Euskal Herriko Unibertsitatea
Universidad del País Vasco

EUSKAL HERRIKO UNIBERTSITATEA / UNIVERSIDAD DEL PAÍS VASCO

Facultad de Ciencia y Tecnología

Departamento de Química Inorgánica

Synthesis and characterization of low-cost materials for aqueous Na-ion batteries

A dissertation submitted to the University of the Basque Country in partial fulfillments of the requirements for the degree of Ph.D.

By

Antonio Jesús Fernández Ropero

Thesis Advisors:

Dr. Montse Casas Cabanas

Dr. Miguel Ángel Muñoz Márquez

Tutor:

Prof. Teófilo Rojo

2016

Resumen

La presente tesis doctoral tuvo su inicio en Enero de 2013 gracias a la contratación por parte del Centro de Investigación Cooperativa (CIC) EnergiGUNE del estudiante de doctorado. La tesis ha sido desarrollada prácticamente en su totalidad en las instalaciones del centro localizado en el Parque Tecnológico de Álava (PTA).

Además, su temática la sitúa dentro del Departamento de Almacenamiento de Energía Electroquímica, en la línea de investigación de ión Na y en el grupo de análisis y caracterización superficial.

Este trabajo ha estado dentro del proyecto de investigación financiado por el proyecto ENE2013-44330-R del Ministerio de Economía y Competitividad del gobierno de España Asimismo, esta Tesis incluye el trabajo realizado durante los tres meses de estancia en Montreal (Quebec) en la empresa pública canadiense Hydro-Québec.

El trabajo aquí expuesto trata de la síntesis y caracterización de materiales de electrodo para baterías de ión sodio acusosas. Este tipo de alternativa está actualmente siendo evaluado como una alternativa más barata y ecológica que los sistemas actuales de almacenaje de energía en la red eléctrica. Aunque tanto el uso de sodio y sobre todo el electrolito acuoso tiene ciertas limitaciones en la densidad energética final del dispositivo, esto no supone un gran problema en el citado caso de instalaciones estacionarias.

Mientras que el número de estudios de baterías de ión sodio con electrolito orgánico ha alcanzado un gran número en los últimos años, los estudios en sistemas acuosos son mucho más escasos. Sin embargo, son prometedores para que la tecnología ión sodio pueda alcanzar el punto de competitividad respectos a los sistemas de almacenamiento energético típicamente comercializados.

Para poder detallar de manera satisfactoria toda la información recabada a lo largo de los tres años de investigación, esta tesis ha sido dividida en siete capítulos independientes.

Capítulo 1: Introducción

En el capítulo 1 se trata toda la problemática ambiental respecto al aumento del consumo energético y el consecuente agotamiento de las fuentes fósiles como carbón, metano y petróleo. Esto ha provocado el auge del uso de fuentes de energía renovables. Sin embargo, este tipo de energía es intermitente y necesita del uso de sistemas de almacenaje. Las represas hídricas y los sistemas de aire comprimido son típicamente utilizados en sistemas de almacenaje a gran escala. Sin embargo, para sistemas a media y pequeña escalas las baterías

son preferidas. Entre estas baterías se pueden encontrar las de plomo, cadmio, litio o sodio-azufre. Las baterías de plomo y cadmio son medioambientalmente poco aconsejables, mientras que las baterías de sodio-azufre trabajan a temperaturas de 350 °C aproximadamente y las cuales conllevan serios riesgos de seguridad. Las baterías de litio tienen buenas prestaciones pero aún resultan costosas para este tipo de aplicaciones y el agotamiento de las reservas de litio augura un aumento del precio de este tipo de tecnología en las próximas décadas.

Las baterías de ion-sodio están por tanto consideradas como una alternativa atractiva a las baterías de litio ya que son potencialmente menos caras, más seguras y ambientalmente benignas. De manera similar a las baterías de ion-litio, los iones Na son transportados entre el electrodo positivo y el negativo durante la carga y descarga de la batería, siendo el electrolito el medio en el que se desplazan estos iones.

Solamente aquellas tecnologías que sean realmente atractivas en términos de coste podrán alcanzar la etapa de comercialización y así contribuir a la implementación de las energías renovables. La vía más prometedora a la hora de reducir costes es la de desarrollar sistemas de electrolito acuoso. Los electrolitos acuosos ofrecen conductividades iónicas muy superiores a las de los solventes orgánicos, son más baratos, más fáciles de producir y pueden ser fabricados con electrodos más gruesos.

Es por todos estos motivos que proponemos identificar y estudiar materiales que sean buenos candidatos para electrodos positivos de sodio-ion en medio acuoso con el fin de desarrollar sistemas de bajo coste para aplicaciones estacionarias. Sin embargo, la búsqueda de materiales de electrodo sodio-ion representa un gran reto. Una de las razones de ello es que los sistemas sodio-ion están basados en reacciones de intercalación de modo que los posibles candidatos deben poder acomodar iones del tamaño del sodio en su estructura. Además, las reacciones secundarias con agua u O_2 por ejemplo deben ser evitadas.

Además, en el contexto de reducción de costes, los materiales deben de estar formados por elementos baratos y a ser posible, medioambientalmente benignos, como es el caso de los aquí descritos: $NaTi_2(PO_4)_3$, $NaFePO_4$ (olivino y maricita), $NaFe_2(CN)_6$ y $Na_4Fe_3(PO_4)_2P_2O_7$.

En este capítulo mientras se exponen los hechos anteriormente descritos y que conducen a la conclusión de porque se elige esta tecnología y materiales como objeto de estudio, se describen las características principales de las baterías comerciales y se ofrece una exhaustiva revisión de los principales materiales de electrodo y electrolitos estudiados en baterías de ión sodio orgánicas. Los principales materiales de electrodo positivo pueden ser divididos en tres

grandes familias: óxidos, polifosfatos y ferrocianidas. Entre los materiales de electrodo negativo destacan los óxidos de Ti y materiales basados en carbon.

Posteriormente se explican los principales estudios en sistemas acuosos. Los electrodos positivos también son clasificados en las mismas familias, mientras que entre los cátodos los óxidos de Ti y los carbones son descartados debido a su bajo potencial que quedaría emplazado en el rango de inestabilidad del agua, siendo el electrodo más destacado el $NaTi_2(PO_4)_3$.

Capítulo 2: Técnicas experimentales

Después de este resumen y de la justificación del proyecto descrito en esta tesis, en el capítulo 2 se da una descripción de las técnicas utilizadas a lo largo de la investigación. Dichas técnicas pueden ser divididas en dos grandes bloques: técnicas de caracterización físico-química y técnicas de caracterización electroquímica.

En el primer bloque se detallan los fundamentos teóricos, equipos utilizados y objeto de uso de las siguientes técnicas: difracción de rayos X, microscopía electrónica de barrido y de transmisión, espectrometría de masas, análisis mediante espectrometría de Mössbauer y análisis termogravimétrico. Estás técnicas se usaron tanto para la caracterización de las muestras obtenidas después del proceso de síntesis como para los materiales después de tratamientos de optimización para mejorar la electroquímica y los materiales después del ciclado electroquímico.

El segundo bloque describe los fundamentos de las dos principales electroquímicas de caracterización utilizadas: voltametría cíclica y estudio galvánico. Así mismo se comentan los dos equipos utilizados y los requerimientos de preparación de baterías dependiendo de la naturaleza del electrolito a utilizar.

Capítulo 3: Estudio de $NaTi_2(PO_4)_3$ como material de ánodo

Una vez descrita la parte experimental, en el capítulo 3 se desarrolla el estudio referente al fosfato de titanio ($NaTi_2(PO_4)_3$). Este es el principal material usado como electrodo negativo en electrolito acuoso debido que su potencial de trabajo entra dentro de la ventana de estabilidad del electrolito. En este trabajo, se han explorado dos métodos de síntesis (Pechini y cerámico). Pechini resultó en una fase pura mientras que el cerámico presentó pequeñas impurezas de pirofosfato de titanio. La mayor pureza de la muestra obtenida mediante el método de Pechini es atribuida a una mezcla más íntima de los precursores. Además, esta mejor mezcla requiere de menores temperaturas de síntesis y la muestra presento menor

cristalización. El efecto del molino de bolas en la electroquímica de las dos muestras fue evaluado con considerables mejoras aumentando el tiempo de tratamiento. No obstante, el recubrimiento de las partículas con C residual procedente de la quema de un polímero resultó en el método más efectivo de mejora. La muestra optimizada en electrolito orgánico fue testeada en electrolito acuoso. El rendimiento a distintos pH fue evaluado. La suma del C-de un una cubierta de carbón y de un pH = 12 resultó en un material de electrodo con alta estabilidad electroquímica y eficiencia coulombica.

Capítulo 4: Estudio de $NaFePO_4$ (olivina) como material de cátodo

En el capítulo 4 se habla del fosfato de hierro ($NaFePO_4$) con estructura olivina. Este material ha despertado un gran interés en baterías de ión sodio orgánico por sus diferencias en el comportamiento electroquímico respecto a su homólogo $LiFePO_4$. De hecho, $NaFePO_4$ con esta estructura es obtenido a partir de $LiFePO_4$ mediante un proceso de oxidación y de reducción química. El material aquí obtenido a partir de $LiFePO_4$ comercial recubierto con carbón es posteriormente testeado en medio orgánico. Una vez comprobado que su funcionamiento se ajusta a lo ya publicado, fue testeado usando electrolito acuoso. El material presentó poca estabilidad durante el ciclado. Mediante el estudio de diferentes rangos de ciclado, una ventana óptima fue determinada. A pesar de la reducción de ventana, el material mostró valores de capacidad específica similares a los obtenidos en el electrolito orgánico y lo que es más destacable, valores mucho menores de sobrepotencial. En ambos medios se estudió el rendimiento electroquímico incrementando la temperatura a 55 °C. Mejoras en términos de capacidad y de sobrepotencial fueron detectadas en ambos medios, especialmente en electrolito acuoso. Finalmente se desarrolló una batería completa con el $NaTi_2(PO_4)_3$.

Capítulo 5: Estudio de $NaFe_2(CN)_6$ como material de cátodo

En el capítulo 5, se describe la caracterización estructural y el rendimiento electroquímico del $NaFe_2(CN)_6$, este material es conocido como Prussian blue y resulta atractivo por la amplitud de su estructura química, la cual le permite albergar iones sodio sin verse alterada. Este material estudiado en electrolito orgánico se caracteriza por tener dos marcados procesos redox. En este estudio se observa la baja estabilidad del material en medio acuoso cuándo ambos procesos son abarcados. Sin embargo, al centrarnos únicamente en un proceso, el material aumenta considerablemente la estabilidad y alcanza eficiencias coulombicas cercanas al 100%. Al igual que $NaFePO_4$, unos valores muy bajos de sobrepotencial son observados. La comparación de ambos materiales nos llevó a la conclusión de que la mayor parte de las diferencias en sobrepotencial en medio acuoso y orgánico se deben principalmente a las diferencias en la energía de activación en el proceso de desolvatación del electrolito.

Capítulo 6: Estudio de $Na_4Fe_3(PO_4)_2P_2O_7$ como material de cátodo

El capítulo 6 trata del polianión mixto $Na_4Fe_3(PO_4)_2P_2O_7$ el cuál ha sido recientemente estudiado en medio orgánico. En este capítulo se describen factores fundamentales en la síntesis del material para obtener una muestra cuasi-pura. La electroquímica fue optimizada en electrolito orgánico siguiendo diferentes estrategias como molienda, recubrimiento o adición de carbón en la etapa de síntesis. La estrategia que dio un mejor rendimiento fue la de adición de carbón. Esta muestra optimizada se estudió usando electrolito acuoso. El material presentó un buen rendimiento en términos de capacidad y polarización y después de analizar las causas de pérdida de capacidad a lo largo del ciclado se proponen distintas estrategias que podrían ser llevadas a cabo para mejorar dicho factor.

Capítulo 7: Estudio de $NaFePO_4$ (maricita) como material de cátodo

Finalmente, en el capítulo 7, el fosfato de hiero $NaFePO_4$ pero en este caso con estructura maricita fue estudiado. Esta estructura a diferencia de la olivina estudiada en el capítulo 4 es obtenida directamente mediante métodos convencionales de síntesis. En este capítulo se describe la optimización de la síntesis y la influencia de la variación de parámetros en dicho proceso. El mecanismo electroquímico en electrolito orgánico es descrito apoyándonos en técnicas como espectrometría de Mössbauer y difracción de rayos X. Finalmente, el material es estudiado en medio acuoso.

Capítulo 8: Conclusiones generales

Por último, el Capítulo 8 incluye las conclusiones más relevantes fruto del trabajo llevado a cabo durante esta tesis doctoral. En este capítulo se discuten los resultados obtenidos en los diferentes capítulos de acuerdo con los objetivos planteados en el Capítulo 1 y el estado del arte.

Summary

Sodium-ion batteries (NIBs) are considered an attractive alternative to lithium-ion batteries. The main drawback of Na-ion systems is the energy density penalty derived from the larger mass of Na when compared to Li. However, in the case of stationary applications, lower energy density is acceptable if the total cost of implementation is disruptively low and the usable device lifetime is extremely long. Even cheaper, safer and more environmentally friendly devices can be designed by using aqueous electrolyte despite of the reduce voltage stability window of water.

The present work is focused on the identification of potential candidate's material as Na-ion electrodes in aqueous electrolyte. The synthesis and the structural characterization of polyanionic compounds as $NaFePO_4$, $NaTi_2(PO_4)_3$ and $Na_4Fe_3(PO_4)_2P_2O_7$, and the Prussian blue $NaFe_2CN_6$, which are being currently studied in organic Na-ion batteries, are here described. Subsequently, they were tested first in organic media for comparative purposes. Once their behaviour was the expected, they were tested in aqueous electrolyte, finding the best conditions of pH and voltage ranges to increase the capacity retention compromising as less as possible the delivered capacity and, consequently, the final energy density of the final device.

In chapter 3 $NaTi_2(PO_4)_3$ which is the most studied anode for aqueous NIBs were explored. Different strategies were used for the electrochemical optimization in organic media and C-coating treatment gave the best results. The optimized material was evaluated in aqueous media at different pH. The selection of a pH = 12 resulted in a good coulombic efficiency and a capacity retention of 100% after 400 cycles.

In chapter 4, $NaFePO_4$ which has been of great interest in the last year's research for organic NIBS was studied. This material was obtained by oxidation and further reduction of a commercial C-coated $LiFePO_4$ sample. After characterizing in organic electrolyte to verify a similar behaviour to that reported in this media, the material was studied in aqueous electrolyte where the overpotential was much lower. The reduction of the operating voltage range was demonstrated to be essential to the cycling stability of this material. The overpotential was notably reduced in aqueous electrolyte. Furthermore, the electrochemical performance of $NaFePO_4$ was evaluated at 55 °C in both media obtaining improved results in terms of overpotential and capacity, especially in aqueous electrolyte. Finally, a full cell battery was built with $NaTi_2(PO_4)_3$ as negative electrode to demonstrate that $NaFePO_4$ is a suitable candidate for aqueous Na-ion cells.

In chapter 5, $NaFe_2(CN)_6$ which is a material easy to synthesize and made of low-cost earth-abundant elements was studied as cathode material. The chemical stability of $NaFe_2(CN)_6$ cells in 1 M Na_2SO_4 was shown to be very dependent of the selected voltage range. Remarkable coulombic efficiencies were achieved focusing only on one of the two main redox process of this material. Moreover, this voltage limitation led to improved cycling stability.

In chapter 6, the synthesis of $Na_4Fe_3(PO_4)_2P_2O_7$ which has been recently reported as a new material for organic NIBs was optimized until obtained a quasi-pure phase. The electrochemical performance in organic electrolyte was optimized by using different strategies as C-coating of the particles, ball-milling or addition of C in the synthesis step. After this, the optimized material was tested in aqueous electrolyte. A good performance in terms of capacity and overpotential was obtained, however, some capacity fading was found after cycling. The causes of this material's fading were found and strategies to increase this capacity are proposed.

Finally, in chapter 7, $NaFePO_4$ with maricite structure, which was supposed to be electrochemically inactive for years but a recently study says the opposite, was studied. Firstly, different parameters during synthesis and its influence in the final result were evaluated. Maricite $NaFePO_4$ was electrochemically study in both media. The electrochemical mechanism is discussed and possible hypothesis were supported by different techniques as Mössbauer and in-situ X-ray diffraction.

Table of contents

1. Introduction

Since the beginning of the industrial revolution, the global energy consumption has continuously grown. During the twentieth century the use of primary energy rose by a factor of twenty and annual growing rates are now around 2% [1]. More than 80% of the used energy comes from fossil fuels, which is the main cause of CO_2 emissions. From 1990 to 2010, the emission of this gas increased more than a 30% (Fig. 1. 1) [2], contributing considerably to global warming.

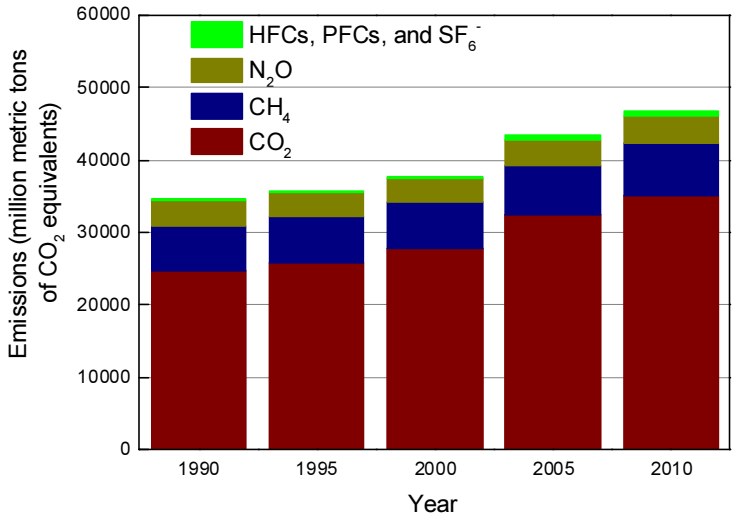

Fig. 1. 1. Worldwide emissions of carbon dioxide (CO_2), methane (CH_4), nitrous oxide (N_2O), and several fluorinated gases from 1990 to 2010. Emissions are expressed in millions tons of dioxide equivalents [2].

These concerning emissions and the depletion of fossil reserves are stimulating the spread of renewable energy sources, which currently represent only 7% of the world's primary energy consumption. The main problem of renewables is its intermittent production that, along with the variation of the demand levels, urgently requires suitable energy storage systems. While pump hydro and compressed air technologies are a good option for large scale systems, for rechargeable batteries are the leading choice medium and low scale applications (Fig. 1. 2) [3].

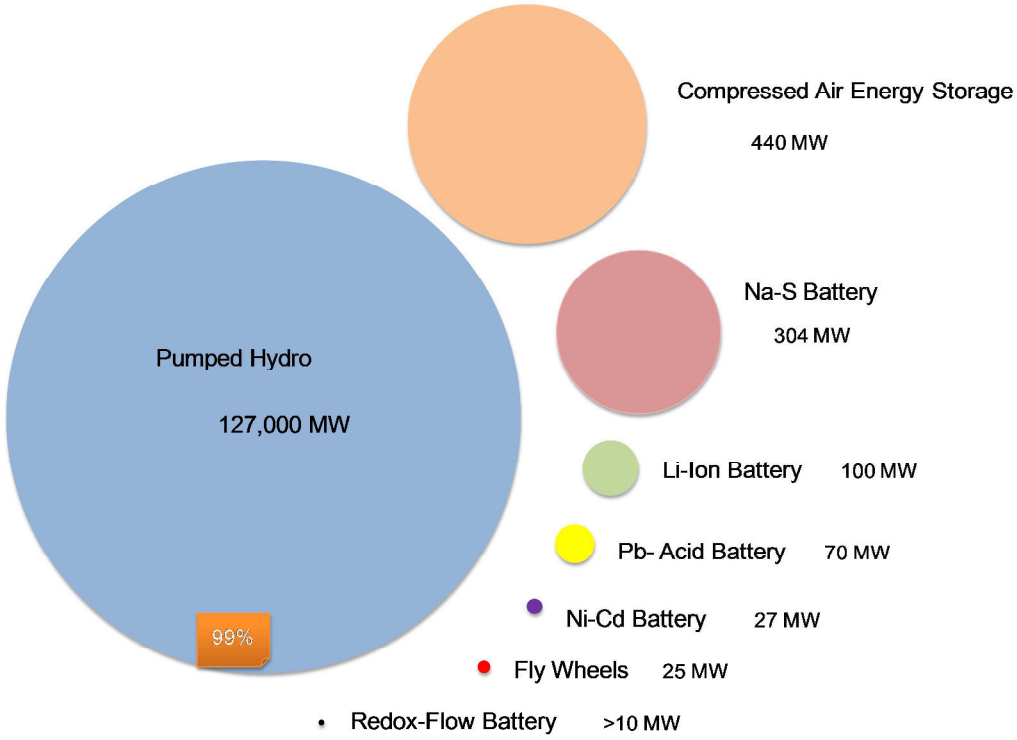

Fig. 1. 2. Worldwide installed storage capacity for electrical energy in 2012 [3].

1.1. Rechargeable batteries in the grid

Rechargeable batteries use reversible electrochemical reactions to store electrical energy. The amount of stored energy depends on the average voltage between two chemical compounds (positive and negative electrodes) and their specific capacity (given by the number of electrons involved in the processes and the molecular weight of the electrode material) [4]. During charge the positive active material is oxidized, producing electrons and the negative material is reduced, consuming them. These electrons constitute the current flow in the external circuit. Reversely, during discharge the negative material is oxidized and the positive material is reduced. The flow of electrons diffuses in this case from the cathode to the anode.

Electrodes are separated by the electrolyte which may serve as a simple medium for internal ion flow between electrodes or it may be an active participant in the electrochemical reaction.

The number of commercially relevant rechargeable battery systems for grid storage is relatively low (see Fig. 1. 2). They can be divided into two main categories according to the electrolyte used: aqueous (Pb-acid, alkaline Ni-Cd or NiMH and more recently redox-flow batteries) and non-aqueous (Na-S batteries and Li-ion batteries (LIBs) [3].

1.1.1. Aqueous batteries

Aqueous electrolytes have much higher ionic mobility than organic solvents, are cheaper, the devices are simpler to manufacture and can be used with thicker electrodes [5]. The electrochemical stability window of aqueous electrolytes is only 1.23 V wide and therefore lower energy densities are achievable compared to organic batteries that operate in a window of 2-3.7 V. Kinetic effects may expand the stability limit to 2 V as is the case of Pb-acid batteries [6]. The main characteristics of commercial aqueous batteries are described below and summarized in Table 1. 1.

1.1.1.1. Pb-acid batteries

The Pb-acid battery is the oldest type of rechargeable battery and was invented in 1859 by Gaston Planté. These systems are still the most commonly used secondary batteries and consume more than 70% of the world's lead production [7]. They are the third most common battery employed in stationary applications and are also widely used by the automobile industry as starter motors. Its success stems from its low price, mostly thanks to lead's abundance and easiness of recycling. Its excessive weight is its major limitation. Other drawbacks are the inability to be stored in low-charge state due to the acid stratification and sulfation [8], the limited number of deep-discharge cycles, the limited use at high temperature, the necessity of slow charge and the fact that contain lead and acid which are environmental hazards [9].

Pb-acid batteries are constituted by a sulfuric acid tank which contains parallel Pb plates, alternately distributed with positive and negative polarity. The positive plates are coated by Pb (II) oxide and the negative plates are made of Pb sponge. This configuration corresponds to the charged state. In the discharged state both the positive and negative plates become Pb (II) sulfate ($PbSO_4$) [10]. Therefore, the elemental processes that occur in the battery are:

$$PbO_2 + 2H_2SO_4 + 2e^- \rightarrow 2H_2O + PbSO_4 + SO_4^{2-}$$

$$Pb + SO_4^{2-} \rightarrow PbSO_4 + 2e^-$$

1.1.1.2. Ni-Cd batteries

Ni-Cd batteries are a kind of alkaline battery and therefore use a basic aqueous electrolyte, typically KOH (although NaOH is cheaper, KOH is preferred for its higher conductance). The first Ni-Cd battery was created by the Swedish Waldemar Jungner in 1899.

Ni-Cd batteries have been in the market for more than a hundred years, but they have been partially displaced by Nickel–Metal Hydride (NiMH) batteries which have two to three times

the capacity of a Ni-Cd battery of equivalent size, less memory effect and no environmental hazards like Cd. However, Ni-Cd battery are preferred in products with low capacity requirements and in renewable energy systems due to their lower prize, high rate capability and availability at low temperatures in comparison to NiMH batteries [11].

The positive electrode in Ni-Cd batteries is Ni oxyhydroxide (NiOOH) and Cd is used as negative electrode. The elemental processes in discharge reaction are:

$Cd + 2OH^- \rightarrow Cd(OH)_2 + 2e^-$

$2NiO(OH) + 2H_2O + 2e- \rightarrow 2Ni(OH)_2$

1.1.2. Non-aqueous batteries

Non-aqueous electrolytes enable the use of redox couples with a larger voltage difference, and historically represented a big step in energy density.

1.1.2.1. Na-S batteries

Na–S batteries, which have been commercialized since the mid-1970s [12], have a high energy density, acceptable charge/discharge efficiency (89-92%), long cycle life, temperature stability and use cheap and easy to recycle components [4]. This technology utilizes molten Na and S as anode and cathode materials respectively, separated with a β''- alumina solid electrolyte and usually operate at 300–350 °C. The entire cell is enclosed by a steel casing that is protected, usually by Cr and Mo, from being corroded on the inside. The container is sealed at the top with an airtight alumina lid. The cells are arranged in blocks for better heat conservation and are encased in a vacuum-insulated box. During the discharge reaction the anode, molten elemental Na at the core, donates electrons to the external circuit. Then, Na^+ migrates through the electrolyte to the S container which consists in an absorbing C sponge [13]. The discharge process can be represented as follows:

$2Na^0 – 2e^- \rightarrow 2\ Na^+$

$xS + 2Na^+ + 2e- \rightarrow Na_2S_x^-$ (x = 5-3)

As the cell discharges, the Na level drops. Once running, the heat produced by charging and discharging cycles is sufficient to maintain the operating temperatures and usually no external heating source is required.

Its main disadvantages are the risk of an uncontained reaction in case of electrolyte breaking and the corrosion produced by Na polysulfides that involve the use of highly resistant containers.

1.1.2.2. Li-ion batteries (LIBs)

A safer technology which usually operates at room temperature is Li-ion . Li is the lightest metal (M = 6.94 g mol^{-1}) and therefore high capacity materials can be developed. Due to their high energy density (up to 210 Wh Kg^{-1} and 650 Wh L^{-1}) and their better shelf life compared to conventional aqueous technologies these batteries have captured an important niche in the market despite their higher cost [4,14].

Prior to their commercialization, three important developments occurred during 1980s. In 1980 John B. Goodenough identified and developed Li_xCoO_2 as cathode material. The first prototypes of these Li batteries suffered from severe safety problems and short lifetimes due to the use of Li metal in the anode side, which was instable due to the formation of dendrites, causing shorts in the cell and subsequent extremely exothermic reactions. Secondly, Rachid Yazami discovered graphite as negative electrode. The replacement of Li metal by graphite in the anode gave up a 90% of capacity but more stability was achieved, which represented a longer cycle life and safety improvements. Finally, these achievements crystallized in the first LIB prototype, built by the research team managed by Akira Yoshino of Asahi Chemical in Japan in 1985, a rechargeable and more stable version of the Li battery; that Sony commercialized in 1991.

LIBs thus comprise two lithium insertion electrodes with a thin layer of electrolyte solution (or a solid matrix) in between, whose role is to enable a fluent and fast transport of Li^+ between the electrodes (Fig. 1. 3). Liquid electrolytes in LIBs consist of Li salts, such as $LiPF_6$, $LiBF_4$ or $LiClO_4$ in an organic solvent, such as ethylene carbonate (EC), dimethyl carbonate (DMC), and diethyl carbonate (DEC) or mixtures of them [15].

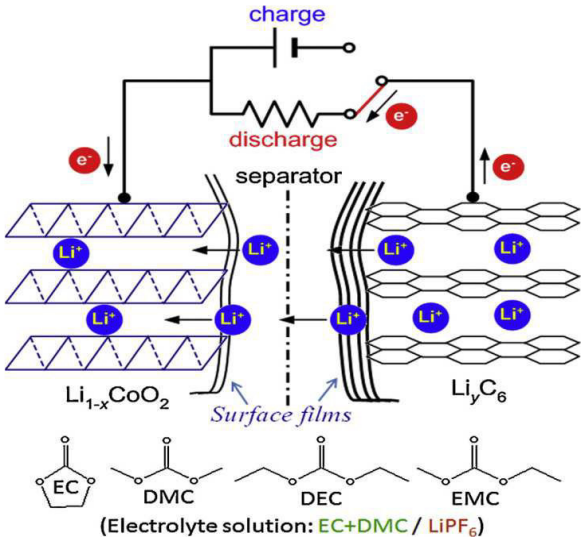

Fig. 1. 3. A representative scheme on how Li-ion batteries usually work via Li ion intercalation processes [15].

The most important cathode materials for commercially available LIBs are $LiCoO_2$ (layered), $LiMn_2O_4$ (spinel), $LiFePO_4$ (olivine) and $LiMn_{1/3}Li_{1/3}Co_{1/3}O_2$ (layered) which operate within a range of the 3.5–4 V *vs*. Li^+/Li. These compounds have practical capacities of 150, 120, 155 and 160 mAh g^{-1} respectively [16,17,18].

The most commonly used anode material is graphite, but non-graphitic carbons (soft carbons, hard carbons) [19] may also be used. Electrodes are casted as thin (micrometric thick) films on Al or Cu sheets which act as current collectors for the cathode and the anode respectively.

Nowadays, on one hand, research is focusing in obtaining electrode materials with higher voltage or larger capacities (which would imply more energy density) to achieved the required autonomy in mobile applications as electrical vehicles. On the other hand, for stationary applications, the most important issue is to reduce the high cost of these batteries and new alternatives as less expensive materials or cheaper production processes are being explored.

Table 1. 1. Secondary Battery Technology Comparison: Electrode and electrolyte materials, voltage, theoretical and practical specific energy, practical energy density and major issues per battery system.

Battery System	Electrodes (Electrolyte)	Nominal Voltage (V)	Theoretical Specific Energy (Wh Kg^{-1})	Practical Specific Energy (Wh Kg^{-1})	Practical Energy Density (Wh L^{-1})	Major Issues
Pb-acid	Pb/PbO_2 (H_2SO_4)	2.1	252	35	70	Heavy, Low Cycle Life, Toxic Materials
Ni-Cd	Cd/NiOOH (KOH)	1.3	244	35	100	Toxic materials, maintenance, costs
Na-S	Na/S (Beta Alumina)	2.1	792	170	345	High Temperature Battery, Safety, Low Power Electrolyte
Li-Ion	Graphite/Li-intercalation compound ($LiPF_6$)	3.5-4	410	150	400	Safety, Calendar Life, Cost

1.2. Na-ion batteries (NIBs) as alternative technology for stationary applications

A potential low cost alternative to LIBs can be obtained by replacing Li for Na. Its low cost due to its natural abundance (Fig. 1. 4) and accessibility; suitable redox potential (E_0 = (Na^+/Na) = -2.71 V *vs.* standard hydrogen electrode, only 0.3 V above that of Li) and similar intercalation chemistry to Li, make this element strategic in innovative research of energy storage systems. It should be noticed that total global Li consumption in 2008 was approximately 21,280 tons; hence mineable Li resources from the present could be sustained only for approximately 65 years if no Li is recycled [20]. In response to the Li increasing demand, Na could be used as complement to Li-based technology and even as replacement when low cost is the main requirement.

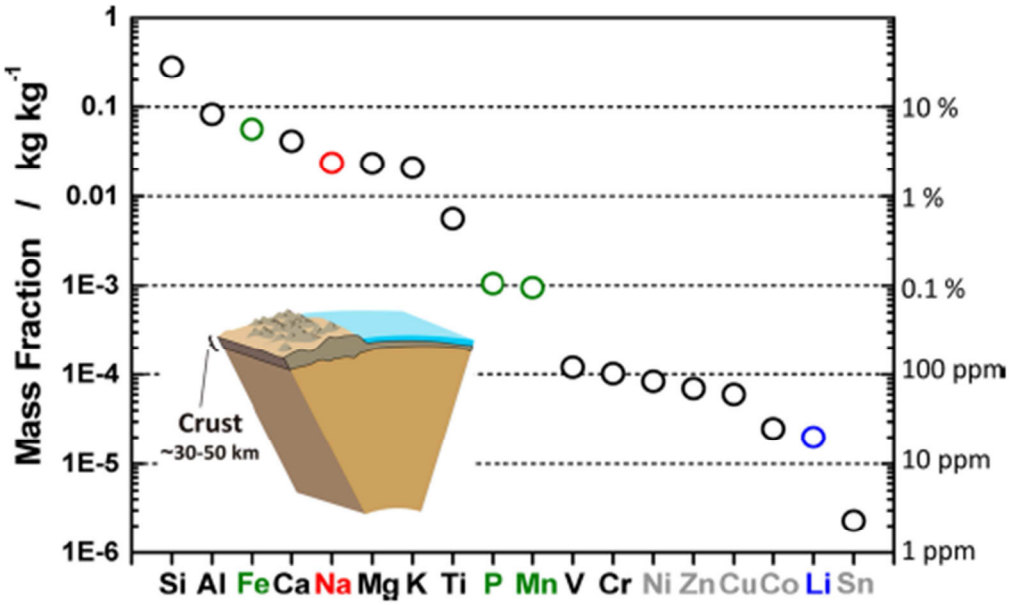

Fig. 1. 4. Elemental abundance in the Earth's crust [21].

This technology has a similar operation principle than its homologous Li-ion system. Indeed, Na ions are shuttled between the positive (cathode) and negative (anode) electrodes upon discharge and charge through a non-aqueous Na-ion electrolyte that is contained between the electrodes [22,23]. The study of Na-ion electrodes has been intensified in the last years. Fig. 1. 5 displays the relationship between the capacity and voltage for most studied electrode materials in NIBS. A non-exhaustive description of the main electrode materials and electrolytes under study is given below.

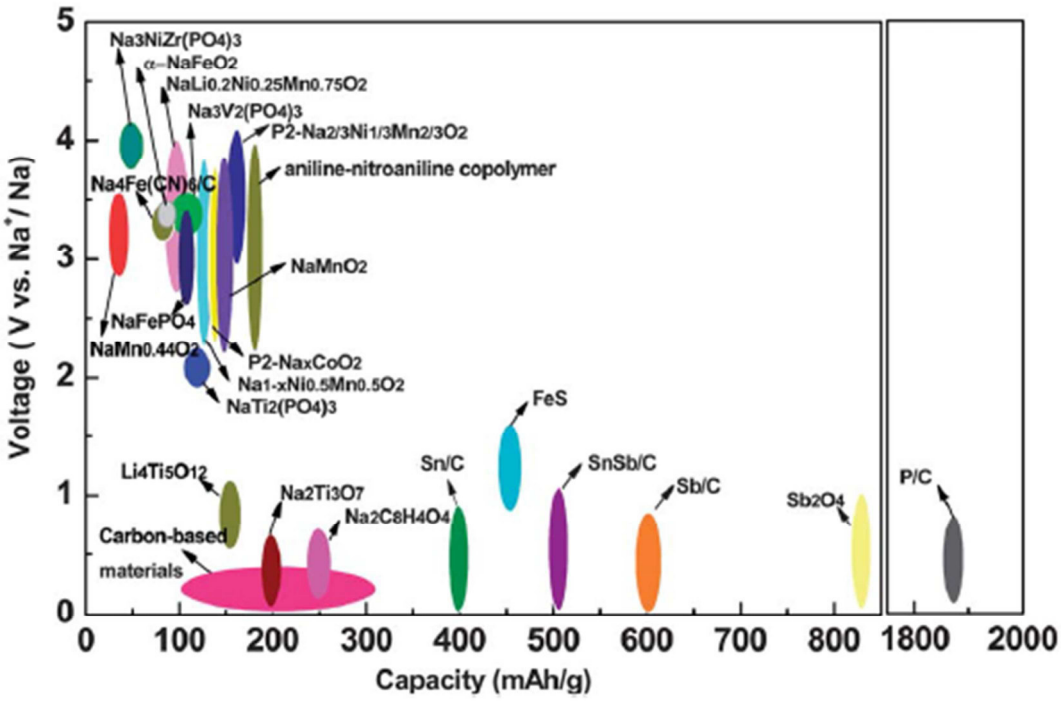

Fig. 1. 5. The relationship between capacity and voltage for present electrodes materials in Na-ion batteries [23]

1.2.1 Cathode materials

A great variety of compounds are being studied as possible cathodic materials for Na-ion batteries but can be roughly grouped in three main families of compounds: oxides, polyanionic compounds and Prussian blue analogues. Each family presents its own advantages and disadvantages and a summary of their features is discussed below.

1.2.1.1. Layered oxides

Layered oxides are considered to be a promising cathode system for Na-ion batteries due to their high capacity and cost [5]. Within this family, Mn and Fe based compounds are the most promising.

All layered oxides can be classified in different polytypes which differ in the stacking of the close-packed oxygen layer. Octahedral ABCABC (O3-type) (Fig. 1. 6a) and prismatic ABBA (P2-type) (Fig. 1. 6b) stackings are of special interest. O3-type layered oxides as $NaMnO_2$ [24] typically exhibit stepwise voltage profiles (Fig. 1. 6c). This fact is related to structural related to Na-ordering and layer gliding.

Better rate capability is displayed by P2-type layered oxides such as P2-$Na_{2/3}Mn_{1/2}Fe_{1/2}O_2$ [25]. The superior rate capability of P2-type oxides compared to O3-type oxides is correlated to the smooth voltage profile (Fig. 1. 6d) which can be interpreted as softer structural changes

due to Na^+ insertion. However, P2-type oxides also show low capacity retention which is attributed to the phase transition of P2 to BACBBCAB (OP4) stacking [26].

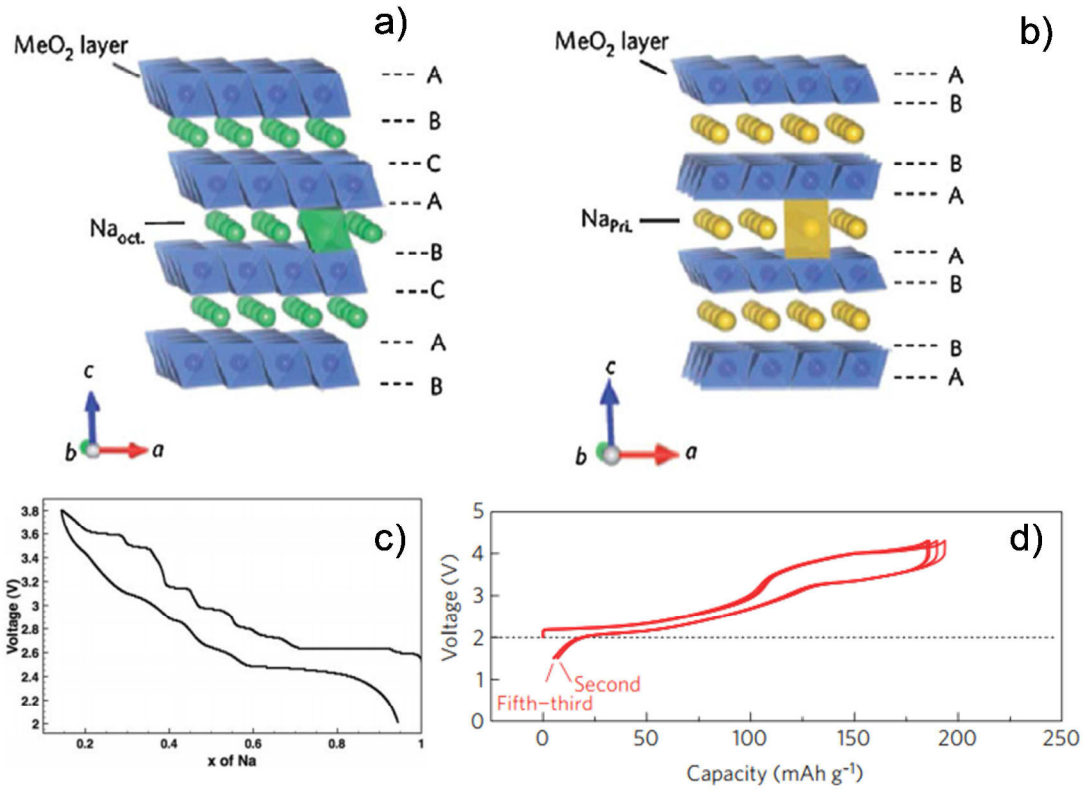

Fig. 1. 6. (a) Stepwise voltage profile of O3-NaxMnO_2 [24] and (b) smooth voltage profile of P2-$Na_{2/3}Mn_{1/2}Fe_{1/2}O_2$ [25]. Layered structure of O3-type (c) and P2-type (d) NaMO2.

Different strategies have been followed to decrease the capacity fading of P2 phase materials. Li rich layered sodium metal oxides [27] or substitution of Mn by Mg [28,29] leaded to improved cyclabilities. However, the use of P2 phases which are deficient in Na requires pre-sodiation strategies as electrochemical sodiation, the use of a sacrificial salt as Na_3N [30] or the recently reported ball milling with metallic Na [31]. Moreover, the air sensitive of layered oxides is a drawback for low-cost applications.

1.2.1.2. Polyanionic compounds

Because of their structural and thermal stability, and tunable redox potential, materials based on phosphate polyanions are attractive as cathodes materials for NIBs.

Extensively tested as cathode for LIBs, $Na_3M_2(PO_4)_3$ NASICON-type compounds have deserved attention as electrode materials for Na-ion batteries thanks to their three-dimensional framework of large interstitial spaces through which Na^+ can diffuse [32,33,34]. $Na_3V_2(PO_4)_3$ is one of the most interesting compounds within this family and exhibits two potential plateaux

related to the V^{4+}/V^{3+} and V^{3+}/V^{2+} redox couples, separated by 1.8V (located at 3.4 V and 1.6 V *vs.* Na^+/Na respectively) with theoretical capacities of 117 mAh g^{-1} and 50 mAh g^{-1} respectively. However, practical capacities are of the order of 80 mAh g^{-1} [35] and the separation between the two plateaux is too large to be utilized in practical devices.

Na-V fluorophosphates are an interesting alternative to phosphates since, in addition to their good theoretical specific capacities, the inclusion of highly electronegative fluorine atoms in the covalent polyanionic framework increases the voltage of the active redox couple [36]. Yamaki *et al*. were the first to report the performance of three isostructural compounds with formula $Na_3M_2(PO_4)_2F_3$ (M = Ti, Fe and V) [37]. Among these, Ti and Fe phases presented poor electrochemical performance, but Na-V fluorophosphate showed an excellent rate capability with specific capacities around 90 mAh g^{-1} related to two plateaux at 3.65 and 4.1 V vs. Na^+/Na. This compound has been recently used as positive active material in recent a prototype *vs*. hard carbon [38]. However, V is a non-abundant and badly spread element (95% in Russia, China and South Africa) that might still be too costly if Na-ion batteries are to compete with LIBs. Moreover, its toxicity (the inhalation of V products produces lung cancer [39]) implies preventive actions in its commercialization.

Despite the lower voltage delivered by the Fe+2/Fe+3 redox couple in comparison to V compounds, Fe-based materials are desirable since are more abundant and environmentally friendly than V. In this context, olivine $NaFePO_4$ has the highest theoretical specific capacity (154 mAh g^{-1}) among phosphate polyanion cathode materials and, since its Li analogue is a successful commercial electrode material [40], has deserved particular interest. It operates around 2.9 V *vs*. Na^+/Na and has a theoretical energy density of 446 Wh kg^{-1} *vs*. Na metal. Although the voltage is somewhat low, good practical capacities (100-120 mAh g^{-1} at low rates) and cyclability have been reported, as well as a different transformation mechanism with respect to $LiFePO_4$ [41,42,43,44,45,46]. It has however the drawback that it has to be obtained by delithiation of LiFePO4 since the olivine polymorph is thermodynamically less stable than maricite [41], and Na-ion lower diffusion coefficients and higher contact and charge transfer resistances compared to its lithium counterpart have been reported [47].

Maricite $NaFePO_4$ was first disregarded as a possible alternative since was thought to be electrochemically inactive in rechargeable batteries [48,49]. However, a recent report by Kim *et al*. showed, for the first time, that nanosized maricite $NaFePO_4$ can function as good cathode material for NIBs [50]. It can deliver a first cycle capacity of 142 mA h g^{-1} (92% of the theoretical value) with outstanding cyclability, with a negligible capacity fade after 200 cycles (95% retention of the initial cycle). It has been proposed that Na ion deintercalation results in the amorphisation of the material.

Another family of compounds that has been recently identified as possible cathode materials are pyrophosphates. These offer a robust and stable three-dimensional $(P_2O_7)^{4-}$ framework with multiple sites for alkali ions. The theoretical capacity of most pyrophosphates ($NaFeP_2O_7$, $NaCoP_2O_7$, $Na_2MnP_2O_7$, $Na_2CuP_2O_7$ and $Na_2VOP_2O_7$) is close to 100 mAh g^{-1} with the exception of the Mn compound that can theoretically reach 195 mAh g^{-1} if two Na+ are extracted [51]. Triclinic (P-1) $Na_2FeP_2O_7$ [52] and (P1) $Na_2MnP_2O_7$ [53] with 3D Na ion channels, and layered orthorhombic Na2CoP2O7 [54] with 2D channels for Na+ mobility have been experimentally studied. All three demonstrated reversible Na-ion storage with a capacity around 80 mAh g^{-1} and an average voltage of 3 V for the Fe and Co compounds and about 3.6 V for the Mn compound. Pyrophosphate-based compounds are therefore stable and have versatile structures, but exhibit low theoretical specific capacities compared to phosphates or oxides due to the large weight of the pyrophosphate anion.

A strategy to increase the theoretical capacity is to combine them with phosphates, as for example $Na_4Fe_3(PO_4)_2(P_2O_7)$ (C_{th} = 129 mAh g^{-1}), recently reported by Kim *et al*. which exhibits an average voltage of 3 V *vs*. Na/Na^+ with 100 mAh g^{-1} of practical reversible capacity [55]. The electrochemical process involves the intercalation of 3 Na^+ and occurs through a one-phase reaction with a reversible structural transformation that includes $(P_2O_7)^{-4}$ distortion. The unusually small volume change observed during cycling is expected to contribute to its stable capacity retention [56].

1.2.1.3. Prussian Blue analogues

Prussian-blue analogues (PBAs) have been investigated as alternative cathode materials to layered oxides and polyanion structures. PBAs can be more generally described as Na2-xMA[MB(CN)6]1-y·zH2O where many different transition metals MA and MB can be accommodated and exhibit large empty sites for Na to intercalate [22], which is particularly interesting since the lattice volume expansion/contraction associated to intercalation reactions is believed to be more problematic for Na+ than for Li+ owing to its larger size [23].

Na (de)intercalation was first explored for PBAs with M = Mn, Fe, Co, Ni and Zn by Lu *et al.* [57]. The largest capacitywas achieved with M = Fe, around 100 mAh g^{-1}, which reacts at 2.95 and 3.64 V *vs*. Na^+/Na. The process at 2.95 V corresponds to the oxidation–reduction of the high-spin Fe(III)–Fe(II) couple bonding to N, and that at 3.64 V to the low-spin Fe(III)–Fe(II) couple bonding to C. As a consequence of their low cost and facile synthesis, PBAs with M_A = M_B = Fe or Mn are particularly attractive for large applications where the cost is a key factor.

Na-Mn hexacyanoferrate ($Na_{2-x}MnFe(CN)_6$) with a high Na concentration was reported to be a promising cathode material because of its high capacity (134 mAh g^{-1}) and voltage resulting from the Mn^{3+}/Mn^{2+} redox couple [58]. However, only 120 mAh g^{-1} was maintained over 30

cycles. The material "Berlin green" $Fe^{3+}[Fe^{3+}(CN)_6]$ was reported to undergo sodium insertion with a reversible capacity of 120 $mAhg^{-1}$ and 87% capacity retention over 500 cycles [59]. More recently, You *et al*. reached the high specific capacity of 170 mAh g^{-1} with sodium PB (Na-PB, $Na_{0.61}Fe[Fe(CN)_6]_{0.94}$) nanocubes, and without an apparent capacity loss for 150 cycles [60].

1.2.2. Anode materials

As in Li-ion batteries, full Na-ion cells do not employ Na metal as the negative electrode due to its high reactivity [61] and dendrite formation [62]. On the other hand, typical graphitic carbons employed in Li-ion cells do not intercalate Na^+ [22]. The discovery of suitable anode materials is therefore a major challenge. Other forms of carbon, alloys and metal oxide intercalation compounds are being studied as negative electrode.

1.2.2.1 Carbons

Among carbonaceous compounds, hard carbons (HCs) are leading NIB anode materials, although their performance is still far from that achieved by graphite in LIBs. HC do not react via an intercalation mechanism and it is generally believed that Na^+ ions fill the porosity generated by the disordered carbon layers instead [63].

The good performance of HC as negative material for NIBs was recently demonstrated in full cells with O3-$NaMn_{0.5}Ni_{0.5}O_2$ as the positive electrode [64]. Despite some electrolyte decomposition, over 70% of the initial capacity (300 mAh g^{-1}) is maintained after 50 cycles at moderate current density. Ponrouch *et al*. have recently shown that, in the case of HC prepared from the pyrolysis of sugar, reversible capacities as high as 300 mA h g^{-1} can be obtained at 0.1C for more than 100 cycles in half cells by optimization of HC processing.

Very recently, the insertion of Na^+ in expanded graphite (EG) has also been reported [65,66]. Different from other carbonaceous NIB anodes, EG stores Na^+ mostly by interlayer intercalation. The interlayer spacing between graphene layers strongly influences the reversible capacity. It increases from 25 $mAhg^{-1}$ in graphite (d = 3.4 Å) to 136 $mAhg^{-1}$ [65] or 174 $mAhg^{-1}$ [66] in highly reduced graphene oxide (d = 3.7 Å), reaching 280 $mAhg^{-1}$ at the optimal spacing of 4.3 Å [65]. The optimized material exhibits a stable reversible capacity of about 280 mAhg-1 at current densities of 20 mAg^{-1}, dropping to 180 $mAhg^{-1}$ when the rate is increased to 100 mAg-1. The capacity retention is more than 70% after 2000 cycles at the latter rate, which suggests that the expanded graphite negative electrodes have very encouraging aging properties. The insertion potential of these materials is a sloping curve from 1.5 V to 0 V with more than 80% of the capacity under 1 V. The higher voltage compared to HC increases the safety at the expense of the energy density.

1.2.2.2. Low potential transition-metal compounds

Anodes based on the insertion of Na^+ into transition metal oxides and phosphates are of particular interest, since benefit from good safety features and high volumetric energy densities. Most of the current research interest focuses on titanates, which generally present acceptable voltages but poor electronic conductivity.

Sodium intercalation into amorphous TiO_2 nanotubes shows that their particle size is critical to obtain significant Na intercalation [109]. Up to 140 mAh g^{-1} can be obtained at 0.15C through a sloppy plateau from 2.5 to 1 V, which is a high voltage for practical cells.

The reversible insertion of 2 Na^+ (180 mAh g^{-1}) into $Na_2Ti_3O_7$ was shown to occur at a voltage as low as 0.3 V *vs*. Na^+/Na [67]. However, to achieve this capacity, a slow cycling rate (0.04C) and a composite electrode with 30% of carbon black are necessary. The rate capability has been significantly improved by reduction of the particle size by either hydrothermal synthesis [68] to obtain 8-nm particles capable of delivering reversible capacities up to 110 mAh g^{-1} at 4C, or high-energy ball milling [69] to reduce the particles down to 100 nm and achieve 75 $mAhg^{-1}$ at 5C. In both cases the capacity retention is improved at higher rates, thus suggesting electrolyte decomposition, which is aggravated by the large surface area of the material [70].

The superior capabilities of cathodes based on P2-layered oxide cathodes led to the investigation of the same structure for negative electrode applications. Thus, $Na_{0.66}Li_{0.22}Ti_{0.78}O_2$ [71], with lithium in the transition-metal site, shows a reversible capacity of approximately 120 mAh g^{-1} at 0.1C with an average voltage of 0.7 V versus Na^+/Na. This material exhibits good rate capability with 75 mAh g^{-1} at 1C and 75% capacity retention after 1200 cycles. The good performance is attributed to the very small volume change (0.8%) upon Na^+ insertion. However, as the previous cited P2-manganese oxides, $Na_{0.66}Li_{0.22}Ti_{0.78}O_2$ is also deficient in sodium.

Another Ti-based anode is NASICON $NaTi_2(PO_4)_3$ (C_{th} = 133 mAh g^{-1}) [72]. Two Na ions can be reversibly deintercalated/intercalated in the three-dimensional structure of $NaTi_2(PO_4)_3$ through a two-phase reaction via Ti^{4+}/Ti^{3+} redox pair. However, the voltage plateau occurs at *ca*. 2.1 V *vs*. Na^+/Na, which is a quite high potential to work as anode in a commercial organic cell. It has been recently discovered that the Ti^{+3}/Ti^{2+} redox pair is also accessible at low voltage [73].

1.2.3. Electrolyte

In addition to providing a stable interface, an electrolyte must achieve good ionic conductivity. This parameter is mostly affected by the concentration of the charge carrier (solubility of the salt), the ionic mobility (viscosity of the media), and the ionic dissociation of

the salt (dielectric constant of the media) [22].The most common organic electrolytes in organic NIBs are analogues to those of LIBs, and consist of an inorganic salt dissolved in an organic solvent (or a mixture of them). Several of these organic liquid electrolytes have been investigated by several groups.

HC is the only anode material that has been systematically studied against different electrolytes, but contradictory results have been obtained. Ponrouch *et al.* found that $NaClO_4$ or $NaPF_6$ in EC : PC solvent mixtures is the best choice for HC [74] . Another report shows good capacity retention in $NaPF_6$ and $NaClO_4$ EC/DMC (50:50 vol%) solutions although the better behavior was obtained with $NaClO_4$ in PC solutions [75]. These discrepancies show the high degree of sensitivity to the nature of the electrode and highlight the necessity of more work to fully characterize these systems.

Fluoroethylene carbonate (FEC) has also been identified to improve the irreversibility in different anode materials when used as additive [76, 77, 78].

Research is now focused in finding other electrolytes that are safer, cheaper and/or more environmentally friendly, like polymer, solid state and aqueous electrolytes.

1.3. Aqueous Na-ion batteries

Promising as NIBs may be, the energy density penalty derived from the larger mass of Na when compared to Li represents a drawback. In the case of stationary applications, lower energy density is acceptable but only if the total cost of implementation is disruptively low and the usable device lifetime is extremely long.

By replacing the organic electrolyte by an aqueous one, the cost can be further reduced while providing environmentally friendly and safety features. Obviously, since the stable voltage window of aqueous electrolytes is narrower, lower energy density is achievable but again, it is an acceptable trade-off in the context of stationary applications where cost is the main driver.

The first aqueous electrolyte full cell using a “rocking chair” system was already reported in 1994 by Dahn’s group. They developed a Li-ion aqueous battery where VO_2 was used as the negative electrode and $LiMn_2O_4$ as the positive electrode. The cell could operate at an average voltage close to 1.5 V with a specific energy density of 75 Wh kg^{-1} based on the total weight of both electrode materials [79]. In the last years, studies on electrodes materials for aqueous NIBs have exponentially grown since combine the advantage of using Na instead of Li and a cheaper and more environmentally friendly electrolyte [5, 80].

Electrode materials for aqueous NIBs should satisfy several conditions to be used in aqueous

systems. First, the electrode redox potentials should be located between those of O_2 and H_2 evolution to avoid water splitting during electrochemical cycling (2.297 and 3.527 V *vs*. Na^+/Na at neutral pH) [81]. Second, the electrode needs to be chemically stable at the operating pH of the aqueous electrolyte to avoid dissolution. Also O_2 should be avoided since residual O_2 can cause side reactions:

$$Na\text{-(intercalated)} + 1/2H_2O + 1/4O_2 \rightarrow Na^+ + OH^-$$

Fig. 1. 7 shows a summary of the different Na-ion reported compounds that comply with the voltage requirement.

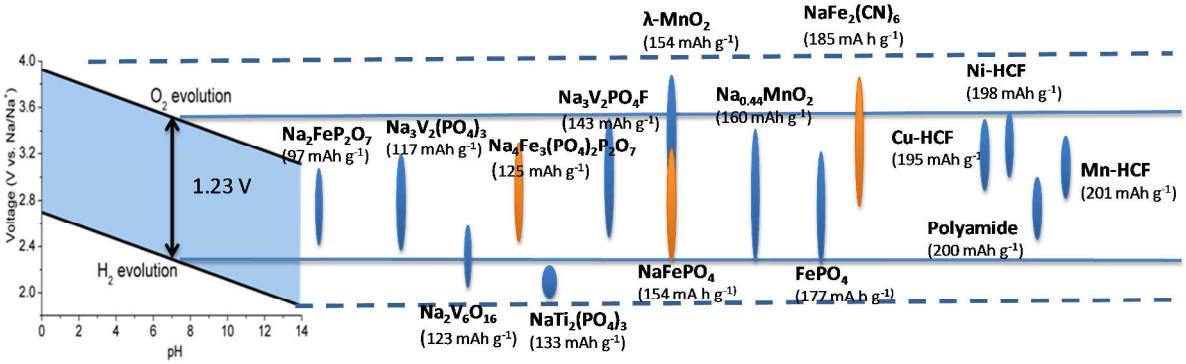

Fig. 1. 7. The main studied electrodes so far in aqueous NIBs in function of their theoretical specific capacity and voltage range. The blue background indicates the stability voltage range of the aqueous electrolyte as a function of the pH.

1.3.1. Cathode materials

As it happens with cathode tested for organic NIBs, the most studied materials belong to three different families: oxides, polyanionic compounds and PBA. Below the most relevant studies for cathodes materials in aqueous media are discussed.

1.3.1.1. Oxides

One of the first reports of an aqueous Na-based cathode material was from Sauvage *et al*., who tested the electrochemical Na^+ insertion/de-insertion into $Na_{0.44}MnO_2$ (C_{th} = 160 mAh g^{-1}, 3.005, 3.225 and 3.455 V *vs*. Na^+/Na) in aqueous media when studying this material for its sensing properties [82]. Soon after, Whitacre *et al*. developed a hybrid cell using the same material as a positive electrode and activated carbon (AC) as negative electrode, obtaining higher energy densities than a supercapacitor and good reversibility, showing a specific capacity of 45 mAh g^{-1} and a voltage of 1.4 V [83].

Several methods of synthesis have been used to improve the electrochemical activities of $Na_{0.44}MnO_2$ in an aqueous electrolyte. Liu *et al*. found that a specific capacitance of 200 F g^{-1},

corresponding to a capacity of 55 mAh g^{-1}, could be obtained from $Na_{0.44}MnO_2$ synthesized using the sol–gel method [84]. Cycle performance of up to 4,000 cycles was achieved with an 84% retention of the initial discharge capacity at a 18 C current density.

The electrochemical activity of $Na_{0.44}MnO_2$ in an aqueous Na ion full cell using an insertion-based counter electrode like $NaTi_2(PO_4)_3$ was recently reported by Wu and Li *et al*. [85]. A capacity of 40 mA h g^{-1} was obtained at 0.6 C with an energy density of ~33 Wh kg^{-1}. This cell demonstrated remarkably high rate performance and comparable to a supercapacitor, but with much higher energy density. Approximately 60% of the initial capacity was retained after 700 cycles for this cell.

Improved results in terms of capacity were obtained using the spinel λ-MnO_2 (C_{th} = 154 mAh g^{-1}). This material was able to deliver a specific capacity up to 100 mAh g^{-1}, leading to a full cell energy density of 25 Wh kg^{-1} for a 5-hour discharge with an AC anode [86]. However, λ-MnO_2 has to be prepared by delithiation of a Li-containing precursor ($LiMn_2O_4$) in acid media. These are now commercialized by Aquion [87].

1.3.1.2. Polyanionic compounds

NASICON-Type cathodes as $Na_3V_2(PO_4)_3$ (C_{th} = 117 mAh g^{-1}) and $NaVPO_4F$ (C_{th} = 143 mAh g^{-1}) have been studied in aqueous electrolyte. In the case of $Na_3V_2(PO_4)_3$ about 50 mAh g^{-1} with an operating voltage of 3.355 V *vs*. Na^+/Na was obtained in a 5 M $NaNO_3$ electrolyte solution at 8.5C rate using Pt as counter electrode [88]. However, the capacity retention was only 30% of the initial capacity after 30 cycles. $NaVPO_4F$ electrode exhibited a capacity of 54 mAh g^{-1} between 3.155 and 3.755 V *vs*. Na^+/Na also in a 5 M $NaNO_3$, with a 70% of capacity retention after 20 cycles in a full cell with polyamide as anode at almost 0.33C rate [89].

More environmentally friendly Fe-based polyanionic compounds have been recently tested as cathode materials in aqueous systems. This is the case of the $Na_2FeP_2O_7$ (C_{th} = 97 mAh g^{-1}) reported by Jung *et al*. [90] in 1 M Na_2SO_4 aqueous electrolyte, which showed a main plateau around 3 V *vs*. Na^+/Na. At 1C rate, the initial discharge capacity was 58 mAh g^{-1} and the capacity retention was approximately 86% after 300 cycles.

Levi and Zhao *et al.* investigated the co-insertion of different ions from mixed aqueous electrolyte solutions and their coexistence in the olivine Li_xFePO_4 matrix [91]. They found that a reversible Na^+ insertion was possible with the two characteristics oxidative peaks also observed in organic systems and which corresponds to the intermediate phase $Na_{0.7}FePO_4$ [41,42]. The same was also observed when Vujkovic *et al.* reversibly cycled $LiFePO_4$ in an aqueous solution of $NaNO_3$ [92]. Another recent work showed the use of $FePO_4$ in aqueous electrolyte when $Na_3Ti_2(PO_4)_3$ was evaluated as Na-bearing anode. The authors reported an

initial full cell capacity at 0.5C of ~110 mAh g^{-1} cathode, with a capacity fade of about 40% after 20 cycles at pH = 11 [93].

1.3.1.3. Prussian Blue (PB) and Prussian Blue analogues (PBAs)

The electrochemical performance of nanostructured nickel hexacyanoferrate (NiHCF) in 1 M $NaNO_3$ and 1 M KNO_3 solutions acidified to pH = 2 was reported by Wessells *et al.* to deliver 52 mAh g^{-1} of reversible capacity at 3.3 V *vs.* Na^+/Na and almost undetectable capacity fading after 5,000 cycles at 8.3C [94]. The same group reported the effect of the insertion of different monovalent cations (K^+, Na^+, Li^+ and NH_4^+) on nanostructured Cu hexacyanoferrate (CuHCF) and NiHCF [95]. Rapid kinetics and long cycle life were observed for K^+ insertion into CuHCF, and for both Na^+ and K^+ insertion into NiHCF. Wu *et al*. later developed a full cell based on the redox couple NiHCF-$NaTi_2(PO_4)_3$, with an average output voltage of 1.27 V, a specific energy of 42.5 Wh kg^{-1} and a capacity retention of 88% after 250 cycles at 5C rate [96]. A full cell based only in PBA was shown by Pasta *et al*. with CuHCF as positive electrode and manganese hexacyanomanganate (MnHCMn) as negative electrode and delivered a maximum specific energy of 27 Wh kg^{-1}at 1C rate with an average voltage of 0.95 V [97]. Regarding the cheaper and less polluting Fe-based compounds, Wu *et al.* [98] have recently reported the electrochemical performance of BG and Na-PB as cathode for aqueous Na-ion batteries with capacities over 100 mAh g^{-1}, although the very poor coulombic efficiency still remains to be improved (around 80% at 1C). The company Alveo Energy is a confirmation of the great potential that this family of compounds offers, since much of its production is based on PBA batteries [99].

As can be observed in Table 1. 2 which summarizes the most relevant studies for cathode materials in aqueous NIBs, the experiments are carried out at very high rate. The major inconvenient with aqueous systems is the large amount of possible secondary reactions that result, among others, in high self-discharge and capacity fading. These phenomena are usually not detected in systems tested at high current densities since are kinetically inaccessible. Therefore, while some systems can look promising at high rates, it is only at lower rates that all the drawbacks become visible.

Table 1. 2. Some electrochemical data obtained for the most relevant materials studied so far in aqueous electrolyte as cathode material

Cathode	Counter	Electrolyte	Rate	Capacity (mAh g^{-1})	Cathode voltage (V *vs.* Na^+/Na)	Cycle (capacity retention)
$Na_{0.44}MnO_2$	AC	1 M Na_2SO_4	18C	55	3.005, 3.225, 3.455	4,000 (84%)
Λ-MnO_2	AC	1 M Na_2SO_4	4C	100		5,000 (no loss)
NaFeP2O7	AC	1 M Na2SO4	1C	58	3	300 (86%)
$Na_3V_2(PO_4)_3$	Pt	1 M Na_2SO_4	8.5C	50	3.355	30 (30%)
$NaVPO_4F$	Polyimide	5 M $NaNO_3$	0.33C	54	3.155	20 (70%)
$FePO_4$	$Na_3Ti_2(PO_4)_3$	1 M Na_2SO_4 (pH = 11)	0.5C	110	2.9 3.1	20 (40%)
NiHCF	Discharged NiHCF	1 M $NaNO_3$ (pH = 2)	8.3C	52	3.3	5,000 (undetectable)
CuHCF	MnHCMn	1 M NaClO4 saturated with $Mn(ClO_4)_2$	10C	50	3.5	1,000 cycles
Na-PB	AC	1 M Na_2SO_4	1C	100 (Efficiency <80%)	3	40 (93%)

1.3.2. Anode materials

In comparison to the cathodes for aqueous NIBs, the number of anodes studied in these kind of systems is more limited. Most of the studies are related to $NaTi_2(PO_4)_3$, although recently, new materials has been reported.

1.3.2.1. Nasicon $NaTi_2(PO_4)_3$

$NaTi_2(PO_4)_3$ is the most studied anode in aqueous NIBs because of its voltage (2.1 V *vs*. Na^+/Na), its high theoretical capacity of 133 mAh g^{-1} and flat plateau.

Sun II Park *et al*. synthesized $NaTi_2(PO_4)_3$ by Pechini method [100] and using Zn foil as counter electrode in 2 M Na_2SO_4 aqueous electrolyte, they achieved 123 mAh g^{-1} of reversible capacity in the first cycle despite a high current of 2 mA cm^{-2} was used. However, only 60 % of the initial capacity was retained after 30 cycles.

A first aqueous full cell with $NaTi_2(PO_4)_3$ as anode combined with $Na_{0.44}MnO_2$ as cathode was developed by Wu *et al*.. They reported a fast synthesized carbon-coated $NaTi_2(PO_4)_3$ which delivered 72 mAh g^{-1} in 1 M Na_2SO_4 at 0.12C rate. The full cell retained 78 % of the initial capacity after 20 cycles [101].

Soon later, the same system was reported by Li *et al*. [102]. In this case, $NaTi_2(PO_4)_3$ was synthesized by an easy solid state reaction. The full cell delivered a reversible capacity based on the $NaTi_2(PO_4)_3$ mass of 120 mAh g^{-1} at 0.6C, however capacity fading was the main limitation of the system even at rates as high as 5C. Improvements in this electrochemical couple were achieved by graphite coating of $NaTi_2(PO_4)_3$ and 86% of the initial capacity (95 mAh g^{-1}) was achieved after 100 cycles at 1C rate [103]. Despite of these last improvements on, $NaTi_2(PO_4)_3$ capacity retention still has to be further improved to develop functional full cells.

1.3.2.2. Other anode materials

Pasta *et al*. reported the use of manganese hexacyanomanganate (MnHCMn) as anode for aqueous NIBs. The Mn-based PBA, with the chemical composition $K_{0.11}Mn[Mn(CN)_6]_{0.83}\cdot 3.64H_2O$, showed a redox plateau at 2.76 V *vs*. Na^+/Na with a specific capacity of 57 mAh g^{-1}. Galvanostatic cycling at different C rates (1, 5, and 10C) revealed low hysteresis, resulting in a high rate capability. Furthermore, as it has been mentioned in the section 1.3.1, a full cell using CuHCFe as cathode delivered a maximum specific energy of 27 Wh kg^{-1} at 1C rate with an average voltage of 0.95 V and almost negligible capacity loss up to 1000 cycles at 10C [97].

Other explored compounds are vanadates. Qu et *al*. reported the electrochemical performance of $V_2O_5\cdot 0.6H_2O$ nanoribbons which exhibited a capacity of 43 mAh g^{-1} in a 0.5 M Na_2SO_4 aqueous electrolyte [104]. More recently, one-dimensional nanostructured V oxide, $Na_2V_6O_{16}\cdot nH_2O$, showed an initial specific capacity of 123 mAh g^{-1} with an average voltage of 2.31 V *vs*. Na^+/Na. However, the subsequent charge capacity was only 42 mAh g^{-1} with a fast fading in the early cycles [105].

Qin *et al*. introduced 1,4,5,8-Naphthalenetetracarboxylic dianhydride (NTCDA)-derived Polyimide as an anode material for aqueous NIBs [89]. The average charge and discharge voltages were 2.21 and 2.32 V vs. Na^+/Na, respectively, in a 5 M $NaNO_3$ electrolyte, which is similar to the redox potential in Li aqueous batteries. The Na ion storage mechanism was not fully described in their report, and further research is required to understand similar potentials for Li^+ and Na^+ insertions. The charge/discharge capacities were 184 and 165 mAh g^{-1} respectively at a current density of 50 mA g^{-1}. However, after 20 cycles the capacity decayed in 17% from the initial capacity.

Considering these results, the only actual plausible alternative to $NaTi_2(PO_4)_3$ is MnHCMn. Depending on the cathode, one of this two materials should be selected.

1.4. Aim of this doctoral thesis

The aim of this work was to find suitable electrode materials for low-cost Na-ion aqueous batteries. At the beginning of this work, the number of works related to this topic was very limited and most studied materials so far were Mn-Based. This is why we focused in Fe-based materials, encouraged by previous studies of $LiFePO_4$ in aqueous electrolyte and the low-cost and environmentally friendly properties of Fe-based materials.

The selected screened materials are $NaFePO_4$, $NaFe_2(CN)_6$ and $Na_4Fe_3(PO_4)_2P_2O_7$ because their operation voltage lies within the electrolyte stability window.

Since the electrochemical performance of $NaTi_2(PO_4)_3$ in aqueous electrolyte had already reported, this material was chosen as anode material to build aqueous full cells. Chapter 3 details the optimization both in organic and aqueous media of $NaTi_2(PO_4)_3$ obtained by two different routes to finally be used as negative electrode in full cells The following chapters (chapters 4-7) correspond to the different cathode materials studied. Once synthesized, all materials were previously studied in organic electrolyte for comparative purposes. Once the material was optimized in organic half-cells, the electrochemical characterization was done using 1 M Na_2SO_4 aqueous electrolyte.

[1] Annual Energy Outlook 2015, U.S. Energy Information Administration, April 2015, http://goo.gl/sW9urI
[2] Climate Change Indicators in the United States, Third Edition, United States Environmental Protection Agency, 2014
[3] Dan Rastler, Electric Power Research Institue (EPRI), "Electricity Energy Storage Technology Options: System Cost Benchmarking", IPHE Workshop "Hydrogen. A Competitive Energy Storage Medium for Large Scale Integration of Renewable Electricity", 15-16 Nov. 2012, Seville, Spain
[4] D. Linden and T. Reddy, Handbook of Batteries, 3rd Edition, McGraw-Hill (2003)
[5] V. Palomares, M. Casas-Cabanas, E. Castillo-Martinez, M.H. Han, T. Rojo, Update on Na-based battery materials. A growing research path, Energy Environ. Science 6 (2013) 2312–2337
[6] J-Y. Luo, W.-J. Cui, P. He, Y-Y. Xia, Raising the cycling stability of aqueous lithium-ion batteries by eliminating oxygen in the electrolyte, Nat.Chem. 2 (2010) 760–765.
[7] http://batteryuniversity.com/learn/article/battery_statistics
[8] H.A. Catherino, F.F. Feres, F. Trinidad, Sulfation in lead-acid batteries, J. Power Sources 129 (2004) 113-120
[9] R. M. Dell, D. Antony, and J. Rand. Understanding batteries. RSC Paperbacks. The Royal Society of Chemistry, 2001
[10] C. Daniel and J.O. Besenhard, editors. Handbook of Battery Materials. Wiley-VCH Verlag GmbH & Co. KGaA, 2011
[11] M. Winter, R.J. Brodd, What are batteries, fuel cells and supercapacitors?, Chem. Rev. 104 (2004) 4245-4270
[12] J. Sudworth and R. Tilley, The Sodium/Sulfur Battery, Chapman and Hall,London (1985)
[13] T. Oshima, M. Kajita, A. Okuno, Development of Sodium-Sulfur Batteries, Int. J. Appl. Ceram. Technol. 1 (2004) 269-76
[14] J. M. Tarascon. Key challenges in future Li-battery research. Phil. Trans. R. Soc. A 368 (2010) 3227–3241
[15] D. Yoo, E. Markevich, G. Salitra, D. Sharon, D. Aurbach, On the challenge of developing advanced technologies for electrochemical energy storage and conversion, Materials Today, 17 (2014) 110-121
[16] M.S. Whittingham, Lithium Batteries and Cathode Materials, Chem. Rev. 104 (2004) 4271-4302
[17] J.B. Goodenough, Cathode materials: a personal perspective, J. Power Sources 174 (2007) 996-1000
[18] J.W. Fergus, Recent developments in cathode materials for lithium ion batteries, J. Power Sources 195 (2010) 939-954
[19] J.R. Dahn, T. Zheng, Y. Liu, J. S. Xue, Mechanism for lithium insertion in carbonaceus materials, Science 270 (1995) 590-593
[20] 8 C.-X. Zu, H. Li, Thermodynamic analysis on energy densities of batteries, Energy Environ. Sci., 4 (2011) 2614–2624.
[21] N. Yabuuchi, K. Kubota, M. Dahbi, S. Komaba, Research development on sodium-ion batteries, Chem. Rev. 114 (2014) 11636-11682
[22] D. Kundu, E. Talaie, D. V. Duffort, L. F. Nazar, The emerging chemistry of sodium ion batteries for electrochemical energy storage, Angew. Chem. Int. Ed. 54 (2015) 3431-3448
[23] H. Pan, Y-S. Hu, L. Chen, Room-temperature stationary sodium-ion batteries for large-scale electric energy, Energy Envron. Sci., 6 (2013) 2338-2360
[24] X. Ma, H. Chen, G. Ceder, Electrochemical properties of monoclinic $NaMnO_2$, J. Electrochem. Soc. 158 (2011), A1307 – 1311.
[25] N. Yabuuchi, M. Kajiyama, J. Iwatate, H. Nishikawa, S. Hitomi, R. Okuyama, R. Usui, Y. Yamada, S. Komaba, Nat. Mater. 2012, P2-type $Na_x[Fe_{1/2}Mn_{1/2}]O_2$ 11, 512 – 517.
[26] G. Singh, J.M. López el Amo, M. Galceran, S. Pérez-Villar, T. Rojo, Structural evolution during sodium deintercalation/intercation in $Na_{2/3}[Fe_{1/2}Mn_{1/2}]O_2$, J. Mater. Chem. A 3 (2015) 6954-6961.
[27] N. Yabuuchi, R. Hara, M. Kajiyama, K. Kubota, T. Ishigaki, A. Hoshikawa, S. Komaba, New O2/P2-type Li-excess layered manganese oxides as promising multi-functions electrode material for rechargeable Li/Na batteries, Adv. Energy Mater. 4 (2014), 1301453.
[28] J. Billaud, G. Singh, A. R. Armstrong, E. Gonzalo, V. Roddatis, M. Armand, T. Rojo, P. G. Bruce, Na0.67Mn1-xMgxO2 (0 ≤ x ≤ 0.2): a high capacity cathode for sodium-ion batteries Energy Environ. Sci. 7 (2014) 1387 – 1391.
[29] N. Sharma, N. Tapia-Ruiz, G. Singh, A.R. Armstrong, J.C. Pramudita, H.E.A. Brand, J. Billaud, P.G. Bruce, T. Rojo, Rate dependent performance related to crystal structure evolution of $Na_{0.67}Mn_{0.8}Mg_{0.2}O_2$

in a Sodium-Ion Battery, Chem. Mater. 27 (2015) 6976-6986
[30]G. Singh, B. Acebedo, M. Casas-Cabanas, D. Shanmukaraj, M. Armand, T. Rojo, An approach to overcome first cycle irreversible capacity in P2-$Na_{2/3}[Fe_{1/2}Mn_{1/2}]O_2$, Electrochemistry Communications 37 (2013) 61–63
[31] B. Zhang, R. Dugas, G. Rousse, P. Rozier, A.M. Abakumov, J.M. Tarascon, Insertion comopounds and composites made by ball milling for advanced sodium ion batteries, Nat. Commun. 7 (2016) art. number 10308
[32] C. Delmas, R. Olazcuaga, F. Cherkaoui, R. Brochu, New family of phosphates with formula $Na_3M_2(PO_4)_3$ (M = Ti, V, Cr, Fe), C.R. Acad. Sc. Paris, Ser. C 287 (1978) 169–171
[33] J. Gopalakrishnan, K. K. Rangan, $V_2(PO_4)_3$ - a novel NASICON-type vanadium phosphate synthesized by oxidative deintercalation of sodium from $Na_3V_2(PO_4)_3$, Chem. Mater., 4 (1992), 745–747
[34] B. L. Cushing and J. B. Goodenough, Li2NaV2(PO4)3: a 3.7 V lithium-insertion cathode with the rhomboedral NASICON structure, J. Solid State Chem. 162 (2001) 176–181
[35] Z. Jian, L. Zhao, H. Pan, Y.-S. Hu, H. Li, W. Chen, L. Chen, Carbon coated $Na_3V_2(PO_4)_3$ as novel electrode material for sodium ion batteries Electrochem. Commun. 14 (2012) 86–89
[36] C. Masquelier, L. Croguennec, Polyanionic (Phosphates, Silicates, Sulfates) frameworks as electrode materials for rechargeable Li (or Na) batteries, Chem. Rev. 113 (2013) 6552-6591
[37] K. Chihara, A. Kitajou, I. D. Gocheva, S. Okada, J.-I. Yamaki, Cathode properties of $Na_3M_2(PO_4)_2F_3$ [M = Ti, Fe, V] for sodium-ion batteries, J. Power Sources, 2013, 227, 80–85
[38] GREENLION European project Newsletter, $Na_3V_2(PO_4)_2F_3$/$NaPF_6$ EC:DEC/Hard Carbon prototype, 6th November 2014
[39] J. M. Wörle-Knirsh, K. Kern, C. Schleh, C. Adelhelm, C. Feldmann, H. F. Krug, Nanoparticulate Vanadium Oxide Potentiated Vanadium Toxicity in Human Lung Cells, Environ. Sci. Technol., 2007, 41 (1), pp 331–336
[40] J.B.Goodenough, A. Padhi, K.S. Nanjundaswamy, C. Masquelier, Cathode materials for secondary (rechargeable) lithium batteries, US5910382 (1999).
[41] P. Moreau, D. Guyomard, J. Gaubicher, F. Boucher, Structure and stability of sodium intercalated phases in olivine $FePO_4$. Chem. Mater. 22 (2010) 4126–4128
[42] M. Casas-Cabanas, V.V. Roddatis, D. Saurel, P. Kubiak, J. Carretero-Gonzalez, V. Palomares, P. Serras, T. Rojo, Crystal chemistry of Na insertion/deinsertion in $FePO_4$-$NaFePO_4$, J. Mater. Chem. 22 (2012) 17421–17423
[43] S.M. Oh, S.T. Myung, J. Hassoun, B. Scrosati, Y. Sun, Reversible $NaFePO_4$ electrode for sodium secondary batteries, Electrochem. Commun. 22 (2012) 149–152
[44] R. Tripathi, S.M. Wood, M.S. Islam, L.F. Nazar, Na-ion mobility in layered Na_2FePO_4F and olivine Na [Fe,Mn]PO4, Energy Environ. Sci., 6 (2013) 2257–2264
[45] M. Galceran, D. Saurel, B. Acebedo, V.V. Roddatis, E. Martin, T. Rojo, M. Casas-Cabanas, The mechanism of $NaFePO_4$ (de)sodiation determined by in situ x-ray diffraction, Phys. Chem. Chem. Phys. 16 (2014) 8837–8842
[46] A. Whiteside, C.A.J. Fisher, S.C. Parker, M.S. Islam, Particle shapes and surface structures of olivine $NaFePO_4$ in comparison to $LiFePO_4$, Phys. Chem. Chem. Phys. 16 (2014) 21788–94
[47] Y. Zhu, Y. Xu, Y. Liu, C. Luo, C. Wang, Nanoscale, Comparison of electrochemical performances of olivine NaFePO4 in sodium-ion batteries and olivine $LiFePO_4$ in lithium-ion batteries, 5 (2013) 780–787
[48] A. Sune, F. R. Beckd, D. Haynese, J. A. Poston Jr., S.R. Narayanana, Prashant N. Kumtab, A. Manivannane, Synthesis, characterization, and electrochemical studies of chemically synthesized $NaFePO_4$, Mater. Sci. Eng. B 177 (2012) 1729-1733
[49] P. P. Prosini, C. Cento, A. Masci, M. Carewska, Sodium extraction from sodium iron phosphate with a Maricite structure, Solid State Ion. 263 (2014) 1–8
[50] J. Kim, D-H. Seo, H. Kim, I. Park, J-K. Yoo, S-K. Jung, Y-U. Park, W. A. G. IIIe and K. Kang, Unexpected discovery of low-cost maricite $NaFePO_4$ as a high-performance electrode for Na-ion batteries, Energy Environ. Sci. 8 (2015) 540-545
[51] P. Barpanda, S.-I. Nishimura, A. Yamada, High-Voltage Pyrophosphate Cathodes, Adv. Energy Mater. 2 (2012) 841–859
[52] P. Barpanda, G. Liu, C. D. Ling, M. Tamaru, M. Avdeev, S. C.Chung, Y. Yamada, A. Yamada, $Na_2FeP_2O_7$: A Safe Cathode for Rechargeable Sodium-ion Batteries Chem. Mater. 25 (2013) 3480 – 3487
[53] P. Barpanda, T. Ye, M. Avdeev, S. C. Chung, A. Yamada, A new polymorph of $Na_2MnP_2O_7$ as a 3.6 V cathode material for sodium-ion batteries, J. Mater. Chem. A 1 (2013) 4194 – 4197

[54] P. Barpanda, J. Lu, T. Ye, M. Kajiyama, S. C. Chung, N. Yabuuchi, S. Komaba, A. Yamada, A layer-structured $Na_2CoP_2O_7$ pyrophosphate cathode for sodium-ion batteries RSC Adv. 3 (2013) 3, 3857 – 3860
[55] H. Kim, I. Park, D-H. Seo, S. Lee, S-W. Kim, W-J. Kwon, Y-U. Park, C-S, Kim, S. Jeon, K. Kang, New iron-based mixed-polyanion cathodes for lithium and sodium rechargeable batteries: combined first principles calculations and experimental study, J. Am. Chem. Soc. 134 (2012) 10369-10372
[56] H. Kim, I. Park, S. Lee, H. Kim, K. Y. Park, Y. U. Park, H. Kim, J. Kim, H.D. Lim, W.S. Yoon, K. Kang, Understanding the Electrochemical Mechanism of the New Iron-Based Mixed-Phosphate $Na_4Fe_3(PO_4)_2(P_2O_7)$ in a Na Rechargeable Battery, Chem. Mater., 25 (2013) 3614–3622
[57] Y. Lu, L. Wang, J. Cheng, and J. B. Goodenough, "Prussian blue: a new framework of electrode materials for sodium batteries", Chemical Communications 48, p. 6544, 2012
[58] L. Wang, Y. Lu, J. Liu, M. Xu, J. Cheng, D. Zhang, J. B. Goodenough, A superior low-cost cathode for a Na-Ion battery, Angew. Chem. Int. Ed. 2013, 52, 1964 – 1969
[59] X. Wu, W. Deng, J. Qian, Y. Cao, X. Ai, H. Yang, Single-crystal FeFe(CN)(6) nanoparticles: a high capacity and high rate cathode for Na-ionbatteries, J. Mater. Chem. A 2013, 1, 10130
[60]Y. You, X.-L. Wu, Y.-X. Yin, Y.-G. Guo, High-quality Prussian blue crystals as superior cathode materials for room-temperature sodium-ion batteries, Energy Environ. Sci. 7 (2014) 1643-1647
[61] D. I. Iermakoba, R. Dugas, M. R. Palacín, A. Ponrouch. On the comparative stability of Li and Na metal anode interfaces in conventional alkyl carbonate electrolytes, J. Electrochem. Soc. 162 (2015) A7060-A7066
[62] M. J. Jäckle, A. Grob, Microscopic properties of lithium, sodium and magnesium battery anode material related to possible dendrite growth, 141 (2014) 17410
[63] D. A. Stevens, J. R. Dahn, High capacity anode materials for rechargeable sodium-ion batteries, J. Electrochem. Soc. 2000, 147, 1271 – 1273
[64] S. Komaba, W. Murata, T. Ishikawa, N. Yabuuchi, T. Ozeki, T. Nakayama, A. Ogata, K. Gotoh, K. Fujiwara, Electrochemical Na insertion and solid electrolyte interphase for hard-carbon electrodes and application to Na-ion batteries, Adv. Funct. Mater. 2011, 21, 3859 – 3867
[65] Y. Wen, K. He, Y. Zhu, F. Han, Y. Xu, I. Matsuda, Y. Ishii, J. Cumings, C. Wang, Expanded graphite as superior anode for sodium-ion batteries Nat. Commun. 2014, 5, 4033
[66] Y.-X.Wang, S.-L. Chou, H.-K. Liu, S.-X. Dou, Reduced graphene oxide with superior cycling stability and rate capability for sodium storage, Carbon 57 (2013) 202 – 208
[67] P. Senguttuvan, G. Rousse, V. Seznec, J.-M. Tarascon, M. R. Palacin, $Na_2Ti_3O_7$: Lowest Voltage Ever Reported Oxide Insertion Electrode for Sodium Ion Batteries, Chem. Mater. 23 (2011) 4109 – 4111
[68] W.Wang, C. Yu, Z. Lin, J. Hou, H. Zhu, S. Jiao, Microspheric $Na_2Ti_3O_7$ consisting of tiny nanotubes: an anode material for sodium-ion batteries with ultrafast charge–discharge rates, Nanoscale 5 (2013) 594 – 599
[69] A. Rudola, K. Saravanan, C. W. Mason, P. Balaya, $Na_2Ti_3O_7$: an intercalation based anode for sodium-ion battery applications, J. Mater. Chem. A 1 (2013) 2653 – 2662
[70] M. Zarrabeitia, E. Castillo-Martinez, J.M.L. Del Amo, A. Eguia-Barrio, M.A. Muñoz-Marquez, T. Rojo, M. Casas-Cabanas, Identification of the critical synthesis for enhanced cycling stability of Na-ion anode material $Na_2Ti_3O_7$, Acta Mater. 104 (2016) 125-130
[71] Y. Wang, X. Yu, S. Xu, J. Bai, R. Xiao, Y.-S. Hu, H. Li, X.-Q. Yang, L. Chen, X. Huang, A zero-strain layered metal oxide as the negative electrode for long-life sodium-ion batteries, Nat. Commun. 4 (2013) 2365
[72] C. Delmas, F. Cherkaoui, A. Nadiri and P. Hagenmuller, A nasicon-type phase as intercalation electrode: $NaTi_2(PO_4)_3$, Mat. Res. Bull. 22 (1987) 631-639
[73] P. Senguttuvan, G. Rousse, M. E. Arroyo y de Dompablo, H. Vezin, J. M. Tarascon and M. R. Palacín, J. Am. Chem. Soc., 2013, 135, 3897–3903.
[74] A. Ponrouch, E. Marchante, M. Courty, J. M. Tarascon, M. R. Palacin. In search an optimized electrolyte for Na-ion batteries, Energy Environ. Sci. 5 (2012) 8572-8583
[75] J. Zhao, L. Zhao, K. Chihara, S. Okada, J.-i. Yamaki, S. Matsumoto, S. Kuze, K. Nakane, Electrochemical and thermal properties of hard carbon-type anodes for Na-ion batteries, J. Power Sources 2013, 244, 752 – 757.
[76] S. Komaba, T. Ishikawa, N. Yabuuchi, W. Murata, A. Ito, Y. Ohsawa, Fluorinated Ethylene Carbonate as Electrolyte Additive for Rechargeable Na Batteries, ACS Appl. Mater. Interfaces 3 (2011) 4165 – 4168.
[77] S. Komaba, Y. Matsuura, T. Ishikawa, N. Yabuuchi,W. Murata, S. Kuze, Redox reaction of Sn-polyacrylate electrodes in aprotic Na cell, Electrochem. Commun. 21 (2012) 65 – 68.

[78] A. Darwiche, C. Marino,M. T. Sougrati, B. Fraisse, L. Stievano, L. Monconduit, Better Cycling Performances of Bulk Sb in Na-Ion Batteries Compared to Li-Ion Systems: An Unexpected Electrochemical Mechanism, J. Am. Chem. Soc. 2012, 134, 20805 – 20811.
[79] W. Li, W.R. McKinnon and J.R. Dahn ,Lithium Intercalation from Aqueous Solutions, J. Electrochem. Soc., 141(1994) 2310-2316
[80] H. Kim, J. Hong, K-Y. Park, H. Kim, S-W. Kim and K. Kang, Aqueous Rechargeable Li and Na Ion Batteries, *Chem. Rev.* 114 (2014) 11788–11827
[81] Luo, J.-Y.; Cui, W.-J.; He, P.; Xia, Y.-Y. Nat. Chem. 2010, 2, 760.
[82] F. Sauvage, E. Baudrin, J. M. Tarascon, Study of the potentiometric response towards sodium ions of $Na_{0.44-x}MnO_2$ for the development of selective sodium ion sensors, Sens. Actuator B-Chem. 120 (2007) 638–644.
[83] J.F. Whitacre, A.Tevar, S.Sharma, $Na_4Mn_9O_{18}$ as a positive electrode material for an aqueous electrolyte sodium-ion energy storage device, Electrochem. Commun. 12 (2010) 463–466.
[84] X. Liu, N, Zhang, J. Ni; L. Gao, Improved electrochemical performance of sol-gel method prepared $Na_4Mn_9O_{18}$ in aqueous hybrid Na-ion supercapacitor, J. Solid State Electrochem. 17 (2013) 1939.
[85] Li, Z.; Young, D.; Xiang, K.; Carter, W. C.; Chiang, Y.-M., Towards High Power High Energy Aqueous Sodium-Ion Batteries: The $NaTi_2(PO_4)_3/Na_{0.44}MnO_2$ System, Adv. Energy Mater. 2013, 3, 290.
[86] J.F. Whitacre, T.Wiley, S.Shanbhag, Y.Wenzhuo, A.Mohamed, S.E. Chun, E.Weber, D.Blackwood, E.Lynch-Bell, J.Gulakowski, C.Smith, D.Humphreys, An aqueous electrolyte, sodium ion functional, large format energy storage device for stationary applications, J. Power Sources 213 (2012) 255–264.
[87] http://www.aquionenergy.com/
[88] W. Song, X. Ji, Y. Zhu, H. Zhu, F. Li, J. Chen, F. Lu, Y. Yao, C.E. Banks, Aqueous sodium-ion battery using a $Na_3V_2(PO_4)_3$ electrode, ChemElectroChem, 1 (2014) 871–876.
[89] H. Qin, Z.P. Song, H.Zhan, Y.H. Zhou, Aqueous rechargeable alkali-ion batteries with polyimide anode, J. Power Sources 249 (2014) 367–372.
[90] Y-H. Jung, C-H. Lim, J-H. Kim, D-K. Kim, $Na_2FeP_2O_7$ as a positive electrode material for rechargeable aqueous sodium-ion batteries, R. Soc. Chem. Adv. 4 (2014) 9799–9802.
[91] M. D. Levi, S. Sigalov, G. Salitra, R. Elazari, D. Aurbach, L. Daikhin and V. Presser, In Situ Tracking of Ion Insertion in Iron Phosphate Olivine Electrodes via Electrochemical Quartz Crystal Admittance, J. Phys. Chem. C, 2013, 117, 1247–1256.
[92] M. Vujkovic, S. Mentus, Fast sodiation/desodiation reactions of electrochemically delithiated olivine $LiFePO_4$ in aerated aqueous $NaNO_3$ solution. J. Power Sources 247 (2014) 184-188
[93] Z. Li, D.B. Ravnsbaek, K. Xiang, Y. M. Chiang, $Na_3Ti_2(PO_4)_3$ as a sodium-bearing anode for rechargeable aqueous sodium-ion batteries, Electrochem. Commun. 44 (2014) 12–15.
[94] C. D. Wessells, S. V. Peddada, R. A. Huggins, Y. Cui, Nickel hexacyanoferrate nanoparticle electrodes for aqueous sodium and potassium ion batteries, Nano Lett. 11 (2011) 5421-5425.
[95] C.D. Wessells, S. V. Peddada, M. T. McDowell, R. A. Huggins, Y. Cui, The effect of insertion species on nanostructured open framework hexacyanoferrate battery electrodes", J. Electrochem. Soc. 159 (2012) A98-A103.
[96] X. Wu, Y. Cao, X. Ai, J. Quian and H. Yang, "A low cost and environmentally benign aqueous rechargeable sodium-ion battery based on $NaTi_2(PO_4)_3$-$Na_2NiFe(CN)_6$", Electrochem. Commun. 31 (2013) 145-148.
[97] M. Pasta, C. D.Wessells, N. Liu, J. Nelson, M. T. McDowell, R. A. Huggins, M. F. Toney, Y. Cui, Full open-framework batteries for stationary energy storage, Nat. Commun. 5 (2014) 3007.
[98] X. Wu, Y. Luo, M. Sun, J. Quian, Y Cao, X Ai, H. Yang, Low-defect Prussian blue nanocubes as high capacity and long life cathodes for aqueous Na-ion batteries, NANO ENERGY 13 (2015) 117-123.
[99] http://www.alveoenergy.com/
[100] S. Park, I. Gocheva, S. Okada, J. Yamaki, Electrochemical properties of $NaTi_2(PO_4)_3$ anode for rechargeable aqueous sodium-ion batteries, J. Electrochem. Soc. 158 (2011) 1067–1070.
[101] W. Wu, A. Mohamed and J.F. Whitacre, Microwave synthesized $NaTi_2(PO_4)_3$ as an aqueous sodium-ion negative electrode, J. Electrochem. Soc. 160 (2013) A497-A504.
[102] Z. Li, D. Young, K. Xiang, W. C. Carter, Y-M. Chiang, Towards high power energy aqueous sodium-ion batteries: the $NaTi_2(PO_4)_3/Na_{0.44}MnO_2$ system, Adv. Energy Mater. 3 (2013) 290-294
[103] W. Wu, J. Yan, A. Wise, A. Rutt, J.F. Whitacre, Using intimate carbon to enhance the performance of $NaTi_2(PO_4)_3$ anode materials: carbon nanotube vs graphite, J. Electrochem. Soc. 161 (2014) A561-A567
[104] Qu, Q. T.; Liu, L. L.; Wu, Y. P.; Holze, R. Electrochim. Acta 2013, 96, 8.

[105] Deng, C.; Zhang, S.; Dong, Z.; Shang, Y. Nano Energy 2014, 4, 49.

2. Experimental techniques

This chapter is divided in two main parts. Firstly, the fundamentals and basics principles of the techniques used for the physico-chemical characterization are explained. Secondly, the electrochemical characterization part is described, and is divided between the fundamentals of the used techniques and the optimization and requirements needed to carry out electrochemical measurements in aqueous media. The synthesis details can be found in the chapter of each material.

2.1. Physico-chemical characterization techniques

Physico-chemical characterization techniques were used to confirm the achievement of the pristine phases after the different synthesis routes. These techniques were also used to study the structural and morphology variation of the samples after optimization treatment (ball-milling, C-coating…) as well as the characterization of the electrodes after cycling. The description of the fundamentals and the equipment used for each of these techniques is detailed below.

2.1.1. X-ray powder diffraction(XRD)

X-ray powder diffraction (XRD) has been the most used technique to confirm that the desired phase was obtained after each synthesis. XRD is a non-destructive technique, essential for the study of materials, and especially, for structural characterization [1]. XRD is used to identify the atomic and molecular structure of a crystal. This technique is based in the irradiation with an X-ray beam, with a determined intensity (I) and a wavelength (λ) with a similar order of magnitude than the interatomic distance between the atoms of the crystal (in inorganic chemistry λ_{Cu} = 1.5406 Å is typically used) . X-rays diffract by atoms are dispersed in particular directions that depend on the crystal structure of the material. Although these waves cancel one another out in most directions through destructive interference (Fig. 2. 1a), some of them add constructively in a few specific directions, determined by Bragg's law (Eq. 1 and Fig. 2. 1b):

$$n\lambda = 2d_{hkl}\, sin\theta \qquad \text{(Eq. 1)}$$

Where n is an integer number which refers to the diffraction order, λ is the wavelength of the incident x-ray beam, d_{hkl} is the spacing between the planes in the atomic lattice and q is the angle between the incident ray and the scattering planes [2].

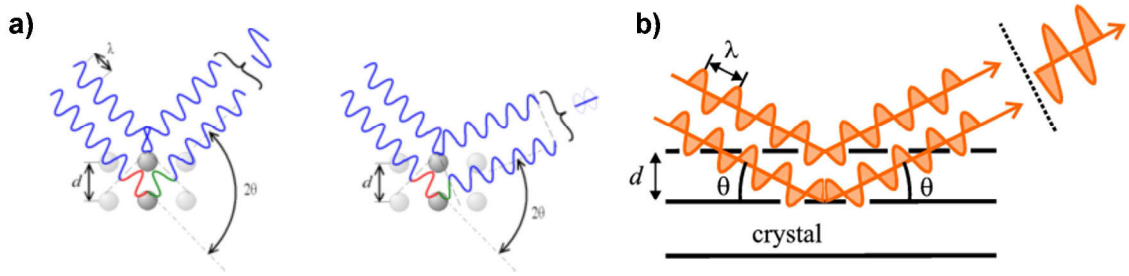

Fig. 2. 1. (a) Constructive interference (left) and destructive interference (right) of a two-wave front and (b) Schematic description of the diffraction of lattice planes according to W.L. Bragg

In XRD measurements, the intensity of the diffracted beam from the sample is scanned in function of the incidence angle. The maxima in a difractogram allow identifying the material and its crystal structure according to Bragg's law, since each maximum of intensity corresponds to a characteristic distance between atomic planes.

XRD data were analyzed by means of the FullProf analysis software [3]. XRD patterns of pure samples were refined by Le bail method to obtain cell parameters and crystallite's sizes according to the Scherrer formula (Eq. 2) and after correcting from instrumental features. In some cases, multiphasic samples were analyzed by the Rietveld method [4] to obtain additional information regarding the weight % of each phase.

$$\tau = \frac{K\lambda}{\beta \cos 2\theta} \qquad \text{(Eq. 2)}$$

X-ray diffraction data were recorded using two different devices: a dichromatic Bruker Advance D8 ($\lambda_{CuK\alpha1,}$=1.54056 Å, $\lambda_{CuK\alpha2}$ =1.5443 Å) (Fig. 2. 2a) and monochromatic Bruker D8 Discover instruments ($\lambda_{CuK\alpha1,}$=1.54056 Å) (Fig. 2. 2b) instruments.

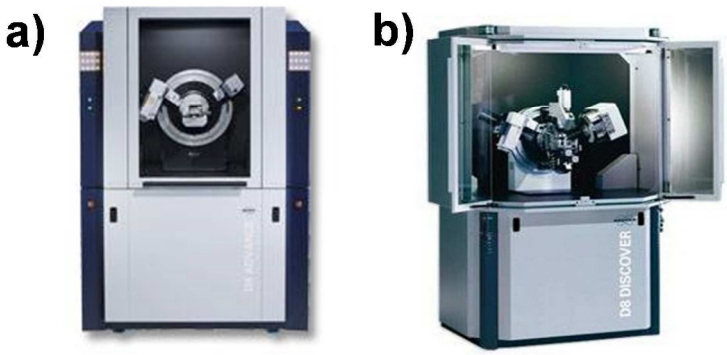

Fig. 2. 2. (a) Bruker Advance D8 with copper radiation and (b) Bruker D8 Discover instruments

2.1.2. Thermogravimetric analysis (TG)

Thermogravimetric analysis is a simple analytical technique used to determine the thermal stability of the sample. It measures changes in the weight of the material as a function of temperature. The amount of water and the presence of volatile species such as carbonate and organic components can also be determined with this technique. In our case, this technique was used to determine the C content in several samples by calcination of the sample in air by means of a simultaneous thermal analyzer NETZSCH STA 449 *F3 Jupiter* (Fig. 2. 3).

Fig. 2. 3. Thermogravimetric analyzer NETZSCH STA 449 *F3 Jupiter*

2.1.3. Inductively Coupled Plasma Optical Emission Spectroscopy (ICP-OES)

ICP-OES is an analytical technique used for elemental determinations. This technique calculates the concentration of ions in a particular sample by ionizing the sample with inductively coupled plasma producing excited atoms and ions that emit electromagnetic radiation at wavelengths characteristic of a particular element. The intensity of this emission is indicative of the concentration of the element within the sample.

The used equipment was an Ultima 2 Optical Emission Spectrometer (Fig. 2. 4). Since the analysed sample has to be liquid in order to be ionized, electrolyte samples from cycled batteries were measured directly, supernatant solutions from solubility tests were filtered prior to measuring and solid samples were digested in a solution of HNO_3 X M.

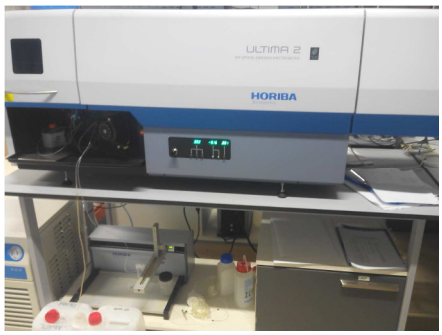

Fig. 2. 4. Ultima 2 Optical Emission Spectrometer

2.1.4. Electron microscopy

Electron microscopy (EM) was used to examine particle size, morphology and distribution. In an electron microscope high energy electrons are generated from a filament by using a large accelerating voltage; electrons interact much more strongly with matter than photons do, and therefore, a better resolution can be achieved.

In EM the electrons are accelerated under vacuum. Beams of these fast-moving electrons are focussed on an object and are absorbed or scattered by the object so as to form an image on an electron-sensitive photographic plate.

In this study both scanning electronic microscopy (SEM) and transmission electron microscopy (TEM) were used, and are described below. Generally, the resolution of a TEM is better than that of a SEM.

2.1.4.1. Scanning electron microscope (SEM)

In a SEM, the surface of the sample is scanned with an electron beam (usually a tungsten or LaB_6 filament) with a fine focal spot size produced by condenser lenses. The spot size determines the resolution of the image (Fig. 2. 5a). Several types of signals (secondary electrons, backscattered electrons, X-rays) are produced when the focused electron beam impacts on the specimen surface, and they can all be used to form a SEM image. The most common signal is that provided by secondary electrons which have higher resolution than others. The accelerating voltage is usually between 1 and 30 kV, and the lower voltages increase the brightness. This technique can provide magnifications between 20 and 300,000x.

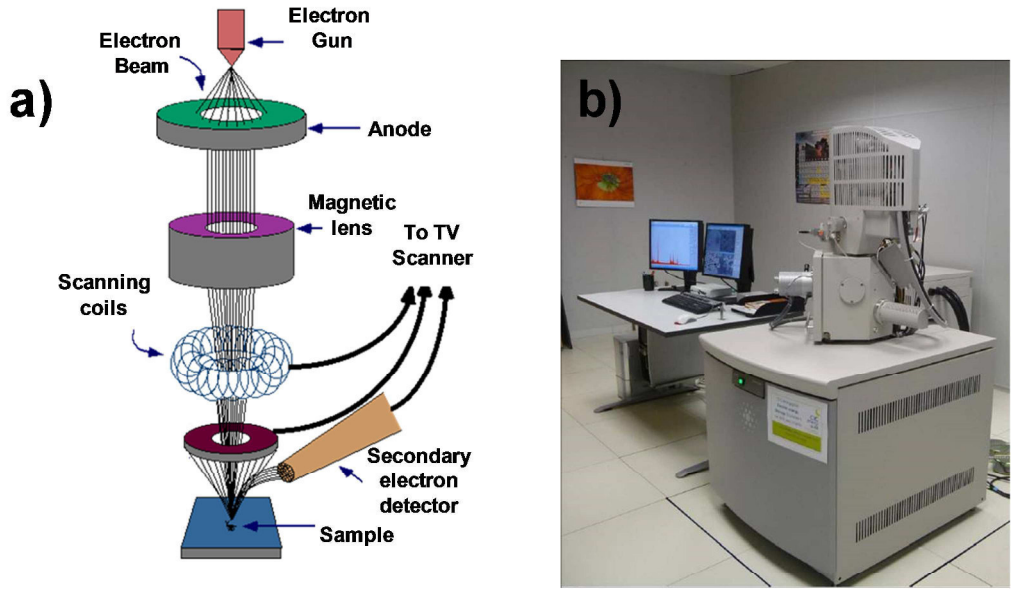

Fig. 2. 5. (a) Schematic diagram of a SEM and (b) Quanta 200 FEG (FEI) SEM from CIC energigune.

Some electronic conductivity in the sample is necessary to avoid charge accumulations and can be coated with C or Au. In this work, coating was not necessary since the samples were conductive enough. The SEM images are produced by detecting secondary electrons which are emitted from the surface due to excitation by the primary electron beam. A Quanta 200 FEG (FEI) scanning electron microscope (Fig. 2. 5b) was used to determine the distribution and size of the particle of different samples. The working voltages of this equipment vary from 3kV (low vacuum mode) to 30 kV (high vacuum mode) and final resolution until 3-5 nm can be achieved.

2.1.4.2. Transmission electron microscope (TEM)

A transmission electron microscope (TEM) has a high voltage of up 100 KeV or higher (up to 1 MeV) and provide both image and diffraction information about samples. Alike the SEM, the electron beam crosses the sample and, therefore, the key requirement is a low thickness of the sample.

The electron beam emitted by a cathode is focused on a specimen using a several condenser lenses causing an enlarged version to appear on a fluorescent screen. This electron beam carries information about the specimen (Fig. 2. 6a).

The FEI Tecnai G2 is a 200kV field emission gun (FEG) high resolution TEM/STEM was used to determine the homogeneity and C-coating distribution of samples (Fig. 2. 6b).

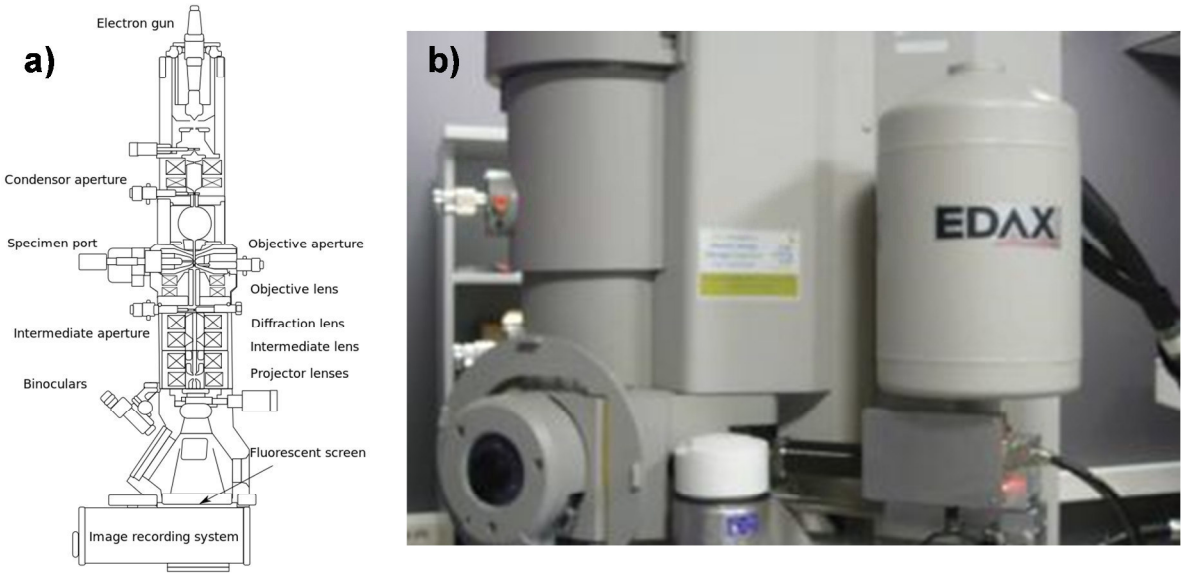

Fig. 2. 6. (a) Schematic diagram of TEM and (b) FEI Tecnai G2 TEM from CIC energigune

2.1.5. Mössbauer spectroscopy

Mössbauer spectroscopy is based on the resonant absorption and emission of gamma rays in solids. This effect was discovered by Rudolf Mössbauer in 1957 and it's called the Mössbauer effect. The most common studied element by this technique is ^{57}Fe.

A sample is exposed to a beam of γ radiation and a detector measures the intensity of the beam transmitted through the sample. The atoms in the source emitting the gamma rays must be of the same isotope as the atoms in the sample absorbing them. To study ^{57}Fe, a ^{57}Co source in a Rh-matrix is used.

In the resulting spectra, gamma ray intensity is plotted as a function of the source velocity. The number, positions, and intensities of the peaks provide information about the chemical environment of the absorbing nuclei and can be used to characterize the sample.

The measurements were performed by Dr. Jose Javier Saiz Garitaonandia from University of the Basque Country using homemade equipment. The velocity was calibrated using a Fe sheet at room temperature. The spectrometry was carried out in the transmission geometry and in the parametric region.

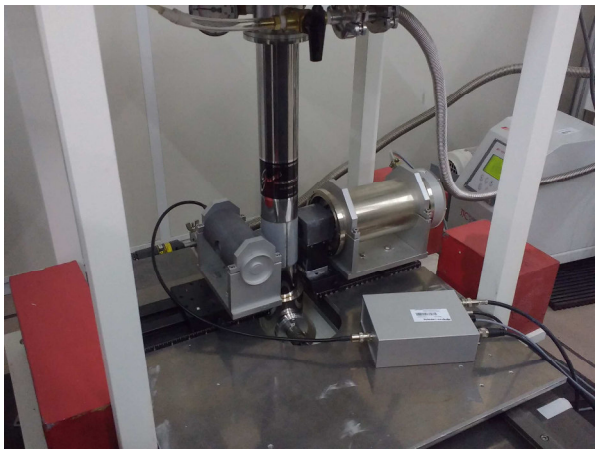

Fig. 2. 7. Homemade equipment used for the Mössbauer spectroscopy.

2.2. Electrochemical characterization

2.2.1. Electrochemical techniques and equipment

Two different technics were used: cyclic voltammetry (CV) and mainly galvanostatic measurements were used to study the materials in this work. A cyclic voltammetry gives qualitative information about electrochemical processes under various conditions, such as the presence of intermediate compounds in oxidation-reduction reactions or the reversibility of a reaction, while galvostatic tests allow obtaining more quantitative values and allow reproducing the behaviour of a battery.

CV is the most widely used technique for acquiring qualitative information about electrochemical reactions. The voltage of the working electrode (WE) is swept between two values: V1 and V2 (see below) at a fixed rate. When the voltage reaches V2 the scan is reversed and the voltage is swept back to V1. It offers a rapid location of potentials at which the different reactions happens and their reversibility [5].

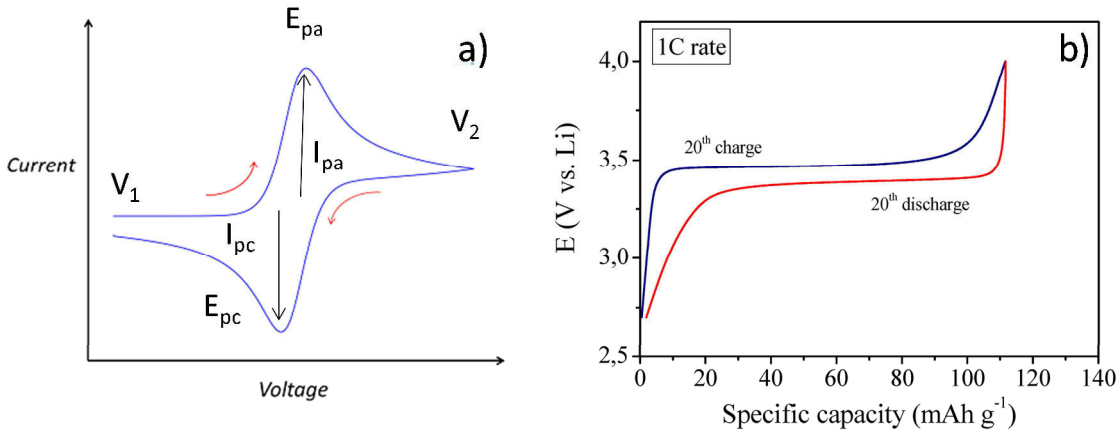

Fig. 2. 8. (a) Typical cyclic voltammogram where i_{pc} and i_{pa} show the peak cathodic and anodic current respectively for a reversible reaction. E_{pc} and E_{pa} represent the potential value for the cathodic and anodic peak respectively [5]. (b) Typical voltage profile obtained for a $LiFePO_4$ cathode in a cell using Li as counter and reference electrode.

For a more quantitative study galvanostatic tests were carried out by applying a current until a V cut-off value is reached [6]. In the case of a full cell, both the WE and the counter electrode (CE) potential were limited.

The applied current for the galavanostatic tests was calculated as a function of the theoretical capacity (C_{th}) of the active material. The C_{th} for determined phase is expressed by:

$$C_{th} = \frac{nF}{3600\ M}\ mAh\ g^{-1}$$

Where *n* is the number of electrons in the reaction, *F* is the Faraday constant and corresponds to the magnitude of electric charge per mole of electrons (96,485.33289(59) C mol^{-1}) [7], and M is the molecular weight of the material expressed in Kg mol^{-1}.

The electrochemical characterization of the materials was carried out using two different according their availabilities:

- A Bio Logic VMP3 Multi-Channel Potential/Galvanostat
- Maccor battery tester

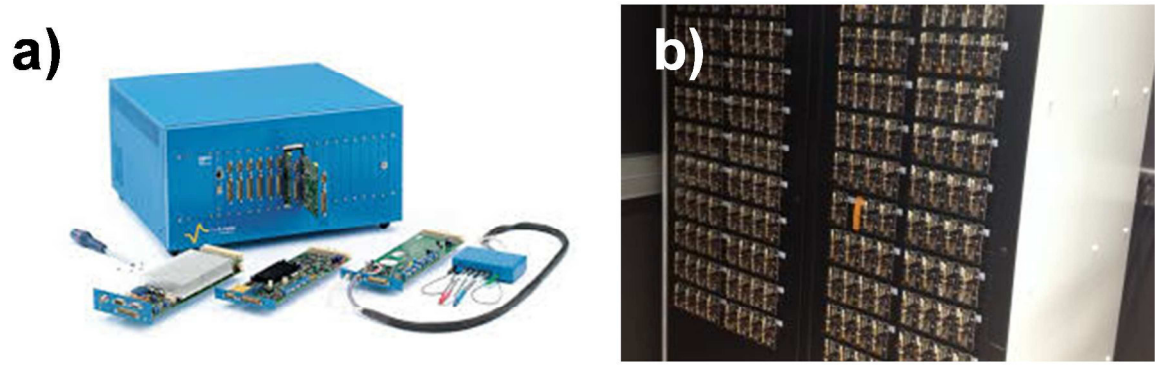

Fig. 2. 9. (a) Bio Logic VMP3 Multi-Channel Potential/Galvanostat and (b) Maccor battery tester from CIC enegigune

All materials were studied in both organic and in aqueous electrolyte. As these media do not have the same requirements, the experimental devices were prepared differently. The characteristics of these devices are detailed below.

2.2.2. Electrochemical characterization in organic media

The different materials studied in this work were always previously cycled in half-cells using an organic electrolyte for comparative purposes. A half-cell is not a real battery with two mass balanced electrodes, but CE is Na-metal in excess and is used also as RE since the voltage is expected to remain constant. A typical 2-electrode Swagelok-type cell is shown in Fig. 2. 10. This device is composed by two stainless steel (SS) plungers which are in the different electrode sides and the battery tester equipment is connected on them. The electrodes and the separator are contained inside a polypropylene body. The separator used is a glass microfiber filter (Whatman, Grade D) impregnated with the organic electrolyte. The cell is assembled thanks to a metallic nut and two nylon ferrules in each electrode side. In order to ensure the electrodes are well pressed a stainless steel spring was used. All organic cells were assembled inside a Glove Box with a dry Ar atmosphere.

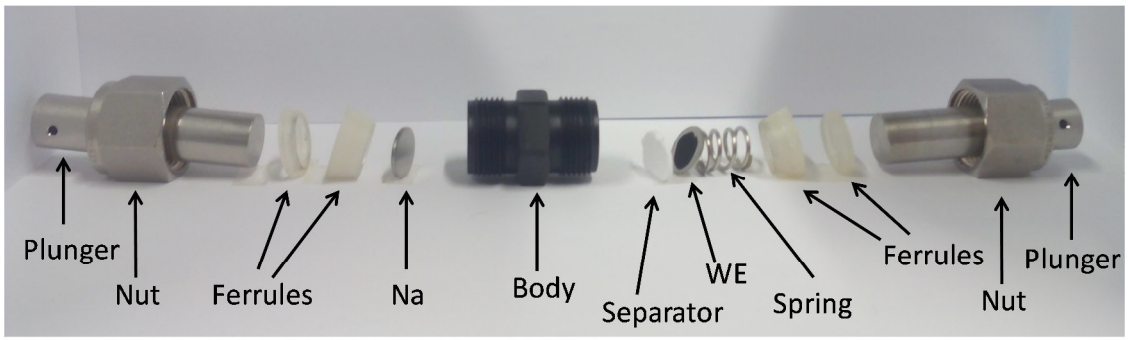

Fig. 2. 10. Schematic diagram of a 2 electrodes Swagelok-type cell.

2.2.3. Electrochemical characterization in aqueous electrolyte

With this thesis, the study of NIBs electrode materials using aqueous electrolyte started as a new subject in CICenergigune. Therefore, the first step was to adapt the previously described methodology to test the studied materials in aqueous media.

1 M Na_2SO_4 was selected as a cheap aqueous electrolyte to test all studied materials. As previously described in the introduction, the O_2 and H_2 evolution potentials are located at 2.297 and 3.527 V *vs*. Na^+/Na at neutral pH, respectively (Fig. 2. 11) [8,9]. Unless mentioned explicitly, the pH of the electrolyte was maintained in its natural value (pH=6). In some cases it was necessary to modify the pH to shift the aqueous stability window so as to avoid electrolyte decomposition by addition of H_2SO_4 or NaOH.

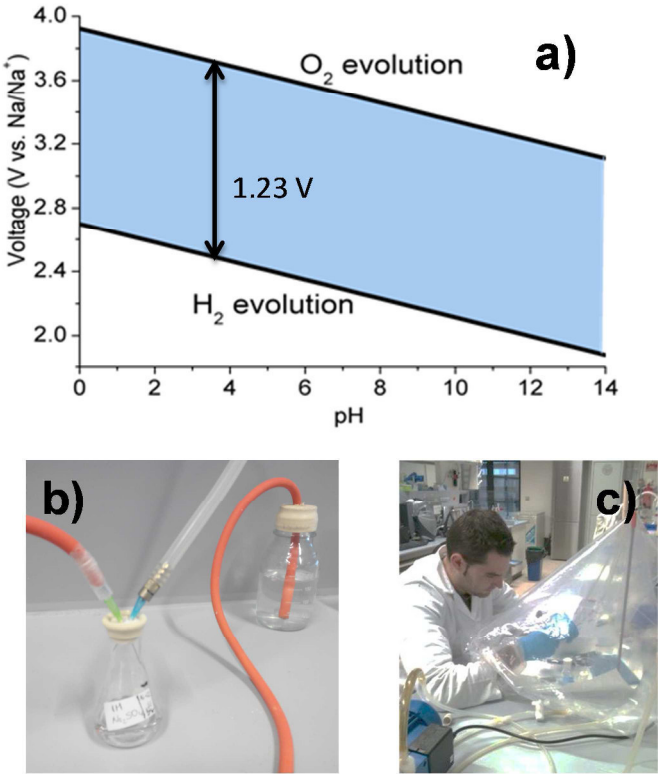

Fig. 2. 11. (a) Aqueous stability voltage window as a function of pH, (b) electrolyte being gasified with N_2 and (c) process of cell assembling inside an Aldrich® AtmosBag with N_2 atmosphere

Moreover, O_2 must be removed to avoid the oxidation of the electrode during the discharge process following the reaction:

Na-(intercalated) + ½ H_2O + ¼ O_2 → $Na^+ + OH^-$ [9]

Therefore, the electrolyte was gasified overnight with N_2 (Fig. 2. 11b) and all electrochemical cells were assembled inside a two-handed Aldrich® AtmosBag (Fig. 2. 11c) with a zipper-lock closure type.

A beaker cell was the first option examined. However, the need of an O_2-free environment required either to seal the system either a continuous N_2 flow. The continuous N_2 flow can be an option in specific experiments; however, it is not a practical solution in systematic studies. Therefore, 3 electrode-Swagelok type cells were selected since are similar in design to those used in organic tests and along with a septum offer an airtight system.

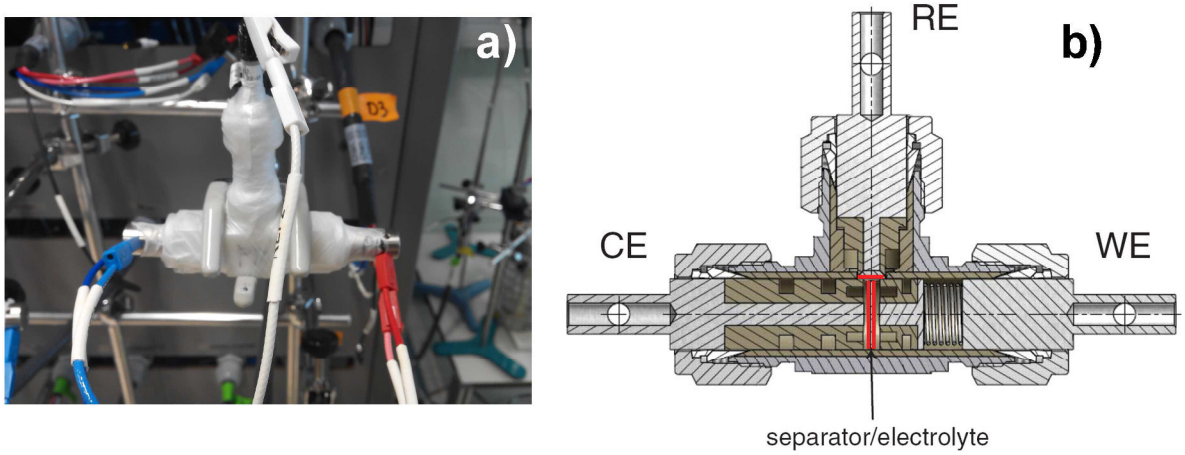

Fig. 2. 12. Picture (a) and scheme (b) of a three-electrode Swagelok-type cell

In this case, a polyoxymethylene T-shaped cell body was used as shown in Fig. 2. 12. A silicon septum was used to seal the cell and a 3 mm diameter hole was punched in the septum to insert the reference electrode. All cells were covered with plastic paraffin film for further protection.

One of the advantages of organic NIBs is that Al can be used as current collector in both negative and positive electrodes, contrary to LIBs, which use Cu foil in the anode side since Al alloys with Li^+ at low potentials.

However, these typical current collector materials react with water to form, depending on the pH and the potential, soluble species or non-soluble oxides which are not electronic conductors [10]. As can be observed in the Pourbaix diagrams represented in Fig. 2. 13 in the case of Al, at pH between 6 and 7 and in the voltage range of the aqueous electrolyte stability window, there is formation of alumina Al_2O_3 which is an electrical insulator [11]. Outside these pH values soluble species such as $AlOH^{2+}$ and Al^{3+} can be found for lower pH and $Al(OH)^{4-}$ at higher pH values.

In the case of Cu, with the exception of a small area close to the lower limit of the electrolyte stability, insoluble oxides as Cu_2O_3, CuO and Cu_2O are formed at moderate basic pH values, and soluble ions as Cu^+ and Cu^{2+} can be formed at acidic pH values and $HCuO^{2-}$ and CuO^{2-} in strong basic media.

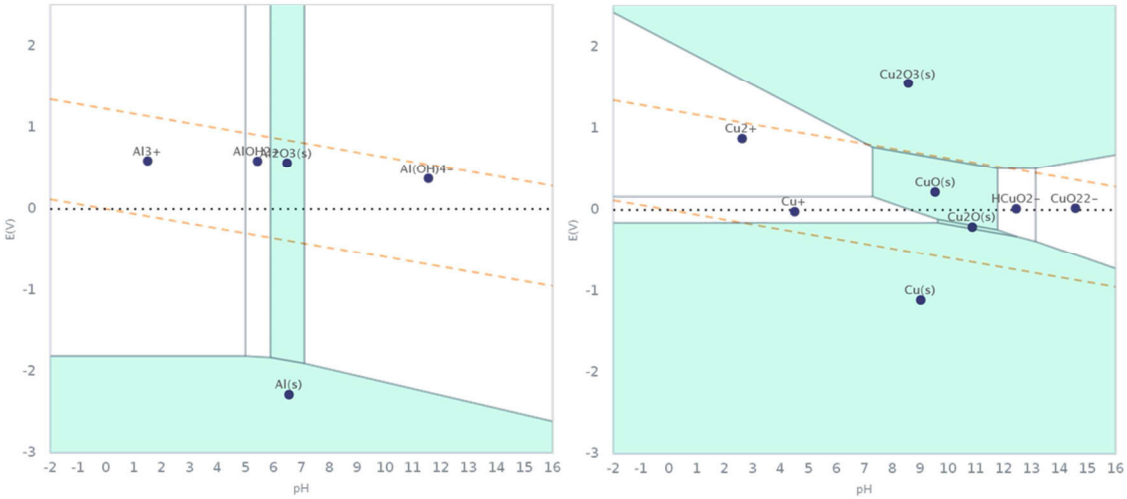

Fig. 2. 13. Pourbaix diagrams of Al (left) and Cu(right). Y-axis represents the voltage *vs*. NHE and X-axis represents the pH. Red line indicates the limits of the aqueous stability range. Green and white polygons correspond to insoluble and soluble phases [12].

Therefore, to avoid the problems of corrosion of the current collector material, stainless steel (SS) disk were used. In some cases, particularly when the potential range was close to the limits of the electrolyte stability window, Ti disks were used since exhibit higher resistance to corrosion and the voltage window is lightly extended.

Slurries with a mass ratio (AM), carbon black conductive additive (Super C65, TIMCAL) and binder in a mass ratio 75 : 20 : 5. Two different binders were evaluated: polyvinylidenefluoride (PVDF) (powder, Alfa Aesar) and polytetrafluoroethylene (PTFE, Aldrich 60%, water dispersion).

EtOH and N- N-Methyl-2-pyrrolidone (NMP) were used as solvent for the PTFE and PVDF slurries. After one hour stirring, they were coated on the current collector and dried overnight under vaccum at 120 ˚C (Fig. 2. 14a). PVDF slurry could be better extended and pressed on the current collector because has better adherence. Fig. 2. 14b shows the voltage profile for the 2nd cycle of two different cells which compare both formulations. While the first electrode prepared with PTFE achieved 60 mAh g^{-1}, the electrode prepared with PVDF 80 mAh g^{-1} were obtained. Therefore, PVDF was chosen as binder additive. However, the electrode had low mass loading between 1-2 mg to be able to extend properly the slurry.

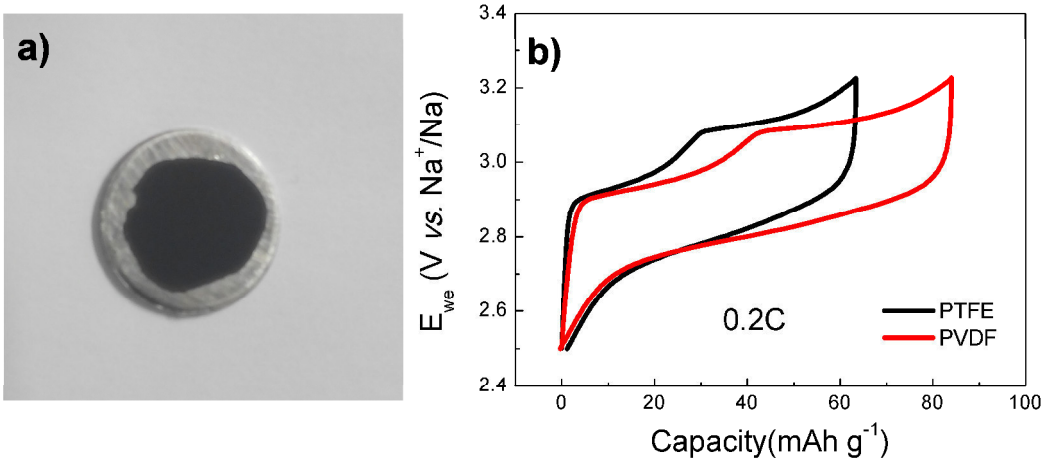

Fig. 2. 14. (a) Electrode prepared by deposition of a drop containing AM, C65 and PVDF in a 75:20:5 ratio in NMP solution. (b) Voltage profiles for the second cycle of $NaFePO_4$ electrodes prepared with two different formulations using 1 M Na_2SO_4 electrolyte at 0.2C in the voltage range from 2.5 to 3.225 V *vs*. Na^+/Na.

Since Na cannot be used as counter and reference electrode in aqueous electrolyte (Na reacts exothermically with water like all alkaline metals to produce NaOH and flammable H_2 gas [13]), Ag/AgCl electrode with 3 M NaCl electrolyte from BioLogic was used as reference electrode in all tests. The electrode has a length of 78 mm and a diameter of 6 mm (Fig. 2. 15a).

$NaTi_2(PO_4)_3$ synthesized by ceramic method was first considered as possible counter electrode but, as will be shown in chapter 3, suffers from some limitations, being coulombic efficiency the main one. Other alternatives were thus explored. Pt is widely used in cyclic voltammetry as counter electrode for academic purposes. However, Pt works as an acceptor and donor of e^- but these electrons come from the O_2 or H_2 evolution of water in the surface of the Pt. Fig. 2. 15b displays the electrochemical behavior of Pt as counter electrode in a galvanostatic $NaFePO_4$ cell. Gas evolution and electrolyte decomposition can finally affect in long measurements, especially in a Swagelock-type cell where the electrolyte is not as abundant as in a beaker cell and WE and CE are closer to each other, and therefore Pt was discarded.

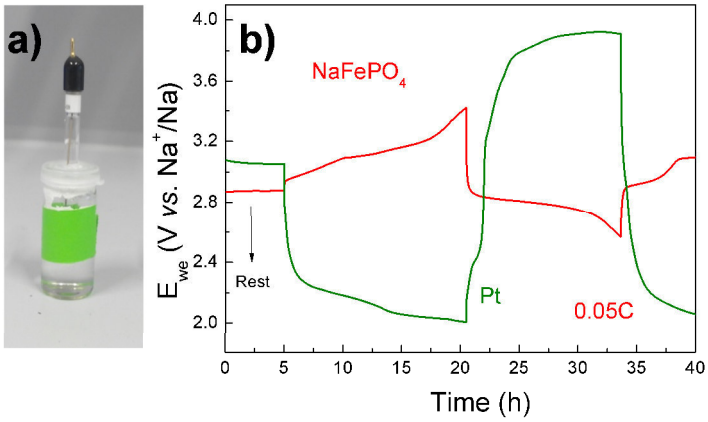

Fig. 2. 15. (a) Ag/AgCl reference electrode with 3 M NaCl from Biologic used as reference electrode in the experiments (c) the same kind of cell but using Pt instead $NaTi_2(PO_4)_3$ as counter electrode

Finally, typical commercial activated carbon (AC) (Norit DLC super30) was selected. AC is a form of carbon processed to have small, low-volume pores that increase the surface area available for adsorption or chemical reactions [14] and are extensively used as supercapacitor electrodes.

Self-standing electrodes were prepared by mixing AC with polytetrafluoroethylene in ethanol in a ratio 95 : 5. The slurry was mixed manually until a paste was formed which was further flattened to achieve a thickness of 250 µm. This paste was punched in 11 mm diameter electrodes with typical loading of 10-20 mg. Then, the AC electrodes were previously tested as symmetric capacitor also using 3-electrodes Swagelok-type cells. Fig. 2. 16 shows the five first cycles of a cyclic voltammetry at 5 mV s^{-1} in a 1.2 V range. The resultant capacitance of AC was 70 F g^{-1}.

To test our materials, the electrode mass balance was calculated to ensure that the AM is the limiting electrode and that the voltage variation owing to the supercapacitative mechanism of AC remains within the voltage window of the aqueous electrolyte (Fig. 2. 16).

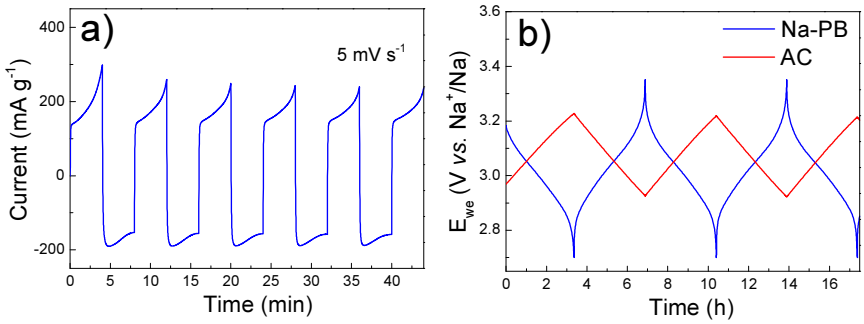

Fig. 2. 16. (a) Anode and cathode galvanostatic curves at 0.2C of a NaPB/Norit DLC super30 (AC) cell with a mass ratio of 1:12. (b) Five first cycles of a cyclic voltammetry at 5 mV s^{-1} in a voltage range of 1.2 V for a symmetrical supercapacitor using activated carbon (AC) Norit DLC super30

[1] A. R. West, Solid State Chemistry and its Applications, Ed. John Wiley and sons, New York (1987)
[2] J. P. Glusker, K. N. Trueblood, Crystal structure analysis: A premier, Oxford University press, New York: 1985
[3] J. Rodríguez-Carvajal, Recent advances in magnetic structure determination by neutron powder diffraction, Physica B: Condensed Matter 192 (1993) 55-69
[4] H. M. Rietveld (1969), A profile refinement method for nuclear and magnetic structures, Journal of Applied Crystallography, 2 (1969) 65–71.
[5] *Bard, Allen J.; Larry R. Faulkner (2000-12-18). Electrochemical Methods: Fundamentals and Applications (2 ed.). Wiley.*
[6] EC-Lab® Software: Techniques and Applications, version 10.34, August 2013
[7] Committee on Data for Science and Technology (CODATA), 2014.
[8] Li, W.; Dahn, J. R.; Wainwright, D. S. Science 1994, 264, 1115
[9] Luo, J.-Y.; Cui, W.-J.; He, P.; Xia, Y.-Y. Nat. Chem. 2010, 2, 760.
[10] https://www.materialsproject.org/
[11] AZO materials web page, http://goo.gl/5RgZ5c
[12] https://www.materialsproject.org
[13] De Leon, N., Reactiviy of Alkali Metals, Indiana University Northwest, 2007.
[14] CPL industries, CPL carbón link: http://www.activated-carbon.com/

3. Study of $NaTi_2(PO_4)_3$ as anode material

In 1987, Delmas *et al*. first introduced $NaTi_2(PO_4)_3$ (C_{th} = 133 mAh g^{-1}) as a Na insertion electrode in nonaqueous electrolyte [1]. They found that two Na ions can be reversibly deintercalated/intercalated at *ca*. 2.1 V *vs*. Na^+/Na, which is a relatively high voltage for organic batteries but suitable for aqueous ones.

It was first reported in an aqueous Na-ion cell by Sun II Park *et al*. [2]. In their report $NaTi_2(PO_4)_3$ was synthesized by Pechini method and, using Zn foil as counter electrode, they achieved 123 mAh g^{-1} of reversible capacity at 2 mA cm^{-2}, although with poor capacity retention (60 % after 30 cycles). As mentioned in chapter 1, several aqueous full cells that use $NaTi_2(PO_4)_3$ as anode have been reported, being capacity fading the main limitation of these systems [3], [4].

In $NaTi_2(PO_4)_3$, PO_4 tetrahedra and TiO_6 octahedra are linked by corners to form a three-dimensional network. Every oxygen atom thus belongs simultaneously to a PO_4 group and a TiO_6 group [5]. Na atoms are located in the center of strongly distorted octahedra formed by the triangular faces of two TiO_6 octahedra stacked on top of each other (Fig. 3. 1).

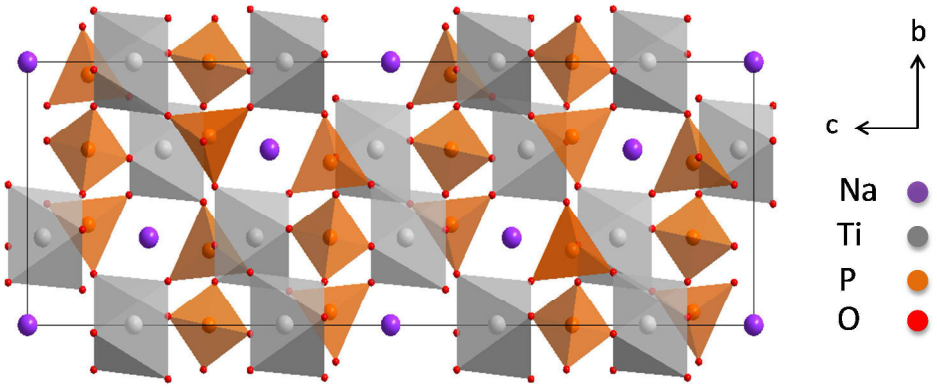

Fig. 3. 1. Hexagonal crystal structure of $NaTi_2(PO_4)_3$.

Since $NaTi_2(PO_4)_3$ is the material with the lowest voltage within the aqueous electrolyte stability window, and had been previously studied in aqueous NIBs, we selected this material at the beginning of the current work for a later utilization as anode in future full cells. Two different routes were employed to prepare the material. The electrochemical performances of the prepared materials as well as their optimization are here shown and discussed.

3.1. Synthesis and physicochemical characterization

3.1.1. Ceramic method

Solid state synthesis was the first selected route we explored to prepare $NaTi_2(PO_4)_3$. Stoichiometric amounts of anhydrous Na_2CO_3 (SIGMA-ALDRICH, $\geq$ 99.5%), TiO_2 anatase (Alfa Aesar, 99.9%) and $(NH_4)_2HPO_4$ (SIGMA-ALDRICH, 98%) were hand-milled for half an hour using an agate mortar. In a first step the mixture was burnt at 500 °C for 5 h in air. After this first treatment, a mixture of TiP_2O_7 and $NaTi_2(PO_4)_3$ is obtained (Fig. 3. 2). This mixture was milled again in the mortar for half an hour and then burnt at 900 °C for 24 h in air [3]. Small peaks which correspond to TiP_2O_7 could still be observed in the XRD pattern of the sample, and therefore the material was heated again for 24 h at 900 °C. After this step the amount of TiP_2O_7 considerably decreased although was still detected (Fig. 3. 2). Small traces of TiP_2O_7 were also found by Wu *et al*. after microwave synthesis, who did not observe any contribution to the electrochemical reaction of this secondary phase [6]. It can also be concluded that the crystallinity of $NaTi_2(PO_4)_3$ increases with longer reaction times, since the diffraction peaks become narrower and better resolved (see for example the reflection at 2θ = 29.5°).

The X-ray diffraction pattern of $NaTi_2(PO_4)_3$ was indexed with R-3cH space group and refined by Le Bail method (Fig. 3. 3), resulting in refined cell parameters of a = 8.4883 (1) Å and c = 21.7923 (3) Å (X^2 = 4.02), in agreement with literature values [7]. In the zoom view, some small peaks matching TiP_2O_7 can be clearly observed.

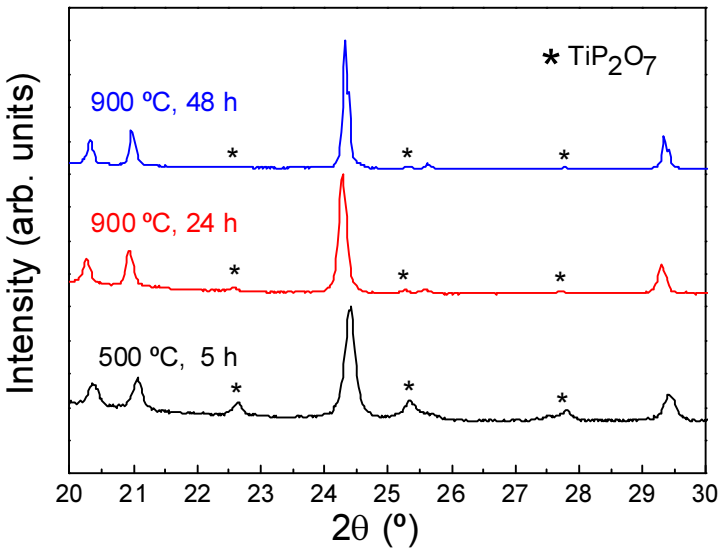

Fig. 3. 2. XRD pattern of $NaTi_2(PO_4)_3$ obtained by ceramic method under different conditions.

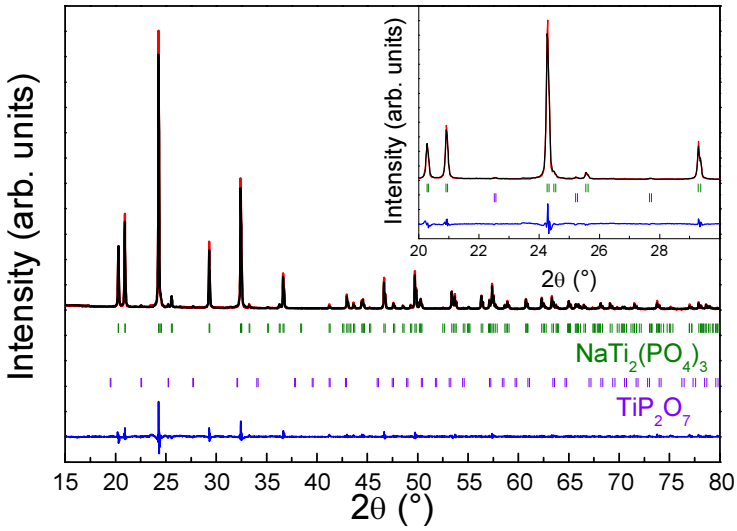

Fig. 3. 3. Refined $NaTi_2(PO_4)_3$ profile using Le Bail method where the observed and calculated intensities are represented by red markers and a black solid line, respectively. The bottom blue line represents the difference between the observed and calculated patterns. Bragg positions are represented as green and purple vertical bars for $NaTi_2(PO_4)_3$ and TiP_2O_7 respectively.

3.1.1.1. Ball-milled sample

Since the large particle sizes usually obtained in ceramic synthesis are usually too large for diffusion-limited processes, and intimate mixtures with carbon are required to ensure electronic conductivity when materials are poor conductors, the obtained material was ball milled in dry conditions with C65 in a 75:20 ratio during 3 and 20 hours using the planetary miller. The XRD patterns before and after the milling treatment for 3 and 20 h are shown in Fig. 3. 4. It can be noticed that the structure is retained in both cases although the larger peak width with increasing ball-milling time indicates a decrease of the domain size.

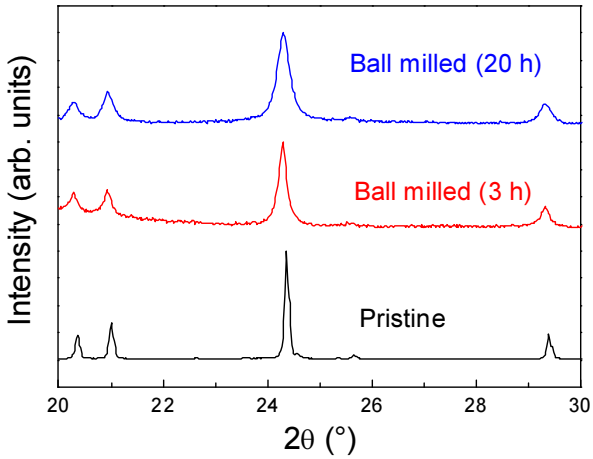

Fig. 3. 4. Comparison of the XRD pattern of pristine $NaTi_2(PO_4)_3$ obtained by ceramic method (black line) and after 3 h (red line) and 20 h (blue line) of ball-milling treatment.

SEM images obtained after ball-milling treatment show that the aggregate size is also reduced. In the as prepared sample, aggregates with sizes between 50 and 125 µm can be observed (Fig. 3. 5a). After 20 hours of ball-milling treatment, although 100 µm aggregates can still be observed, most aggregates measure between 5 and 50 µm (Fig. 3. 5b).

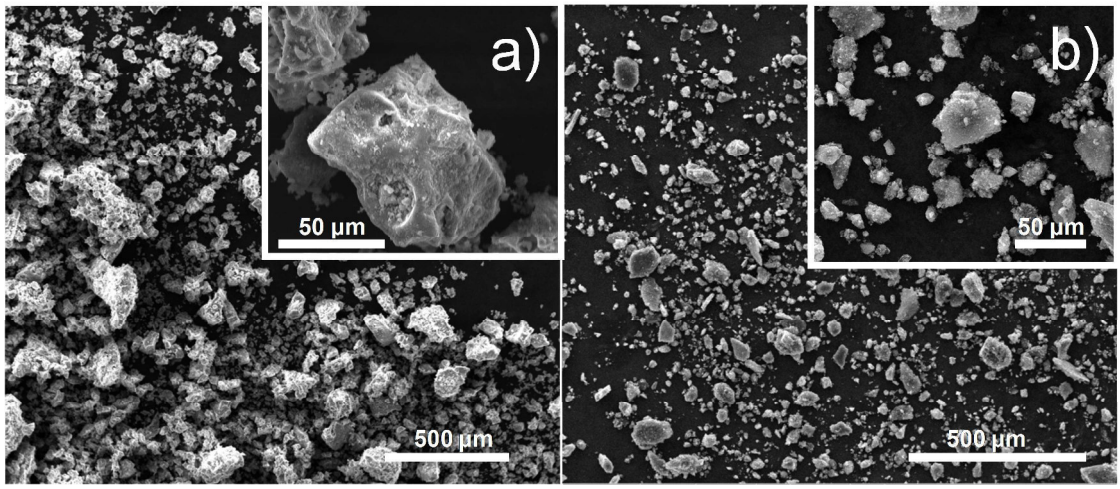

Fig. 3. 5. (a) SEM images of the as prepared material and (b) after 20 hours of ball-milling treatment (b).

3.1.2. Pechini method

Using an alternative approach, $NaTi_2(PO_4)_3$ was prepared following the Pechini method as reported by Sun II Park *et al.* [2]. The Pechini method is an interesting alternative since allows obtaining materials at low temperature by homogeneous mixing of the precursors and avoids further crystallization of the sample. 3.5 g of titanium (IV) butoxide (97%, Sigma-Aldrich) were dissolved in a 55 mL solution formed by H_2O_2 (30 vol%, Fisher Scientific) and NH_4OH (30 vol%, Sigma-Aldrich) in a volume ratio 40:15. Extra pure citric acid monohydrate (Scharlau) was added in a molar ratio of 2:1 with respect to titanium (IV) butoxide. After achieving a green solution, stoichiometric amounts of $NH_4H_2PO_4$ (98.5% Sigma-Aldrich) dissolved in 10 mL of distilled water (18 MΩ·cm) and Na_2CO_3 dissolved in 10 mL of HNO_3 (65%, Scharlau) were added to the main solution. The later was then brought to pH = 5 by adding NH_3 (70 %, Scharlau) and an orange solution was obtained. Then, ethylene glycol (99.8%, Sigma-Aldrich) was introduced in a molar ratio of 1:1 with respect to citric acid and the mixture was heated 80 min at 90 ºC until became a brown gel. Finally, the obtained gel was further heated at 350 ºC during 3 hours at 800 ºC and for 12 more hours in a second step.

The X-ray diffraction pattern of $NaTi_2(PO_4)_3$ was refined by Le Bail method resulting in refined cell parameters of a = 8.4789 (5) Å and c = 21.817 (2) Å (X^2 = 3.937) (Fig. 3. 6a). These values are comparable to those of the material prepared by ceramic synthesis although a very slight

decrease of the *a* parameter and a slight increase in *c* is found. Contrary to the material prepared by the ceramic method, no impurities were found in the XRD pattern of this sample. As expected from the lower temperature and shorter reaction time used in the Pechini method, the diffraction peaks are wider compared to the phase obtained by the ceramic method (Fig. 3. 6b) and are indicative of a smaller domain size.

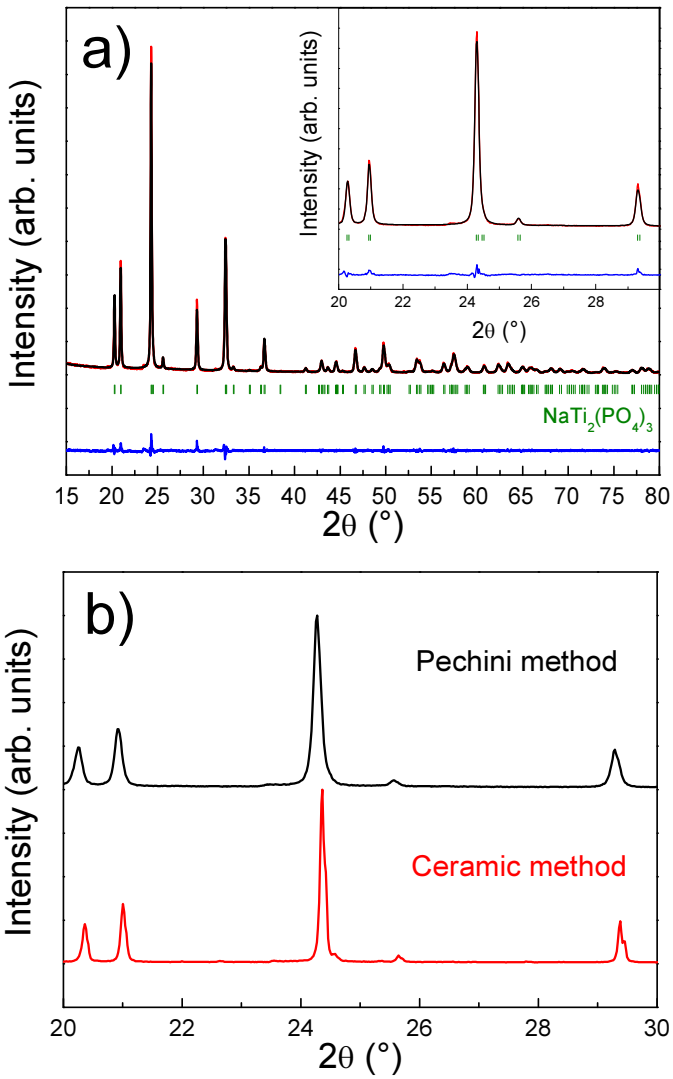

Fig. 3. 6. (a) Refined $NaTi_2(PO_4)_3$ profile using Le Bail method where the observed and calculated intensities are represented by red markers and a black solid line, respectively. The bottom blue line represents the difference between the observed and calculated patterns. Bragg positions are represented as green vertical bars. (b) Comparison of the XRD pattern for $NaTi_2(PO_4)_3$ obtained by Pechini (black line) and ceramic (red line) methods.

3.1.2.1. Ball-milled sample

Using the same equipment and ratio of materials used for the ceramic sample, a ball-milling treatment was carried out. However, since the initial material already exhibited a smaller size, the duration of the treatment was reduced by half (10 h instead of 20 h), resulting in a very similar FWHM of the XRD peaks for both ball-milled samples (Fig. 3. 7).

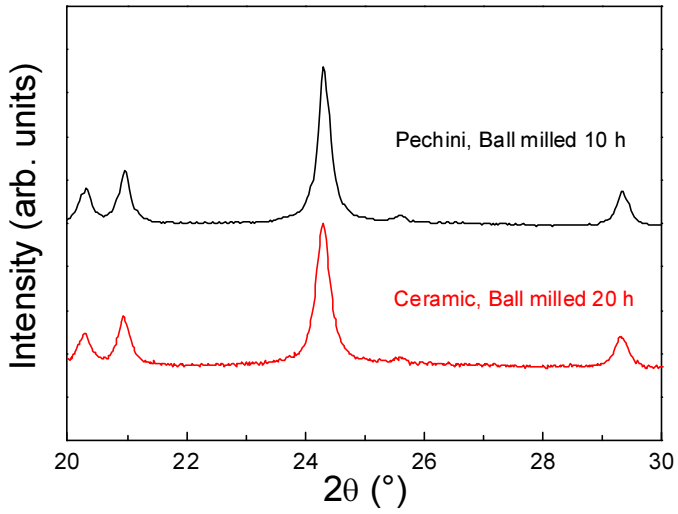

Fig. 3. 7. Comparison of ball-milled $NaTi_2(PO_4)_3$ XRD patterns obtained by Pechini (black line) and ceramic (red line) methods.

3.1.2.2. C-coating

As an alternative to the ball-milling treatment the as prepared sample was C-coated to improve its electronic conductivity using polyethylene-black-poly(ethylenglycol) (Mn≈1400, Sigma-Aldrich) as C-precursor in 1:1 mass ratio. The mixture of active material and polymer was ball milled for 5 h in the planetary mill to obtain a good mixture. The annealing was done at 700 °C during 1 hour in a tubular furnace under a constant Ar flow (100 ml/min).

From TG analysis the material was found to contain 1 wt% of C. The TEM image of the sample after the treatment shows that the distribution of C around the particle was not homogeneous, most probably due to a too low amount of C precursor and therefore, the treatment was repeated (Fig. 3. 8a). A homogeneous 3 nm thick coating can now be observed in a representative TEM image of the sample after the second treatment (Fig. 3. 8b). The C content after the second treatment determined from TG analysis is 2.5 wt%.

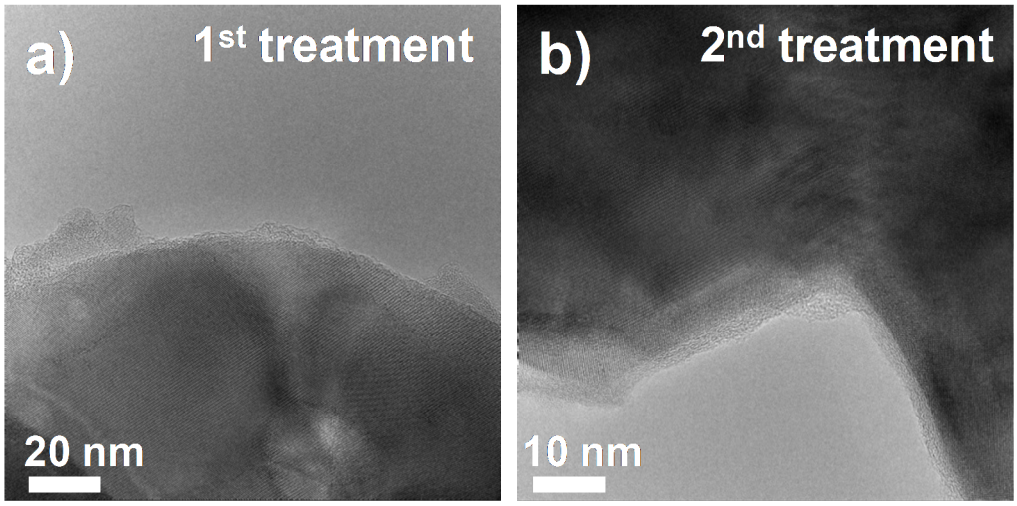

Fig. 3. 8. TEM images of the C-coated sample after a (a) first and a (b) second coating treatment.

3.2. Electrochemical characterization

In this section, the electrochemical characterization of the samples obtained by the different routes detailed above is shown. Since our aim here was to obtain a performing anode to be finally used in full cells, the following results were carried out at different stages of the thesis, which is why in some cases the experimental cell design exhibits slight differences as will be mentioned throughout this section.

3.2.1. Electrochemical characterization in organic electrolyte

3.2.1.1. $NaTi_2(PO_4)_3$ synthesized by the ceramic method

Electrodes were prepared for the pristine and ball-milled samples. Active material, C65 and PVDF were grounded in a mortar for 30 min in a ratio 75:20:5. Then NMP was added and the slurry was kept under stirring for 1 hour. The slurry was casted onto Al foil, and then dried at 120 °C under vacuum overnight. 11 mm-diameter electrodes with a mass loading of 4 mg cm^{-2} were cut and pressed at 5 t cm^{-2}.

1 M $NaClO_4$ (EC: PC) was used as electrolyte in Swagelok half cells with metallic Na as counter (and reference) electrode. All cells were cycled in a voltage range between 1.8 and 2.5 V *vs*. Na^+/Na at 0.1C. The voltage profile of the first 2 cycles can be observed in Fig. 3. 9 for the as prepared and ball-milled samples, and the characteristic plateau at 2.15 V *vs*. Na^+/Na which corresponds to the Ti^{4+}/Ti^{3+} redox couple can be observed in all cases.

The as prepared ceramic material (Fig. 3. 9a) delivered 104 mAh g^{-1} in the first discharge, with 71% of reversible capacity. Both ball-milled samples exhibit a better capacity, delivering 114 mAh g^{-1} in the first discharge (Fig. 3. 9b and Fig. 3. 9c) with slightly better reversibility in the

case of the 3 h ball-milled sample. Indeed, despite at this voltage no electrolyte decomposition is expected, all samples exhibit a first cycle irreversible capacity, a phenomenon that has already been reported both for $LiTi_2(PO_4)_3$ [8] and $NaTi_2(PO_4)_3$ although nobody has given a satisfactory explanation for its origin [2].

Polarization (considered as the difference between plateau in charge and in discharge) is also improved with increased ball-milling time. Indeed polarization values in the second cycle changes from 254 mV, obtained for the as prepared sample, to 173 mV, obtained for the 20h ball-milled sample. Only in the case of the as prepared material the polarization increases upon cycling.

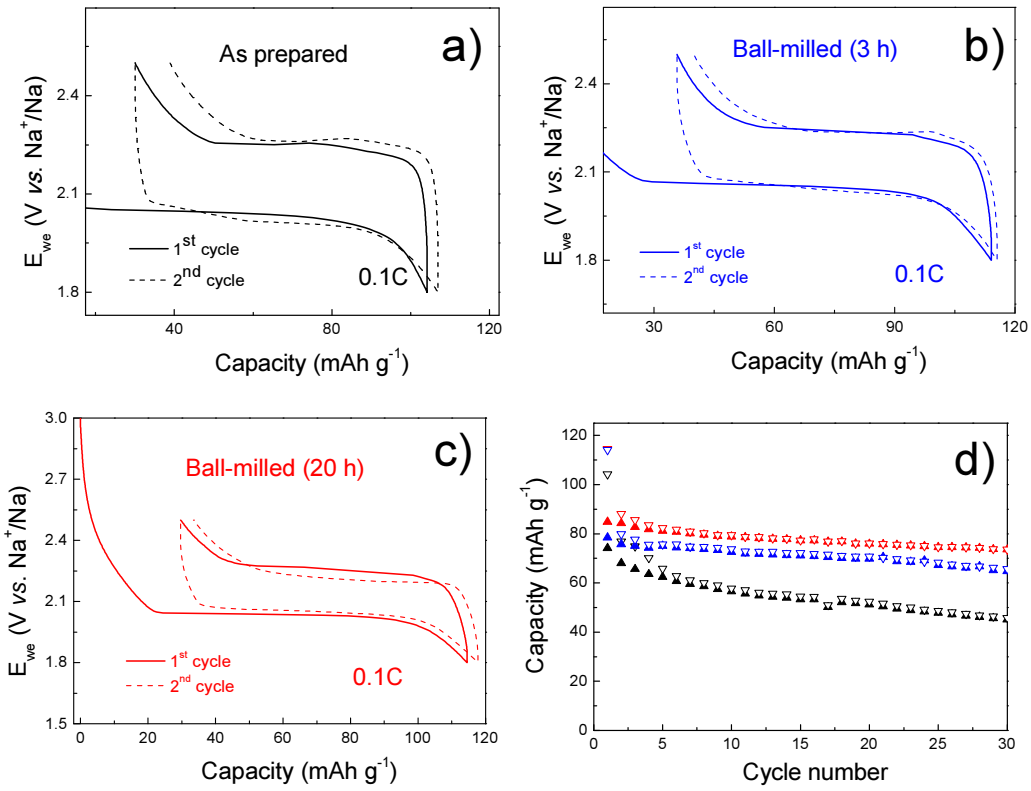

Fig. 3. 9. (a) Voltage *vs.* capacity plot for the first two cycles of the as prepared sample and (b) 3 h ball-milled and (c) 20 h ball-milled sample tested at 0.1C in a voltage range from 1.8 to 2.5 V *vs.* Na^+/Na in organic half-cells. (d) Specific capacity in charge (filled triangle) and in discharge (empty triangle) for the 30 first cycles of the previous three cells.

Fig. 3. 9d shows the capacity of the three samples *vs.* cycle number for the first 30 cycles. Only 62% of capacity retention is achieved by the pristine sample, while 83% and 87% of capacity retention are achieved by the 3 h and 20 h ball-milled samples respectively. These results show that, as reported for the Li-homologous $LiTi_2(PO_4)_3$ [8], ball-milling treatment is effective in improving the electrochemical performance of $NaTi_2(PO_4)_3$.

Despite the improvement in capacity and cyclability, the irreversibility of 25% would imply a previous pre-cycling in half cells if the material is to be used later as counter electrode in the characterization of the cathodes studied in this work.

3.2.1.2. $NaTi_2(PO_4)_3$ synthesized by the Pechini method

The as-prepared material and 10 h ball-milled sample were hand-grounded in a mortar for 30 minutes with C65 and PTFE in a ratio 75:20:5. Isopropyl alcohol was added as solvent and the slurry was kept under stirring for 1 hour. In this case, and to use the same electrode preparation methodology as in the tests carried out in aqueous cells, the slurry was casted on a stainless steel current collector with loadings of 4 mg cm^{-2}. The electrodes were dried overnight at 120 °C and pressed a 0.5 t cm^{-2}.

Fig. 3. 10a shows the voltage profile of the first 2 cycles for an organic half-cell with 1 M $NaClO_4$ (EC:PC) as electrolyte at 0.1C between 1.8 and 2.5 V *vs*. Na^+/Na. 98 mAh g^{-1} were delivered in the first discharge with a 22% of first cycle irreversible capacity, a value that is similar to that obtained for the as prepared ceramic sample. However, in this case, the polarization measured in the second cycle was lower than all ceramic samples (117 mV). Fig. 3. 10b compares the cyclability of the ceramic and Pechini pristine samples and clearly shows that capacity fading is more significant in the Pechini sample (36% of capacity retention after 30 cycles).

Both the lower polarization and the highest capacity fading for the sample synthesized by this route can be explained by the lowest particle size obtained. Indeed, a higher amount of surface area results in a larger effective amount of interface open to ion insertion and shorter diffusion distances but also to a major exposition to the electrolyte, which would enhance secondary reactions.

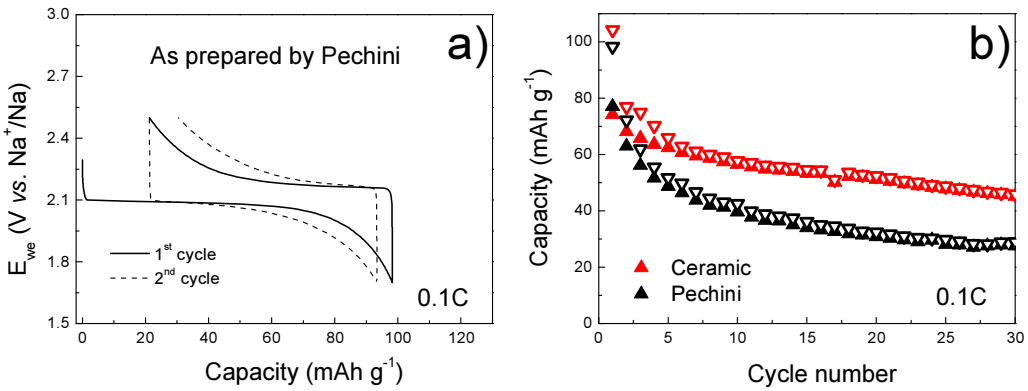

Fig. 3. 10. (a) Voltage *vs*. capacity plot for the first two cycles of the as prepared Pechini sample tested at 0.1C in a voltage range from 1.8 to 2.5 V *vs*. Na^+/Na in an organic Na half- cell (b) Specific capacity in charge (filled triangle) and in discharge (empty triangle) *vs*. cycle number for the as prepared samples obtained by Pechini and ceramic methods at 0.1C.

Fig. 3. 11a shows the first two cycles for the Pechini ball-milled sample in an organic half-cell cycled from 1.8 to 2.5 V *vs*. Na^+/Na at 0.05C. The cell delivered 127 mAh g^{-1} in discharge from which 79 mAh g^{-1} were reversibly charged (38% of irreversibility). This reversible capacity was similar to that obtained for the ceramic ball-milled material (40% of irreversibility) cycled in the same conditions Fig. 3. 11b.

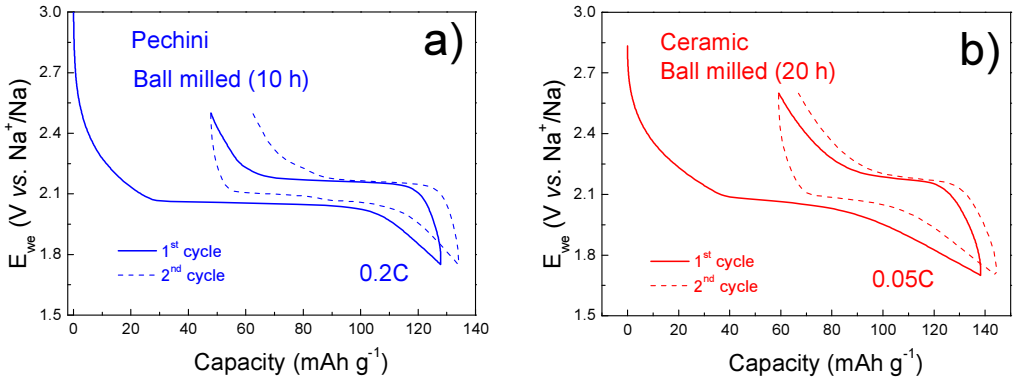

Fig. 3. 11. (a) Voltage *vs*. capacity plot for the first two cycles of the 10 h ball-milled Pechini sample and (b) 20 h ball-milled ceramic sample tested at 0.05C in organic half-cells in a voltage range from 1.8 to 2.5 V and 1.7 to 2.6 V *vs*. Na^+/Na respectively.

Electrodes of the C-coated sample after 1 and 2 treatments were prepared following the same methodology. Fig. 3. 12a and b display the voltage profile of the first two cycles at 0.05C for both samples. After the first coating treatment, the sample delivered a capacity of 139 mAh g^{-1} in the first discharge, with an irreversibility of 24%. The fact that the capacity obtained exceeds the theoretical capacity (C_{th} = 133 mAh g^{-1}) is indicative of a parasitic reaction. The first cycle irreversible capacity of the sample coated twice was reduced to less than 2% and 121 mAh g^{-1} of reversible capacity were achieved. Therefore, C-coating improves the electrochemical performance by reducing the first cycle irreversibility and increases the capacity in comparison to ball-milled samples. The presence of a parasitic reaction is further demonstrated in the inset of Fig. 3. 12 which shows the first ten cycles for each sample. The coulombic efficiencies were around 110% in the first five cycles for the sample coated once, while around 103% were obtained in the sample coated twice. In this case we believe that the C-coating protects the surface of the material from parasitic reactions, an issue that might be particularly critical in aqueous electrolyte since the operating potential is close to that of electrolyte decomposition. In this case the capacity fading is also significantly reduced, with 83% of capacity retention after 10 cycles with respect to 60% obtained for sample coated once. This indicates that with a more homogeneous and thicker coating the material gains in stability since surface reactions are reduced. In terms of polarization no significant differences are observed for the two samples with values close to 40 mV in both cases at the 2nd cycle.

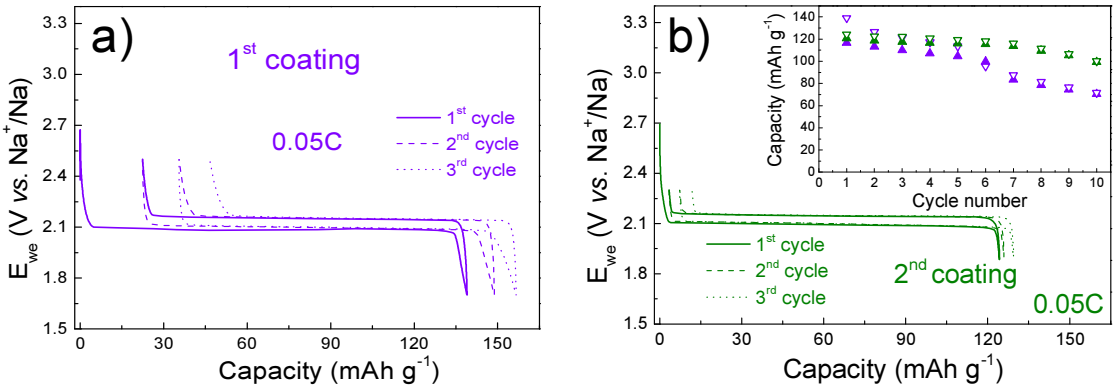

Fig. 3. 12. (a) Voltage *vs*. capacity plot for the sample coated once and (b) twice, tested at 0.05C in organic half-cells with Na metal as counter electrode using 1 M $NaClO_4$ electrolyte. Inset: specific capacity in charge (filled triangle) and in discharge (empty triangle) *vs*. cycle number for the two previous cells.

3.2.2. Electrochemical characterization in aqueous electrolyte

The optimized material was tested in aqueous electrolyte. Electrodes of the Pechini C-coated sample with a mass loading of 1-2 mg cm^{-2} were from a slurry using NMP as solvent, dried overnight at 120 °C and pressed at 4 t cm^{-2}. The voltage profile for the first two cycles of this sample tested *vs*. AC at 1C using 1 M Na_2SO_4 as electrolyte (pH = 6) is shown in Fig. 3. 13a. The cell delivered a reversible capacity of 90 mAh g^{-1} with a 92% of capacity retention after 20 cycles. However, even at this high rate, the coulombic efficiency is of 250% in the first cycle and ca. 140% in the next cycles. There are two factors responsible of this bad coulombic efficiency. On one hand, electrolyte decomposition, since the operation voltage of the material is outside the stability window of the aqueous electrolyte at this pH (H_2 evolution starts at 2.35 V *vs*. Na^+/Na) and therefore decomposes. On the other hand, electrode oxidation during the discharge process which involves the reaction of intercalated Na^+ with H_2O to produce Na^+, OH^- and H_2 at low potentials (see experimental chapter) [9].

If the pH is raised to 8 by NaOH addition the cell delivers 100 mAh g^{-1} and similar capacity fading (ca. 90% after 20 cycles). Electrolyte decomposition is shifted towards lower voltage, and, as it can be observed in Fig. 3. 13b, the irreversibility is mitigated to some extent (174% in the first cycle, and ca. 120% in subsequent cycles). The pH needs therefore to be raised even more in order to shift the lower stability limit of the electrolyte towards lower V values and obtain good coulombic efficiencies (even for high rates).

At pH = 12 both electrolyte decomposition and oxidation of the material start below 2 V *vs.* Na^+/Na. $NaTi_2(PO_4)_3$ was first cycled at 0.1C in a voltage range between 2.05 and 2.2 V (Fig. 3. 14a). A reversible capacity of 115 mAh g^{-1} was achieved, close to that obtained in organic electrolyte. However, after 17 cycles a capacity retention of 83% was found, with coulombic efficiencies around 105%. The same battery was then tested at 0.2C with an initial capacity of 87.5 mAh g^{-1} and a capacity retention of 94% after 11 cycles. Despite doubling the rate, the coulombic efficiencies are still around 103%. When the rate was increased up to 0.5C, the reversible capacity was still 64 mAh g^{-1} and the capacity retention after 11 cycles was ca. 95%. More importantly coulombic efficiencies were close to 100 %.

Fig. 3. 14b shows the voltage profile for the second cycle at each rate. As mentioned before from the calculated values of coulombic efficiency, the process in discharge is not totally reversible for 0.2C and 0.1C rates. The dQ/dV plot shown as inset reveals very low overpotential at all rates (from 40 mV obtained at 0.1C up to 59 mV at 0.5C), which is an important factor to achieve the maximum average voltage in the full cell discharge .

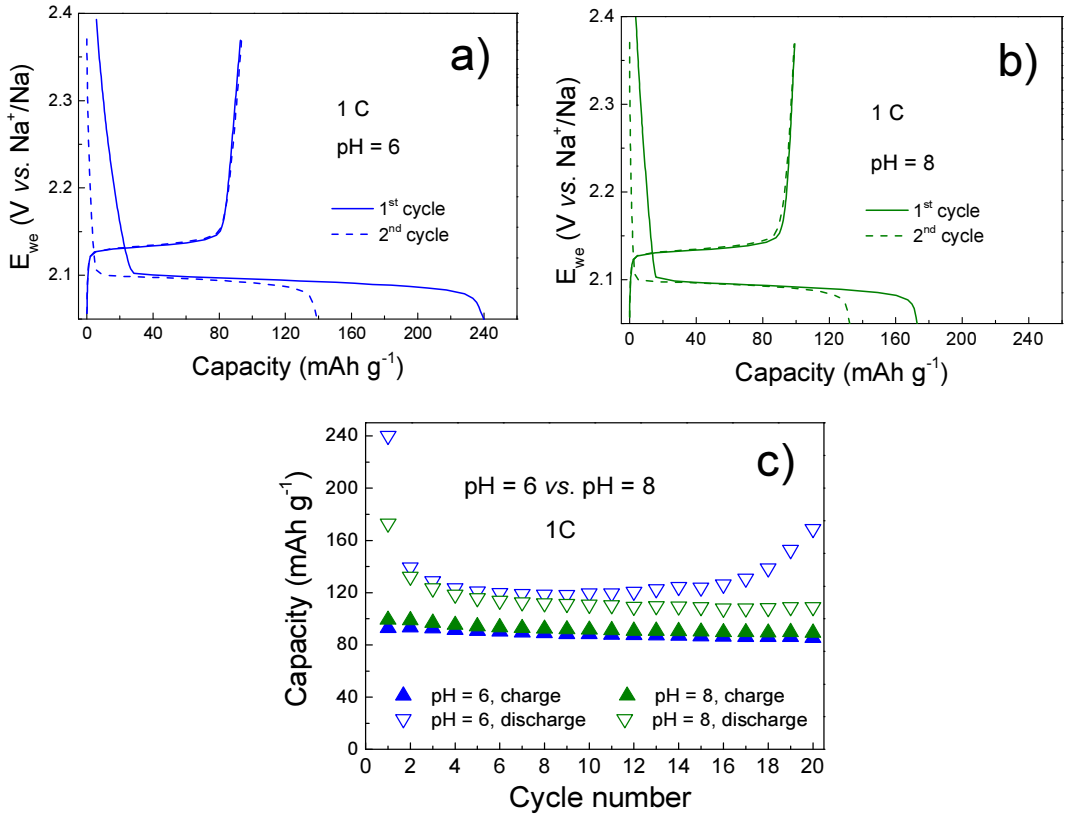

Fig. 3. 13. Voltage *vs.* capacity plot for sample coated twice tested at 1C in a voltage range from 2.05 to 2.37 V *vs.* Na^+/Na in aqueous half-cells using 1 M Na_2SO_4 aqueous electrolyte at (a) pH = 6 and (b) pH = 8. (c) Specific capacity in charge (filled triangle) and in discharge (empty triangle) *vs.* cycle number for each cell.

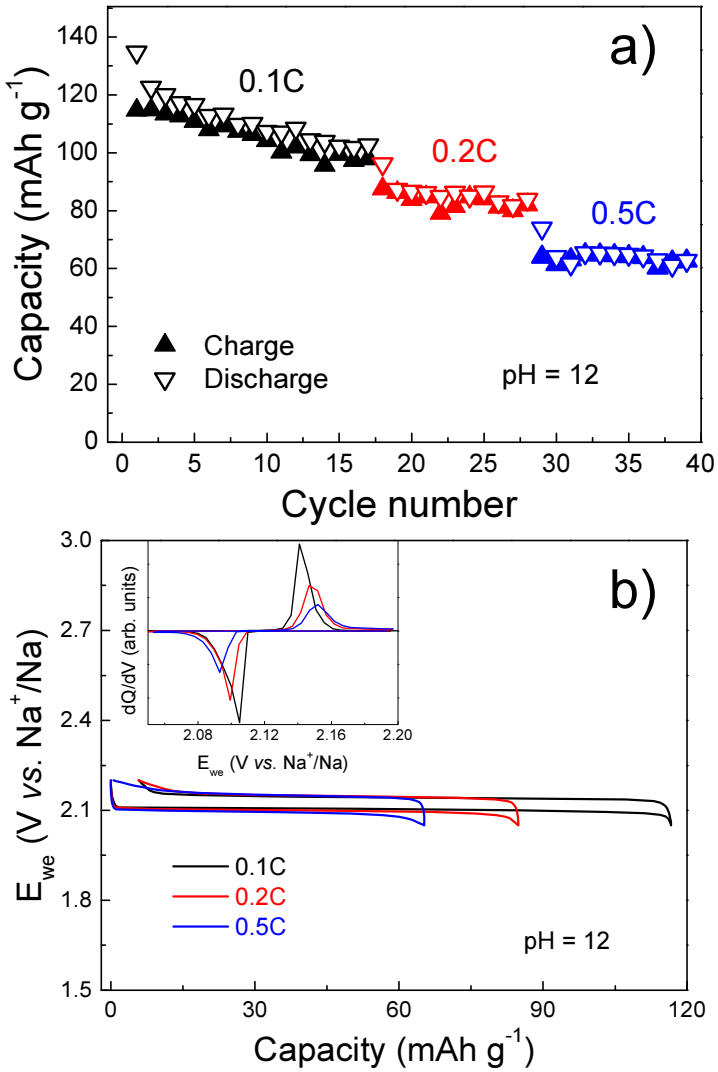

Fig. 3. 14. (a) Specific capacity *vs.* cycle number for the sample coated twice in charge (filled triangle) and in discharge (empty triangle) for each rate (a) 0.1C (black), 0.2C (red) and 0.5C (blue) tested in a voltage range from 2.05 to 2.2 V *vs*. Na^+/Na in an aqueous half-cell using 1 M Na_2SO_4 electrolyte with pH = 12. (b) Voltage *vs*. capacity plot for the 2nd cycle for each rate. Inset: the corresponding dQ/dV plot.

When cycled at 1C, the initial reversible capacity was 90 mAh g^{-1} with a capacity retention of 79.33% after 100 cycles (Fig. 3. 15a). These values are close to that reported for this material in aqueous NIBs. However, we observed that if the electrodes are not pressed (red), there is no fading after 400 cycles (although 20 cycles are needed to achieve the maximum of capacity delivered in these conditions (65 mAh g^{-1})). Non-pressed electrodes also showed a slightly higher overpotential (65 mV) than pressed electrodes (50 mV) (Fig. 3. 15b). Despite the lower capacity and lower polarization, the stability of the systems make $NaTi_2(PO_4)_3$ a suitable anode for aqueous NIBs.

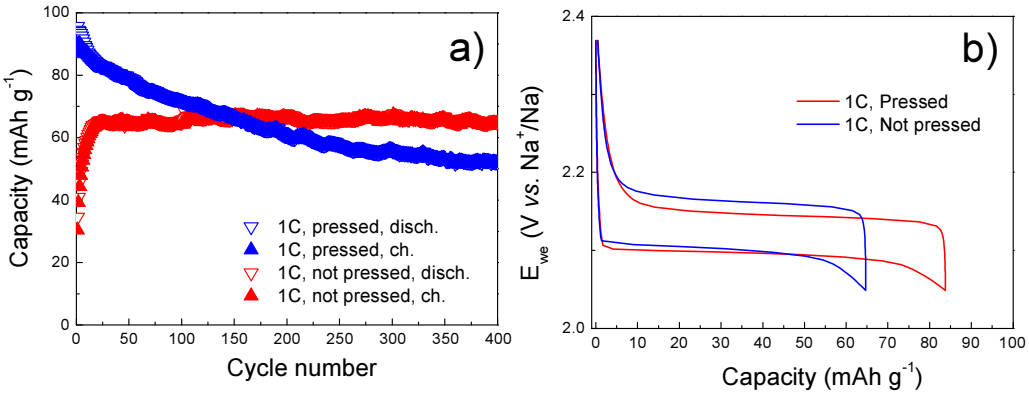

Fig. 3. 15. (a) Specific capacity *vs*. cycle number for a pressed electrode (blue) and non-pressed electrode (red) of the sample coated twice in charge (filled triangle) and in discharge (empty triangle) at 1C in a voltage range from 2.05 to 2.2 V *vs*. Na^+/Na in an aqueous half-cell using 1 M Na_2SO_4 electrolyte at pH = 12. (b) Voltage *vs*. capacity plot at cycle 20th for both kinds of electrode.

3.3. Conclusions

Two different synthesis routes for $NaTi_2(PO_4)_3$ were explored. The sample obtained by ceramic method showed some impurities of TiP_2O_7, while by Pechini method the sample was obtained pure due to a better mixing of precursors.

Both samples improved notably in terms of capacity, cyclability and polarization with a ball-milling treatment. However, an irreversibility of 25% in the first cycle was observed. This irreversibility is mitigated with an effective C-coating. Moreover, capacities close to the theoretical capacity and overpotential values as low as 40 mV were achieved at 0.05C in organic electrolyte.

The improved material was tested in aqueous electrolyte. The influence of the pH on the sample was studied, showing much better results in terms of coulombic efficiency at pH = 12 than at pH = 6 and pH = 8. But, even at pH = 12, the material had to be cycled at high rates to achieve coluombic efficiencies close to 100%.

Finally, by using non-pressed electrodes, $NaTi_2(PO_4)_3$ achieved 400 cycles with 100% of capacity retention despite a lower capacity and a slightly higher overpotential are achieved. Also, 20 conditioning cycles are needed to reach the maximum of capacity (65 mAh g^{-1}). Therefore, a stable anode was achieved to use in future full cells.

[1] C. Delmas, F. Cherkaoui, A. Nadiri and P. Hagenmuller, A nasicon-type phase as intercalation electrode: $NaTi_2(PO_4)_3$, Mat. Res. Bull. 22 (1987) 631-639
[2] S. Park, I. Gocheva, S. Okada, J. Yamaki, Electrochemical properties of $NaTi_2(PO_4)_3$ anode for rechargeable aqueous sodium-ion batteries, J. Electrochem. Soc. 158 (2011) 1067–1070
[3] Z. Li, D. Young, K. Xiang, W. C. Carter, Y-M. Chiang, Towards high power energy aqueous sodium-ion batteries: the $NaTi_2(PO_4)_3/Na_{0.44}MnO_2$ system, Adv. Energy Mater. 3 (2013) 290-294
[4] W. Wu, J. Yan, A. Wise, A. Rutt, J.F. Whitacre, Using intimate carbon to enhance the performance of $NaTi_2(PO_4)_3$ anode materials: carbon nanotube vs graphite, J. Electrochem. Soc. 161 (2014) A561-A567
[5] L. Hagman, P. Kierkegaard, The Crystal Structure of $NaM_2^{IV}(PO_4)_3$; Me^{IV} = Ge, Ti, Zr, Acta Chem. Scand. 22 (1968) 1822-1832
[6] W. Wu, A. Mohamed, J.F. Whitacre, Microwave synthesized $NaTi_2(PO_4)_3$ as an aqueous sodium-ion negative electrode, J. Electrochem. Soc. 160 (2013) A497-A504
[7] J.L. Rodrigo, P. Carrasco, J. Alamo, Thermal-expansion of $NaTi_2(PO_4)_3$ studied by Rietveld method from x-ray-diffraction data, Mat. Res. Bull. 24 (1989) 611–618
[8] X-H. Liu, T. Saito, T. Doi, S. Okada, J-I. Yamaki, Electrochemical properties of rechargeable aqueous lithium ion batteries with an olivine-type cathode and a Nasicon-type anode, J.Power Sources 189 (2009) 706–710
[9] J-Y. Luo, W.-J. Cui, P. He, Y-Y. Xia, Raising the cycling stability of aqueous lithium-ion batteries by eliminating oxygen in the electrolyte, Nat.Chem. 2 (2010) 760–765

4. Study of Olivine $NaFePO_4$ as cathode material

Among polyanionic Na-ion materials studied so far, olivine $NaFePO_4$ has the highest theoretical capacity (154 mAh g^{-1}). Its operation voltage (2.9 V *vs.* Na^+/Na) is somewhat low for organic cells but lies within the aqueous electrolyte stability limit (2.297 and 3.527 V *vs.* Na^+/Na at neutral pH) and is therefore an interesting aqueous positive electrode to explore.

$NaFePO_4$ is analogue to $LiFePO_4$ [1], which is a commercial success in Li-ion batteries for its low cost, safe voltage and power capability. Good capacity (100-120 mAh g^{-1} at low rates) and cyclability have been reported for $NaFePO_4$ in organic electrolyte, as well as a different reaction mechanism with respect to $LiFePO_4$ [2,3,4,5,6,7].

The olivine structure can be described as a hexagonal, close-packed array of oxygen atoms with half of the octahedral sites occupied with iron atoms and one-eighth of the tetrahedral sites occupied by phosphorous ions, resulting in isolated phosphate tetrahedra (Fig. 4. 1). There are three distinct oxygen sites, two distinct metal sites (M1 and M2) and only one phosphorous site. In olivine, the M1 site holds the alkali metal while the M2 site holds the transition metal. The diffusion of Na ions occurs through the channels along the b-axis, as in its Li-counterpart [5].

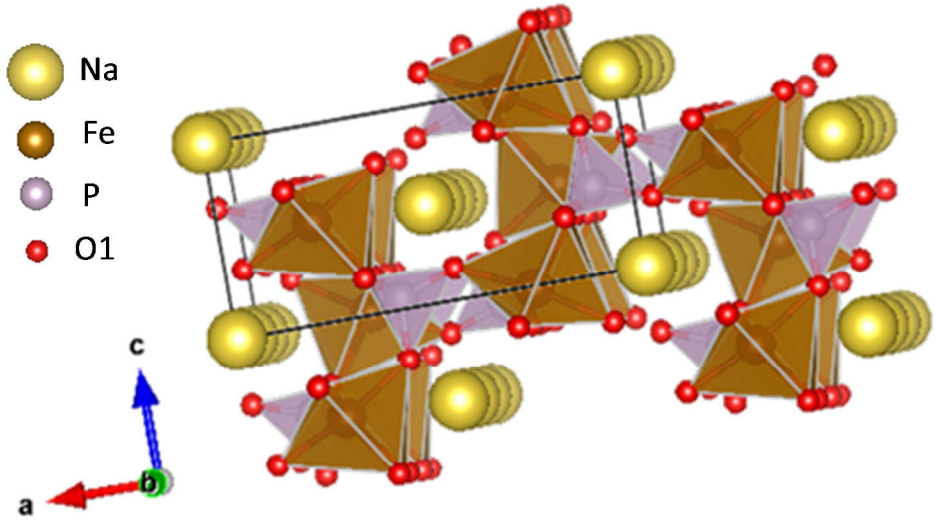

Fig. 4. 1. Crystal structure of olivine $NaFePO_4$.

In the course of our work $FePO_4$ was evaluated in aqueous electrolyte in a report focussed in $Na_3Ti_2(PO_4)_3$. The authors reported an initial full cell capacity at 0.5C of ~110 mAh $g^{-1}_{cathode}$, with a capacity fade of about 40% after 20 cycles at pH = 11 [8]. Another recent work showed that $LiFePO_4$ could be reversibly cycled in an aqueous solution of $NaNO_3$ [9]. In view of these promising preliminary results we decided to further evaluate the electrochemical performance of $FePO_4/NaFePO_4$ in aqueous electrolyte.

4.1. Synthesis and physicochemical characterization

$NaFePO_4$ was prepared by chemical delithiation and further sodiation of commercial carbon-coated (6 wt. %) $LiFePO_4$ with an average primary particle size of 800 nm, according to the supplier's specifications. The X-ray diffraction pattern of $LiFePO_4$ was refined by Le Bail method using Pnma space group (Fig. 4. 2a) resulting in refined cell parameters of *a* = 10.3198(1) Å, *b* = 6.00294(7) Å, and *c* = 4.69009(6) Å (Table 4.1), in agreement with literature values [10].

$LiFePO_4$ was oxidized using NO_2BF_4 (95%, Sigma-Aldrich) in a 2.5 molar excess and CH_3CN as solvent. The reaction was carried out in a glove box under Ar atmosphere ($\leq$ 5 O_2 and H_2O ppm) for 1 day at room temperature. Once the reaction was completed the solution was vacuum filtered outside the glove box and the delithiated collected powder was washed with acetonitrile twice and dried under vacuum at 80 ºC overnight [6].

The refined X-ray diffraction pattern of the obtained $FePO_4$ is shown in figure 1b. The pattern was indexed with Pnma space group (Fig. 4. 2b) resulting in refined cell parameters (as obtained by Le Bail method) of *a* = 9.8115(2) Å, *b* = 5.7863(1) Å, and *c* = 4.7798(1) Å (Table 4.1), in agreement with literature values [10]. The fact that no $LiFePO_4$ was detected in the X-ray diffraction pattern is a first indication that delithiation was complete.

The chemical sodiation of the previously obtained $FePO_4$ powder was carried out by treatment with NaI (99.5%, Sigma-Aldrich) in CH_3CN in a 3:1 molar ratio. The reaction was done in Ar atmosphere at 85°C for one day [6]. The X-ray diffraction pattern of the obtained $NaFePO_4$ sample was also indexed with Pnma space group (Fig. 4. 2c), and the refined cell parameters *a* = 10.4043(3) Å, *b* = 6.2213(1) Å and *c* = 4.9485(1) Å (Table 4. 1) are also in agreement with literature values [2]. The Na/Fe ratio of the final $NaFePO_4$ compound was verified by ICP and found to be equal to 0.95 ± 0.03.

In Fig. 4. 2d a comparison of $LiFePO_4$, $FePO_4$ and $NaFePO_4$ XRD patterns can be observed. $FePO_4$ peaks are displaced to the right with regard to those of $LiFePO_4$ in agreement with the cell contraction that results from deinsertion of Li ions, changing the total volume from 290.5 to 270.8 $Å^3$. The *a* parameter is the more affected one while the *c* parameter almost does not change and even slightly increases after oxidation.

On the other hand, the insertion of sodium into the olivine structure results in a larger cell volume compared to the lithium counterpart (319.8 $Å^3$), which represents a total increase of about 18% with respect to $FePO_4$, in agreement with recent literature results [3]. Despite this volume change is very high for a Na-insertion material, $NaFePO_4$ exhibits a good cyclability as will be shown below.

From the profile of diffraction peaks, and after subtracting the instrumental contribution using an Instrument Resolution File (IRF) determined with an Al_2O_3 standard, average domain sizes of 128(2) nm, 110(1) nm and 91(1) are obtained for $LiFePO_4$, $FePO_4$ and $NaFePO_4$ respectively. From these values it can be concluded that the domain size is slightly reduced during both oxidation and reduction treatments, most probably because the differences in volume between the different compositions cause internal strains that are relaxed by the creation of internal interfaces. Additionally, TEM was used to verify that C-coating remains around the particle after oxidation and reduction treatments (Fig. 4. 3).

Table 4. 1. *a*,*b* and *c* cell parameters (Pnma space group) and X^2 agreement factors obtained after Le Bail refinement of the XRD patterns of the different studied samples: $LiFePO_4$, $FePO_4$ and $NaFePO_4$.

$LiFePO_4$	a (Å)	10.3198(1)
	b (Å)	6.00294(7)
	c (Å)	4.69009(6)
	X^2	5.96
$FePO_4$	a(Å)	9.8115(2)
	b (Å)	5.7863(1)
	c (Å)	4.7798(1)
	X^2	2.023
$NaFePO_4$	a(Å)	10.4043(3)
	b (Å)	6.2213(1)
	c (Å)	4.9485(1)
	X^2	1.564

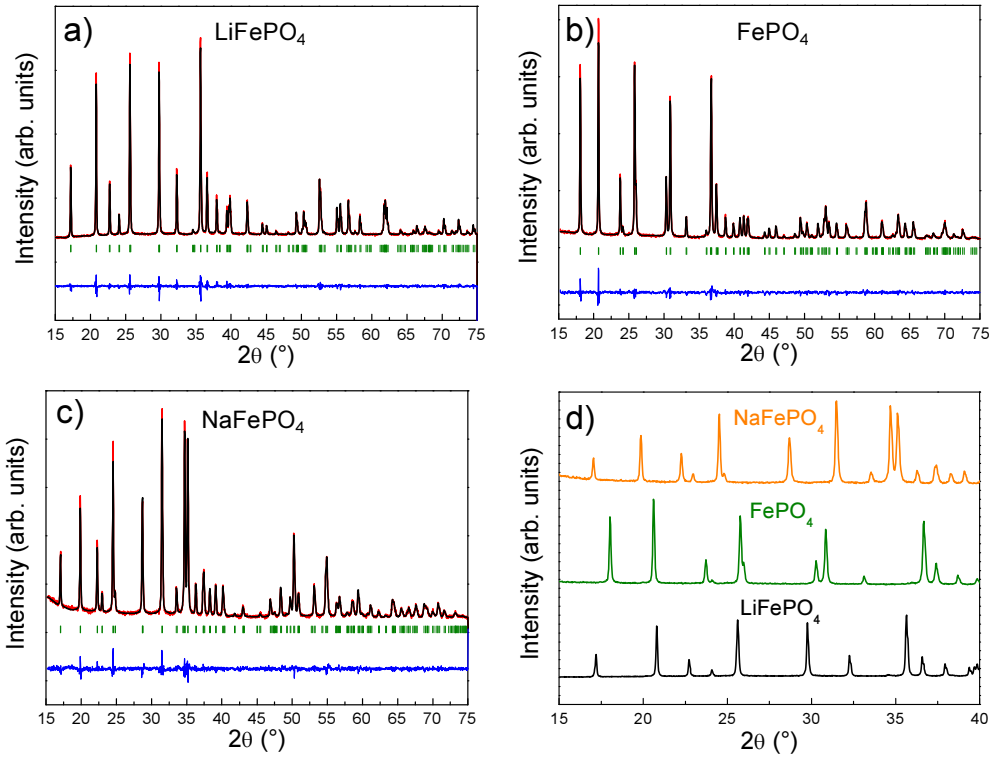

Fig. 4. 2. Refined profiles using Le Bail method of (a) $LiFePO_4$, (b) $FePO_4$ and (c) $NaFePO_4$. The observed and calculated intensities are represented by the red markers and the black solid line, respectively. The bottom blue line represents the difference between the observed and calculated patterns. Bragg positions are represented as green vertical bars. (d) Comparison of the XRD patterns of the three different samples.

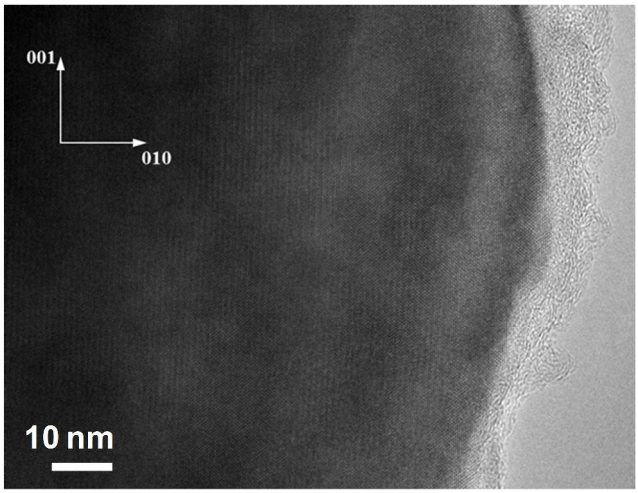

Fig. 4. 3. TEM image of a $NaFePO_4$ particle border

4.2. Electrochemical characterization

Electrodes of C-coated $NaFePO_4$ were prepared by casting a slurry of formulation 75:20:5 (active material: C65: PVdF) on stainless steel. The electrodes were dried overnight at 120 °C under vacuum and pressed at 4 t cm^{-2} as described in the experimental chapter. The material was electrochemically characterized both in organic and aqueous electrolyte for comparative purposes.

4.2.1. Electrochemical characterization in organic electrolyte

The electrochemical characterization of $NaFePO_4$ was first carried out in organic electrolyte 1 M $NaClO_4$ (EC:PC with 2% FEC) in Na half-cells. Fig. 4. 4a shows the rate capability test for a battery cycled at different rates (0.05C, 0.1C, 0.2C, 0.4C, C and 2C) in the range from 2.2 to 4.3 V *vs*. Na^+/Na. After cycling at 2C the cell was cycled for five additional cycles at a slower rate (0.2C) to verify that the material is able to deliver the same capacity after fast cycling. At 0.05C a capacity of 105 mAh g^{-1} is achieved, which is comparable to what has been found in the literature for a similar rate in a similar voltage window [4]. Fig. 4. 4b shows the voltage profile at the 5th cycle for each of the six different rates. As expected, the voltage profile is not symmetric with two plateaus at around 2.93 and 3.1 V *vs*. Na^+/Na in charge and one at 2.75 V in discharge at 0.05C. Contrary to the symmetrical 2-phase mechanism observed in micrometric $LiFePO_4$ [10], Na^+ extraction occurs in two voltage plateaus separated by an intermediate phase Na_xFePO_4 (x = 2/3), whereas three phases ($FePO_4$, $Na_{2/3}FePO_4$ and $NaFePO_4$) appear simultaneously in discharge, reflected in the galvanostatic profile as a single plateau during Na^+ insertion [3].

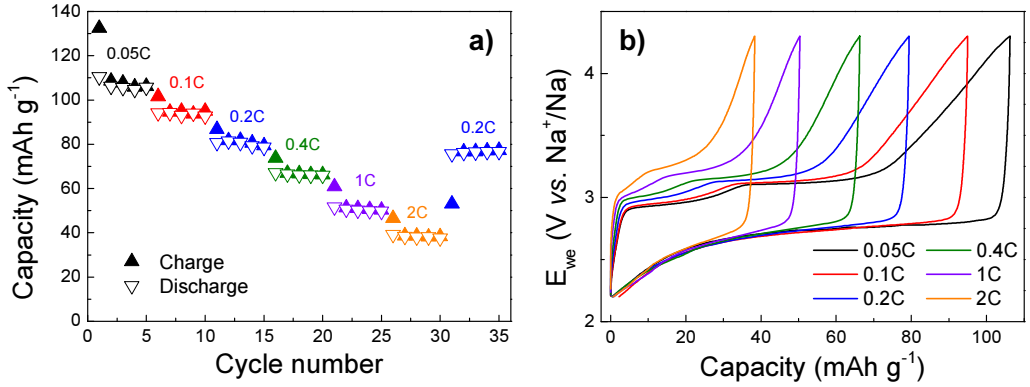

Fig. 4. 4. (a) Specific capacity in charge (filled triangle) and in discharge (empty triangle) *vs*. cycle number for an organic Na half-cell cycled at different rates between 2.2 and 4.3 V *vs*. Na^+/Na (a) and voltage *vs*. capacity plot for the 5th cycle at 0.05C (black line), 0.1C (red line), 0.2C (blue line), 0.4C (green line), 1C (violet line) and 2C in the same battery (b).

In general terms, $NaFePO_4$ shows a major overpotential in comparison to its homologous $LiFePO_4$. This fact is due a lower Na^+ diffusion coefficient in the structure compared to Li^+ [5,7]. Furthermore, this overpotential is aggravated inasmuch the rate increases, as expected for diffusion-controlled processes, going from 0.265 V at 0.05C to 0.510 V at 2C (Table 4. 2). This results in a drop of capacity of about 12 mAh g^{-1} every time the rate is doubled, showing that the rate capability of the material must be improved. The polarization is particularly aggravated at the end of charge, which will result in a considerable loss of capacity when the material is used in aqueous electrolyte because of the voltage limitation due to the narrower stability window of water.

Table 4. 2. Values of capacity and overpotential obtained from the profiles shown in Fig. 4. 4b. The polarization has been calculated as the difference between the average voltage in charge and discharge for the plateau at the highest potential.

Rate	Capacity (mAh g^{-1})	Polarization (V)
0.05C	105	0.380
0.1C	93	0.410
0.2C	79	0.450
0.4C	66	0.490
1C	50	0.600
2C	38	0.710

4.2.2. Electrochemical characterization in aqueous electrolyte

After testing the material in organic electrolyte and verifying that a similar behaviour to what has been already reported in the bibliography is obtained, $NaFePO_4$ was tested in 1 M Na_2SO_4 electrolyte using a three-electrode Swagelok configuration with Ag/AgCl (3 M NaCl) as reference electrode and AC as counter electrode.

Fig. 4. 5a shows a test at 0.2C performed in a quite conservative voltage range (from 2.5 to 3.3 V *vs*. Na^+/Na). The battery delivered an initial capacity of 92.27 mAh g^{-1} and, after 35 cycles, retained 77.26 % of the capacity (71.28 mAh g^{-1}). The exact origin of this capacity fading has not been identified yet, although material dissolution can be ruled out according to ICP analysis of the electrolyte after cycling (less than 0.4 % of the initial Fe content was detected in the electrolyte after 35 cycles, while the capacity faded down to 77.26 % of the initial capacity); and no extra peaks (Fig. 4. 5b) were detected in the XRD pattern of the cycled

electrode, where the peaks of $Na_{2/3}FePO_4$ are observed meaning that not all Na insertion is reversible. There are some extra peaks from the current collector and the clay used to hold the electrode during the measurement.

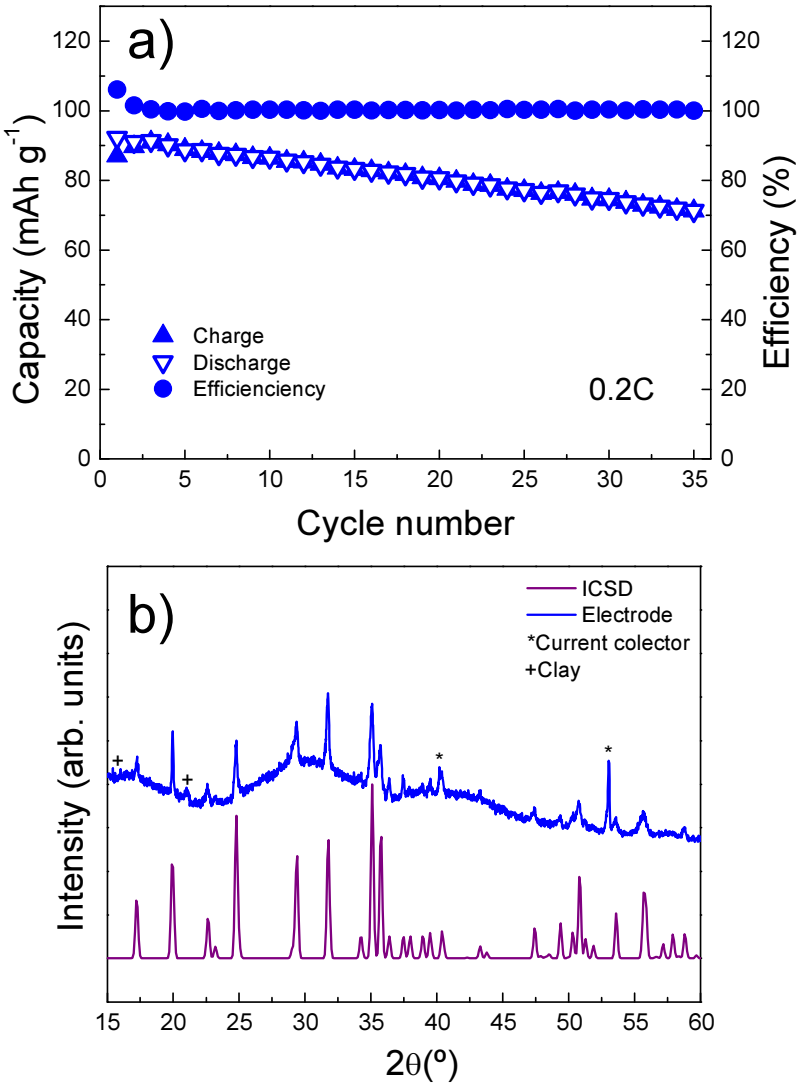

Fig. 4. 5. (a) Specific capacity in charge (filled triangle) and in discharge (empty triangle) and coulombic efficiency (circle) *vs*. cycle number for an aqueous battery cycled at 0.2C between 2.5 and 3.3 V *vs*. Na^+/Na. (b) XRD pattern of an electrode after 35 cycles (blue) and calculated $Na_{2/3}FePO_4$ pattern obtained from ICSD database [2].

Next step was to try to stabilize the cyclability by reduction of the voltage window. To determine the optimum voltage range for $NaFePO_4$, two batteries were cycled starting from 2.625 to 3.2 V *vs.* Na^+/Na at 0.2C. In one of them, the upper limit was increased 0.025 V every 5 cycles (Fig. 4. 6a). Above 3.2 V, it can be observed that there is a severe capacity fading.

In the other battery, the lower limit was decreased 0.025 V every five cycles (Fig. 4. 6b). There is a little increase in the capacity (5 mAh g^{-1}) when lower cut-off limit was reduced from 2.625 to 2.550 V, but no extra capacity was observed by further opening the voltage range.

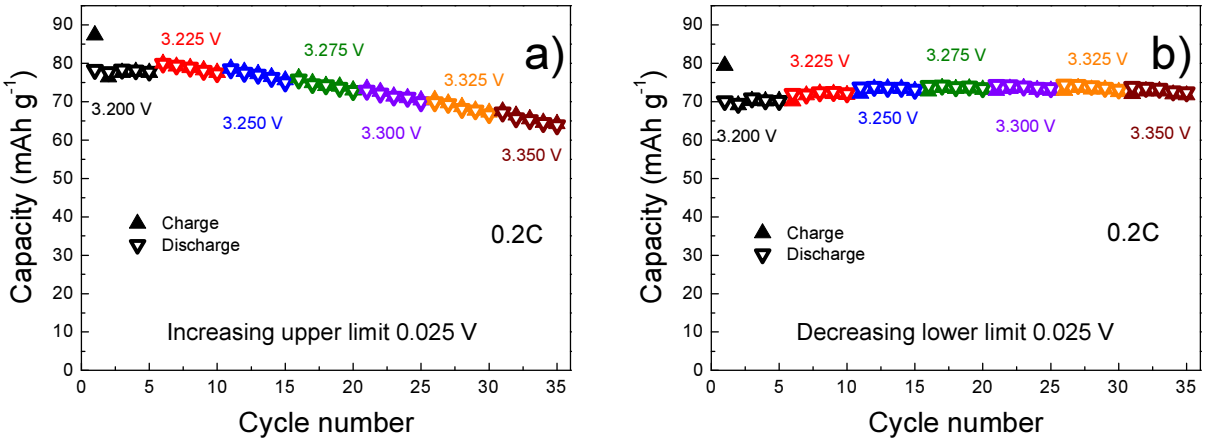

Fig. 4. 6. (a) Evolution of the capacity *vs*. cycle number of $NaFePO_4$ cells at 0.2C using AC as anode in 1 M Na_2SO_4 with increasing upper cut-off voltage (0.025 V every 5 cycles) and (b) with decreasing lower cut-off voltage (0.025 V every 5 cycles) from starting values of 2.625 - 3.2 V *vs*. Na^+/Na .

In view of the results obtained, the window from 2.55 to 3.2 V *vs*. Na^+/Na was considered as the optimum range for the cyclability of the $NaFePO_4$ at this rate and was used in further experiments.

When cycling the cells at 0.2C inside the selected voltage range, the capacity retention significantly improved, reaching 90% after 35 cycles, in contrast to 77% achieved with the previous voltage window (Fig. 4. 7). The obtained capacity was obviously lower, 81 mAh g^{-1} instead of 92 mAh g^{-1}, but the significant improvement in stability is a trade-off that compensates the 12% of capacity loss, since after 30 cycles a comparable capacity is obtained with both voltage ranges.

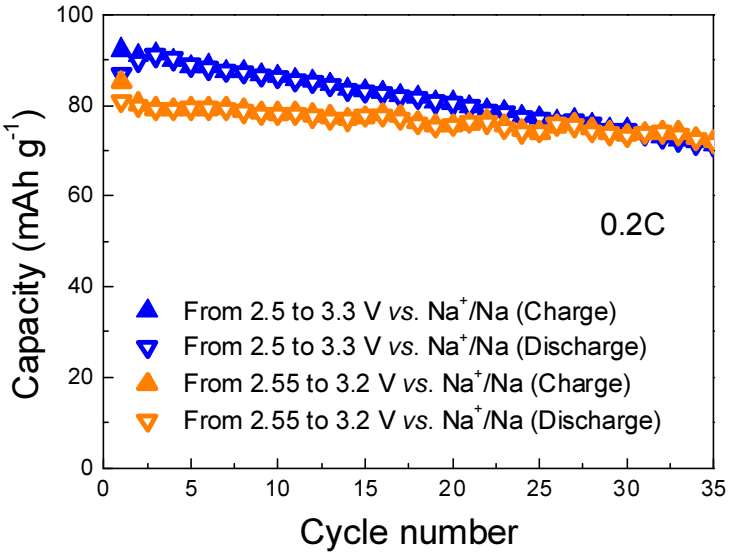

Fig. 4. 7. Specific capacity *vs*. cycle number of $NaFePO_4$ in 1 M Na_2SO_4 using AC as anode at 0.2C rate from 2.55 to 3.2 V *vs*. Na^+/Na (orange) and from 2.5 to 3.3 V *vs*. Na^+/Na (blue).

Fig. 4. 8 shows a comparison of the cycling stability obtained with this more conservative window when cycling the cell at 0.2C and 1C rates. At this latter rate excellent capacity retention has been obtained (more than 95% after 35 cycles) but the capacity decreases in 30% reaching only 45 mAh g^{-1}. This can be improved by slightly widening the voltage window since the 2.55-3.2 V window has been selected for best low rate stability, but it can be opened to 2.45-3.3 V for higher rates. Indeed, a capacity retention of about 90% is observed at 1C for this wider voltage window (Fig. 4. 8) and the capacity increases up to 67 mAh g^{-1}. Remarkably, the three cells shown in this figure resulted in energy efficiencies around 100%.

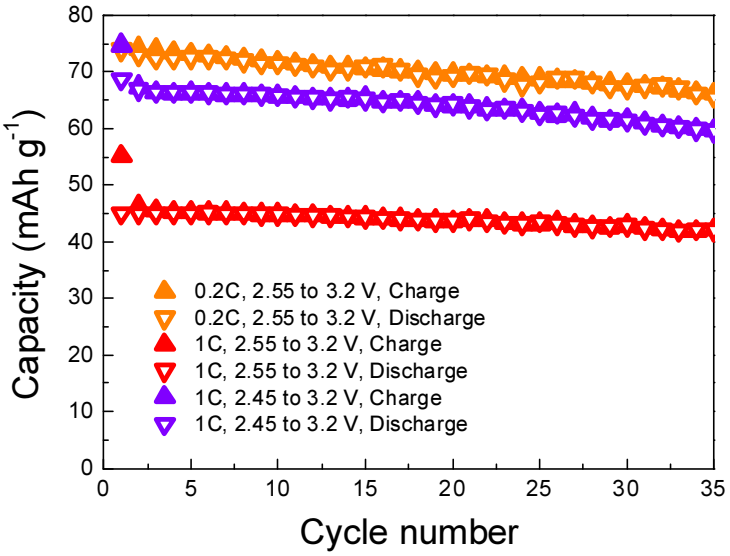

Fig. 4. 8. Specific capacity *vs*. cycle number of $NaFePO_4$ in 1 M Na_2SO_4 in a hybrid cell *vs*. AC at 0.2C rate from 2.55 to 3.2 V *vs*. Na^+/Na (orange) and two batteries at 1C rate in the same range (red) and from 2.45 to 3.3 V *vs*. Na^+/Na (violet).

Rate capability tests were performed at 0.2C, 0.4C, 1C, 2C, 0.2C, 0.1C and 0.2C rates (Fig. 4. 9) in the conservative voltage window that had led to the best results at 0.2C rate (2.55 to 3.2 V vs. Na^+ /Na). As previously seen, this very conservative window limits the reaction before it is completed. Therefore, if the capacity of the aqueous cell is compared with the performance obtained in organic electrolyte with the extended window (Fig. 4. 4 and Table 4. 2), a somewhat lower capacity is obtained at the slowest rates, with 75 mAh g^{-1} at 0.1C and 71 mAh g^{-1} at 0.2C (Table 4. 3). However, the same capacity as in the organic electrolyte is obtained for the fastest rates (> 0.4C) despite the much smaller voltage window, being able to deliver 32% and 25% of the theoretical capacity at 1C and 2C, respectively.

Table 4. 3. Values of capacity and polarization in the 5th cycle obtained for NaFePO4 cycled at different rates in an aqueous cell using AC and Ag/AgCl (3 M NaCl) as counter and reference electrodes, respectively.

Rate	Capacity (mAh g^{-1})	Polarization (V)
0.1C	75	0.249
0.2C	71	0.264
0.4C	61	0.270
1C	48	0.300
2C	38	0.321

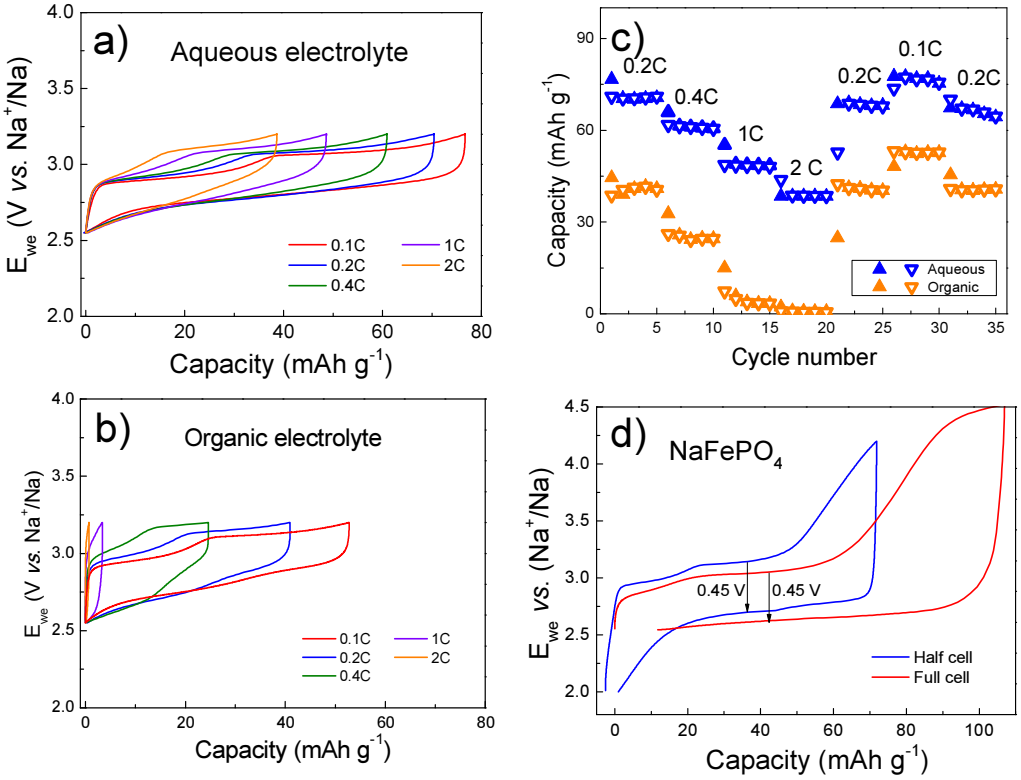

Fig. 4. 9. Voltage *vs*. capacity plot at different rates (0.1C (red), 0.2C (blue), 0.4C (green), 1C (violet) and 2C (orange) for (a) an aqueous cell and (b) an organic cell, both cycled between 2.55-3.2 V *vs*. Na^+/Na. (c) Summary of the rate capability tests for the different electrolytes and voltage windows (aqueous cell in blue, and organic cell in orange). (d) Voltage profile of NaFePO4 tested in an organic half-cell and organic 3-electrodes cell with metallic Na and $Na_3Ti_2O_7$ as reference and counter electrode respectively.

On the other hand, if the same window is used for the organic electrolyte, the lower performance of the organic cell at the highest rates becomes more visible (Fig. 4. 9b). In this case, the capacity of the aqueous cell exceeds that of the organic cell at all rates and the organic cell completely fails to cycle at 1C and 2C.

The better results obtained in aqueous medium are due to a reduction of the overpotential as it is observed in table 4.3, where the values of polarization at the different rates are given for the aqueous electrolyte. Compared to those obtained in organic electrolyte (Table 4. 3), these are notably reduced. In aqueous electrolyte, 0.264 and 0.321 V are obtained at 0.2C and 2C respectively while in organic electrolyte the overpotential at 0.2C is 450m V and increases up to 0.710 V when cycling at 2C.

In order to exclude the possibility that the Na counter electrode used in the half-cell was at the origin of the larger overpotential of organic cells, a full cell using $NaTiO_2$ was built. The voltage profile of this cell, cycled at 0.1C, is compared to an aqueous cell cycled at the same rate in figure Fig. 4. 9d. Both exhibit the same overpotential despite Na is only used as reference and does not participate in the reaction occurring in the full cell.

The lower polarization in aqueous electrolyte has been already reported for some materials such as $NaTi_2(PO_4)_3$ [11], $LiFePO_4$ [12] and $Na_{0.44}MnO_2$ [13]. Although aqueous electrolytes have typically a higher ionic diffusion coefficient compared to organic electrolyte, the electrolyte's conductivity contribution on the overall cell polarization in Li-ion and Na-ion batteries is generally negligible [14,15]. Moreover, several materials have been reported as Na-ion electrode materials in organic electrolyte with significantly smaller polarization at the same rate than $NaFePO_4$ (layered oxides as P2-$Na_{2/3}[Fe_{1/2}Mn_{1/2}]O_2$ [16], hard-carbons [17], titanates as $Na_2Ti_3O_7$ [18]). We can thus reasonably rule out the intrinsic conductivity of the aqueous electrolyte as origin of the lower polarization.

On the other hand, although the electrode's ionic diffusivity has an important contribution to the overall polarization; it is an intrinsic property of the material and should not be affected by the electrolyte choice. The origin of the lower polarization of the aqueous electrolyte must thus reside in the electrode-electrolyte interfacial region rather than in the ionic diffusivities of the individual components. One can cite for instance the overpotential due to the less facile desolvation step of the Na ion in non-aqueous electrolyte, which would be translated in a larger charge-transfer resistance [19] or the better wetting of the active materials due to the lower viscosity of aqueous electrolyte [11], which would reduce the polarization related to the diffusion of the electrode material by increasing the effective amount of interface open to ion insertion. This later hypothesis is further supported by the fact that it has been demonstrated that the delithiation of $LiFePO_4$, a necessary step in the synthesis of $FePO_4$ and $NaFePO_4$, generates an important porosity of the materials surface due to the release of mechanical stress between Li-rich and Li-poor phases [20]. This could be additionally accentuated in the $FePO_4$/$NaFePO_4$ system since the cell mismatch is much higher than for the Li counterpart, although it is likely that the carbon coating may buffer this effect to some extent. This suggests that the electrochemical performance of $NaFePO_4$ in organic electrolyte may be greatly improved by optimizing the characteristics of the materials surface and/or coating.

Another mean to reduce polarization is to increase the operating temperature [3]. Fig. 4. 10 shows the comparison of aqueous and organic cells cycled at 55 ˚C with a window of 2.55 to 3.2 V *vs*. Na^+/Na. Since this material exhibits a rather flat voltage-composition profile, the effect is notable and much larger capacity values are obtained in both media. In particular, the effect is quite drastic in organic electrolyte, as the 0.2C capacity has more than doubled reaching 85 mAh g^{-1} (Fig. 4. 10a), a value that overcomes that obtained at the same rate in a wider window (see figure 4.3). A reduction of 50% in polarization can be observed in this medium at 0.2C, from 0.450 V at room temperature to 0.220 V at 55 ˚C.

In aqueous electrolyte the improvement is also noticeable and an excellent performance is obtained. Indeed the capacity at 0.2C reaches now 110 mAh g^{-1} and almost 87 mAh g^{-1} at 1C,

while this is the capacity value achieved at 0.2C in organic electrolyte at this temperature for the same voltage window. At 2C the capacity is still above 70 mAh g^{-1} (Fig. 4. 10b), demonstrating that aqueous $NaFePO_4$ cells can be considered a very interesting candidate for low-cost high rate applications. While the reduction in polarization in the aqueous electrolyte was not as drastic as in organic medium, a change from 0.270 V at room temperature to 0.200 V at 0.2C is still obtained.

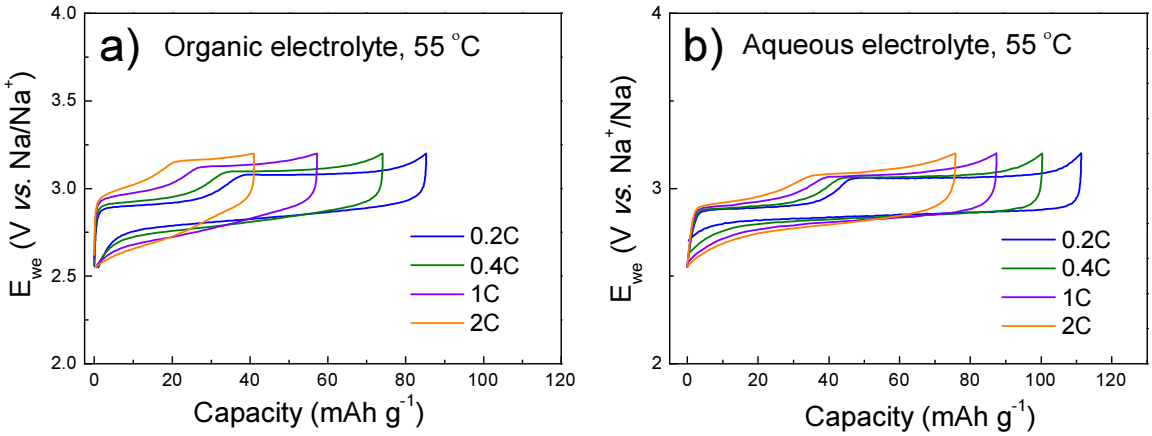

Fig. 4. 10. (a) Voltage *vs*. capacity plot at different rates for an organic cell and (b) an aqueous cell cycled between 2.55-3.2 V *vs*. Na^+/Na at 55 °C.

Table 4. 4. Values of capacity and polarization obtained for NaFePO4 cycled at 55 °C at different rates in an aqueous and in an organic half cells at the 5th cycle.

Medium	Rate	Capacity (mAh g^{-1})	Polarization (V)
Aqueous	0.2C	116	0.200
	0.4C	102	0.220
	C	89	0.250
	2C	76	0.290
Organic	0.2C	85	0.220
	0.2C	75	0.270
	C	57	0.330
	2C	41	0.370

4.2.3. Development of an aqueous full cell

To demonstrate the feasibility of this material in a real system, a full cell was built with $NaTi_2(PO_4)_3$ as anode material in a mass ratio 1 : 1. Pressed $NaTi_2(PO_4)_3$ electrodes were used. The pH here was raised to 12 to avoid the oxidation of the anode [21]. Therefore, as the electrochemical characterization of $NaFePO_4$ has been carried pH = 6, $NaFePO_4$ was previously characterized at pH = 12. In Fig. 4. 11a, it can be observed that the behaviour at both pHs is comparable.

The resulting full cell delivers an average voltage of 0.6 V, with an initial capacity of 70 mAh g^{-1} and capacity retention of 76% after 20 cycles (Fig. 4. 11b). The initial capacity may seem modest compared to the 100 mAh g^{-1} reported by Li *et al.* on $FePO_4$ [22], even taking into account the larger molecular weight of $NaFePO_4$. However, it is important to note that our voltage window (2.45 V to 3.3 V *vs*. Na^+/Na) is slightly narrower than theirs (2.55 V to 3.5 V *vs*. Na^+/Na) and we greatly improved the stability upon cycling (although at the cost of a slightly lower capacity). As a matter of fact, since the $NaFePO_4$/AC half cells presented a much better stability upon cycling than the full cell, we can reasonably argue that the major source of capacity fading is in the anode side, which is observed in the chapter 3 of the present work for the pressed electrodes. As these results have been finally obtained in non-optimized lab-scale electrodes and using a very conservative voltage window, we believe that major improvements can be expected if both are optimized according to the application.

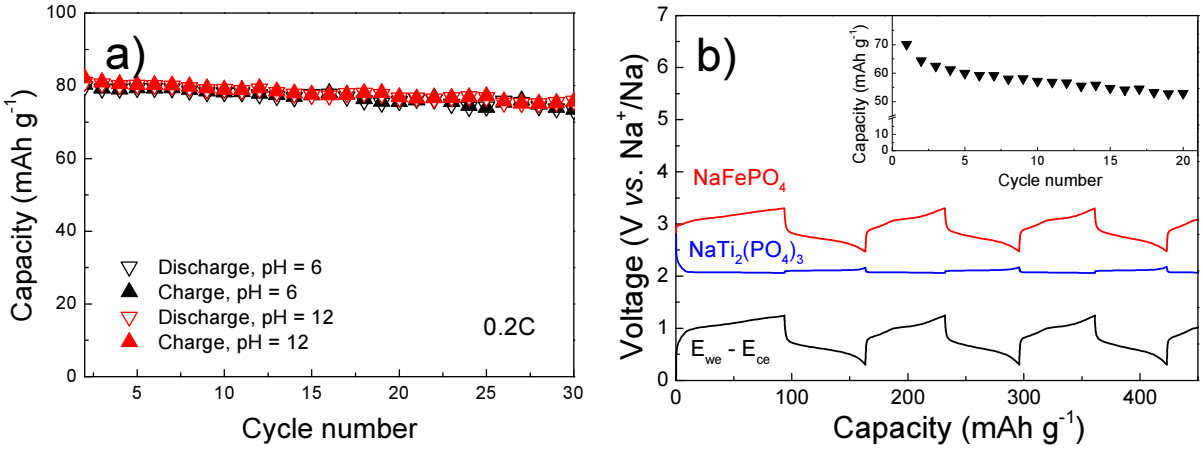

Fig. 4. 11. (a) Specific capacity *vs*. cycle number of two batteries cycled at pH = 6 (black) and pH =12 (red). (b) Voltage *vs*. capacity plot of a $NaFePO_4$ (red line)/$NaTi_2(PO_4)_3$ (blue line) cell with 1 M Na_2SO_4 as electrolyte at pH = 12 (black line: average cell voltage). Inset: Capacity in mAh $g^{-1}_{NaFePO4}$ of the full cell for the first 20 cycles.

4.3. Conclusions

The electrochemical properties of $NaFePO_4$, obtained by chemical delithiation and further sodiation of $LiFePO_4$, in both aqueous and organic media have been studied.

The reduction of the voltage range was demonstrated to be essential to the cycling stability of this material. The origin of capacity fading if the voltage range is not reduced has not been identified, although material dissolution can be ruled out and the XRD pattern of the cycled material does not exhibit extra peaks.

The overpotential in aqueous electrolyte is significantly lower than in organic electrolyte. This notable reduction in polarization, which is discussed in terms of interfacial properties, allows better performances at high rates despite the lower voltage window used in the aqueous cells, reaching a capacity of 70 mAh g^{-1} at 0.2C and 40 mAh g^{-1} at 2C.

At 55 ˚C, the overpotential in both electrolytes is significantly reduced and a much larger capacity is obtained in both media, with a superior performance of the aqueous cells, especially at high rates, achieving 110 mAh g^{-1} at 0.1C and 74 mAh g^{-1} at 2C.

Finally, a full cell battery was built with $NaTi_2(PO_4)_3$ as negative electrode. The cell delivered 0.6 V and 70 mAh g^{-1} and demonstrated that $NaFePO_4$ is a promising candidate for aqueous Na-ion cells.

[1] R. Malik, A. Abdellahi, Ceder, G. A Critical Review of the Li Insertion Mechanisms in $LiFePO_4$ Electrodes, J. Electrochem. Soc. 160 (2013) A3179-A3197
[2] P. Moreau, D. Guyomard, J. Gaubicher, F. Boucher, Structure and stability of sodium intercalated phases in olivine $FePO_4$. Chem. Mater. 22 (2010) 4126–4128
[3] M. Casas-Cabanas, V.V. Roddatis, D. Saurel, P. Kubiak, J. Carretero-Gonzalez, V. Palomares, P. Serras, T. Rojo, Crystal chemistry of Na insertion/deinsertion in $FePO_4$-$NaFePO_4$, J. Mater. Chem. 22 (2012) 17421–17423
[4] S.M. Oh, S.T. Myung, J. Hassoun, B. Scrosati, Y. Sun, Reversible $NaFePO_4$ electrode for sodium secondary batteries, Electrochem. Commun. 22 (2012) 149–152
[5] R. Tripathi, S.M. Wood, M.S. Islam, L.F. Nazar, Na-ion mobility in layered Na_2FePO_4F and olivine Na [Fe,Mn]PO4, Energy Environ. Sci., 6 (2013) 2257–2264
[6] M. Galceran, D. Saurel, B. Acebedo, V.V. Roddatis, E. Martin, T. Rojo, M. Casas-Cabanas, The mechanism of $NaFePO_4$ (de)sodiation determined by in situ x-ray diffraction, Phys. Chem. Chem. Phys. 16 (2014) 8837–8842
[7] A. Whiteside, C.A.J. Fisher, S.C. Parker, M.S. Islam, Particle shapes and surface structures of olivine $NaFePO_4$ in comparison to $LiFePO_4$, Phys. Chem. Chem. Phys. 16 (2014) 21788–94
[8] Z. Li, D.B. Ravnsbaek, K. Xiang, Y. M. Chiang, $Na_3Ti_2(PO_4)_3$ as a sodium-bearing anode for rechargeable aqueous sodium-ion batteries, Electrochem. Commun. 44 (2014) 12–15
[9] M. Vujkovic, S. Mentus, Fast sodiation/desodiation reactions of electrochemically delithiated olivine $LiFePO_4$ in aerated aqueous $NaNO_3$ solution. J. Power Sources 247 (2014) 184-188
[10] Padhi AK, Nanjundaswamy KS, Goodenough JB. Phospho-olivines as positive-electrode materials for rechargable lithium batteries. J Electrochem Soc 144 (1997) 1188–1190
[11] S. Park, I. Gocheva, S. Okada, J. Yamaki, Electrochemical properties of $NaTi_2(PO_4)_3$ anode for rechargeable aqueous sodium-ion batteries, J. Electrochem. Soc. 158 (2011) 1067–1070
[12] P. He, X. Zhang, Y. G. Wang, L. Cheng, Y. Y. Xia, Lithium-ion intercalation behavior of $LiFePO_4$ in aqueous and nonaqueous electrolyte solutions, J. Electrochem. Soc. 155 (2008) A144–A150
[13] D.J. Kim, R. Ponraj, A.G. Kannan, H-W. Lee, R. Fathi, R. Ruffo, C. M. Mari, D. K. Kim, Diffusion behavior of sodium ions in $Na_{0.44}MnO_2$ in aqueous and non-aqueous electrolytes, J. Power Sources, 244 (2013) 758–763
[14] A. Ponrouch, E. Marchante, M. Courty, J-M. Tarascon, M. R. Palacin, In search of an optimized electrolyte for Na-ion batteries, Energy Environ. Sci. 5 (2012) 8572–8583
[15] Y.J. Zhu, Y.H. Xu, Y.H. Liu, C. Luo, C.S. Wang, Comparison of electrochemical performances of olivine $NaFePO_4$ in sodium-ion batteries and olivine $LiFePO_4$ in lithium-ion batteries. Nanoscale, 5 (2013) 780–787
[16] N. Yabuuchi, M. Kajiyama, J. Iwatate, H. Nishikawa, S. Hitomi, R. Usui, Y. Yamada, S.Komaba, P2-type $Na_x[Fe_{1/2}Mn_{1/2}]O_2$ made from earth-abundant elements for rechargeable Na batteries, Nat. Mater. 11 (2012) 512–517
[17] S. Komaba, T. Ishikawa, N. Yabuuchi, W. Murata, A. Ito, Y. Ohsawa, Fluorinated ethylene carbonate as electrolyte additive for rechargeable Na batteries, ACS Appl Mater. Interfaces 3 (2011) 4165–4168
[18] P. Seguttuvan, G. Rousse, V. Seznec, J-M. Tarascon, $Na_2Ti_3O_7$: Lowest voltage ever reported oxide insertion electrode for sodium ion batteries, Chem. Mater. 23 (2011) 4109-4111
[19] P. He, X. Zhang, Y. G. Wang, L. Cheng, Y. Y. Xia, Lithium-ion intercalation behavior of $LiFePO_4$ in aqueous and nonaqueous electrolyte solutions, J. Electrochem. Soc. 155 (2008) A144–A150
[20] K. Weichert, W. Sigle, P.A. van Aken, J. Jamnik, C. Zhu, R. Amin, T. Acartark, U. Starke, J. Maier, Phase boundary propagation in large $LiFePO_4$ single crystals on delithiation, J. Am. Chem. Soc. 134 (2012) 2988–2992
[21] J-Y. Luo, W.-J. Cui, P. He, Y-Y. Xia, Raising the cycling stability of aqueous lithium-ion batteries by eliminating oxygen in the electrolyte, Nat.Chem. 2 (2010) 760–765
[22] Z. Li, D.B. Ravnsbaek, K. Xiang, Y. M. Chiang, $Na_3Ti_2(PO_4)_3$ as a sodium-bearing anode for rechargeable aqueous sodium-ion batteries, Electrochem. Commun. 44 (2014) 12–15

5. Study of $NaFe_2(CN)_6$ Prussian Blue as cathode material

PB has been widely used as pigment by artists since its discovery in 1704. In 1936, J.F. Keggin and F.D. Miles Neff described its structure determined by X-ray diffraction data as well as that of some related compounds [1].They determined that Na-PB has a cubic framework (space group $Fm\bar{3}m$) with Fe^{2+} and Fe^{3+} located on alternate corners of a cube of corner-shared octahedra bridged by linear $(C{\equiv}N)^-$ anions (Fig. 5. 1). In the late 1970s-early 1980s, different studies highlighted the appealing electrochemical behaviour of PB family of materials due to the presence of open channels for ion diffusion and the redox Fe^{+2}/Fe^{+3} pair [2, 3, 4, 5].

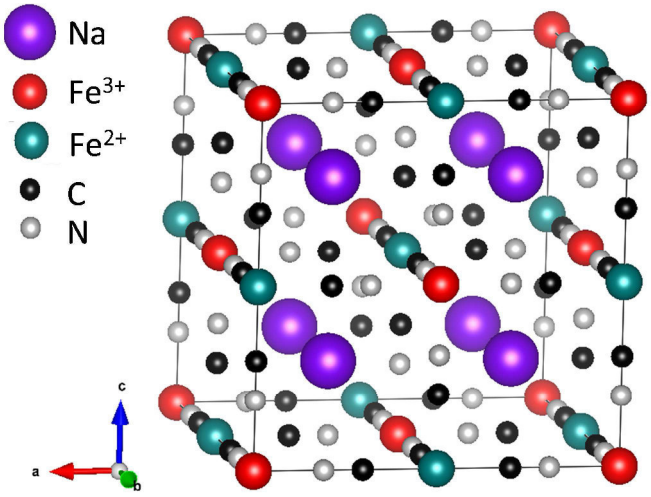

Fig. 5. 1. Crystal structure of Prussian Blue

More recently, PB and PBAs of the type $AMFe(CN)_6{\cdot}xH_2O$ (A = Na, K and M = transition metal), have been revisited as cathode materials for rechargeable alkali-ion batteries (LIBs [6], K-ion batteries (KIBs) [7] and, more recently, NIBs [8]) with encouraging results.

Na (de)intercalation was explored by Lu *et al.* for PBA with M = Mn, Fe, Co, Ni and Zn [8]. The largest capacity, around 100 mAh g^{-1}, was achieved with M = Fe, which reacts at 2.9 and 3.6 V vs. Na^+/Na. You *et al*. later reached a capacity of 170 mAh g^{-1} with sodium PB (Na-PB), $Na_{0.61}Fe[Fe(CN)_6]_{0.94}$, crystallized in the form of nanocubes (Cth = 184 mAh g^{-1}) [9].

The electrochemical performance of this Fe-based compound in aqueous electrolyte was reported during the course of this work by Wu *et al.* with capacities over 100 mAh g^{-1}, although the coulombic efficiency still remains to be improved (around 80% at 1C) [*10*].

Our work has focussed in the study of different cycling conditions (voltage range, pH) to improve the cycling stability of this material. This work has been done in collaboration with M.J. Piernas-Muñoz and Dr. Elizabeth Castillo also from CIC energiGUNE, which also synthesized the material and carried out the electrochemical characterization in organic electrolyte (wide voltage window).

5.1. Synthesis and physicochemical characterization

Na-PB was obtained at room temperature by mixing 100 mL of 40 mM $Na_4[Fe(CN)_6]\cdot 10H_2O$ with 100 mL of 40 mM $FeCl_3\cdot 6H_2O$. When the two solutions came in contact, a blue colour suspension containing PB was formed according to equation 1. No aging time was allowed once the Na-PB suspension was formed.

Since the small PB particles resisted 10 min of centrifugation at 4000 rpm it was necessary to force its precipitation by adding ethanol. Then, after 24 h filtering, washing with ethanol (3 x 10 ml) and drying, dark blue crystal-like aggregates of PB were formed.

$$(1 + (x/3))\ FeCl_3 + Na_4[Fe(CN)_6] \rightarrow Na_{1-x}Fe^{III}_{1+(x/3)}[Fe^{II}(CN)_6]\cdot yH_2O + (3 + x)\ NaCl \qquad \text{(Eq. 1)}$$

The successful formation of Na-PB was confirmed from XRD data. The Le Bail refinement of the material is shown in Fig. 5. 2a. The pattern has been indexed with $Fm\bar{3}m$ space group with a refined *a* cell parameter of 10.221(5) Å. From the profile of diffraction peaks, and after substracting the instrumental contribution using an Instrument Resolution File (IRF) determined with an Al_2O_3 standard, average domain sizes of 5 nm were obtained. Since the presence of the alkaline ion does not affect the length of the cell parameters due to the large volume [1], further analysis are necessary to determine the total amount of Na^+.

A Na: Fe ratio of 0.75: 2.08 was obtained from atomic absorption analysis. TG analysis (Fig. 5. 2b) revealed a mass loss of 18% at T > 300 ˚C which corresponds to 3.5 H_2O molecules per formula unit. By combining both atomic absorption and TGA, $Na_{0.75}Fe_{1.08}[Fe(CN)_6]\cdot 3.5H_2O$ was determined to be the exact composition.

SEM images (see Fig. 5. 2c as example) show a non-homogeneous particle size distribution ranging from ca. 50 nm to 1 µm. An average value of 272 nm was obtained by measuring the size of a representative sample (100 particles). The resulting histogram fits to a log-normal distribution (Fig. 5. 2d). The fact that the particle size observed in the SEM image does not coincide with the crystallite size obtained by XRD indicates Na-PB is formed by polycrystalline particles.

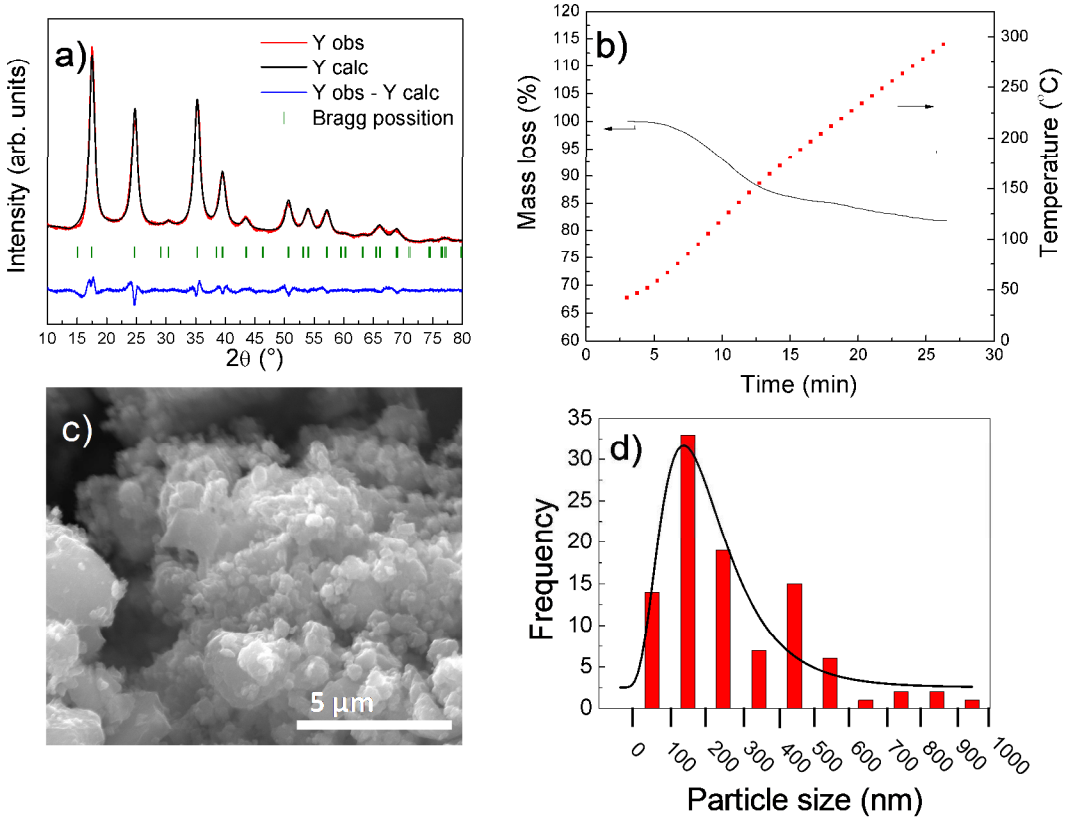

Fig. 5. 2. (a) Le Bail refinement of Na-PB XRD pattern. Experimental (black) and calculated (red) patterns are shown along with the difference curve (blue) and Bragg reflections (vertical bars). (b) Thermogravimetric analysis carried out under N_2 atmosphere, in the temperature range from 30 to 300 °C at 10 °C min^{-1}. (c) SEM image of Na-PB at x20,000 magnification. (d) Histogram of the particle size distribution of a representative sample area (100 particles).

5.2. Electrochemical characterization

Na-PB electrodes were prepared by grounding previously in a mortar the active material, C65 and PVDF in a mass ratio 85:10:5. A slurry of the above-mentioned composition dispersed in *N*-Methyl-2-pyrrolidone (NMP) (99.5% anhydrous, Sigma-Aldrich) was deposited on a stainless steel current collector disk except for the galvanostatic tests up to 4.1 V *vs*. Na^+/Na, at which voltage the oxygen evolution produces steal corrosion and, therefore, the steel current collector was replaced by Ti. The electrodes were dried overnight at 120 ºC under vacuum and pressed at 5 t cm^{-2}.

5.2.1. Electrochemical characterization in organic electrolyte

Fig. 5. 3 shows a cyclic voltammogram of Na-PB from 1.5 to 4.75 V *vs*. Na^+/Na at 1 mV s^{-1} in a half-cell using organic electrolyte 1 M $NaPF_6$ EC:PC (2% vol. FEC). 1 M $NaPF_6$ in EC: PC: FEC (49:49:2) was chosen as organic electrolyte since has been shown to result in the highest

coulombic efficiency and the best capacity retention amongst several studied Na-PB half-cells with different $NaClO_4$-$NaPF_6$ carbonate mixtures [11].

As expected, two main reversible processes are observed upon charge [8,9], located at 3.22 and 3.83 V *vs*. Na^+/Na, and upon discharge, at 2.55 and 3.15 V *vs*. Na^+/Na. The charge and discharge peaks are significantly separated, which is indicative of a considerable polarization. The process at lower potential corresponds to the reduction from Na-PB to sodium Prussian White (Na-PW), $Na_2Fe^{II}[Fe^{II}(CN)_6]\cdot yH_2O$, and the process at higher potential corresponds to oxidation from Na-PB to Berlin Green (BG), both reversible, as shown in Fig. 5. 3 and in accordance with Eq1.

$$\underset{\text{(Na-PW)}}{Na_{2-x}Fe^{II}_{1+x/3}[Fe^{II}(CN)_6]\cdot yH_2O} \underset{\leftarrow}{\rightarrow} \underset{\text{(Na-PB)}}{Na_{1-x}Fe^{III}_{1+x/3}[Fe^{II}(CN)_6]\cdot yH_2O} \underset{\leftarrow}{\rightarrow} \underset{\text{(BG)}}{Fe^{III}_{1+x/3}[Fe^{III}_{1-x}Fe^{II}_{x}(CN)_6]\cdot yH_2O}$$

(Eq. 1)

In the process at higher potential, a small shoulder appears at 4 V in agreement with the several plateaux observed in other publications (Fig. 5. 3). This shoulder could be indicative of a more complex mechanism that includes an intermediate phase, although further investigation is needed to confirm this hypothesis.

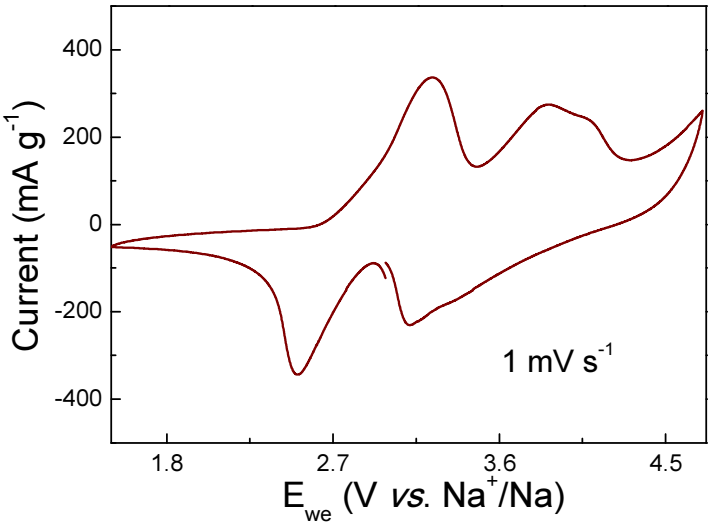

Fig. 5. 3. (a) Cyclic voltammogram of the 2nd cycle at 1 mV s^{-1} of Na-PB in 1 M $NaPF_6$ EC: PC: FEC 49:49:2, in the voltage range from 1.5 to 4.75 V *vs*. Na^+/Na.

5.2.2. Electrochemical characterization in aqueous electrolyte

5.2.2.1. Electrochemical characterization in a large voltage range

When Na-PB was tested in aqueous electrolyte by cyclic voltammetry from 2.6 to 4.2 V *vs*. Na^+/Na both processes are also observed (Fig. 5. 4) although the peaks are shifted to somewhat higher values (3 V and 3.8 V *vs.* Na^+/Na in aqueous electrolyte with respect to the average voltage of 2.9 V and 3.5 V *vs.* Na^+/Na observed in organic media), in agreement with the values observed in a previous report [10]. A strong decrease in polarization (from ca. 0.67 V for both redox processes in organic electrolyte to around 0.35 V in aqueous electrolyte) is also noticed. The oxidation of PB to BG partially overlaps with H_2O decomposition, which is at the origin of the significant observed irreversibility (the theoretical O_2 evolution onset is 3.58 V *vs*. Na^+/Na at pH = 6).

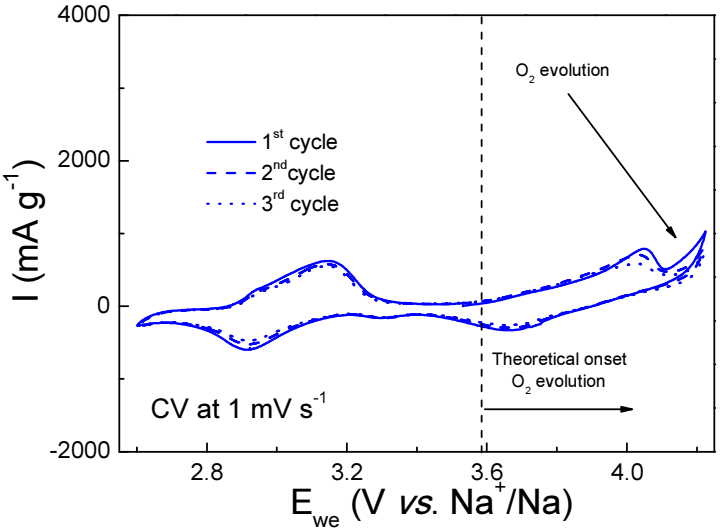

Fig. 5. 4. Cyclic voltammograms (3 first cycles) at 1 mV s^{-1} of Na-PB in the voltage window from 2.6 to 4.2 V using 1 M Na_2SO_4 aqueous electrolyte.

The instability of Na-PB in aqueous electrolyte at high potential is further demonstrated when it is galvanostatically cycled between 2.7 and 4.1 V vs. Na^+/Na at a slow rate such as 0.2C, since a continuous charge at around 3.55 V *vs*. Na^+/Na is observed that impedes achieving the second process and only stops when the time limitation is reached (Fig. 5. 5a). On the other hand, when the material is cycled at a higher rate such as 14C the oxidation to BG is kinetically favoured with respect to electrolyte decomposition and can be partially achieved (inset Fig. 5. 5b), but the battery quickly self-discharges during relaxation periods and the voltage of the cell decreases to a value close to its initial OCV (3.165 V *vs*. Na^+/Na) in less than one hour (Fig. 5. 5b).

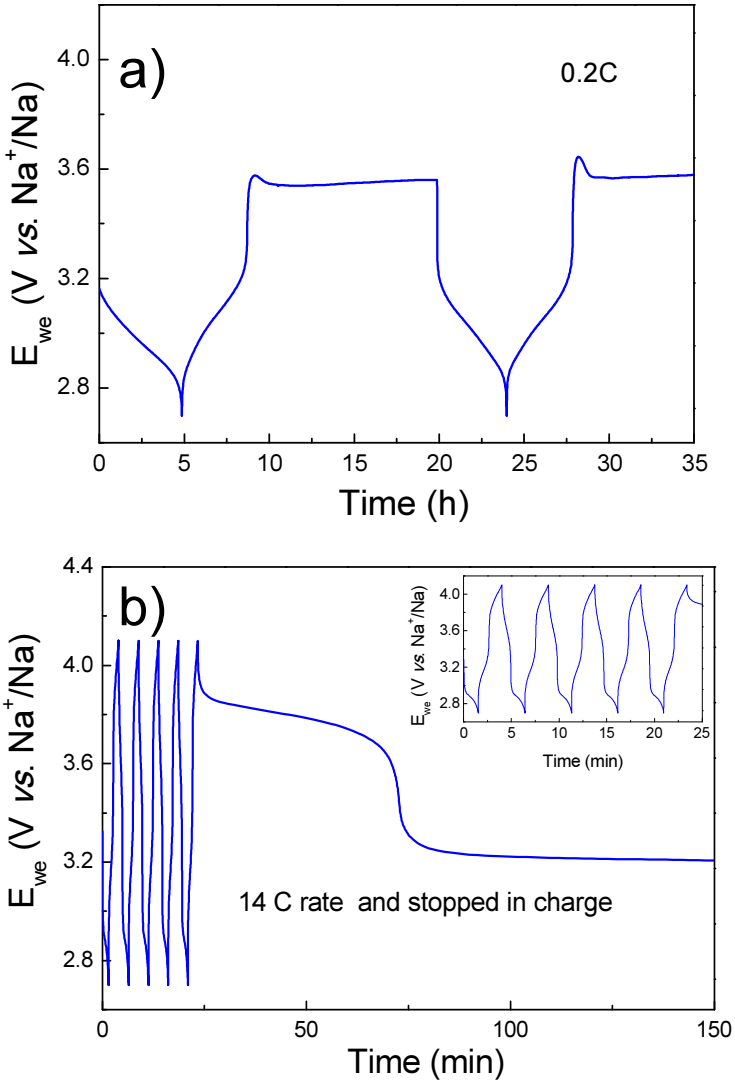

Fig. 5. 5. (a) Voltage *vs*. time plot of Na-PB between 2.7 and 4.1 V *vs*. Na^+/Na at 0.2C in aqueous electrolyte and (b) Voltage *vs*. time plot at 14C between 2.7 and 4.1 V *vs*. Na^+/Na in aqueous electrolyte and OCV variation of the charged battery (inset: zoom of the 5 cycles before stopping).

In order to evaluate whether the irreversibility was due to material dissolution or to the loss of electrical contact between electrode material and current collector originated by the formation of O_2 gas, cycled batteries were disassembled and further analysed. Solubility tests done by dissolving 3 mg of active material in 20 ml of water and the electrolyte proved that pristine Na-PB is soluble in water but not in the electrolyte (Fig. 5. 6a). BG was also found to be insoluble when an electrode was charged at 0.05C in an organic half-cell hold 20 h at 4.25 V (Fig. 5. 6b) and immersed in 20 ml of aqueous electrolyte (Fig. 5. 6c). Solubility can thus be ruled out. On the contrary, an important part of the active material was found deposited on the separator (Fig. 5. 6d). Therefore, bubble formation from evolution of O_2 is most likely responsible of the detachment of PB particles from the electrode film and capacity fading.

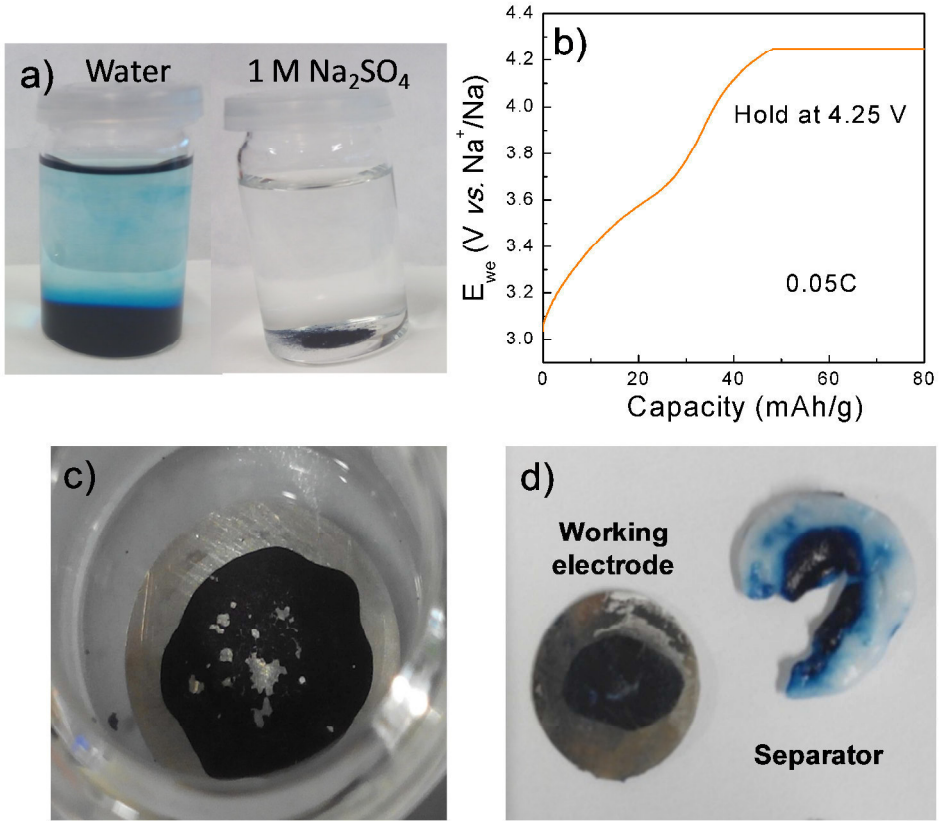

Fig. 5. 6. (a) Solubility test of the recovered electrode and solubility test in 20 ml of 1 M Na_2SO_4 electrolyte.(b) Solubility tests of Na-PB in aqueous electrolyte and water by addition of 3 mg of powder in 20 ml of solution. (c) Voltage *vs.* capacity plot of a battery after a first charge at 0.05C and hold 20 hours at 4.25 V *vs*. Na^+/Na. (d) Working electrode and separator from the disassembled battery represented in Fig. 5. 5a.

One possibility to avoid O_2 evolution at the end of charge is to reduce the electrolyte's pH to shift the stability voltage range of the aqueous electrolyte towards higher potentials. For this purpose, the 1 M Na_2SO_4 solution used as electrolyte was acidified by addition of H_2SO_4 to achieve a pH = 2. As can be observed in Fig. 5. 7a, the second process is partially achieved but there is still competition with electrolyte decomposition and the oxidation of the Na-PB is not totally completed. Furthermore, as occurred with previous experiments at pH = 6, the active material was partially deposited on the separator (Fig. 5. 7b). Therefore, even using an acid electrolyte, the formation of O_2 hampers the utilization of Na-PB in a practical device.

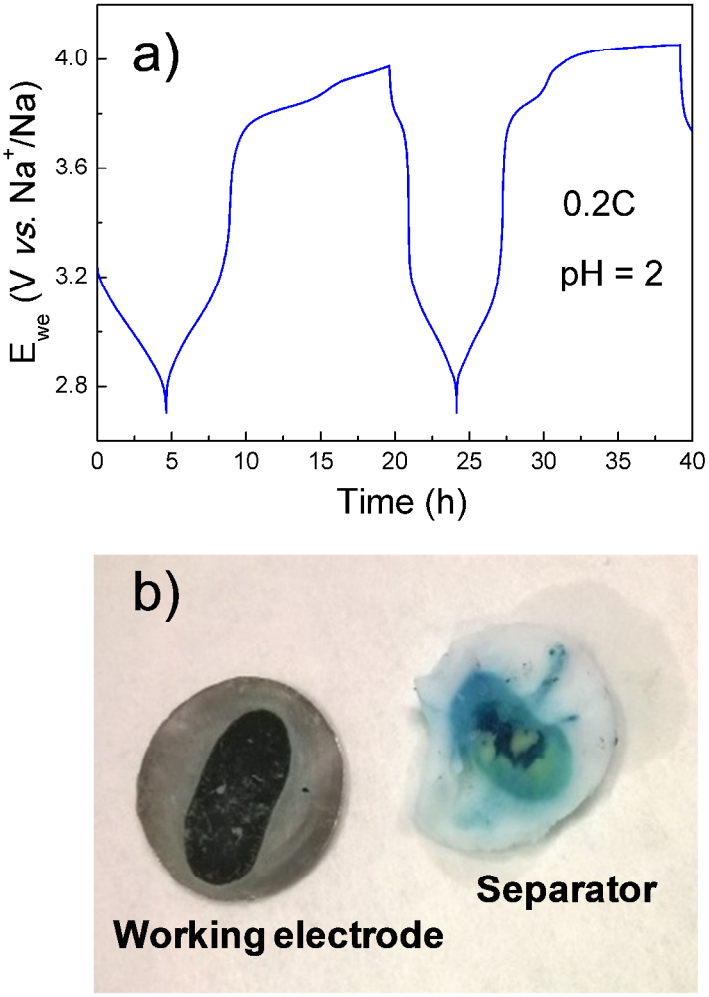

Fig. 5. 7. (a) Voltage vs. time plot of Na-PB between 2.7 and 4.1 V *vs.* Na^+/Na at 0.2C in aqueous electrolyte acidified at pH = 2 (b) Working electrode and separator from the dissembled battery.

5.2.2.2. Electrochemical characterization in a reduced voltage range

Since concurrent electrolyte decomposition results in impractical cells (electrode detachment, need to cycle at high rate, self-discharge), the strategy was changed and, to obtain a better cycling stability, the voltage window was reduced to only include the process from Na-PB to Na-PW (2.6 to 3.45 V *vs.* Na^+/Na). As expected, a much higher stability can be observed (Fig. 5. 8) and no active material was found on the separator. The choice of this narrower window obviously results in a lower capacity, but in this case such a trade-off is required for a good system's stability.

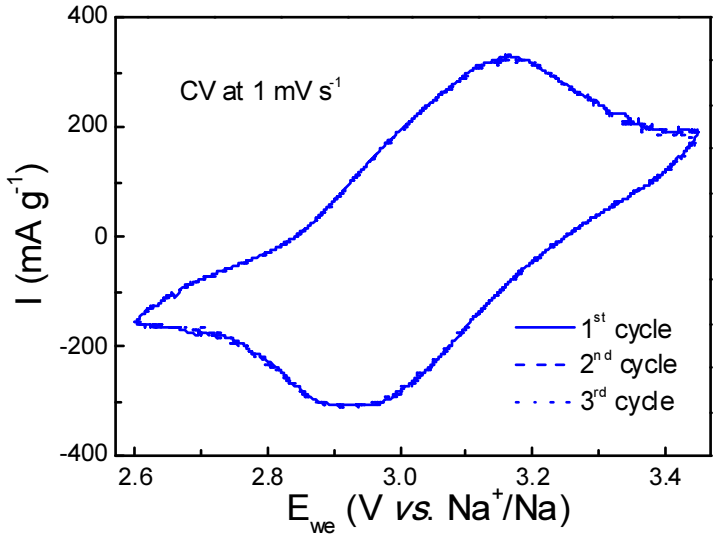

Fig. 5. 8. Cyclic voltammogram (3 first cycles) at 1 mV s^{-1} of Na-PB in the voltage window from 2.6 to 3.45 V *vs*. Na^+/Na using 1 M Na_2SO_4 aqueous solution.

This good stability is further confirmed in the galvanostatic tests carried out at 0.2C and 1C between 2.7 and 3.35 V *vs*. Na^+/Na (see Fig. 5. 9). As can be seen in this figure, the initial reversible capacity at 0.2C is 61 mAh g^{-1}. These capacities are similar to those reported by Wessells *et al.* [12,13], Pasta *et al.* [14] and Wu *et al.* [15] for other PB analogues such as CuHCF, NiHCF and MnHCF. After 50 cycles, 53 mAh g^{-1} are still retained, corresponding to 87% of capacity retention (capacity retention has been calculated with respect to the 2nd discharge).

At 1C (Fig. 5. 9b), the initial reversible capacity was 50 mAh g^{-1} with a capacity retention of 84% (42 mAh g^{-1}) after 200 cycles. Wu *et al*. reported 93% of capacity retention over 40 cycles using a current density of 125 mA g^{-1} when the 2 redox processes were studied. Here, with the reduced voltage window, the capacity retention after 40 cycles is still 98% even using a lower current density (92.16 mA g^{-1}). The absence of O_2 evolution leads to significantly improved coulombic efficiencies close to 100% at 1C (Fig. 5. 9b), compared to 80% obtained at 1C when the voltage window is opened to form BG.

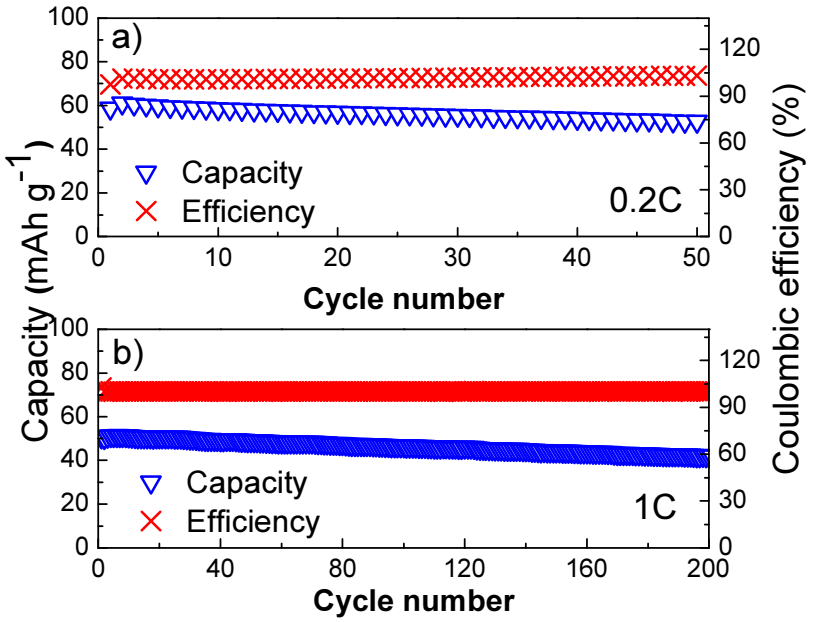

Fig. 5. 9. (a) Discharge specific capacity and coulombic efficiency of two Na-PB aqueous cells cycled in the voltage range from 2.7 to 3.35 V *vs.* Na^+/Na at (a) 0.2C and (b) 1C rates.

The XRD pattern of the cycled electrode is shown in Fig. 5. 10. From its Le Bail refinement it can be concluded that no structural deformations occur after 200 cycles. The refinement did not show changes in the cell parameter value (a = 10.232(3) Å). The 2θ range between 40 º and 52 º was not refined due to the overlap with the current collector.

Rate capability tests carried out from 2.7 to 3.35 V *vs*. Na^+/Na by changing the rate every 5 cycles at 0.2C, 0.4C, 1C, 2C, 5C and 10C for both organic and aqueous cells are shown in (Fig. 5. 11 and Table 1). Since the overpotential in organic electrolyte (Fig. 5. 11a) is larger than in aqueous electrolyte (Fig. 5. 11b), the voltage range in organic media was extended from 2.4 to 3.35 V *vs*. Na^+/Na to complete the discharge process. Slightly higher capacities values were achieved for aqueous cells. In organic electrolyte, at 0.2C, 1C and 5C, the displayed capacities were 63, 50 and 39 mAh g^{-1}, respectively, while in aqueous electrolyte, 65, 56 and 42 mAh g^{-1} were achieved at 0.2C, 1C and 5C.

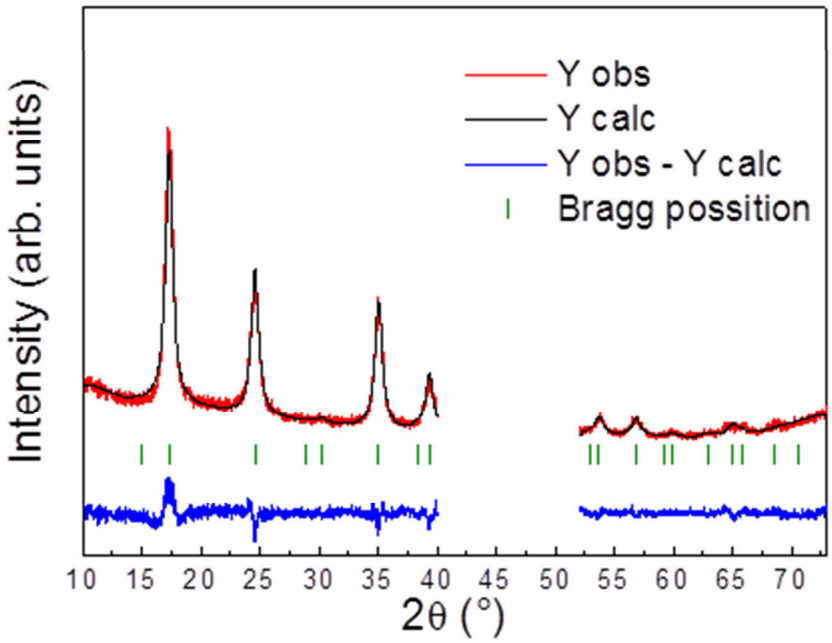

Fig. 5. 10. Le Bail refinement of the XRD pattern of a cycled electrode (200 cycles at 1C, see Fig.5.9 of the manuscript). Experimental (black) and calculated (red) patterns are shown along with the difference curve (blue) and Bragg reflections (vertical bars).

The main differences between both media can be found in the overpotential values which have been calculated as the difference between the average charge and discharge voltages. The overpotential in organic electrolyte is quite significant at all rates and 0.178, 0.259 and 0.540 V were obtained at 0.2C, 1C and 10C, respectively. In aqueous electrolyte the overpotential at 0.2C was almost undetectable (0.018 V). At 1C rate the overpotential was only 0.046 V, and at 10C only increased up to 0.198 V (less than half of the value obtained in organic media). It is worth mentioning that at this C-rate the cell still retained around 40% of the initial capacity with a drastically improved round trip efficiency with respect to organic electrolyte. When the battery is cycled at lower rates after the rate capability tests, the initial capacity is still maintained after at least 45 cycles in both electrolytes (see Fig. 5. 11c), indicating a good cycling stability.

Table 1. Capacity and polarization values at different rates (0.2C, 0.4C, 1C, 2C, 5C and 10C) for an aqueous battery cycled from 2.7 to 3.35 V *vs.* Na^+/Na and an organic battery cycled from 2.4 to 3.35 V *vs.* Na^+/Na.

	Aqueous electrolyte		Organic electrolyte	
Rate	**Capacity**	**Polarization**	**Capacity**	**Polarization**
0.2C	65(1)	0.018(2)	63	0.178
0.4C	62(3)	0.027(1)	55	0.200
1C	56(4)	0.046(3)	50	0.259
2C	51(6)	0.072 (5)	46.5	0.340
5C	42(8)	0.133 (4)	39	0.348
10C	35(9)	0.198 (2)	28	0.540

As in the case of $NaFePO_4$ [16], a lower overpotential was found in aqueous cells. At 0.2C, there is a reduction of 90% of the polarization with respect to organic one. Since the contribution of the conductivity of the electrolyte on the overall cell overpotential in Li-ion and Na-ion batteries is negligible (despite aqueous electrolytes have typically a higher ionic diffusion coefficient compared to organic electrolyte) [17,18], the lower polarization should be related with the more facile desolvation step of sodium in aqueous electrolyte [19] and/or with the lower viscosity and subsequent better wettability [20]. Na-PB experiences a major reduction than $NaFePO_4$, which suggests that indeed the electrode-electrolyte interface also influences in the observed overpotential. An exhaustive comparison between materials and media will be found at the end of this work to better understand the influence of each factor (wettability and desolvation).

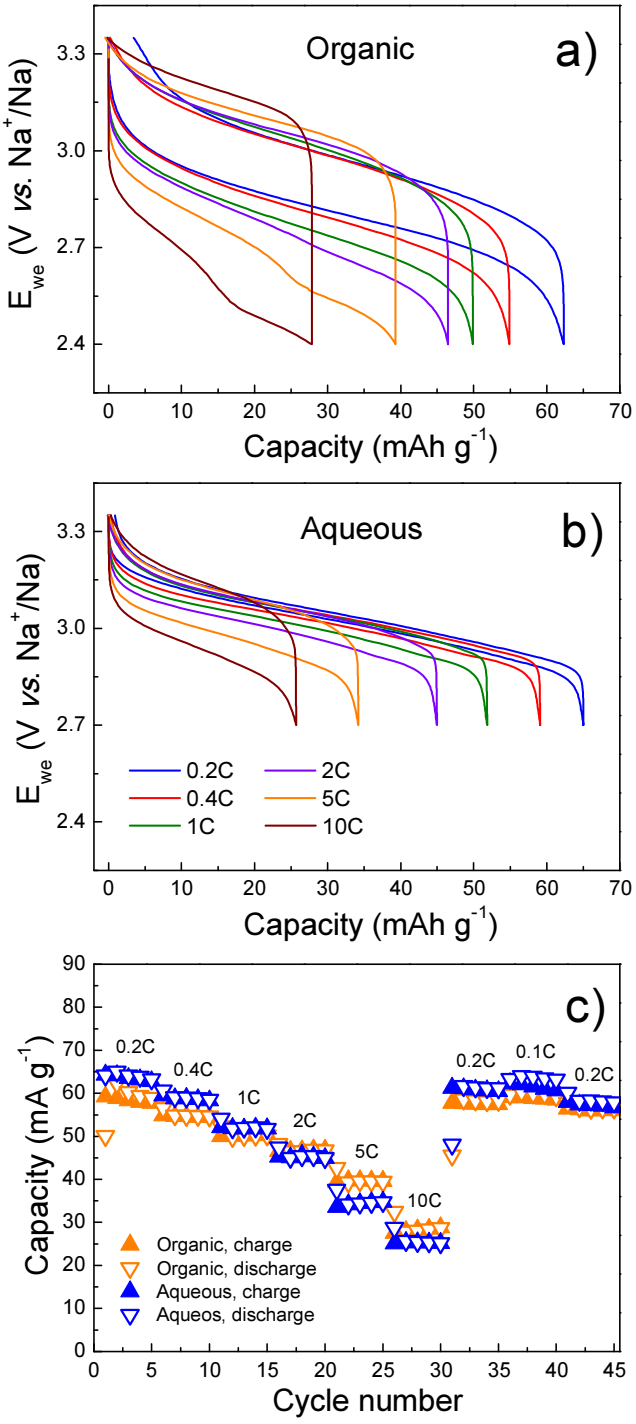

Fig. 5. 11. (a) Voltage *vs*. capacity plots for Na-PB at different rates (0.2C, 0.4C, 1C, 2C, 5C and 10C) for an aqueous cell cycled between 2.7-3.35 V *vs*. Na^+/Na and (b) an organic cell cycled between 2.4-3.35 V *vs*. Na^+/Na, (c) Capacity *vs*. cycle number plot of the rate capability tests carried out for the two different electrolytes.

5.3. Conclusions

The chemical stability of Na-PB cells in 1 M Na2SO4 has been shown to be very dependent on the selected voltage range. At pH = 6, the second process from Na-PB to BG cannot be achieved when cycling at low rate (0.2C) because of electrolyte decomposition. Even at high rate there is competition with the electrolyte decomposition which leads to low coulombic efficiencies and detachment of the material from the current collector due to bubble formation, which would result in impractical cells. At pH = 2, this process at high potential can be only partially achieved, with severe fading and low coulombic efficiencies. Therefore, to achieve a better electrochemical stability, the voltage range should be limited.

Remarkable coulombic efficiencies over 99% at 1C and over 98% at 0.2C can be achieved focussing on the first redox process from Na-PB to Na-PW. Moreover, this voltage limitation led to improved cycling stability (87% and 97% at 0.2C and 1C after 50 cycles) in comparison to reported values.

Reversible capacities of 65 and 52 mAh g^{-1} at 0.2C and 1C respectively have been obtained despite limiting the voltage range and a very low overpotential has been measured (0.018 V at 0.2C), which results in an excellent round trip efficiency.

The promising performance of Na-PB together with the fact that it is a material easy to synthesize and made of low-cost earth-abundant elements, make it a very appealing candidate for aqueous systems able to compete with current stationary storage systems.

[1] J.F. Keggin, F.D. Miles, Structures and formulae of the Prussian Blues and related compounds, Nature 137 (1936) 577-578

[2] V. D. Neff, Electrochemical oxidation and reduction of thin films of Prussian Blue, J. Electrochem. Soc. 125 (1978) 886-887
[3] D. Ellis, M. Eckhoff, V. D. Neff, Electrochromism in the mixed-valence hexacyanides. 1. Voltammetric and spectral studies of the oxidation and reduction of thin films of prussian blue, J. Phys. Chem. 85 (1981) 1225-1231
[4] V. D. Neff, Some performance characteristics of a Prussian Blue battery, J. Electrochem. Soc. 132 (1985) 1382-1384
[5] K. Itaya, H. Akahoshi, S. Toshima, Electrochemistry of Prussian Blue modified electrodes: an electrochemical preparation method", J. Electrochem. Soc. 129 (1982) 1498-1500.
[6] N. Imanishi , T. Morikawa, J. Kondo, Y. Takeda, O. Yamamoto, N. Kinugasa, T. Yamagishi, Lithium intercalation behavior into iron cyanide complex as positive electrode of lithium secondary battery, J. Power Sources 79 (1999) 215–219
[7] A. Eftekhari, Potassium secondary cell based on Prussian blue cathode, J. Power Sources 126 (2004) 221-228
[8] Y. Lu, L. Wang, J. Cheng, and J. B. Goodenough, Prussian blue: a new framework of electrode materials for sodium batteries, Chem. Commun. 48 (2012) 6544-6546
[9] Y. You, X.-L. Wu, Y.-X. Yin, Y.-G. Guo, High-quality Prussian blue crystals as superior cathode materials for room-temperature sodium-ion batteries, Energy Environ. Sci. 7 (2014) 1643-1647
[10] X. Wu, Y. Luo, M. Sun, J. Quian, Y Cao, X Ai, H. Yang, Low-defect Prussian blue nanocubes as high capacity and long life cathodes for aqueous Na-ion batteries, NANO ENERGY 13 (2015) 117-123
[11] M.J. Piernas-Muñoz, E. Castillo-Martínez, J.L. Gómez-Cámer, T. Rojo, "Optimizing the electrolyte and binder composition for Sodium Prussian Blue, $Na_{1-x}Fe_{x+(1/3)}(CN)_6 \cdot yH_2O$, as cathode in sodium ion batteries", Electrochim. Acta (accepted, 2016)
[12] C. D. Wessells, S. V. Peddada, R. A. Huggins, Y. Cui, Nickel hexacyanoferrate nanoparticle electrodes for aqueous sodium and potassium ion batteries, Nano Lett. 11 (2011) 5421-5425
[13] C.D. Wessells, S. V. Peddada, M. T. McDowell, R. A. Huggins, Y. Cui, The effect of insertion species on nanostructured open framework hexacyanoferrate battery electrodes", J. Electrochem. Soc. 159 (2012) A98-A103
[14] M. Pasta, C. D.Wessells, N. Liu, J. Nelson, M. T. McDowell, R. A. Huggins, M. F. Toney, Y. Cui, Full open-framework batteries for stationary energy storage, Nat. Commun. 5 (2014) 3007
[15] X. Wu, Y. Cao, X. Ai, J. Quian and H. Yang, "A low cost and environmentally benign aqueous rechargeable sodium-ion battery based on $NaTi_2(PO_4)_3$-$Na_2NiFe(CN)_6$", Electrochem. Commun. 31 (2013) 145-148
[16] A.J. Fernández-Ropero, D. Saurel, B. Acebedo, T. Rojo, M. Casas-Cabanas, Electrochemical characterization of $NaFePO_4$ as positive electrode in aqueous sodium-ion batteries, J. Power Sources, 291 (2015) 40-45
[17] A. Ponrouch, E. Marchante, M. Courty, J-M. Tarascon, M. R. Palacin, In search of an optimized electrolyte for Na-ion batteries, Energy Environ. Sci. 5 (2012) 8572–8583
[18] Y.J. Zhu, Y.H. Xu, Y.H. Liu, C. Luo, C.S. Wang, Comparison of electrochemical performances of olivine $NaFePO_4$ in sodium-ion batteries and olivine $LiFePO_4$ in lithium-ion batteries, Nanoscale, 5 (2013) 780–787
[19] P. He, X. Zhang, Y. G. Wang, L. Cheng, Y. Y. Xia, Lithium-ion intercalation behavior of $LiFePO_4$ in aqueous and nonaqueous electrolyte solutions, J. Electrochem. Soc. 155 (2008) A144–A150
[20] S. Park, I. Gocheva, S. Okada, J. Yamaki, Electrochemical properties of $NaTi_2(PO_4)_3$ anode for rechargeable aqueous sodium-ion batteries, J. Electrochem. Soc. 158 (2011) 1067–1070

6. Study of $Na_4Fe_3(PO_4)_2P_2O_7$ as cathode material

The combination of different polyanion groups with transition metals offers multiple choices to discover new cathode materials for both Li and Na-ion batteries with the desired requirements [1,2]. In this regard, the combination of phosphate $(PO_4)^{3-}$ and pyrophosphate $(P_2O_7)^{4-}$ groups has been recently explored as an interesting strategy to raise the voltage of polyanionic materials [3,4] and the synthesis and the electrochemical performance in organic electrolyte of $Na_4Fe_3(PO_4)_2P_2O_7$ has been recently reported by Kim *et al.*[5,6].

Fig. 6. 1 shows a schematic representation of the crystal structure of this material. The crystal framework is composed of a 3D network of $[Fe_3P_2O_{13}]_\infty$ infinite layers parallel to the b−c plane. These $[Fe_3P_2O_{13}]_\infty$ layers are connected along the a-axis by P_2O_7 groups, that produces large tunnels for Na-diffusion along the b-axis. There are four symmetrically distinguishable Na sites in the crystal, and these are connected to each other throughout the 3D framework. Two Na sites (Na2 and Na3), formed by seven coordinated NaO_7 polyhedra and NaO_6 octahedra, are present along the a-axis. Two other Na sites (Na1 and Na4), formed by NaO_6 octahedra, are located on the b−c plane [6].

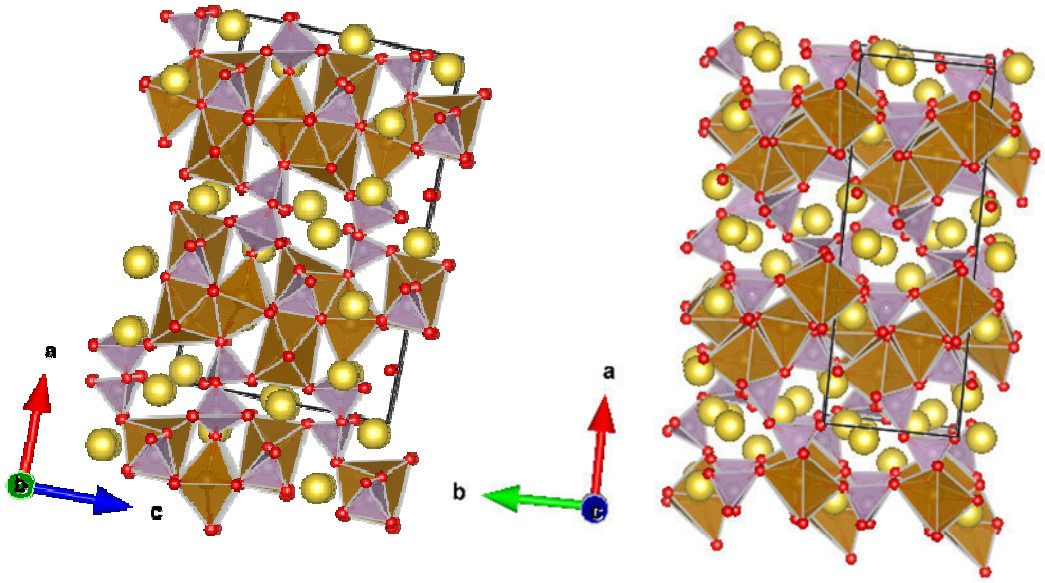

Fig. 6. 1. Crystal structure of the $Na_4Fe_3(PO_4)_3P_2O_7$crystal structure.

$Na_4Fe_3(PO_4)_3P_2O_7$ theoretically deinserts three Na^+ if all the Fe^{2+} is oxidized to Fe^{3+} (C_{th} = 129 mAh g^{-1}). About 82% of the theoretical capacity was obtained at 0.05C with an average voltage of 3.2 V *vs*. Na^+/Na and with relatively good cycle stability. Good cycle performance was also observed at higher C-rates (0.1C and 0.2C) with only a slight reduction of capacity [6]. The electrochemical process occurs as a one-phase reaction with a reversible structural evolution that includes P_2O_7 distortion. The unusually small volume change (4%) observed during cycling is expected to contribute to its stable cycle retention.

Although polyanionic compounds as phosphates [7] and pyrophosphates [8] have already been explored in aqueous systems, mixed polyanion materials still remain unexplored. Since $Na_4Fe_3(PO_4)_2P_2O_7$ meets the requirements set for aqueous systems (inexpensive elements, operation voltage), we decided to include this material in our investigation. This work has been done in collaboration with Marine Reynaud also from CIC energigune who participated in the synthesis of the material.

6.1. Synthesis and physicochemical characterization

$Na_4Fe_3(PO_4)_2P_2O_7$ was synthesized via a conventional two-step solid-state route from low-cost precursors, following a procedure similar to the one described by Kim *et al*. [5] A mixture of sodium pyrophosphate $Na_4P_2O_7$ (95%, Aldrich), iron oxalate $FeC_2O_4{\cdot}2H_2O$ (99%, Aldrich) and ammonium phosphate monobasic $NH_4H_2PO_4$ (98.5%, Aldrich) or dibasic $(NH_4)_2HPO_4$ (98 % Aldrich) in a 1.2:3:2 molar ratio was thoroughly mixed by dry ball-milling under Ar (Planetary ball mixer Fritsch at 200 rpm for 24h with Zirconia balls with a-sample mass ratio of 30). The mixture of precursors was then pelletized and calcined at 300 ˚C for 6-8 hours under Ar/H_2 flow. After this first heating treatment, the sample was grounded with a mortar and re-pelletized to be annealed a second time under Ar/H_2 flow.

For this second annealing step, the temperature and annealing time were screened from 350 ˚C to 475 ˚C and from 6 to 24 hours. Fig. 6. 2 shows the XRD patterns of the different samples obtained. It was determined that lower temperatures favored the formation of maricite $NaFePO_4$ at the expense of the targeted phase $Na_4Fe_3(PO_4)_2P_2O_7$, while the dwelling time was not a critical parameter. Moreover, impurities of $Na_2FeP_2O_7$ appeared simultaneously to evolution of $Na_4Fe_3(PO_4)_2P_2O_7$. From pseudo-Rietveld refinements (Rietveld refinements without refining the atomic content of the different phases) a quantitative phase analysis was carried out. An example is shown in Fig. 6. 3 for a representative sample obtained after a first calcination treatment at 300ºC for 6 hours and a second heat treatment at 450 ˚C for 12 hours. $Na_4Fe_3(PO_4)_2P_2O_7$ was indexed with $Pn2_1$ space group and $NaFePO_4$ and $Na_2FeP_2O_7$ were indexed with *Pnma* and *P-1* respectively. The final mass ratio for this sample was 79:12:9 ($Na_4Fe_3(PO_4)_2P_2O_7$:$NaFePO_4$:$Na_2FeP_2O_7$). It should be noted that, since it was assumed that each phase was stoichiometric and that exhibited an ideal structure, these values should be taken only as orientative but can give an indication of the trends followed when changing the synthesis conditions. The cell parameters of $Na_4Fe_3(PO_4)_2P_2O_7$ were a = 18.091(1) Å, b = 6.5379(4) Å and c = 10.650(6) Å, in agreement with literature values [5]. This sample is referred as *as prepared* sample.

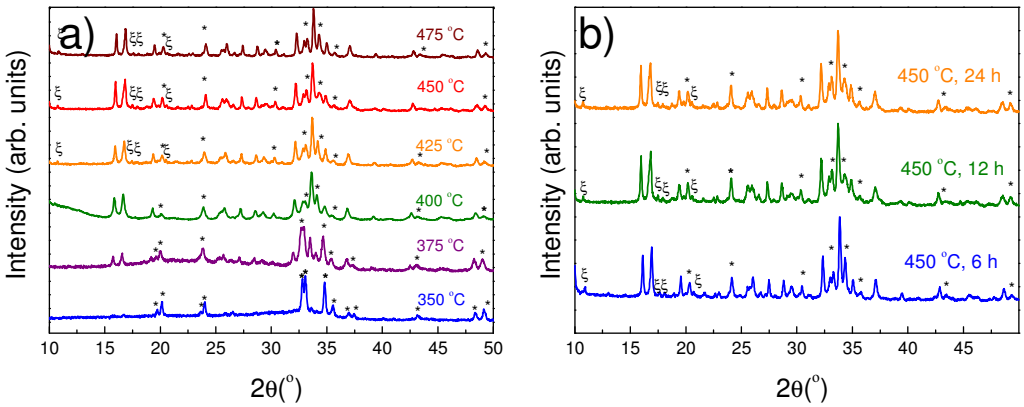

Fig. 6. 2. (a) XRD patterns of $Na_4Fe_3(PO_4)_2P_2O_7$ obtained at different temperatures and (b) at different heating times with the temperature set at 450 ˚C for the second step. The peaks which correspond to $NaFePO_4$ and $Na_2FeP_2O_7$ are highlighted by * and *ξ*, respectively.

A summary of the results obtained in the different synthesis attempts is given in Table 1. As was observed in Fig. 6. 2, at lower temperatures maricite formation is favored. From 400 to 475 no clear correlation between the temperature and final phase ratio can be observed, as occurs with reaction time. Only the sample heated for 24 h had more impurities than others prepared at the same temperature (450 ˚C).

In all the above examples, Ar/H_2 was chosen to prevent the formation of Fe-III compounds such as $Na_3Fe_2(PO_4)_3$, or Fe_2O_3. However, despite these precautions the pellet was often not homogeneous in color after the second heating treatment, with a reddish outer part containing mostly NASICON $Na_3Fe_2(PO_4)_3$ and maricite $NaFePO_4$, and a brown inner part containing mostly the targeted phase $Na_4Fe_3(PO_4)_2P_2O_7$ and maricite $NaFePO_4$ and $Na_2FeP_2O_7$ as secondary phases, as we have shown.

Table 1. Ratio of $Na_4Fe_3(PO_4)_2P_2O_7$, $NaFePO_4$ and $Na_2FeP_2O_7$ determined by pseudo-Rietveld refinement for samples prepared under different the temperature and dwelling time for the second treatment.

Sample	Temperature (˚C)	Dwelling Time (h)	$Na_4Fe_3(PO_4)_2P_2O_7$	$NaFePO_4$	$Na_2FeP_2O_7$
140825_2C1	350	12	12.53	82.96	4.51
140825_1C1	375	12	36.36	52.13	11.51
140818_2C1	400	12	76.52	20.14	3.34
140825_2D1	425	12	69.10	20.74	10.16
140912_C1_in	450	12	66.21	19.47	14.32
140912_F1_in	475	12	74.18	18.99	6.84
140912_D1_in	450	24	64.65	18.55	16.79
140912_E1_in	450	6	73.92	13.9	12.18
140605_2C1	450	6	71.06	14.54	14.40
140605-3D1	450	12	79.2	12.3	8.51
140818-2C1in	450	12	79.9	19.32	0.78

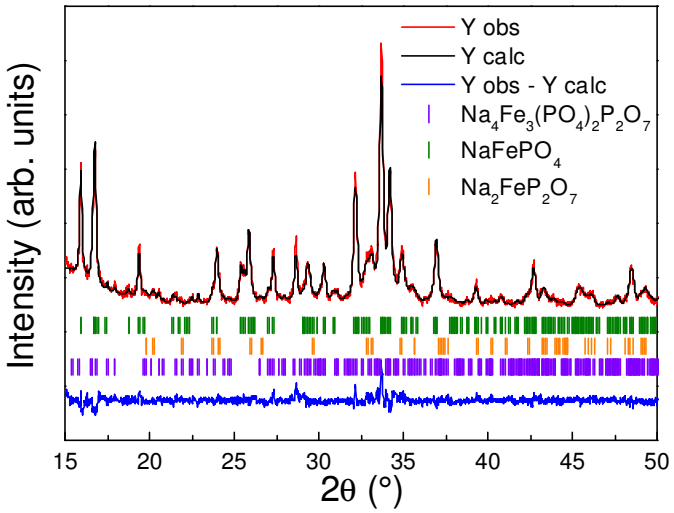

Fig. 6. 3. Pseudo-Rietveld refined XRD pattern of a sample obtained after a first calcination treatment at 300°C for 6 hours and a second heat treatment at 450°C for 12 h. The red line, black line, and blue line represent the observed pattern, calculated pattern, and difference between them, respectively. Vertical markers represent the Bragg position for $Na_4Fe_3(PO_4)_2P_2O_7$ (green), $NaFePO_4$ (orange) and $Na_2FeP_2O_7$ (violet).

In order to reduce the amount of impurities other parameters were additionally modified as the coating of the pellet with C ketjen black powder to avoid surface oxidation. In this case the use of Ar/H_2 was estimated unnecessary and was replaced by cheaper N_2. The use of a Na excess was also avoided. Unfortunately, although there was not oxidation around the pellet, all these attempts resulted unfruitful and a similar phase's mass ratio was obtained (Fig. 6. 4.).

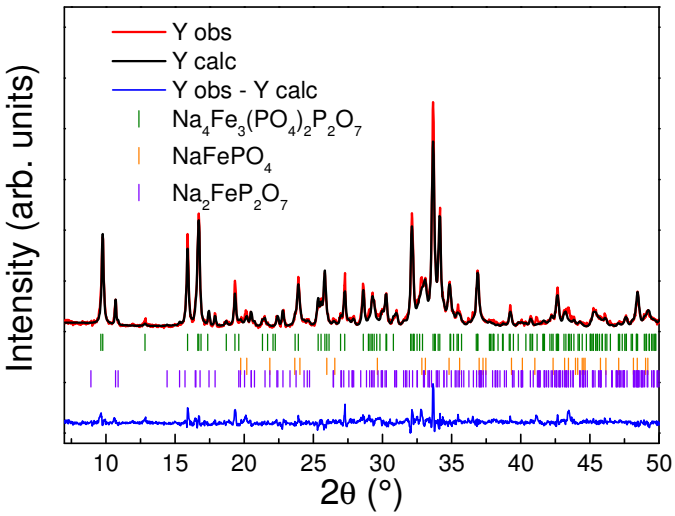

Fig. 6. 4. Pseudo-Rietveld refined XRD pattern of a sample obtained by covering the pellet with C and with stoichiometric ratio Na:Fe. The red line, black line, blue line, and blue line represent the observed pattern, calculated pattern, and difference between them, respectively. Vertical markers represent the Bragg position for $Na_4Fe_3(PO_4)_2P_2O_7$ (green) and maricite $NaFePO_4$ (orange).

On the other hand, when the dry ball-milling step was replaced by wet ball-milling using acetone, a pure phase was obtained and only 2.5% of maricite was detected as impurity from the pseudo-Rietveld refinement (Fig. 6. 5). The obtained $Na_4Fe_3(PO_4)_2P_2O_7$ cell parameters are in agreement with those of the previous samples (a = 18.091(9) Å, b = 6.538(3) Å and c = 10.650(5) Å).

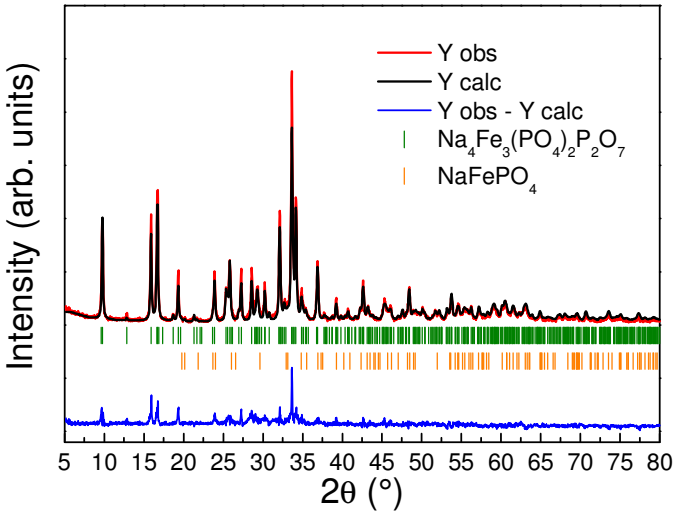

Fig. 6. 5. Pseudo-Rietveld refined XRD pattern of a sample obtained by wet milling of the precursors. The red line, black line, blue line, and blue line represent the observed pattern, calculated pattern, and difference between them, respectively. Vertical markers represent the Bragg position for $Na_4Fe_3(PO_4)_2P_2O_7$ (green) and maricite $NaFePO_4$ (orange).

6.1.1. Ball-milled sample

Since the ceramic method usually results in too large particles for diffusion-limited processes (see Chapter 3) the sample was ball-milled with carbon C65 using the Spex Mixer during 15 minutes in a 80:20 ratio. The purpose was two-fold: (i) to reduce the size of agglomerates and (ii) to obtain a more homogeneous distribution of carbon and electroactive material. This sample had a $Na_4Fe_3(PO_4)_2(P_2O_7)$: $NaFePO_4$: $Na_2FeP_2O_7$ ratio of 79:12:9. XRD patterns recorded before and after the ball-milling process show that the structure of the sample is maintained, with no phase evolution, but the peaks are broader after the ball-milling process, which indicates a decrease of the size of the crystallites (Fig. 6. 6). From the profile of diffraction peaks, and after subtracting the instrumental contribution using an Instrument Resolution File (IRF) determined with an Al_2O_3 standard, average domain sizes were 50 (1) nm and 17 (1) nm before and after the milling treatment. This sample is referred as *ball-milled* sample.

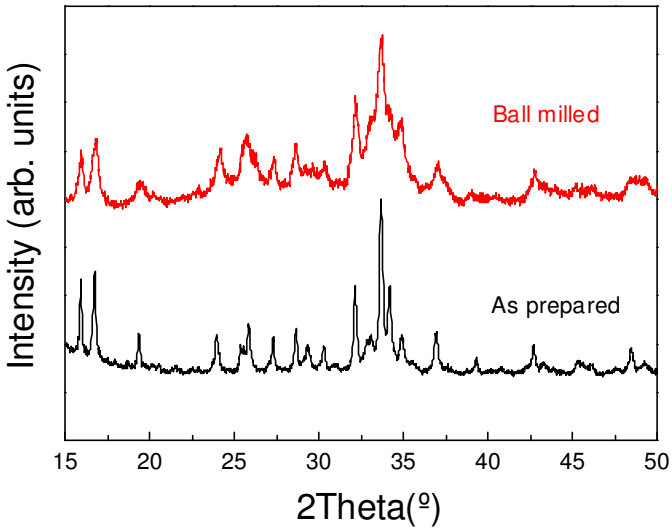

Fig. 6. 6. Comparison of the XRD pattern of the sample before (black line) and after (red line) ball-milling.

6.1.2. C-coated sample

A second approach was carried out to improve electronic conductivity of the material and a carbon coating treatment was done using the method described in chapter 3 for $NaTi_2(PO_4)_3$.

The pristine sample chosen for this treatment had a $Na_4Fe_3(PO_4)_2(P_2O_7)$: $NaFePO_4$: $Na_2FeP_2O_7$ ratio of 81:19:1. The sample was first mixed in a mortar with POE-block-PEG polymer (previously dried under vacuum) in an equimassic ratio (1:1 wt.). Then this mixture was ball-milled for 6 hours under argon at 300 rpm in a Fritsh planetary mixer using zirconia balls in a powder-to-balls ratio of 1:20 wt. The resulting black-brown powder was then calcined at 470°C for 3 hours under Ar/H_2 flow.

TEM images taken after C-coating treatment showed the presence of an amorphous coating with heterogeneous distribution and thickness (Fig. 6. 7). The large amount of amorphous material presumably indicates that not all the polymer was burnt out. However, an increase in temperature, according to Kim *et al*. would imply an increase in maricite $NaFePO_4$ impurities [5]. This sample was referred as *C-coated.*

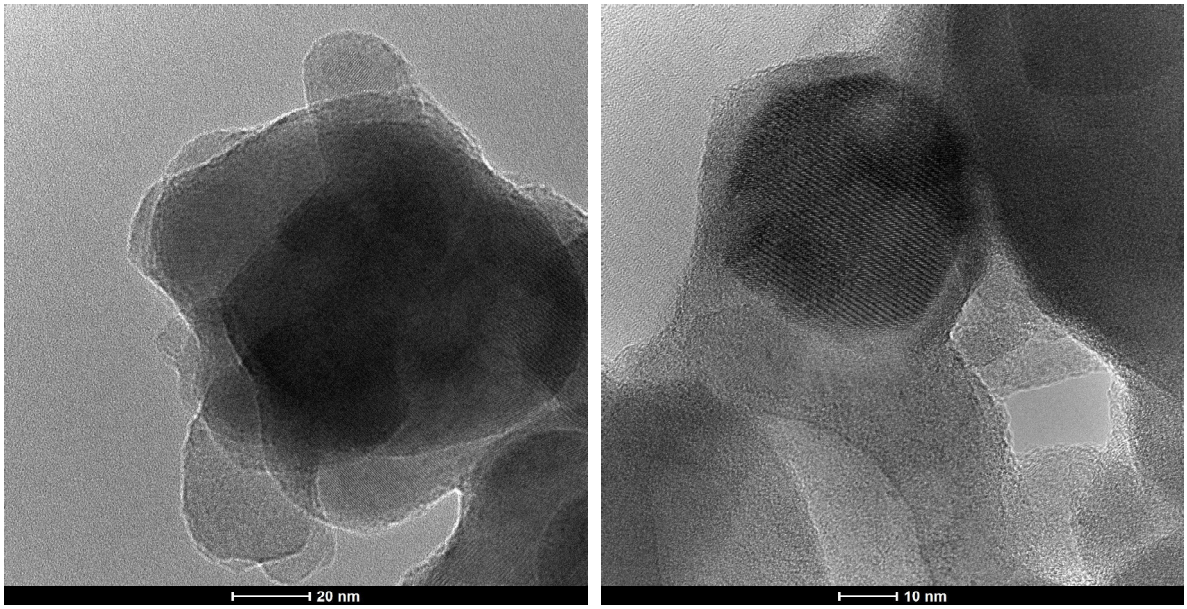

Fig. 6. 7. TEM images of the C-coated sample.

6.1.3. Addition of C to the precursor's mixture

A third strategy was followed to increase the conductivity and carbon was added before calcination of the precursors.

In a first attempt, 10 wt% of carbon C65 was added to the mixture of precursors ($Na_4P_2O_7$ + $FeC_2O_4{\cdot}2H_2O$ + $NH_4H_2PO_4$) before the two-step heating treatment described above. This resulted in a ratio of 19:10:71 of $Na_4Fe_3(PO_4)_3P_2O_7$:$NaFePO_4$:$Na_2FeP_2O_7$ (as determined by pseudo-Rietveld) and the strategy was therefore modified and carbon was added after the first heat treatment in a a lower amount. To do so, the three precursors ($Na_4P_2O_7$ + $FeC_2O_4{\cdot}2H_2O$ + $NH_4H_2PO_4$) were mixed as described earlier, and a pellet of this mixture was calcined at 300 ºC for 6h under Ar/H_2 flow. Then, the pellet was crunched in a mortar and the resulting powder was mixed with 5wt% of carbon C65 using the Spex mixer for 15 min under argon. This mixture was pressed into a pellet and annealed for 6 hours at 450 °C under Ar/H_2. In this case, the pseudo-Rietveld refinement determined the presence of residual precursor $Na_4P_2O_7$ and a ratio of 75:13:8:5 was obtained for $Na_4Fe_3(PO_4)_3P_2O_7$: $NaFePO_4$:$Na_2FeP_2O_7$:$Na_4P_2O_7$ (Fig. 6. 8.). This sample is referred as *C-precursor* sample.

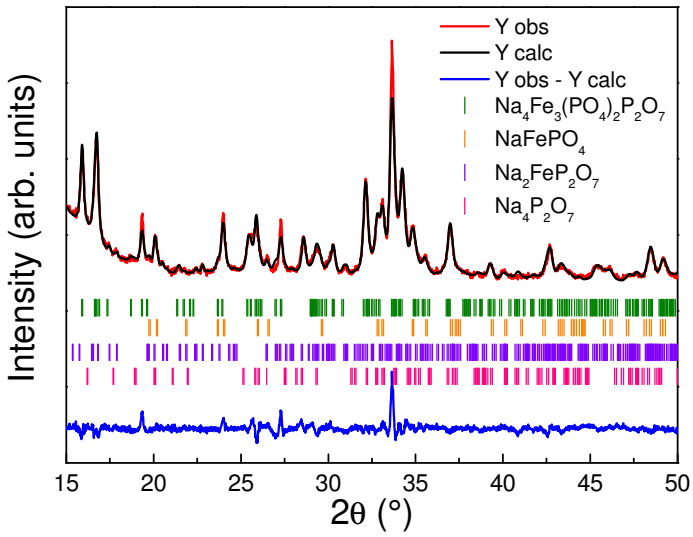

Fig. 6. 8. Pseudo-Rietveld refined pattern of a sample obtained after adding 5% of C65 before the 2nd heat treatment. The red line, black line, and blue line represent the observed pattern, calculated pattern, and difference between them, respectively. Vertical markers represent the Bragg position for $Na_4Fe_3(PO_4)_2P_2O_7$ (green), $NaFePO_4$ (orange) and $Na_2FeP_2O_7$ (violet) and $Na_4P_2O_7$ (pink).

When the dry ball-milling step was replaced by wet ball-milling using acetone, a pure phase was obtained and only 3.6% of maricite was detected as impurity from the Rietveld refinement (Fig. 6. 5). The obtained $Na_4Fe_3(PO_4)_2P_2O_7$ cell parameters are in agreement with those of the previous samples (a = 18.103(2) Å, b = 6.535(6) Å and c = 10.644(1) Å). This sample is referred as *WM C-precursor* sample.

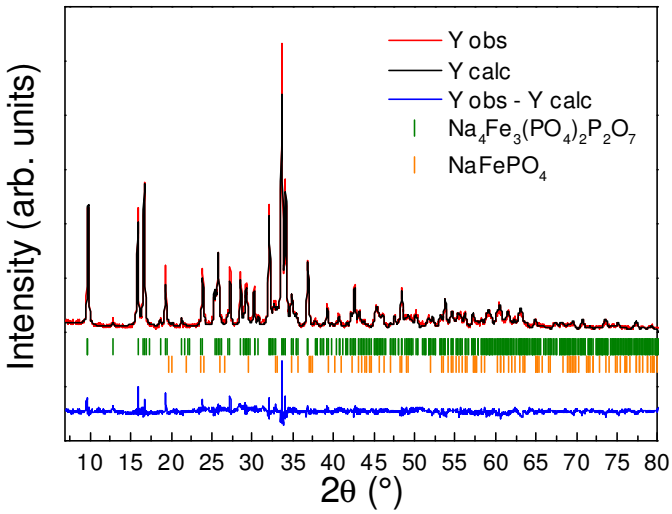

Fig. 6. 9. Pseudo-Rietveld refined pattern of a with 5% of C65 using wet-milling treatment to mix the precursors. The red line, black line, and blue line represent the observed pattern, calculated pattern, and difference between them, respectively. Vertical markers represent the Bragg position for $Na_4Fe_3(PO_4)_2P_2O_7$ (green), $NaFePO_4$ (orange) and $Na_2FeP_2O_7$ (violet) and $Na_4P_2O_7$ (pink).

6.2. Electrochemical characterization of $Na_4Fe_3(PO_4)_2P_2O_7$

Electrodes were prepared on stainless steel disks with a 75:20:5 ratio of active material, C65 and PVDF, respectively. The samples were hand-grounded in a mortar for 30 minutes with C65 and PVDF and, after NMP was added, the slurry was kept under stirring for one hour. The slurry was then casted on stainless steel disk current collectors. NMP was dried overnight at 120 ^{o}C and pressed 5 t cm^{-2}. The C content in the C-coated and C-precursor samples was considered as part of the active material. When maricite $NaFePO_4$ and $Na_2FeP_2O_7$ impurities were present, they were considered as part of the active material and therefore the capacity of $Na_4Fe_3(PO_4)_2P_2O_7$ was underestimated in these samples.

6.2.1. Electrochemical characterization in organic media

6.2.1.1. Preliminary electrochemical studies on non-pure samples

The electrochemical characterization of $Na_4Fe_3(PO_4)_2P_2O_7$ was carried out in parallel to the optimization of the synthesis parameters and therefore some of the previous impure samples were tested to select the best electrochemical conditions and materials.

Organic electrolyte cells were first mounted in order to compare the behaviour of the obtained material with reported data and to determine the operating voltage and capacity. Half cells were tested in a voltage window of 1.8 to 4.3 V *vs*. Na^+/Na using 1 M $NaClO_4$ in EC:PC with 2% FEC as the electrolyte.

The *as prepared* sample delivered a reversible capacity of 79.4 mAh g^{-1} at 0.1C (Fig. 6. 10a) although a somewhat lower capacity (73 mAh g^{-1}) is obtained in the first charge. The *ball-milled* (Fig. 6. 10b) and the *C-coated* (Fig. 6. 10 c) samples are those with the highest reversible first cycle capacity values of 98 and 116 mAh g^{-1} respectively. On the other hand, the *C-precursor* sample delivered a reversible capacity of 84 mAh g^{-1} (Fig. 6. 9a).

Despite the high capacity obtained in the *C-coated* sample, it must be pointed out that the coulombic efficiency increased though cycling up to 110% at the 6th cycle, which implies an irreversible process during discharge. We believe that this is related to the reduction of the residual amount of polymer that remained in the sample after the heating treatment, in agreement with the TEM images observed in Fig. 6. 7 On the other hand, the rest of samples exhibited good coulombic efficiencies close to 100% Fig. 6. 12a).

The average voltage was around 3 V in all cases, as expected [5]. A high overpotential is observable in the first charge/discharge profile for all the studied samples and is slightly reduced for the next cycles with the exception of the *as prepared* sample. The average

overpotential is given in Table 2 for the second cycle. The overpotential decreases following the sequence *as prepared* > *ball-milled* > *C-coated* > *C-precursor*, the latter with an average value of 0.160 V. In the case of the *C-coated* sample the polarization is similar to *the ball-milled* sample (0.230 V). However, the best results in terms of polarization were obtained for *C-precursor* sample which had only 0.160 V of polarization in the 2nd cycle.

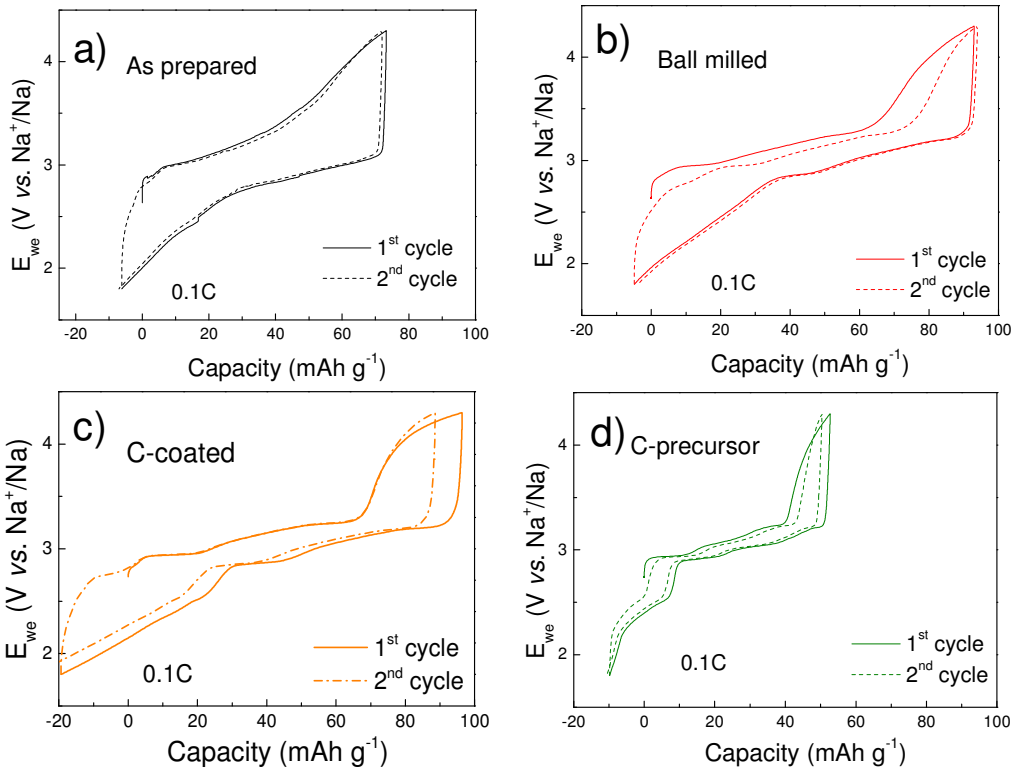

Fig. 6. 10. Voltage *vs.* specific capacity plot for the 1st (solid line) and 2nd (dash) cycles at 0.1C in 1 M $NaClO_4$ EC:PC with 2 % of FEC for the four different samples: as prepared (a), ball-milled (b), C-coated (c) and C-precursor (d).

Table 2. Summary of the reversible capacity and polarization values for the first cycle and average voltage and polarization values for the second cycle obtained for the different samples at 0.1C (as prepared, ball-milled, C-coated and C-precursor).

	1st cycle		2nd cycle	
Sample	**Capacity (mAh g^{-1})**	**Polarization (V)**	**Average voltage (V *vs.* Na^+/Na)**	**Polarization (V)**
As prepared	80	0.400	3.03	0.420
Ball-milled	98	0.330	3.00	0.240
C-coated	116	0.270	3.04	0.230
C-precursor	85	0.220	3.06	0.160

After cycling at 0.1C, the same cells where tested at 1C. Fig. 6. 11 shows the first two cycles for the bal-milled, C-coated and C-precursor samples. The capacity values, polarization and average voltage for the first two cycles are summarized in Table 3. The capacity decreased drastically in the ball-milled sample from 97.8 mAh g^{-1} at 0.1C to 51 mAh g^{-1} of reversible capacity at 0.1C (48% less). Even a worse rate capability was displayed by the C-coated sample which delivered 116.1 mAh g^{-1} at 0.1C and 48.2 at 1C (58.5% less). In contrast, C-precursor sample maintained 75% of the 0.1C capacity at 1C, resulting in 63.49 mAh g^{-1}.

This better rate capability for the *ball-milled* sample with respect to the *C-coated* one is in agreement with the polarization values. The overpotential for the *C-precursor* sample was 0.240 V, while the *ball-milled* and *C-coated* phases obtained polarization values of 0.620 V and 0.740 V (Table 3).

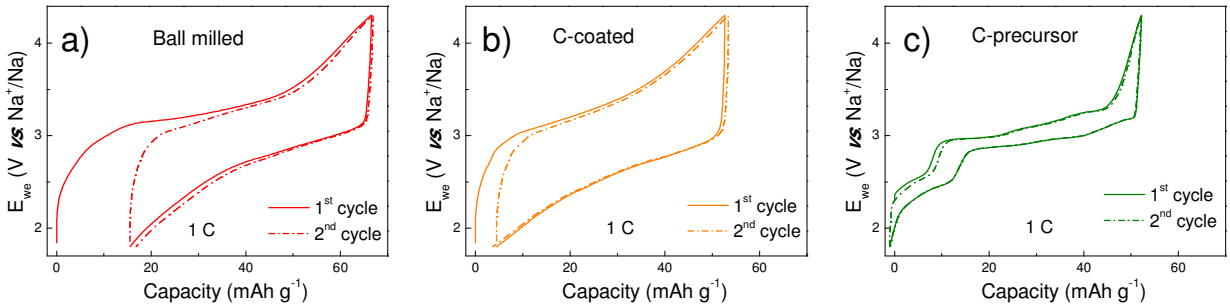

Fig. 6. 11. Voltage profile *vs*. specific capacity for the 1st(solid line) and 2nd(dash) cycles at 1C in 1 M $NaClO_4$ EC:PC with 2 % of FEC for ball-milled (a), C-coated (b) and C-precursor (c) samples.

Table 3. Reversible capacity in the first discharge and polarization and average voltage values in the 2nd cycle at 0.1 C for the ball-milled, C-coated and C-precursor sample

Sample	Capacity (mAh g^{-1})	Polarization (V)	Average voltage (V *vs*. Na^+/Na)
Ball-milled	50.99	0.620	3.02
C-coated	48.17	0.740	2.93
C-precursor	63.49	0.240	3.02

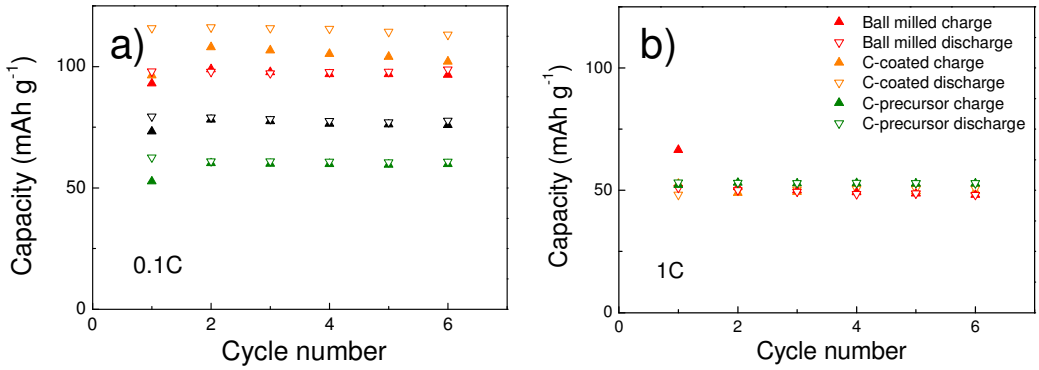

Fig. 6. 12. Capacity vs. cycle number in charge and in discharge at 0.1C (a) in 1 M $NaClO_4$ EC:PC with 2 % of FEC for the four different samples: as prepared (black), ball-milled (red), C-coated (orange) and C-precursor (green). Capacity vs. cycle number in charge and in discharge at 1C (b) in 1 M $NaClO_4$ EC:PC with 2 % of FEC, ball-milled (red), C-coated (orange) and C-precursor (green) samples.

In order to maximize the extent of reaction within the smaller voltage window of in aqueous electrolyte, the addition of C in the precursor results in a good approach to get it.

6.2.1.2. Electrochemical studies on the pure sample

Previously to the aqueous tests, the WM C-precursor was tested in organic media. At 0.1C the reversible capacity increases from 85 mAh g^{-1} of the non-pure C-precursor sample to 108 mAh g^{-1} and similar overpotential values (ca. 0.150 V) (Fig. 6. 13a). When the rate was increased to 1C, the reversible capacity was 77 mAh g^{-1} (13 mAh g^{-1} more than non-pure C-precursor sample) and and the overpotential in the second cycle was 0.3 V (Fig. 6. 13b).

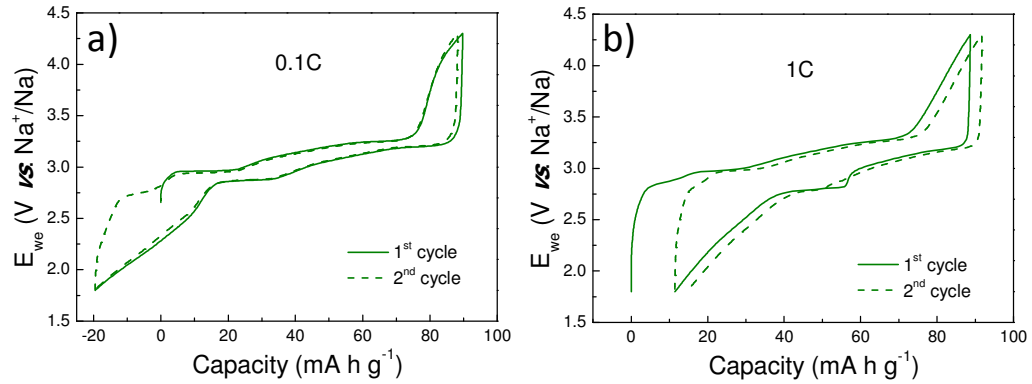

Fig. 6. 13. (a) Voltage profile *vs*. capacity for the first two cycles of WM C-precursor sample tested in an aqueous half-cell between 2.5 to 3.4 V at (a) 0.1C and (b) 1C

Once the material was electrochemically optimized in organic media, was tested using aqueous electrolyte.

6.2.2. Electrochemical characterization in aqueous media

These measurements were done in aqueous electrolyte 1M Na_2SO_4 using AC and Ag/AgCl (3 M NaCl) as counter and reference electrodes, respectively. The WM C-precursor material was cycled at 1C from 2.5 to 3.4 V *vs*. Na^+/Na.

Fig. 6. 14a shows the voltage profile for the first two cycles. In aqueous electrolyte the cell also delivered 77 mAh g^{-1}, which is similar to that obtained in organic electrolyte at the same rate despite the smaller voltage range used in aqueous electrolyte. An overportential of 0.09 V was achieved *vs.* 0.3 V achieved in organic electrolyte at the same rate.

After 50 cycles, the cell still retained 75% of the initial capacity (Inset of Fig. 6. 14). In order to understand this fading in aqueous medium, solubility tests were carried out. 100 mg of sample were immersed in two different solutions: water and 1 M Na_2SO_4. After 72 h, the powder was filtered and the recovered supernatants were analyzed by ICP (Fig. 6. 15 and Table 4).

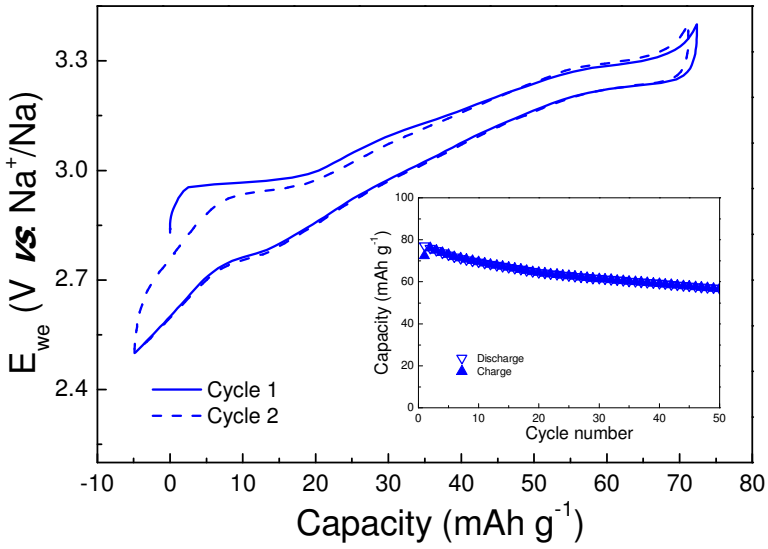

Fig. 6. 14. (a) Voltage profile *vs*. capacity for the first two cycles of WM C-precursor sample tested in an aqueous half-cell at 1C between 2.5 to 3.4 V vs. Na^+/Na using 1 M Na_2SO_4 electrolyte. Inset: Capacity *vs*. cycle number for the first 50 cycles for the same cell.

In the water sample, an intense yellow color can be observed in the supernatant, possibly due to dissolved Fe. ICP results are shown in Table 4 and confirm the much high solubility of Fe in water. Fe is also found in the electrolyte, although in a much lesser extent.

The amount of Na was analyzed only in the water solution since the other already contains a high amount of Na. A 15 wt% of Na, 3.4 wt% of Fe and 5.9% of P were solved. However, these values do not have a direct relation with the stoichiometry of the compound, where the ratio Na/Fe and P/Fe are 1.33 (see Table 4). We therefore believe that the higher solubility of Na

with respect to Fe should be related with the hydrolysis of pyrophosphates forming Fe oxides and Na phosphates because Na phosphates are more soluble than iron oxides [9]. If the supernatant of the electrolyte solution is analyzed, P and Fe solubility decrease. Although the addition of C in the precursor improves notably the electrochemistry reducing the polarization and increasing the rate capability, it does not form a protective coating and cannot avoid hydrolysis of the material.

The XRD pattern of the powder recovered from these tests was measured and refined by Rietveld method (Fig. 6. 16). All diffraction peaks correspond to $Na_xFe_3(PO_4)_3P_2O_7$, with x<4 since appear shifted to the right with respect to the *as-prepared* material[6], but no new peaks from other phases appear. For the sample aged in non-deoxygenated water the refined cell parameters are *a* = 17.833(2), *b* = 6.5080(6) and *c* = 10.717(1). Using the experimental cell parameters reported by Kim *et al*. for different x values in $Na_xFe_3(PO_4)_3P_2O_7$ obtained by desodiation using NO_2BF_4, and assuming a linear Vegard's law from the results obtained by, the refined cell parameters would correspond to $Na_{\sim 2.26}Fe_3(PO_4)_3P_2O_7$. On the other hand, the cell parameters for the sample aged in oxygenated 1 M Na_2SO_4 are *a* = 17.8860(2), *b* = 6.5292(5) and *c* = 10.711(1). The higher values for *a* and *b* correspond to a slightly more reduced phase that, according to Vegard's law, would be close to $Na_{\sim 2.64}Fe_3(PO_4)_2P_2O_7$.

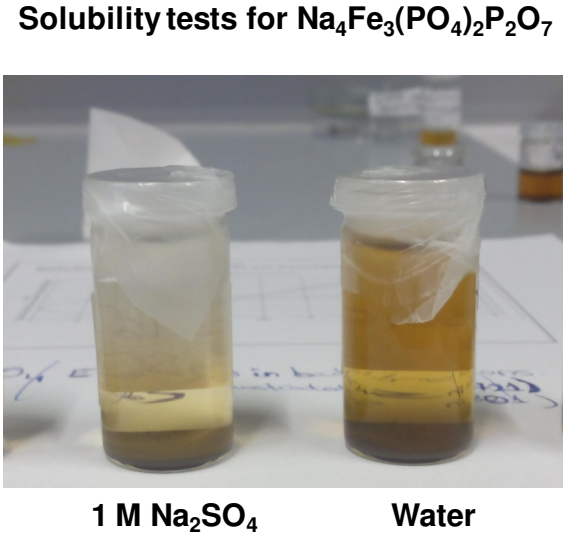

Fig. 6. 15. Solubility tests for $Na_4Fe_3(PO_4)_2P_2O_7$ by addition of 100 mg of $Na_4Fe_3(PO_4)_2P_2O_7$ in 10 mL of 1 M Na_2SO_4 solution and water.

Table 4. Results from ICP of supernatants of solubility tests.

Solution	Na (ppm)	Fe (ppm)	P (ppm)	Molar ratio (Na/Fe)	Molar ratio (P/Fe)
Water	208.74	92.52	118.74	5.5	2.65
1 M Na_2SO_4	-	2.922	41.8	-	4.18

We can conclude that there are two factors that affect to $Na_4Fe_3(PO_4)_2P_2O_7$ stability in aqueous electrolyte: oxidation of the sample, which implies a Na loss, and hydrolysis resulting in more or less soluble species. Therefore, these secondary reactions should be mitigated following different strategies if this material is to be used in aqueous cells. On one hand, to avoid the oxidation process, a concentrated electrolyte or an adequate pH could work. On the other hand, to avoid the hydrolysis of the sample, an effective coating is needed. Moreover, both problems could be alleviated by increasing the ratio active material: electrolyte so that the electrolyte saturates faster.

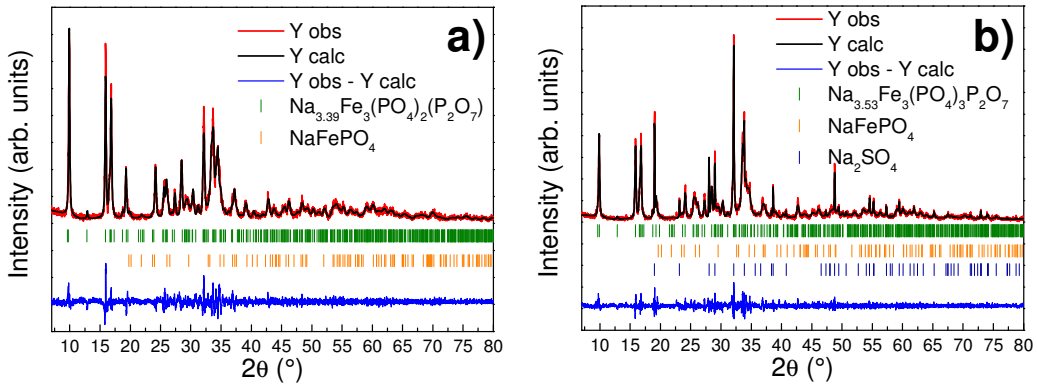

Fig. 6. 16. Pseudo-Rietveld refined XRD patterns of two samples aged for 72 h in (a) water and (b) 1 M Na_2SO_4 by ball-milling of the precursors. The red line, black line, blue line, and blue line represent the observed pattern, calculated pattern, and difference between them, respectively. Vertical markers represent the Bragg position for $Na_4Fe_3(PO_4)_2P_2O_7$ (green), maricite $NaFePO_4$ (orange) and Na_2SO_4 (navy blue).

6.3. Conclusions

Several parameters of $Na_4Fe_3(PO_4)_2P_2O_7$ ceramic synthesis have been analyzed. The effect of temperature and dwelling time were analyzed. However, a purity of 75-80% was only achieved and maricite $NaFePO_4$ and $Na_2FeP_2O_7$ appeared as secondary phases. On the other hand, changing from dry milling of the precursor's mixture to wet milling finally resulted in a quasi-pure sample, with only 2.5-3.6% of maricite.

Three different strategies have been tested to improve the conductivity of the material (ball-milling, C-coating, adding C to the precursors mixtures before and after the first heat treatment) and the obtained materials have been characterized in Na half-cells. The best results in terms of polarization were obtained for the C-precursor sample. When the quasi pure phase with C in the precursors was tested, it exhibited 108 mAh g^{-1} and 77 mAh g^{-1} at 0.1C and 1C good overpotential values (0.09 and 0.30 V at the respective rates).

This sample was studied for the first time in aqueous electrolyte. Despite of the lower voltage range used in this media, the same capacity obtained in organic media at the same rate was achieved. As was observed in the previous materials, a much lower overpotential was observed (0.09 V at 1C). A capacity fading of 75% after 50 cycles was observed. The ICP results obtained from solubility tests show that Na and Fe dissolve, most probably as a result of the hydrolysis of the material. We found that the solubility is much higher in pure water than in the electrolyte solution. Furthermore, the analysis of aged material revealed oxidation of the samples.

As conclusion, this material shows promising capacity and overpotential values to be used in aqueous NIBs. Work should be directed towards increasing its stability in aqueous medium. Different strategies could be simultaneously considered. On one hand, to avoid the oxidation process, a concentrated electrolyte or an adequate pH could work. On the other hand, to avoid the hydrolysis of the sample, an effective coating is needed. Moreover, both problems could be alleviated by increasing the ratio active material: electrolyte so that the electrolyte saturates faster.

[1] G. Hautier, A. Jain; H. Chen, C. Moore, S. P. Ong, G. Ceder, Novel mixed polyanions lithium-ion battery cathode materials predicted by high-throughput *ab initio* computations, J. Mater. Chem. 21 (2011), 17147−17153.
[2] A. Jain, G. Hautier, C. Moore, B. Kang, J. Lee, H. Chen, N. Twu, G. J. Ceder., G. J. Electrochem. Soc. 2012, 159 (5), 622−633.
[3] M. Nose, H. Nakayama, K. Nobuhara, H. Yamaguchi, S. Nakanishi, H. Iba, $Na_4Co_3(PO_4)_2P_2O_7$: A novel storage material for sodium-ion batteries, J. Power Sources 234 (2013) 175-179
[4] S. M. Wood, C. Eames, E. Kendrick, M. Saiful Islam, Sodium Ion Diffusion and Voltage Trends in Phosphates $Na_4M_3(PO_4)_2P_2O_7$ (M = Fe, Mn, Co, Ni) for Possible High-Rate Cathodes, J. Phys. Chem. C 119 (2015) 15935−15941
[5] H. Kim, I. Park, D.H. Seo, S. Lee, S-W. Kim, W. J. Kwon, Y.U. Park, C.l S. Kim, S. Jeon‖, K. Kang, New Iron-Based Mixed-Polyanion Cathodes for Lithium and Sodium Rechargeable Batteries: Combined First Principles Calculations and Experimental Study, J. Am. Chem. Soc., 134 (2012) 10369–10372
[6] H. Kim, I. Park, S. Lee, H. Kim, K. Y. Park, Y. U. Park, H. Kim, J. Kim, H.D. Lim, W.S. Yoon, K. Kang, Understanding the Electrochemical Mechanism of the New Iron-Based Mixed-Phosphate $Na_4Fe_3(PO_4)_2(P_2O_7)$ in a Na Rechargeable Battery, Chem. Mater., 25 (2013) 3614–3622
[7] A.J. Fernández-Ropero, D. Saurel, B. Acebedo, T. Rojo, M. Casas-Cabanas, Electrochemical characterization of $NaFePO_4$ as positive electrode in aqueous sodium-ion batteries, J. Power Sources, 291 (2015) 40-45.
[8] Y-H. Jung, C-H. Lim, J-H. Kim, D-K. Kim, $Na_2FeP_2O_7$ as a positive electrode material for rechargeable aqueous sodium-ion batteries, R. Soc. Chem. Adv. 4 (2014) 9799–9802.
[9] W. Porcher, P. Moreau, B. Lestriez, S. Jouanneau, D. Guyomard, Is $LiFePO_4$ stable in water?, Electrochem. Solid State. Lett.

7. Study of Maricite $NaFePO_4$ as cathode material

Contrary to $LiFePO_4$, whose thermodynamically stable polymorph is isostructural to olivine ($(Mg, Fe)_2SiO_4$), maricite is the thermodynamically stable polymorph of $NaFePO_4$. Fig. 7. 1 shows the comparison between olivine and maricite $NaFePO_4$ structures, where it can be observed that M1 and M2 sites have reverse occupancies making their structures different. In olivine, M1 site hosts the alkali metal while the M2 site holds the transition metal, whereas in maricite, the M1 site holds the transition metal and the M2 site holds the alkali metal (see chapter 4). This configuration results in channels for Na^+ diffusion along the *b* axis in the olivine structure, while no obvious channels for ion diffusion appear in the maricite structure.

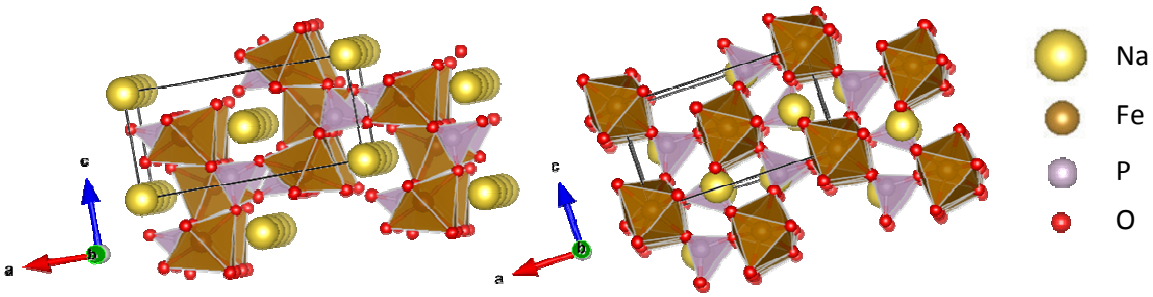

Fig. 7. 1. Comparison of the structure of olivine (a) and maricite (b) $NaFePO_4$. Fe is surrounded by six O forming an octahedron and P by four O forming an octahedron.

For this reason maricite has been considered as electrochemically inactive for a long time [1]. Indeed, a couple of research works had reported a very low capacity (< 30 mAh g^{-1}) when studied in Na half-cells [2, 3], certainly insufficient for its practical use in a battery. However, Kim *et al*. recently reported that nano-$NaFePO_4$ maricite can function as an excellent cathode delivering 142 mAh g^{-1} [4]. In their work they claim that reaction vs. Na is possible because maricite transforms into amorphous $FePO_4$, which substantially minimizes the energetic barriers for Na to hop from site to site. Since no reports of maricite in aqueous electrolyte exist to date, we decided to test this material in aqueous electrolyte and compare its behavior to olivine $NaFePO_4$, already described in chapter 4.

Maricite material has here been synthesized by the ceramic method and the study of several synthesis parameters, its electrochemical behavior and its reaction mechanism using ex-situ and in-situ characterization techniques have been investigated. This work has been done in collaboration with IREQ (Institut de Recherche d'Hydro-Québec) during a 3-month stay from May to August 2015 under the supervision of Dr. Abdel Guerfi and Dr. Karim Zhaguib and with Dr. Jose Javier Saiz Garitaonandia from University of the Basque Country who performed the Mossbauer analysis.

7.1. Synthesis and physico-chemical characterization

Maricite $NaFePO_4$ was synthesized via a conventional two-step solid-state route from low-cost precursors, following a procedure similar to the one described by Kim *et al*. (4). Na_2CO_3 (≥ 99.5%, Sigma-Aldrich), $FeC_2O_4{\cdot}2H_2O$ (99%, Aldrich) and ammonium phosphate monobasic $NH_4H_2PO_4$ (≥ 98.5%, Sigma-Aldrich) were thoroughly mixed in a stoichiometric ratio by dry ball-milling (Planetary mill at 350 rpm for 24h with a balls : sample mass ratio of 40:1). The mixture of precursors was then calcined at 350 ˚C for 5 hours under Ar flow (180-200 mL min^{-1}). After this first heating treatment, the sample was grounded with a mortar and re-pelletized using a disk-shaped mold. The pellet was annealed a second time also under Ar flow at 600 ˚C for 10 h.

After this second heating treatment the pellet was often not homogeneous in color, with the outer part of the pellet being reddish and containing small impurities of $Na_3Fe_2(PO_4)_3$ together with maricite and the inner part of the pellet being grey-white and containing the targeted phase maricite $NaFePO_4$ (Fig. 7. 2a) .

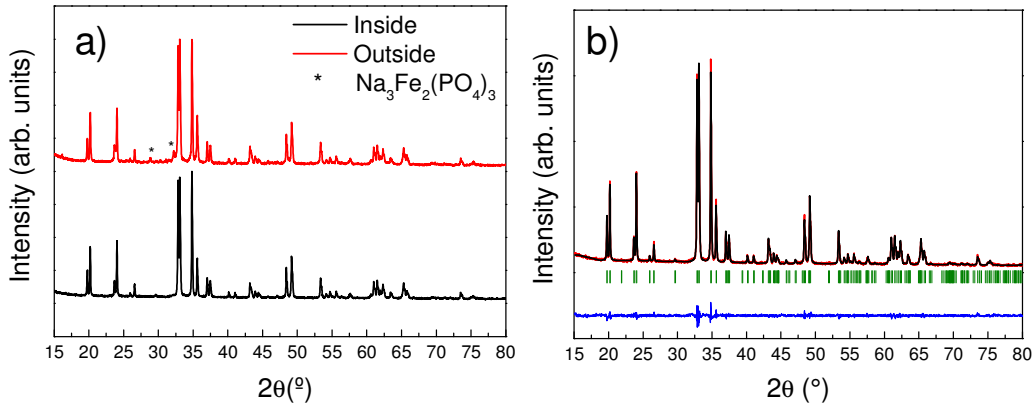

Fig. 7. 2. (a) XRD patterns of the outer (red) and inner (black) parts of the pellet. (b) Le Bail refinement of the obtained pure maricite phase.

The X-ray diffraction pattern of the $NaFePO_4$ sample was refined by Le-Bail Method and indexed with Pnma space group (Fig. 7. 2b), with refined cell parameters of *a* = 8.9809(2) Å, *b*

= 6.8639(1) Å and *c* = 5.0420(9), in agreement with literature values [5]. The sample is referred as DM5-10 (which indicates dry milling and dwelling times). From the profile of the diffraction peaks, and after subtracting the instrumental contribution using an Instrument Resolution File (IRF) determined with an Al_2O_3 standard, an average domain size of 120 nm was obtained.

Once the reported synthesis was reproduced, different parameters were changed to study their influence in the resulting compound and to improve its purity. A C-trap, a graphite crucible and a N_2 flow (cheaper than Ar) were used during the calcination steps to avoid oxidation around the pellet. The ball milling process was also suppressed and the precursors were just hand-milled for 30' to mix the precursors. Contrary to the previously ball milled samples, which showed a homogeneous grey color, the sample was black with white spots after the first treatment at 350 ˚C. After the second treatment at 600 ˚C, the pellet still was multicolor (see Fig. 7. 3a). In the XRD pattern of the sample (referred as HM5-10, which indicates hand milling and dwelling times) several peaks that do not correspond to the targeted phase are detected (Fig. 7. 3b).

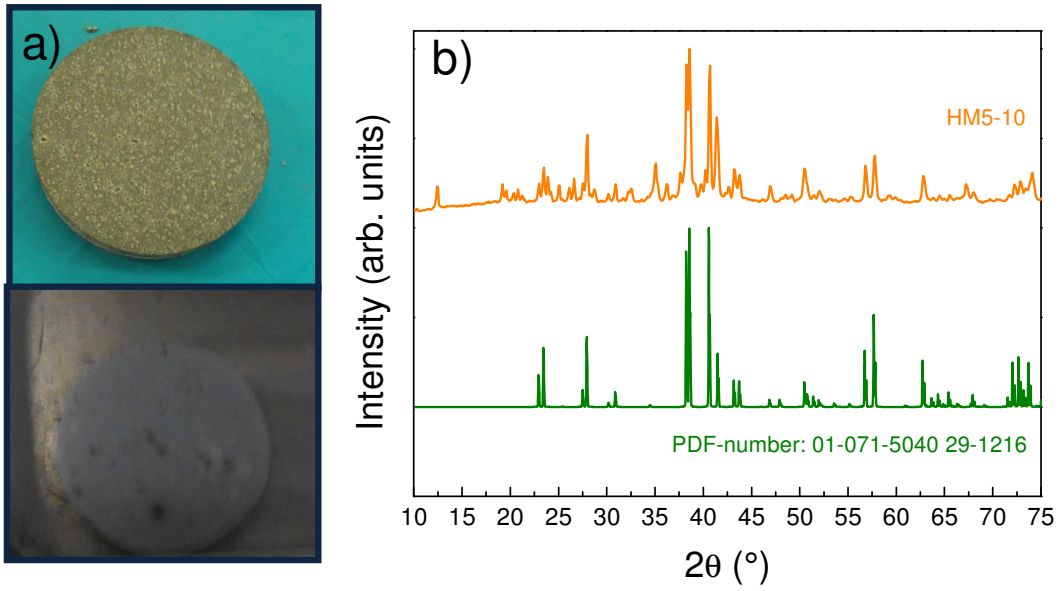

Fig. 7. 3. (a) Pellets after the heating treatments using C trap of a sample without milling treatment (above) and with milling treatment (below). (b) XRD of the HM5-10 sample (orange) and from the database (green).

The next step was to perform a 2 h wet ball milling with EtOH as solvent. The wet ball milling allows a better mixture in lower time than dry milling. The obtained sample (referred as WM5-10) (see Fig. 7. 3a below) had a homogeneous grey color which indicated there was no oxidation in the outer part of the pellet. The Le Bail refinement confirmed the achievement of the pure phase. The refined parameters were *a* = 8.9802(4) Å, *b* = 6.8652(3) Å and *c* =

5.0420(2) Å and the average crystal size 70 nm. In this case, the sample crystallized in smaller particles than the one synthesized with dry milling of the precursors.

Once the need of a previous ball milling treatment was confirmed, shorter dwelling times for the second step were tested (5 h (WM5-5) and 3 h (WM5-3)). In all cases pure maricite was obtained and a similar broadening of diffraction peaks, which indicates a similar cristallinity (Fig. 7. 4). Next step was to reduce the precursors' calcination time from 5h to 2h. Maricite was also obtained in all cases with the same cristallinity (Fig. 7. 4). In conclusion, the synthesis time can be significantly reduced from 5h to 2h and from 10 h to 3h for the first and second heat treatments respectively.

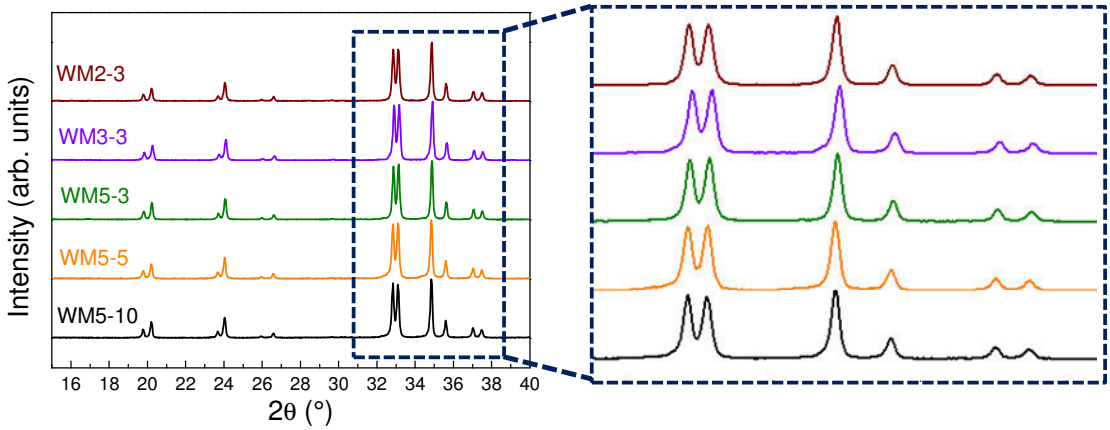

Fig. 7. 4. XRD patterns for five samples synthesized by previous wet ball-milling of the precursors and treated with different dwelling times.

Fig. 7. 5 shows the SEM images for three different samples: (a) DM5-10 (b) WM10-5 and (c) WM3-3. The particle size is clearly larger in (a) than (b), in agreement with the average domain size extracted from Le Bail refinements. From these results, it can be concluded that the type of ball-milling treatment influences on the domain and particle size, while the dwelling time does not affects to these values.

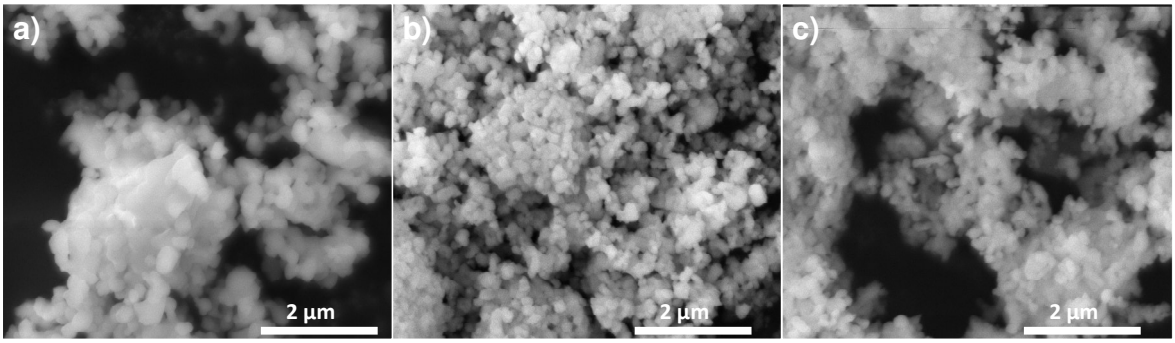

Fig. 7. 5. SEM images at 20,000x magnification of three different samples: (a) DM5-10, (b) WM5-10 and (c) and (c) WM3-3.

7.1.1. Ball milled sample

To increase the conductivity and to reduce the size of agglomerates two different samples (DM5-10 and WM3-3) were ball milled in the planetary mill for 12 hours in an active material : C65 ratio of 80:20. In both cases a speed of 300 rpm was selected and the treatment lasted 24h, with a balls : sample mass ratio of 40:1.

In SEM images a particle size for both materials can be observed and the average domain size obtained by Le-bail refinement decreases down to 30 nm for both samples.

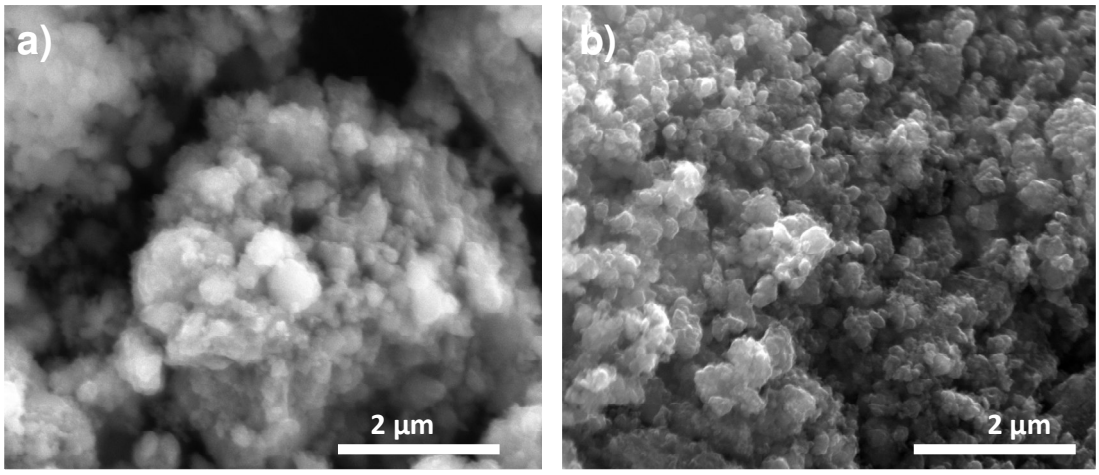

Fig. 7. 6. SEM images at 20,000x magnification of two different samples after ball-milling treatment: (a) DM5-10 and (b) WM3-3.

7.2. Electrochemical characterization of maricite $NaFePO_4$

Electrodes of the samples ball milled with C65 were prepared by casting a slurry of formulation 68:27:5 (active material: C65: PVdF) on stainless steel to reproduce the reported results [4]. The electrodes were further dried overnight at 120 ˚C under vacuum and pressed at 4 t cm^{-2} as described in the experimental chapter. Both materials were electrochemically characterized both in organic and aqueous electrolyte for comparative purposes.

7.2.1. Electrochemical characterization in organic media

Batteries were cycled between 4.5 V and 1.5 V at 0.05C rate (7.7 mAh g^{-1}). 1 M $NaPF_6$ in EC:DEC was used as electrolyte because it was the one used by Kim *et al*. [4] and $NaPF_6$ decomposes at higher potential than $NaClO_4$ [6]. Both samples exhibited exactly the same behavior (Fig. 7. 7a) and therefore no distinction will be done hereafter.

Only 56 mAh g^{-1} were achieved in the first charge (Fig. 7. 7b) but surprisingly a capacity of 110 mAh g^{-1} was obtained in the following discharge. After that the cell stabilized around 75 mAh g^{-1} (Fig. 7. 7c). Since the first discharge capacity was almost twice the charge capacity, and electrolyte decomposition is not expected to occur in the voltage window used here, another battery was cycled starting in discharge using the same voltage range and C-rate (Fig. 7. 7d). Strikingly the cell delivered 100 mAh g^{-1} in the first discharge and 110 mAh g^{-1} in charge. After that, the cell stabilizes at 75 mAh g^{-1} with a similar behavior to that obtained when starting in charge (Fig. 7. 7c).

These results are totally unexpected since the first discharge capacity would involve a very large amount of Fe^{+3} (> 70%) in the starting material if the capacity delivered is attributed to the Fe^{+2}/Fe^{+3} redox couple, and oxidation from Fe^{2+} to Fe^{0} is difficult to believe at these working potentials. To understand these results the starting material was further characterized.

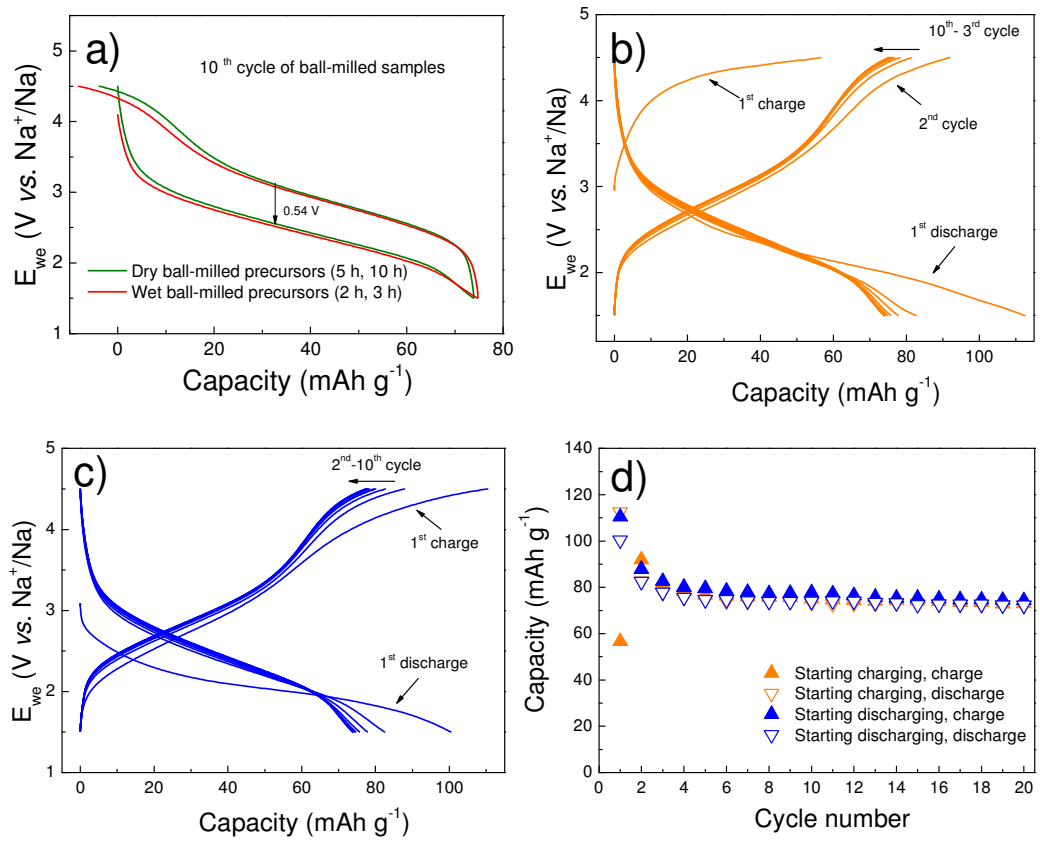

Fig. 7. 7. (a) Comparison of DM5-10 and DM2-3 cycled in organic half-cells at 0.05C between 1.5 and 4.5 V *vs*. Na^+/Na of two organic half-cells. (b) Voltage profiles for the first ten cycles starting in charge. (c) Voltage profiles for the first ten cycles starting in discharge. (d) Comparison of the first 20 cycles of a battery starting in charge and another starting in discharge.

In order to verify if the sample was partially oxidized, the Na/Fe ratio of the ball-milled powder was analyzed by ICP and a value of 0.9 was obtainedHowever, it does not explain the achieved capacity values.

To obtain further information of the oxidation state of the ball-milled powder, Mössbauer spectroscopy was carried out. Fig. 7. 8a shows the obtained spectrum, where only two symmetrical peaks can be observed, and therefore, only one kind of iron contributes to the spectrum. Moreover, the narrow peak width at half-height (WID) of 0.29 mm s^{-1} indicates that all Fe has exactly the same chemical environment. The spectrum was fitted to the theoretical values for Fe^{2+} whith an isomer shift (IS) related to bcc-Fe of 1.19 mm s^{-1} and a quadrupolar splitting (QUA) of 2.2 mm s^{-1}.

Ex-situ Mössbauer spectroscopy and XRD measurements were also carried out on cycled electrodes. To do so, a laminate was prepared with the same formulation (68% of AM) and casted on Al foil. Al foil was used instead of stainless steel since Fe^0 would be detected in Mössbauer spectroscopy. In the spectrum of the pristine electrode (Fig. 7. 8b), Fe^{2+} with similar parameters ((ISO: 1.2 mm s^{-1}, QUA: 2.21 mm s^{-1}, WID: 0.3 mm s^{-1}) and Fe^{3+} contributions (ISO: 0.38 mm s^{-1}, QUA: 0.84 mm s^{-1}, WID: 0.55 mm s^{-1}) were observed, which corresponds to a 36% of Fe^{+3} in laminated electrodes. The origin of the formation of Fe^{3+} still has to be confirmed but it probably appears in the ball-milling step.

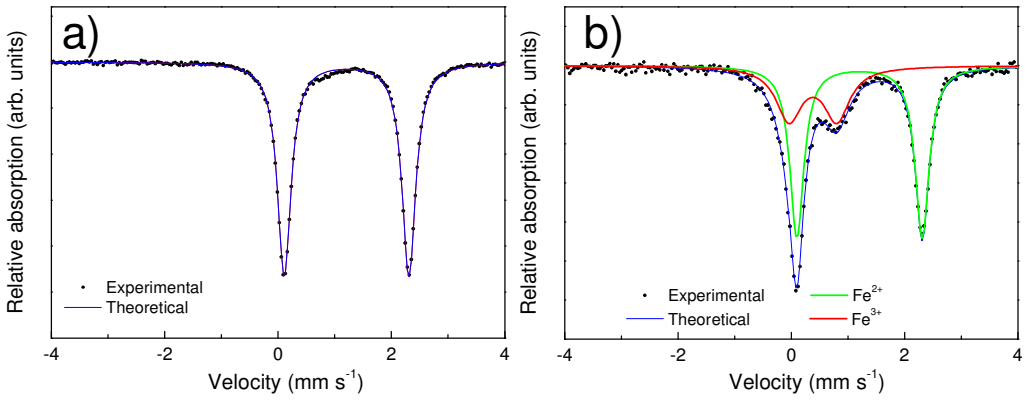

Fig. 7. 8. Mössbauer spectra of the (a) pristine maricite powder and (b) a pristine electrode

Then four organic half-cells were assembled and stopped at different voltage values: (a) after one charge, (b) after one discharge, (c) after one cycle starting in charge and (d) after one cycle starting in discharge (Fig. 7. 9). Table 7. 1 shows the values of Mössbauer parameters for the different recovered electrodes.

The batteries stopped in charge (a and d) had 13% more Fe^{3+} than the pristine electrode, which means oxidation of Fe^{+2} to Fe^{+3} occurs during charge. However, the batteries stopped in

discharge have a similar amount of Fe^{3+} than the pristine electrode. Therefore, the oxidation process is reversible but the reversible oxidation of Fe^{+2} to Fe^{+3} cannot account for all the capacity obtained.

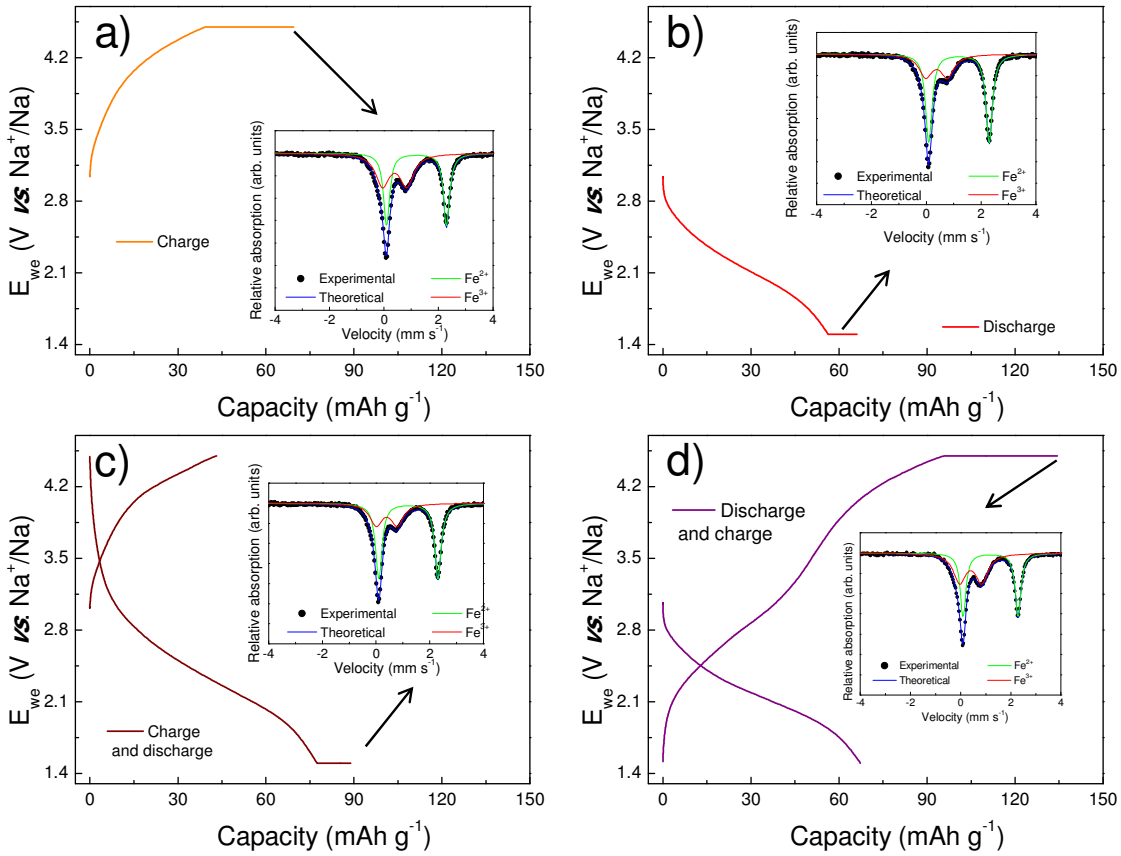

Fig. 7. 9. Voltage profile of four organic half-cells stopped at different voltage values (inset: Mössbauer spectra of the recovered electrodes).

Table 7. 1. Mössbauer spectroscopy parameters of the cell organic half-cells stopped at different voltages

		ISO (mm s^{-1})	QUA (mm s^{-1})	WID (0.3 mm s^{-1})	Fe%
a	**Fe^{2+}**	1.2	2.2	0.27	50.5
	Fe^{3+}	0.39	0.88	0.61	49.5
b	**Fe^{2+}**	1.2	2.2	0.28	66
	Fe^{3+}	0.38	0.79	0.58	34
c	**Fe^{2+}**	1.2	2.21	0.28	65
	Fe^{3+}	0.39	0.79	0.56	35
d	**Fe^{2+}**	1.19	2.19	0.27	50.8
	Fe^{3+}	0.4	0.88	0.59	49.2

The same electrodes were analyzed by XRD. The samples maintain the initial crystallinity, contrary to that reported by Kim *et al*. [4]. Slight displacements can be observed which are of instrumental origin and due to the sample position in the holder. It is difficult to conclude on the differences observed (peak position, change in the intensity distribution of the different reflections) thus in situ XRD measurements were carried out.

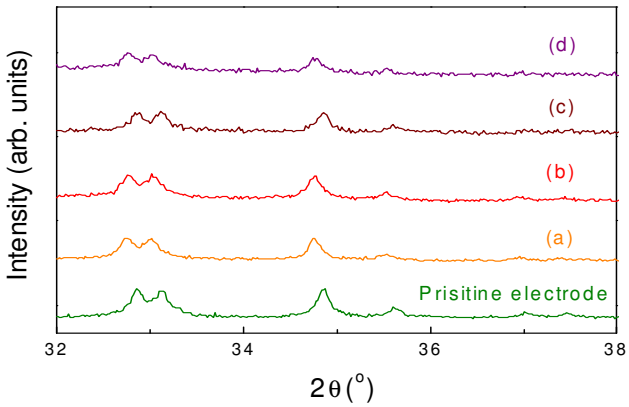

Fig. 7. 10. Ex-situ XRD patterns of the recovered electrodes from organic half-cells stopped at different voltage values

The in-situ cell was tested at 0.025C between 1.5 and 4.3 V *vs*. Na^+/Na. At the end of the charge a slight electrolyte leakage occurred, and can be observed in the voltage profile (Fig. 7. 11a). The leakage produced a slight displacement of the pattern but the reflection (3 0 1) of the maricite (Fig. 7. 11b) was corrected with the displacement of the Al which theoretically should not change. The position of reflection (3 0 1) was followed using a pseudo-Voigt fit. The variation in position is shown in (Fig. 7. 11b) where it can be observed that changes in peak position follow the charge and discharge curves, decreasing during discharge (which means that the cell parameters increase, which would be in agreement with Na^+ insertion) and decreasing in charge, despite being very subtle (the total 2θ variation is only 0.95 °).

The Le Bail refinement of the diffraction patterns confirms the previous results. Although the variation is small, the *a* cell parameter clearly increases when the battery is discharged and decreases when the battery is charged. The *b* and *c* cell parameter suffer from even less variations and, while *b* parameter does not seem to be related to any structural change, the *c* parameter follows a similar trend as *a* parameter but in a lower degree.

From these results can be concluded that insertion occurs to some extent. However, the small changes in cell volume together with relative the amount of Fe^{+2} and Fe^{+3} at different voltage values may indicate that other processes can contribute to the obtained capacity. At present we do not discard the possible existence of a capacitive process and in situ Mossbauer

is planned to clarify the reaction mechanism, which is clearly different from what was previously reported.

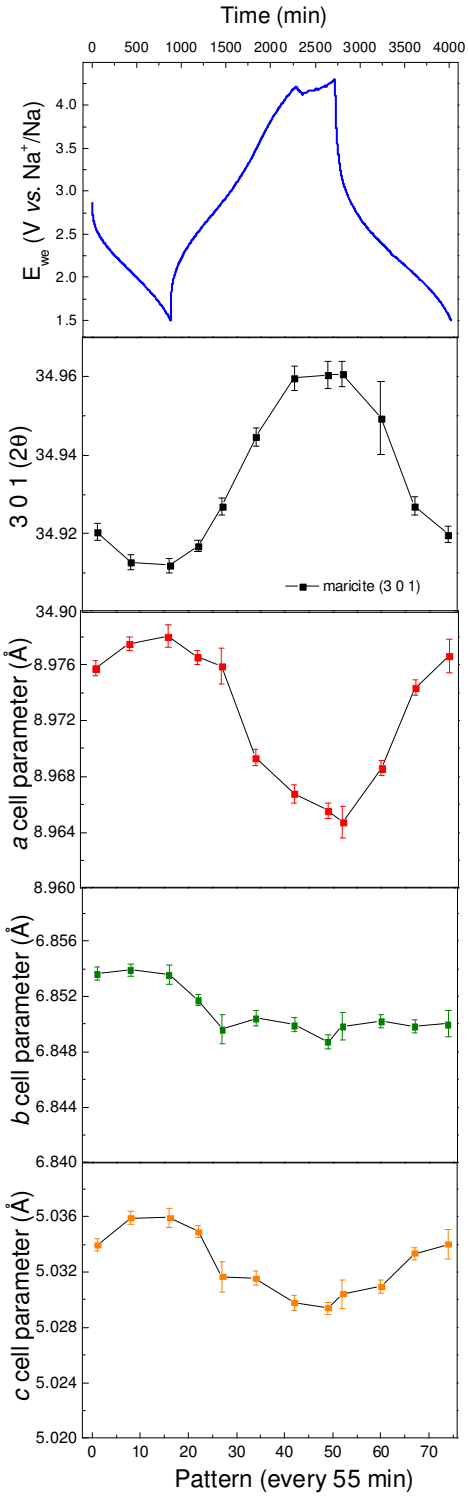

Fig. 7. 11. From top to bottom: voltage profile of a XRD in-situ cell cycled at 0.025C, 2θ of the reflection (3 0 1) and values of the a, b and c cell parameters for different XRD patterns.

7.2.2. Electrochemical characterization in aqueous media

Electrodes of the WM3-3 sample were prepared with same ratio AM:C65:PVDF but using Ti foil as current collector. Ti foil was used as current collector to avoid the SS oxidation since the used voltage limits were close to the electrolyte decomposition. A wider voltage window was used than in previous chapters (2.35 V) to allow complete reaction of maricite since a large overpotential was observed in the organic electrochemical tests.

Aqueous half-cells were tested at 0.2C between 2.4 and 3.5 V *vs.* Na^+/Na. Only 2 mAh g^{-1} of reversible capacity were achieved after cycling, and as it happens in organic media a lower first charge was observed (6 mAh g^{-1}). These results evidence the need to reduce overpotential so as to improve the electrochemical performance of maricite $NaFePO_4$. Maricite $NaFePO_4$ also showed a significant capacity fading when cycled at 0.2C (Fig. Xb). In the first 3 cycles there is a little increase of the capacity but between cycle 4 and cycle 100 a 68 % of capacity fading was found.

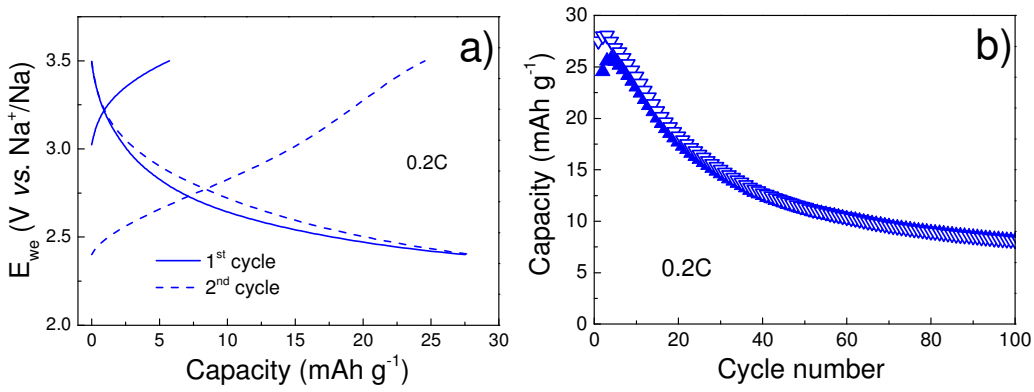

Fig. 6. 1. (a) Voltage profile for maricite WM3-3 in an aqueous half-cell at 0.2C in the voltage range from 2.4 to 3.5 V *vs.* Na^+/Na using 1 M Na_2SO_4 (b) Specific capacity vs. cycle number for the same battery

This fading indicates a low stability of the material in aqueous electrolyte and therefore, a solubility test was carried out by dissolving 100 mg of material in water. From the ICP results of the supernantants (Table 7. 2) solubility of Na, Fe and P was lower than 0.1% after 2 days of immersion.

Table 7. 2. ICP results obtained from the supernatant of a 100 mg solution of material in 10 mL of water

Na (mg L^{-1})	Fe (mg L^{-1})	P (mg L^{-1})
17.83	225.47	28.8

The chemical instability can be ruled out and therefore electrochemical stability is the main issue to be solved. Therefore, further optimization should be done to decrease the polarization (C-coating, ball-milling) and to increase the stability along cycling (protective coating).

7.3. Conclusions

Different parameters during synthesis and its influence in the final result were evaluated. Mechanical mix of precursors it is necessary to obtain the pure phase. The type of ball milling treatment influences on the domain and particle size, while the dwelling time does not affect to these values.

Maricite $NaFePO_4$ was first electrochemically study in organic media. The electrochemical mechanism is discussed and possible hypothesis were supported by different techniques as Mössbauer and in-situ X-ray diffraction. From these results can be concluded that insertion occurs to some extent. However, the small changes in cell volume together with relative the amount of Fe^{+2} and Fe^{+3} at different voltage values may indicate that other processes can contribute to the obtained capacity. At present we do not discard the possible existence of a capacitive process and in situ Mossbauer is planned to clarify the reaction mechanism, which is clearly different from what was previously reported.

This material was finally tested in aqueous electrolyte, however the high polarization does not allow to complete the reaction in the smaller voltage window used in aqueous electrolyte. Moreover, maricite NaFePO4 showed good chemical stability in aqueous solution regarding to the results obtained by ICP but low stability during cycling. Therefore, further optimization has to be done on this material to improve capacity and stability in aqueous media.

[1] P. Moreau, D. Guyomard, J. Gaubicher, F. Boucher, Structure and stability of sodium intercalated phases in olivine $FePO_4$. Chem. Mater. 22 (2010) 4126–4128
[2] P.P. Prosini, C. Cento, A. Masci, M. Carewska, Sodium extraction from sodium iron phosphate with a Maricite structure, Solid State Ion. 263 (2014) 1-8
[3] A. Sune, F. R. Beckd, D. Haynese, J. A. Poston Jr., S.R. Narayanana, P. N. Kumtab, A. Manivannan, Synthesis, characterization, and electrochemical studies of chemically synthesized $NaFePO_4$, Mater. Sci. and Eng. B 177 (2012) 1729– 1733
[4] J. Kim, D-H. Seo, H. Kim, I. Park, J-K. Yoo, S-K. Jung, Y-U. Park, W. A. Goddard III, and K. Kang, Unexpected discovery of low-cost maricite $NaFePO_4$ as a high-performance electrode for Na-ion batteries, Energy Environ. Sci. 8 (2015) 540-545
[5] O. V. Yakubovich, E. L. Belokoneva, V. G. Tsirel'son, V. S. Urusov, Electron densitiy distribution and chemical bond in maricite $NaFePO_4$, Vestnik Moskovskogo Universiteta, Geologiya 47(1992) 46-56
[6] A. Ponrouch, E. Marchante, M. Courty, J-M. Tarascon, M. R. Palacín, In search of an optimized electrolyte for Na-ion batteries, Energy Environ. Sci., 5 (2012) 8572-83

8. General conclusions

$NaTi_2(PO_4)_3$, which is the most promising anode for Na ion aqueous batteries, was synthesized by two different routes. The sample obtained by ceramic method showed some impurities of TiP_2O_7, while by Pechini method the sample was obtained pure due to a better mixing of precursors. In organic electrolyte, both samples improved notably in terms of capacity, cyclability and polarization with a ball-milling treatment. However, an irreversibility of 25% in the first cycle was observed. This irreversibility is mitigated with an effective C-coating. Moreover, capacities close to the theoretical capacity and overpotential values as low as 40 mV were achieved at 0.05C in organic electrolyte. The improved material was tested in aqueous electrolyte. The influence of the pH on the sample was studied, showing much better results in terms of coulombic efficiency at pH = 12 than at pH = 6 and pH = 8. But, even at pH = 12, the material had to be cycled at high rates to achieve coluombic efficiencies close to 100%. By using non-pressed electrodes, $NaTi_2(PO_4)_3$ achieved 400 cycles with 100% of capacity retention despite a lower capacity and a slightly higher overpotential were obtained. Although further studies should be done to study the influence of the calendaring effects, a stable anode was achieved to use in future full cells.

Three different materials based on Fe and other abundant, cheap and environmentally friendly elements were studied as cathode for aqueous Na-ion batteries.

The electrochemical properties of olivine $NaFePO_4$, obtained by chemical delithiation and further sodiation of $LiFePO_4$, in both aqueous and organic media were studied. The reduction of the operating voltage range was demonstrated to be essential to the cycling stability of this material. The origin of capacity fading if the voltage range is not reduced has not been identified, although material dissolution can be ruled out and the XRD pattern of the cycled material does not exhibit extra peaks. The overpotential measured in aqueous electrolyte is significantly lower than in organic electrolyte. This notable reduction in polarization, which is discussed in terms of interfacial properties, allows better performances at high rates despite the lower voltage window used in aqueous cells, reaching a capacity of 70 mAh g^{-1} at 0.2C and 40 mAh g^{-1} at 2C. At 55 ˚C, the overpotential in both electrolytes is significantly reduced and a much larger capacity is obtained in both media, with a superior performance of the aqueous cells, especially at high rates, achieving 110 mAh g^{-1} at 0.1C and 74 mAh g^{-1} at 2C. Finally, a full cell battery was built with $NaTi_2(PO_4)_3$ as negative electrode. The cell delivered 0.6 V and 70 mAh g^{-1} and demonstrated that $NaFePO_4$ is a suitable candidate for aqueous Na-ion cells. However, studies should be done to increase the stability of $NaFePO_4$ in aqueous electrolyte and Mn-doped samples should be explored to increase the voltage, and therefore the energy density, of the final full cell.

, We explored other Fe based materials as $NaFe_2(CN)_6$. The chemical stability of $NaFe_2(CN)_6$ cells in 1 M Na_2SO_4 has been also shown to be very dependent on the selected voltage range. At pH = 6, the second process from Na-PB to BG cannot be achieved when cycling at low rate (0.2C) because of electrolyte decomposition. Even at high rate there is competition with electrolyte decomposition which leads to low coulombic efficiencies and detachment of the material from the current collector due to bubble formation, which would result in impractical cells. At pH = 2, this process at high potential can be only partially achieved, with severe fading and low coulombic efficiencies. Therefore, to achieve a better electrochemical stability, the voltage range should be limited to the first redox process. Remarkable coulombic efficiencies over 99% at 1C and over 98% at 0.2C can be achieved focussing on the first redox process from Na-PB to Na-PW. Moreover, this voltage limitation led to improved cycling stability (87% and 97% at 0.2C and 1C after 50 cycles) in comparison to reported values. Reversible capacities of 65 and 52 mAh g^{-1} at 0.2C and 1C respectively have been obtained despite limiting the voltage range and a very low overpotential has been measured (0.018 V at 0.2C), which results in an excellent round trip efficiency. The promising performance of Na-PB together with the fact that it is a material easy to synthesize and made of low-cost earth-abundant elements, make it a very appealing candidate for aqueous systems if a proper sodiated counter electrode is found.

The strong reduction of overpotential in aqueous electrolyte has been discussed. Fig. 1 shows the comparison of the obtained overpotential values for $NaFePO_4$ and $Na_2Fe_2(CN)_6$ at 4 different rates. Although $NaFePO_4$ exhibits a larger overpotential in both cases, both materials follow the same trend with increasing rate in aqueous electrolyte. This improvement is explained by the easier desolvation of Na^+ in H_2O that results in a fast Na^+ charge transfer at the interface. But the fact that $NaFePO_4$ experiences a major reduction when changing from organic to aqueous electrolyte suggests a major improvement in wettability, which depends on surface topology and chemical composition.

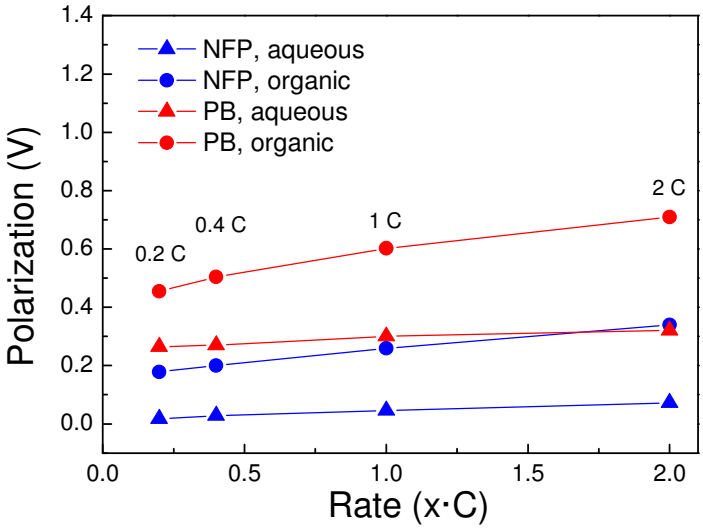

Fig. 1. Overpotential *vs.* rate obtained for aqueous and organic cells measured at 4 different rates (0.2C, 0.4C, 1C and 2C) for Na-PB and olivine $NaFePO_4$.

$Na_4Fe_3(PO_4)_2P_2O_7$ has also been explored as aqueous cathode material. This compound was prepared by synthesis and the effect of temperature and dwelling time were analyzed. However, a purity of 75-80% was only achieved and *maricite* $NaFePO_4$ and $Na_2FeP_2O_7$ appeared as secondary phases. On the other hand, changing from dry milling of the precursor's mixture to wet milling finally resulted in a quasi-pure sample, with only 2% of *maricite*. Three different strategies have been tested to improve the conductivity of the material (ball-milling, C-coating and adding C to the precursors mixture before and after the first heat treatment) and the obtained materials have been characterized in Na half-cells. The best results in terms of polarization were obtained for the C-precursor sample, although it exhibited a lower capacity. This sample was then studied in aqueous electrolyte and an important capacity fading, especially in the first 30 cycles, was observed. ICP results obtained from solubility tests show that Na and Fe dissolve, most probably as a result of the hydrolysis of polyphosphates. We found that the solubility is much higher in pure water than in the electrolyte solution and is intensified with the presence of O_2 in both media. As conclusion, future work on $Na_4Fe_3(PO_4)_2P_2O_7$ as electrode material in aqueous NIBs should be directed towards increasing its stability in aqueous medium. Two different strategies could be simultaneously considered: (i) the preparation of an effective protective coating and (ii) the preparation of thicker electrodes to limit the hydrolysis reaction to the surface of the electrode.

Finally for the maricite $NaFePO_4$, different parameters during synthesis and its influence in the final result were evaluated. Mechanical mix of precursors it is necessary to obtain the pure phase. The type of ball milling treatment influences on the domain and particle size, while the dwelling time does not affect to these values.

Maricite $NaFePO_4$ was first electrochemically study in organic media. The electrochemical mechanism is discussed and possible hypothesis were supported by different techniques as Mössbauer and in-situ X-ray diffraction. From these results can be concluded that insertion occurs to some extent. However, the small changes in cell volume together with relative the amount of Fe^{+2} and Fe^{+3} at different voltage values may indicate that other processes can contribute to the obtained capacity. At present we do not discard the possible existence of a capacitive process and in situ Mossbauer is planned to clarify the reaction mechanism, which is clearly different from what was previously reported.

This material was finally tested in aqueous electrolyte, however the high polarization does not allow to complete the reaction in the smaller voltage window used in aqueous electrolyte. Moreover, maricite NaFePO4 showed good chemical stability in aqueous solution regarding to the results obtained by ICP but low stability during cycling. Therefore, further optimization has to be done on this material to improve capacity and stability in aqueous media.

Journal of Power Sources 291 (2015) 40–45

Contents lists available at ScienceDirect

Journal of Power Sources

journal homepage: www.elsevier.com/locate/jpowsour

Electrochemical characterization of $NaFePO_4$ as positive electrode in aqueous sodium-ion batteries

A.J. Fernández-Ropero [a], D. Saurel [a], B. Acebedo [a], T. Rojo [a, b], M. Casas-Cabanas [a, *]

[a] CIC energiGUNE, Parque Tecnológico de Álava, Albert Einstein 48, ED.CIC, 01510 Miñano, Spain
[b] Departamento de Química Inorgánica, Universidad del País Vasco UPV/EHU, P.O. Box. 644, 48080 Bilbao, Spain

HIGHLIGHTS

- $NaFePO_4$ exhibits low polarization and high rate capability in aqueous electrolyte.
- The material delivered 70 mAh g^{-1} at 2 C and 110 mAh g^{-1} at C/5 at 55 °C.
- A $NaFePO_4/NaTi_2(PO_4)_3$ full cell of 0.6 V and delivering 70 mAh $g^{-1}_{NaFePO4}$ is shown.

GRAPHICAL ABSTRACT

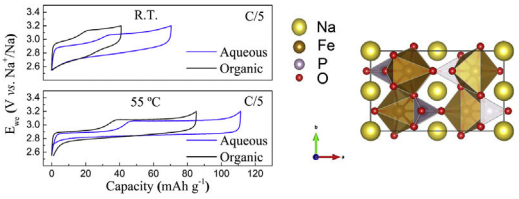

ARTICLE INFO

Article history:
Received 10 December 2014
Received in revised form
10 April 2015
Accepted 4 May 2015
Available online 15 May 2015

Keywords:
Na-ion
Aqueous battery
$NaFePO_4$
$NaTi_2(PO_4)_3$
Full cell

ABSTRACT

Here we report the rate capability and cycling stability of $NaFePO_4$ in aqueous electrolyte at various temperatures and voltage windows and compare it to its performance in organic electrolyte under similar conditions. In aqueous electrolyte the polarization was strongly reduced, leading to superior capacity at all tested rates compared to organic electrolyte with a comparable voltage window. Moreover, by fine tuning the voltage window, the capacity retention was notably improved, indicating that this material is a good candidate for aqueous Na-ion batteries, which we have confirmed by reporting the cycling stability of a $NaFePO_4/NaTi_2(PO_4)_3$ aqueous full cell.

1. Introduction

The alarming increase of contaminants' emissions to the atmosphere as well as the depletion of fossil fuels' reserves are motivating the need for renewable energies and large-scale rechargeable energy storage devices. Current technologies used in grid storage include Na–S, Li-ion, Lead-acid and Nickel–Cadmium, with a clear predominance of the first. Sodium-based systems are potentially less expensive and more environmentally friendly than Li-ion systems given that sodium is more abundant, evenly distributed and easier to extract than lithium [1–4]. Nevertheless, molten sodium and sulphur, operating at 300–350 °C, represent a safety hazard, and thus research efforts are now being directed towards room temperature systems, i.e. Na-ion and Na–O_2 batteries [1–4]. Within this context Na-ion batteries in aqueous media show promise for stationary application. Despite the lower cell voltage with respect to Li-ion batteries, they are safer than the above mentioned technologies and may represent a disruptively low-cost system [2,5].

One of the first reports of an aqueous Na-based cathode material was from Sauvage et al., who tested the electrochemical Na^+ insertion/de-insertion into $Na_{0.44}MnO_2$ (C_{th} = 160 mAh g^{-1}, 3.005,

* Corresponding author.
E-mail address: mcasas@cicenergigune.com (M. Casas-Cabanas).

http://dx.doi.org/10.1016/j.jpowsour.2015.05.006
0378-7753/

3.225 and 3.455 V *vs.* Na^+/Na) in aqueous media when studying this material for its sensing properties [6]. Soon after, Whitacre et al. developed a hybrid cell using the same material as a positive electrode and activated carbon (AC) as negative electrode, obtaining higher energy densities than a supercapacitor and good reversibility, showing a specific capacity of 45 mAh g^{-1} and a voltage of 1.4 V [7–10]. Improved results on this type of cells have been reported using λ-MnO_2 (C_{th} = 154 mAh g^{-1}), as this material was able to deliver a specific capacity up to 100 mAh g^{-1}, leading to a full cell energy density of 25 Wh kg^{-1} for a 5-h discharge with an AC anode [11]. Despite λ-MnO_2 was prepared from a lithium containing precursor, *i.e.* $LiMn_2O_4$, the authors calculated its higher energy density results in a much lower specific cost in $ per Ah than $Na_{0.44}MnO_2$ [11].

Concomitantly, Wessells et al. proposed copper and nickel Prussian blue analogues ($KCuFe(CN)_6$ and $KNiFe(CN)_6$) as positive electrode materials for K^+ and Na^+ aqueous batteries [12,13]. These materials have a theoretical specific capacity of about 60 mAh g^{-1}. While $KNiFe(CN)_6$ was found to react with sodium at 3.3 V *vs.* Na^+/Na, $KCuFe(CN)_6$ reacted at 3.48 V *vs.* Na^+/Na in addition to a second process that was observed near 3.71 V *vs.* Na^+/Na. Promising rate capabilities, round trip energy efficiencies and good cyclabilities have also been reported for both materials.

More recently, the polyanionic compound $Na_2FeP_2O_7$ (C_{th} = 97 mAh g^{-1}) has been reported by Jung et al. [14] in 1 M Na_2SO_4 aqueous electrolyte, with a main plateau around 3 V *vs.* Na^+/Na. At 1 C rate, the initial discharge capacity was 58 mAh g^{-1} and the capacity retention was approximately 86% after 300 cycles. NASICON-Type cathodes as $Na_3V_2(PO_4)_3$ (C_{th} = 117 mAh g^{-1}) and $NaVPO_4F$ (C_{th} = 143 mAh g^{-1}) have also been studied in aqueous electrolyte. In the case of $Na_3V_2(PO_4)_3$ about 50 mAh g^{-1} with an operating voltage of 3.355 V *vs.* Na^+/Na were obtained in a 5 M $NaNO_3$ electrolyte solution at 8.5 C rate [15], while $NaVPO_4F$ electrode exhibited a capacity of 54 mAh g^{-1} between 3.155 and 3.755 V *vs.* Na^+/Na also in a 5 M $NaNO_3$, with a 70% of capacity retention after 20 cycles in a full cell with polyamide as anode at almost C/3 rate [16].

Among polyanionic materials studied so far for Na-ion batteries, olivine $NaFePO_4$ has the highest theoretical capacity (154 mAh g^{-1}) and operates around 2.9 V *vs.* Na^+/Na. The theoretical energy density of this material (446 Wh kg^{-1}) is therefore close to that of $NaVPO_4F$, with the advantage that its operation voltage lies within the electrolyte stability limit and therefore does not need to be cycled at very fast rates to avoid decomposition. $NaFePO_4$ is analogue to the most studied Li-ion electrode material $LiFePO_4$, and its study in organic systems has been intensified in the last two years. Good capacity (100–120 mAh g^{-1} at low rates) and cyclability have been reported, as well as a different transformation mechanism with respect to $LiFePO_4$, [17–22]. The use of $FePO_4$ in aqueous electrolyte has been recently evaluated in a report regarding the use of $Na_3Ti_2(PO_4)_3$ as Na-bearing anode. The authors reported an initial full cell capacity at C/2 of ~110 mAh $g^{-1}_{cathode}$, with a capacity fade of about 40% after 20 cycles at pH = 11 [23]. Another recent work showed that $LiFePO_4$ could be reversibly cycled in an aqueous solution of $NaNO_3$ [24]. These promising preliminary results demand additional effort to further evaluate the electrochemical performance of $FePO_4/NaFePO_4$ in aqueous electrolytes and to find the optimum conditions to reduce the capacity fading upon cycling.

Here we report the rate capability and cycling stability of $NaFePO_4$ in aqueous electrolyte at various temperatures and voltage windows and compare it to its performance in organic electrolyte under similar conditions. The cycling stability of a $NaFePO_4/NaTi_2(PO_4)_3$ full cell in aqueous electrolyte is also reported.

2. Experimental

2.1. Synthesis and structural characterization

$NaFePO_4$ was prepared by chemical delithiation of commercial carbon-coated $LiFePO_4$ using NO_2BF_4 (95%, Sigma–Aldrich) in a molar ratio of 1:2.5 in a CH_3CN solution. The chemical sodiation of the obtained $FePO_4$ was carried out by treatment with NaI (99.5%, Sigma–Aldrich) in CH_3CN in a 3:1 M ratio [18]. On the other hand, $NaTi_2(PO_4)_3$ was obtained through the Pechini method as reported by Sun II Park et al. [25]. In order to improve the electronic conductivity, the material was C-coated using polyethylene-block-poly(ethylenglycol) (Mn ≈ 1400, Sigma–Aldrich) in 1:1 mass proportion, by an anneal at 700 °C during 1 h in a furnace tube with a constant Ar flow. This operation was done twice until a material with 2 wt% of C was obtained as determined by TGA, with a 3 nm thick coating, as determined with a FEI – TECNAI G2 Transmission Electron Microscope (S1).

X-ray diffraction data were recorded using a Bruker Advance D8 instrument with copper radiation ($\lambda_{CuK\alpha1}$ = 1.54056 Å, $\lambda_{CuK\alpha2}$ = 1.5443 Å). Profile matching refinements were performed with the FullProf software [26].

Inductively Coupled Plasma Atomic Emission Spectroscopy (ICP-AES, Horiba Yobin Yvon Activa) has been used to determine the Fe content in the electrolyte after cycling.

2.2. Electrochemical characterization

Electrodes were composed of 75 wt% C-coated material, 20 wt% carbon black conductive additive (Super C65, TIMCAL) and 5 wt% poly(vinylidene fluoride) binder (powder, Alfa Aesar). A slurry of the above-mentioned composition dispersed in *N*-methyl-2-pyrrolidone (NMP) (99.5% anhydrous, Sigma–Aldrich) was deposited on the top of a stainless steel current collector disk, dried overnight at 120 °C and pressed at 5 T cm^{-2}. 1 M Na_2SO_4 was chosen as aqueous electrolyte (previously deoxygenated with N_2). The measurements were done in three electrodes Swagelok-type cells, using Ag/AgCl (3 M NaCl) as reference electrode and AC as counter electrode (Norit DLC super30) in a weight ratio of ≈12:1 to ensure that $NaFePO_4$ is the limiting electrode and that the voltage swing of the carbon electrode remains within the voltage window (S2). Self-standing active carbon electrodes were prepared from the slurry with 5% of polytretafluoroethylene in ethanol and were previously tested as symmetric capacitor also using a three electrodes Swagelok-type cell. A capacitance of 70 F g^{-1} (≈12 mAh g^{-1}) for each electrode and a total voltage of 1.2 V was achieved (S3). All aqueous cells were assembled inside a glove bag (Aldrich) containing N_2 to eliminate any chance of O_2 entrance in the cell, since this would produce the oxidation of the electrode materials [27].

Organic Swagelok half-cells were assembled with Na-metal as counter and reference electrode, and $NaClO_4$ EC:PC with 2% of FEC was used as electrolyte. Organic cells were assembled inside a Glove Box with a dry Ar atmosphere. Glass fibre separators (Whatman, Grade D) were used in both media.

Finally, an aqueous full cell $NaFePO_4/NaTi_2(PO_4)_3$ was assembled using 1 M Na_2SO_4 at pH = 12 after addition of NaOH to avoid the oxidation of the anode material [27].

Galvanostatic and rate capability tests were measured in a Bio Logic VMP3 Multi-Channel Potential/Galvanostat in a 3 electrodes configuration.

3. Results and discussion

The X-ray diffraction pattern of $NaFePO_4$ is shown in Fig. 1a. The pattern has been indexed with Pnma space group and the refined

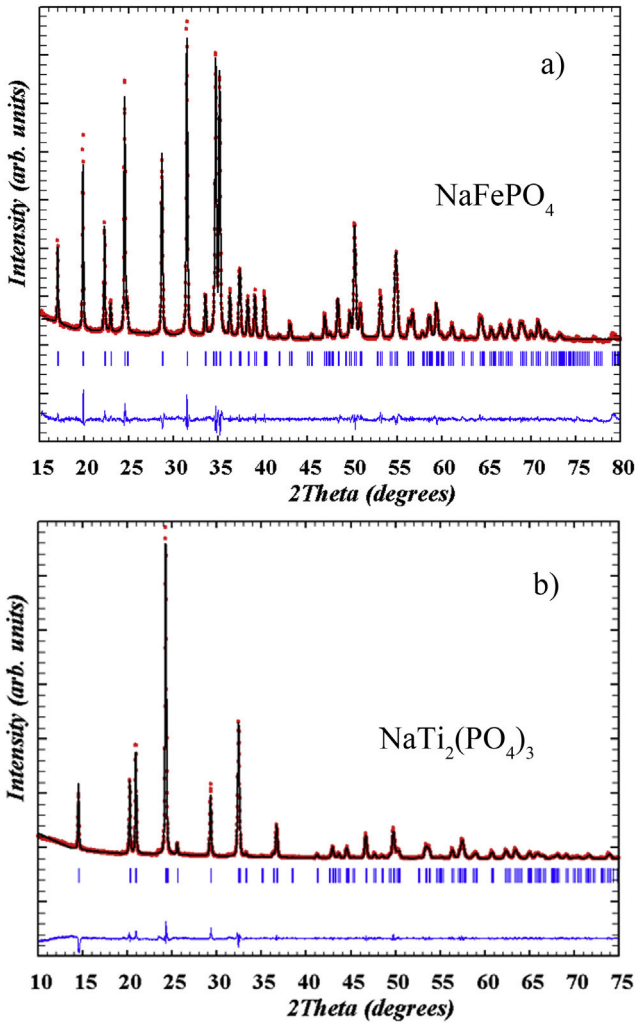

Fig. 1. Profile matching refinement of (a) $NaFePO_4$ obtained by chemical oxidation of $LiFePO_4$ and subsequent reduction, and (b) $NaTi_2(PO_4)_3$ obtained by Pechini method.

cell parameters are a = 10.4032 (4) Å, b = 6.2188 (2) Å, and c = 4.9465 (2) Å (Fig. 1a), in agreement with literature values [17,18,21]. The XRD of $NaTi_2(PO_4)_3$ (Fig. 1b) has been indexed with the R-3cH trigonal structure [28] with refined cell parameters a = 8.4789 Å (5), b = 8.4789 (5) Å, and c = 21.817 (2) Å.

The galvanostatic voltage profiles of $NaFePO_4$ electrodes cycled at different rates in an organic cell within the 2.2–4.3 V voltage window are represented in Fig. 2a. The material suffers from a rather strong polarization of 0.44 V at C/10, comparable to previous reports at similar rate [18,19], which is accentuated at high rates to reach 0.7 V at 2 C. The capacity obtained at C/10 is 100 mAh g^{-1} and decreases to 40 mAh g^{-1} at 2 C, also in agreement with previous reports [18,19,29] – with minor differences attributable to different cycling conditions (relaxation, voltage window, etc.) and electrode preparation. Preliminary experiments using aqueous electrolyte resulted in a continuous fading of the capacity that was stabilized by reducing the voltage range to 2.55 V–3.2 V *vs.* Na^+/Na, which was selected as the optimum window for a C/5 rate (S4). The exact origin of this fading has not been identified yet, although material dissolution can be ruled out according to ICP analysis of the electrolyte after cycling (less than 0.4% of the initial Fe content was detected in the electrolyte after 35 cycles while the capacity faded down to 79% of the initial capacity), and no extra peaks were detected in the XRD patterns of cycled electrodes. This very conservative voltage window limits the reaction before it is completed and therefore a somewhat lower capacity is obtained at the slowest rates, with 77 mAh g^{-1} at C/10 and 70 mAh g^{-1} at C/5 (Fig. 2b and d). However, the same capacity as in the organic electrolyte is obtained for the fastest rates (>C/2.5) despite the much smaller voltage window. In fact, the polarization of the electrode in aqueous electrolyte is notably reduced (0.27 V at C/10, 0.33 V at 2 C) which allows a better performance at high rates regardless of the voltage limit. This fact is even more visible when the organic cell is cycled using the same voltage window, as can be seen in Fig. 2c and d. In this case the capacity of the aqueous cell exceeds that of the organic cell at all rates and is able to deliver 32% and 25% of the theoretical capacity at 1 C and 2 C, respectively, while the organic cell completely fails to cycle.

Since this material has a rather flat voltage-composition profile, further reduction of the polarization should lead to significant increase of the capacity. This can be achieved if the cells are cycled above room temperature [18]. In Fig. 3 we show the comparison of aqueous and organic cells cycled at 55 °C with a window of 2.55–3.2 V *vs.* Na^+/Na. At 55 °C, which actually is a more realistic operation temperature, the polarization in both electrolytes is significantly reduced (insets in Fig. 3) and much larger capacity values are obtained in both media. The effect is quite drastic in organic electrolyte as the C/5 capacity has more than doubled reaching 85 mAh g^{-1}. In aqueous electrolyte the improvement is also noticeable and an excellent performance is obtained. Indeed the capacity at C/5 reaches now 110 mAh g^{-1} and almost 87 mAh g^{-1} at 1 C, while this is the capacity value achieved at C/5 in organic electrolyte at this temperature for the same voltage window. At 2 C the capacity is still above 70 mAh g^{-1} (Fig. 3b), demonstrating that aqueous $NaFePO_4$ cells can be considered a very interesting candidate for low-cost high rate applications.

The lower polarization in aqueous electrolyte has been already reported for some materials such as $NaTi_2(PO_4)_3$ [25], $LiFePO_4$ [30] and $Na_{0.44}MnO_2$ [31]. Although aqueous electrolytes have typically a higher ionic diffusion coefficient compared to organic electrolyte, the electrolyte's conductivity contribution on the overall cell polarization in Li-ion and Na-ion batteries is generally negligible [32,33]. Moreover, several materials have been reported as Na-ion electrode materials with significantly smaller polarization at the same rate than $NaFePO_4$ (layered oxides as P2-$Na_{2/3}[Fe_{1/2}Mn_{1/2}]O_2$ [34], hard-carbons [35], titanates as $Na_2Ti_3O_7$ [36]). We can thus reasonably rule out the intrinsic conductivity of the aqueous electrolyte as origin of the lower polarization. On the other hand, although the electrode's ionic diffusivity has an important contribution to the overall polarization, it is an intrinsic property of the material and should not be affected by the electrolyte choice. The origin of the lower polarization of the aqueous electrolyte must thus reside in the electrode–electrolyte interfacial region rather than in the ionic diffusivities of the individual components. One can cite for instance the overpotential due to the less facile desolvation step of the sodium ion in non-aqueous electrolyte, which would be translated in a larger charge-transfer resistance [30] or the better wetting of the active materials due to the lower viscosity of aqueous electrolyte [25], which would reduce the polarization related to the diffusion of the electrode material by increasing the effective amount of interface open to ion insertion. This later hypothesis is further supported by the fact that it has been demonstrated that the delithiation of $LiFePO_4$, a necessary step in the synthesis of $FePO_4$ and $NaFePO_4$, generates an important porosity of the materials surface due to the release of mechanical stress between Li-rich and Li-poor phases [37]. This could be additionally accentuated in the $FePO_4/NaFePO_4$ system since the cell mismatch is much higher than for the Li counterpart, although it is likely that carbon coating may buffer this effect to some extent. This suggests

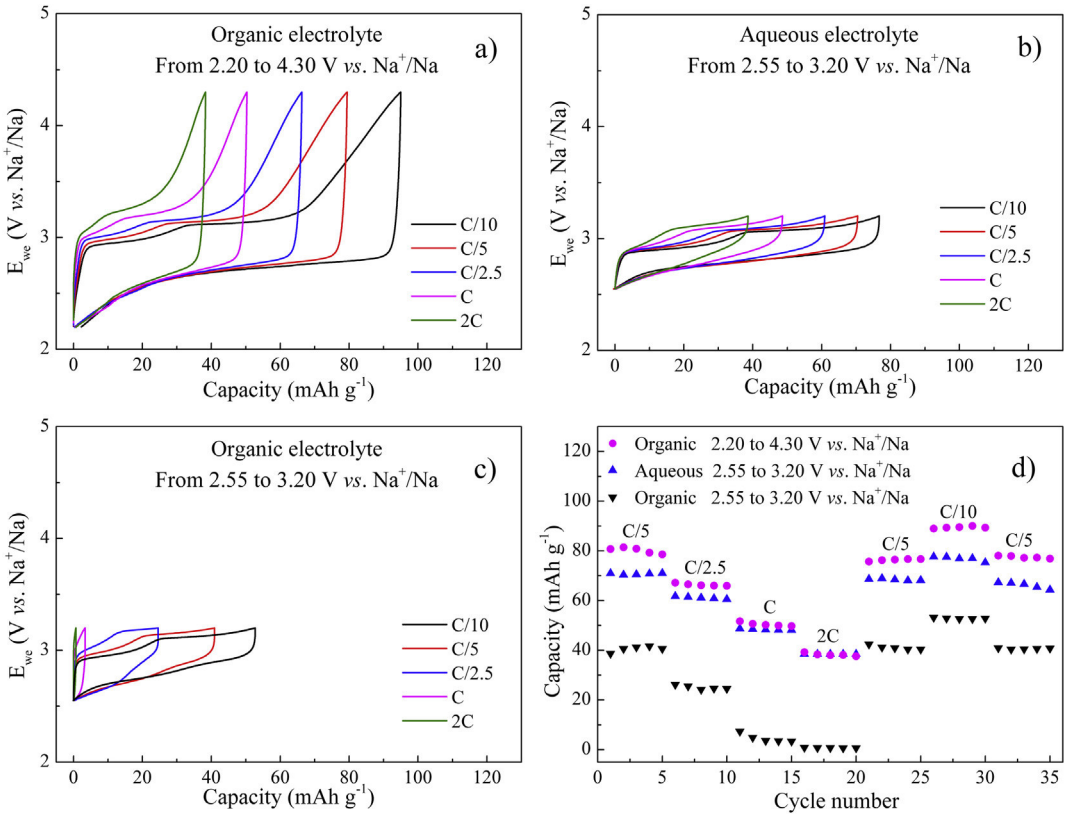

Fig. 2. (a) Electrochemical profiles at different rates for a non-aqueous cell cycled between 2.2–4.3 V *vs.* Na^+/Na and (b) an aqueous cell and (c) an organic cell both cycled between 2.55–3.2 V *vs.* Na^+/Na. (d) Summary of the rate capability tests for the different electrolytes and voltage windows.

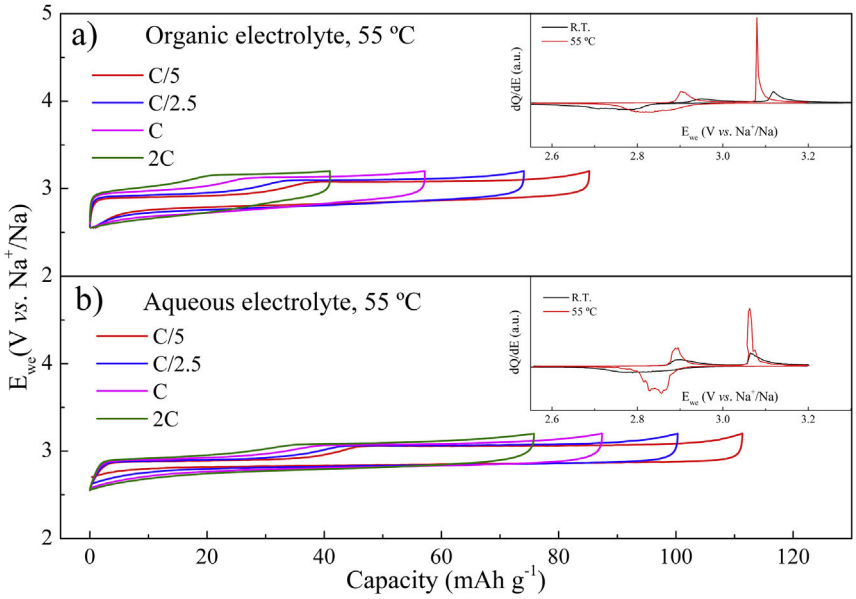

Fig. 3. (a) Electrochemical profiles at different rates for an organic cell and (b) an aqueous cell cycled between 2.55–3.2 V *vs.* Na^+/Na at 55 °C. Inset: dQ/dE plots for a C/5 rate at room temperature and 55 °C.

that the electrochemical performance of $NaFePO_4$ in organic electrolyte may be greatly improved by optimizing the characteristics of the materials surface and/or coating.

Further improvement can be obtained extending the voltage window, as shown in Fig. 4 for a cell operating at room temperature. While the 2.55–3.2 V window has been selected for best low rate stability, it can indeed be opened to 2.45–3.3 V for higher rates without appreciating important capacity fading after 30 cycles, as a capacity retention of about 90% is observed in both cases. Moreover, the capacity at 1 C rate has increased 30% with this

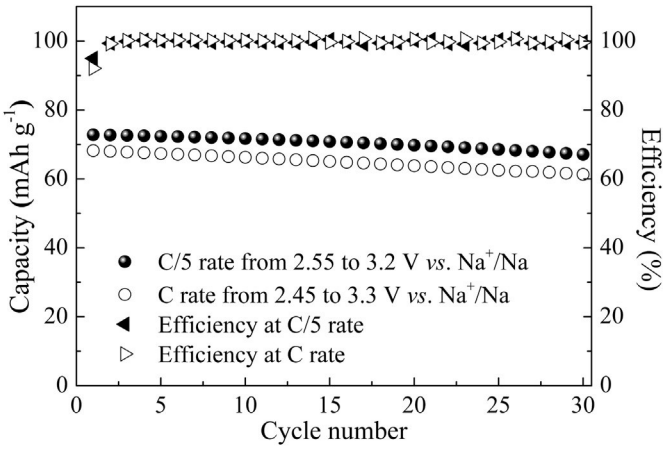

Fig. 4. Comparison of the cyclability of $NaFePO_4$ in 1 M Na_2SO_4 at C/5 rate from 2.55 to 3.2 V *vs.* Na^+/Na and at 1 C rate from 2.45 to 3.3 V *vs.* Na^+/Na.

slight opening of the voltage window, getting close to the value initially obtained at C/5 (Fig. 4), while both cells showed an energetic efficiency around 100%.

Fig. 5 shows a full cell built with $NaTi_2(PO_4)_3$ as anode material. The pH here has been raised to 12 to avoid the oxidation of the anode [27]. The cell delivers an average voltage of 0.6 V, with an initial capacity of 70 mAh g^{-1} and a capacity retention of 76% after 20 cycles. The initial capacity may seem modest compared to the 100 mAh g^{-1} reported by Li et al. on $FePO_4$ [23], even taking into account the major molecular weight of $NaFePO_4$. However, it is important to note that our voltage window (2.45 V–3.3 V *vs.* Na^+/Na for our $NaFePO_4$ electrode) is slightly narrower than theirs (2.55 V–3.5 V *vs.* Na^+/Na). Although at the price of slightly lower capacity, we greatly improved the stability upon cycling by adjusting the voltage window. As a matter of fact, since the $NaFePO_4$/AC half cells presented a much better stability upon cycling as seen in Fig. 4, we can reasonably argue that the major source of the capacity fading is in the anode side, which is confirmed by the 40% capacity fading after 30 cycles observed by Park et al. for this anode material [25]. Finally, as these results have been obtained in non-optimized lab-scale electrodes and using a very conservative voltage window, we believe that major improvements can be expected if both are optimized according to the application.

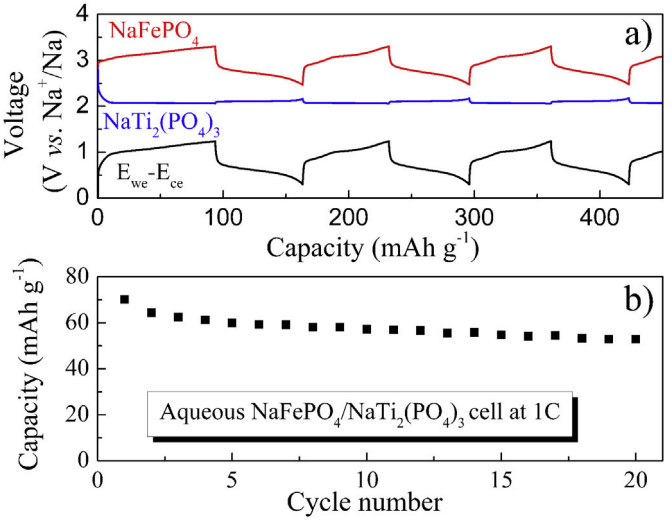

Fig. 5. (a) Voltage profiles *vs.* capacity of a $NaFePO_4/NaTi_2(PO_4)_3$ cell with 1 M Na_2SO_4 as electrolyte basified to pH = 12 by addition of NaOH. (b) Capacity in mAh $g^{-1}{}_{NaFePO4}$ of the full cell for the first 20 cycles.

4. Conclusions

The electrochemical properties of $NaFePO_4$ in aqueous media have been reported. At room temperature, the polarization of the aqueous electrolyte is significantly lower than in organic electrolyte. This notable reduction in polarization, which is discussed in terms of interfacial properties, allows better performances at high rates despite the lower voltage window used in the aqueous cells, reaching a capacity of 70 mAh g^{-1} at C/5 and 40 mAh g^{-1} at 2 C.

At 55 °C, which is closer to the actual temperature within a working battery pack, the polarization in both electrolytes is significantly reduced and much larger capacity is obtained in both media, with a superior performance of the aqueous cells, especially at high rates, achieving 110 mAh g^{-1} at C/10 and 74 mAh g^{-1} at 2 C. In addition, a full cell battery was built with $NaTi_2(PO_4)_3$ as negative electrode, which delivered 0.6 V and 70 mAh g^{-1} and demonstrated that $NaFePO_4$ is a promising candidate for aqueous Na-ion cells.

Associated content

TEM images of C-coated $NaTi_2(PO_4)_3$ and several electrochemical profiles (anode and cathode galvanostatic curves of a $NaFePO_4$/Norit DLC super30 (AC) cell, CV curve of Norit DLC super30 at 5 mV s^{-1} and capacity vs. cycle number of $NaFePO_4$ electrodes in aqueous electrolyte operating at different voltage windows) are available in the Supporting information.

Conflict of interest

The authors declare no competing financial interest.

Acknowledgements

The authors would like to thank the Ministerio de Economía y Competitividad of the Spanish Government for financial support through Project (EE2013-44330R), V.V. Roddatis for the acquisition of TEM images, J. Ségalini for helping in the electrochemical characterization and A. Llordés for a critical revision of the text.

Appendix A. Supplementary data

Supplementary data related to this article can be found at http://dx.doi.org/10.1016/j.jpowsour.2015.05.006.

References

[1] V. Palomares, P. Serras, I. Villaluenga, K.B. Hueso, J. Carretero-González, T. Rojo, Na-ion batteries, recent advances and present challenges to become low cost energy storage systems, Energy Environ. Sci. 5 (2012) 5884–5901.
[2] V. Palomares, M. Casas-Cabanas, E. Castillo-Martinez, M.H. Han, T. Rojo, Update on Na-based battery materials. A growing research path, Energy Environ. Sci. 6 (2013) 2312–2337.
[3] H.L. Pan, Y.S. Hu, L.Q. Chen, Room-temperature stationary sodium-ion batteries for large-scale electric energy storage, Energy Environ. Sci. 6 (2013) 2338–2360.
[4] N. Yabuuchi, K. Kubota, M. Dahbi, S. Komaba, Research development on sodium-ion batteries, Chem. Rev. 114 (2014) 11636–11682.
[5] H. Kim, J. Hong, K.-Y. Park, H. Kim, S.-W. Kim, Aqueous rechargeable Li and Na ion batteries, Chem. Rev. 114 (2014) 11788–11827.
[6] F. Sauvage, E. Baudrin, J.M. Tarascon, Study of the potentiometric response towards sodium ions of $Na_{0.44-x}MnO_2$ for the development of selective sodium ion sensors, Sens. Actuator B Chem. 120 (2007) 638–644.
[7] J.F. Whitacre, A. Tevar, S. Sharma, $Na_4Mn_9O_{18}$ as a positive electrode material for an aqueous electrolyte sodium-ion energy storage device, Electrochem. Commun. 12 (2010) 463–466.

[8] J.F. Whitacre, Sodium Ion Based Aqueous Electrolyte Electrochemical Secondary Energy Storage Device. Patent US 20090253025 A1. 8 October 2009.
[9] J.F. Whitacre, Sodium Based Aqueous Electrolyte Electrochemical Secondary Energy Storage. Patent US 20090052945 A1. 3 March 2011.
[10] J.F. Whitacre, High Voltage Battery Composed of Anode Limited Electrochemical Cells. Patent US 20090274950 A1. 10 November 2011.
[11] J.F. Whitacre, T. Wiley, S. Shanbhag, Y. Wenzhuo, A. Mohamed, S.E. Chun, E. Weber, D. Blackwood, E. Lynch-Bell, J. Gulakowski, C. Smith, D. Humphreys, An aqueous electrolyte, sodium ion functional, large format energy storage device for stationary applications, J. Power Sources 213 (2012) 255–264.
[12] C.D. Wessells, R.A. Huggins, Y. Cui, Copper hexacyanoferrate battery electrodes with long cycle life and high power, Nat. Commun. 2 (2011) 550.
[13] C.D. Wessells, S.V. Peddada, R.A. Huggins, Y. Cui, Nickel hexacyanoferrate nanoparticle electrodes for aqueous sodium and potassium ion batteries, Nano Lett. 11 (2011) 5421–5425.
[14] Y.-H. Jung, C.-H. Lim, J.-H. Kim, D.-K. Kim, $Na_2FeP_2O_7$ as a positive electrode material for rechargeable aqueous sodium-ion batteries, R. Soc. Chem. Adv. 4 (2014) 9799–9802.
[15] W. Song, X. Ji, Y. Zhu, H. Zhu, F. Li, J. Chen, F. Lu, Y. Yao, C.E. Banks, Aqueous sodium-ion battery using a $Na_3V_2(PO_4)_3$ electrode, ChemElectroChem 1 (2014) 871–876.
[16] H. Qin, Z.P. Song, H. Zhan, Y.H. Zhou, Aqueous rechargeable alkali-ion batteries with polyimide anode, J. Power Sources 249 (2014) 367–372.
[17] P. Moreau, D. Guyomard, J. Gaubicher, F. Boucher, Structure and stability of sodium sntercalated shases in olivine $FePO_4$, Chem. Mater. 22 (2010) 4126–4128.
[18] M. Casas-Cabanas, V.V. Roddatis, D. Saurel, P. Kubiak, J. Carretero-Gonzalez, V. Palomares, P. Serras, T. Rojo, Crystal chemistry of Na insertion/deinsertion in $FePO_4$-$NaFePO_4$, J. Mater. Chem. 22 (2012) 17421–17423.
[19] S.M. Oh, S.T. Myung, J. Hassoun, B. Scrosati, Y. Sun, Reversible $NaFePO_4$ electrode for sodium secondary batteries, Electrochem. Commun. 22 (2012) 149–152.
[20] R. Tripathi, S.M. Wood, M.S. Islam, L.F. Nazar, Na-ion mobility in layered Na_2FePO_4F and olivine Na [Fe, Mn]PO4, Energy Environ. Sci. 6 (2013) 2257–2264.
[21] M. Galceran, D. Saurel, B. Acebedo, V.V. Roddatis, E. Martin, T. Rojo, M. Casas-Cabanas, The mechanism of $NaFePO_4$ (de)sodiation determined by in situ x-ray diffraction, Phys. Chem. Chem. Phys. 16 (2014) 8837–8842.
[22] A. Whiteside, C.A.J. Fisher, S.C. Parker, M.S. Islam, Particle shapes and surface structures of olivine $NaFePO_4$ in comparison to $LiFePO_4$, Phys. Chem. Chem. Phys. 16 (2014) 21788–21794.
[23] Z. Li, D.B. Ravnsbaek, K. Xiang, Y.M. Chiang, $Na_3Ti_2(PO_4)_3$ as a sodium-bearing anode for rechargeable aqueous sodium-ion batteries, Electrochem. Commun. 44 (2014) 12–15.
[24] M. Vujkovic, S. Mentus, Fast sodiation/desodiation reactions of electrochemically delithiated olivine $LiFePO_4$ in aerated aqueous $NaNO_3$ solution, J. Power Sources 247 (2014) 184–188.
[25] S. Park, I. Gocheva, S. Okada, J. Yamaki, Electrochemical properties of $NaTi_2(PO_4)_3$ anode for rechargeable aqueous sodium-ion batteries, J. Electrochem. Soc. 158 (2011) 1067–1070.
[26] J. Rodríguez-Carvajal, Phys. B 192 (1993) 55.
[27] J.-Y. Luo, W.-J. Cui, P. He, Y.-Y. Xia, Raising the cycling stability of aqueous lithium-ion batteries by eliminating oxygen in the electrolyte, Nat. Chem. 2 (2010) 760–765.
[28] J.L. Rodrigo, P. Carrasco, J. Alamo, Thermal-expansion of $NaTi_2(PO_4)_3$ studied by Rietveld method from x-ray-diffraction data, Mat. Res. Bull. 24 (1989) 611–618.
[29] J.C. Lu, S.C. Chung, S. Nishimura, A. Yamada, Phase diagram of olivine Na_x-$FePO_4$ ($0 < x < 1$), Chem. Mater. 25 (2013) 4557–4565.
[30] P. He, X. Zhang, Y.G. Wang, L. Cheng, Y.Y. Xia, Lithium-ion intercalation behavior of $LiFePO_4$ in aqueous and nonaqueous electrolyte solutions, J. Electrochem. Soc. 155 (2008) A144–A150.
[31] D.J. Kim, R. Ponraj, A.G. Kannan, H.-W. Lee, R. Fathi, R. Ruffo, C.M. Mari, D.K. Kim, Diffusion behavior of sodium ions in $Na_{0.44}MnO_2$ in aqueous and non-aqueous electrolytes, J. Power Sources 244 (2013) 758–763.
[32] A. Ponrouch, E. Marchante, M. Courty, J.-M. Tarascon, M.R. Palacin, In search of an optimized electrolyte for Na-ion batteries, Energy Environ. Sci. 5 (2012) 8572–8583.
[33] Y.J. Zhu, Y.H. Xu, Y.H. Liu, C. Luo, C.S. Wang, Comparison of electrochemical performances of olivine $NaFePO_4$ in sodium-ion batteries and olivine $LiFePO_4$ in lithium-ion batteries, Nanoscale 5 (2013) 780–787.
[34] N. Yabuuchi, M. Kajiyama, J. Iwatate, H. Nishikawa, S. Hitomi, R. Usui, Y. Yamada, S. Komaba, P2-type $Na_x[Fe_{1/2}Mn_{1/2}]O_2$ made from earth-abundant elements for rechargeable Na batteries, Nat. Mater. 11 (2012) 512–517.
[35] S. Komaba, T. Ishikawa, N. Yabuuchi, W. Murata, A. Ito, Y. Ohsawa, Fluorinated ethylene carbonate as electrolyte additive for rechargeable Na batteries, ACS Appl. Mater. Interfaces 3 (2011) 4165–4168.
[36] P. Seguttuvan, G. Rousse, V. Seznec, J.-M. Tarascon, $Na_2Ti_3O_7$: lowest voltage ever reported oxide insertion electrode for sodium ion batteries, Chem. Mater. 23 (2011) 4109–4111.
[37] K. Weichert, W. Sigle, P.A. van Aken, J. Jamnik, C. Zhu, R. Amin, T. Acartark, U. Starke, J. Maier, Phase boundary propagation in large $LiFePO_4$ single crystals on delithiation, J. Am. Chem. Soc. 134 (2012) 2988–2992.

Meeting Abstracts
ma.ecsdl.org

Abstract MA2015-01 297

Na-Ion Aqueous Batteries for Stationary Energy Storage Systems

Antonio Jesús Fernández-Ropero[a], María José Piernas-Muñoz[a], Marine Reynaud[a], Begoña Acebedo[a], Elizabeth Castillo-Martínez[a], Damien Saurel[b], Teófilo Rojo[a,c] and Montserrat Casas-Cabanas[a]

+ Author Affiliations

Abstract

The worrying increase in the emission of contaminants to the atmosphere and the depletion of the fossil fuels' reserves are motivating the development of renewable energies and large-scale rechargeable energy storage devices. Current technologies used in grid storage include Na-S, Li-ion, Lead-acid and Nickel-Cadmium. With a clear predominance of sodium-based systems which have been implanted as an alternative to Li-ion since they are potentially less expensive and more environmentally friendly (sodium is more abundant, evenly spread and easier to extract than lithium) [1]. Nevertheless, the use of molten sodium and sulphur at 300-350 ºC present safety hazards and now research is being directed towards room temperature systems, such as Na-ion and Na-O_2 batteries [1]. Within this context, Na-ion aqueous batteries hold promise for stationary applications since, although the cell voltage is lower, they are safer than the above mentioned technologies and could represent a disruptively low cost system [1, 2]. Several electrode materials have been proposed for aqueous systems, such as manganese oxide [3], $Na_2FeP_2O_7$ [4] and Prussian blue analogues [5] for the positive side and $NaTi_2(PO_4)_3$ [6] as negative electrode.

During the presentation, we will show the results of our study [7] of low-cost Fe-based cathode materials for aqueous sodium-ion batteries: on one hand,

polyanionic materials with higher capacity than $Na_2FeP_2O_7$, and on the other hand, Prussian-blue analogues which so far have demonstrated promising rate capabilities, round trip energy efficiencies and good cyclabilities [5]. The different materials have been tested in both organic and aqueous electrolyte at different rates and temperatures in order to evaluate their performances for possible applications in stationary storage. Ultimately, full cells using some of the possible anodes for this kind of systems will be also presented.

References

[1] V. Palomares, M. Casas-Cabanas, E. Castillo-Martinez, M.H. Han, T. Rojo. Update on Na-based battery materials. A growing research path. Energy Environ. Science 6(2013) 2312-2337.

[2] H. Kim,. J. Hong, K-Y. Park, H. Kim, S-W. Kim, Aqueous Rechargeable Li and Na ion batteries, Chem. Rev. DOI: 10.1021/cr500232.

[3] J.F. Whitacre, T.Wiley, S.Shanbhag, Y.Wenzhuo, A.Mohamed, S.E. Chun, E.Weber, D.Blackwood, E.Lynch-Bell, J.Gulakowski, C.Smith, D.Humphreys, An aqueous electrolyte, sodium ion functional, large format energy storage device for stationary applications, J. Power Sources 213(2012) 255-264.

[4] Y-H. Jung, C-H. Lim, J-H. Kim, D-K. Kim. $Na_2FeP_2O_7$ as a positive electrode material for rechargeable aqueous sodium-ion batteries. R. Soc. Chem. Adv., 4(2014) 9799-9802.

[5] C.D. Wessells, S.V. Peddada, R.A. Huggins, Y.Cui, Nickel hexacyanoferrate nanoparticle electrodes for aqueous sodium and potassium ion batteries. Nano Lett. 11(2011):5421-5425

[6] S. Park, I. Gocheva, S. Okada, J. Yamaki, Electrochemical properties of $NaTi_2(PO_4)_3$ anode for rechargeable aqueous sodium-ion batteries. J. Electrochem. Soc. 158(2011) 1067-1070.

[7] A.J. Fernández-Ropero, D. Saurel, B. Acebedo, T.Rojo, M.Casas-Cabanas. Submitted.